2017

The role of the heat shock response in protein aggregation and neuroinflammation associated with neurodegenerative diseases

Rebecca San Gil
University of Wollongong

The role of the heat shock response in protein aggregation and neuroinflammation associated with neurodegenerative diseases

Rebecca San Gil

A thesis submitted in fulfilment of the requirements for the award of the degree

Doctor of Philosophy

from the

School of Biological Sciences and Illawarra Health and Medical Research Institute

University of Wollongong

UNIVERSITY OF WOLLONGONG AUSTRALIA

December 2017

Declaration

This thesis is submitted in accordance with the University of Wollongong guidelines in fulfilment of the requirements for the award of the degree Doctor of Philosophy. This thesis does not contain material that has been previously published by another person except where referenced or acknowledged, and has not been submitted for the award of any degree at any other academic institution.

_____

Rebecca San Gil

December 2017

Acknowledgements

I would like to thank A/PR Heath Ecroyd for being a fantastic supervisor over the course of my PhD (and undergraduate studies!). Heath encouraged my interests in researching heat shock proteins, the heat shock response, and their roles in neurodegenerative diseases. I am extremely grateful for the support that I have received from Heath in tackling the ups and downs in the lab, the opportunity to travel to London for a research exchange, presenting my research, and editing thesis and manuscript drafts. We have had a very successful and productive partnership over the last 4 years and I sincerely hope that we continue to collaborate throughout my postdoctoral career. I am extremely grateful to my co-supervisors A/PR Justin Yerbury and Dr Lezanne Ooi, who have also been invaluable in helping me throughout my PhD. Justin's passion for finding new treatments and a cure for MND sparked my initial interest in targeting my PhD research to MND-associated pathologies. Under Lezanne's mentorship, I have developed an interest in neuroscience and neurochemistry. As my super squad of supervisors, Heath, Justin and Lezanne, have also been invaluable to my professional development and have always provided career advice regarding networking, fellowship and project grant applications.

I would like to thank Prof Linda Greensmith and Dr Bernadett Kalmar for taking a chance on a PhD student from the other side of the world and allowing me to undertake a research exchange at University College London. I was incredibly fortunate to work (and share a pint or two) with the bright and talented scientists in the Graham Watts Laboratory, UCL.

Thank you to the IHMRI technical officers, Linda, Katie, Tanya, Clare, Nadia, Di, Poppy for the technical support. IHMRI is also filled with some absolutely quirky, strange, downright crazy scientists who have made my PhD such memorable years. A massive thank you to my fantastic friends in the Ecroyd lab (Dezerae, Anthea, BJ, Caitlin, Nick, and Shannon), Yerbury lab (Natalie, Di, Raf, Luke, Bella, Clare and Liyu), and Ooi lab (Mon, Dzung, Rachelle, Sonia,

and Jeremy). I am very thankful for all the opportunities this PhD has given me to learn new skills, and make friendships and connections that I hope will last long into our lives and postdoctoral research careers.

Finally, a big thank you to my grandparents Abuelo Faustino, Abuela Angelines, and Abuela Mercedes for their unwavering support. Thank you Mum for the brain food, Dad for the scientific arguments, Roslyn and Hugh for the fun times living in London together, and David for being my personal cheerleader, particularly in the final months of writing. The love, encouragement and support from my family and friends has gotten me through the last 4 years of PhD research, I couldn't have done it without them.

Abstract

Neurodegenerative diseases, such as amyotrophic lateral sclerosis and Huntington's disease, are complex diseases that can be characterised by protein inclusion formation and chronic neuroinflammation in the central nervous system. Investigating whether pro-survival mechanisms are induced in cells in response to protein aggregation and inflammatory stimuli is an important area of research. The heat shock response is one such pro-survival pathway that results in the upregulation of heat shock proteins, which have demonstrated anti-aggregation, anti-inflammatory and anti-apoptotic activities in the cell.

Heat shock proteins are dynamic and oligomeric proteins that interact with various co-factors and client proteins, and this can represent a challenge when studying their function in cells. The work described in Chapter 3 outlines a new strategy for the expression of non-tagged Hsps and a fluorescent reporter protein using bicistronic constructs. This method sought to overcome the disadvantages of traditional methods for examining proteins in cells; *i.e.*, tagging the N- or C-termini with a fluorescent protein, which can compromise protein dynamics. The Hsp-encoding bicistronic expression constructs were tested in a cell-based model of protein aggregation to compare the ability of different heat shock proteins to inhibit the aggregation of an aggregation-prone protein, a double mutant isoform of firefly luciferase. These studies showed that Hsp40, Hsp70, and Hsp40+Hsp70 expressed in combination were more efficacious in inhibiting the aggregation of firefly luciferase compared to Hsp90, Hsp27 and αB-c. These Hsp-encoding bicistronic constructs can be used in future experiments to compare the ability of heat shock proteins to inhibit the activation of the inflammatory pathway, cell-death pathways, or the aggregation of a range of disease-associated proteins.

A current limitation in the field of neurodegenerative diseases is the lack of techniques that can be used to non-subjectively quantify the number of inclusions formed in cells. In Chapter 4, a

new technique is described called FloIT (flow cytometric quantification of inclusions and trafficking), which allows for the rapid quantification of protein inclusions and protein translocation between subcellular compartments by flow cytometry. FloIT was shown to be able to quantify the number of inclusions formed in cells by a range of different aggregation-prone proteins including, superoxide dismutase 1, TAR DNA-binding protein-43, huntingtin, and a double mutant isoform of firefly luciferase. FloIT successfully measured the translocation of two different proteins from the nucleus to the cytoplasm after treatment (*e.g.* TAR DNA-binding protein 43 translocation from the nucleus to the cytoplasm after MG132 treatment). FloIT is non-subjective, quantitative, rapid, easy to implement, amenable to medium-high throughput screens of compounds, and therefore, a significant development with regard to techniques that can be used to assess the impact of various treatments on inclusion formation in cells.

The absence of a heat shock response in affected cells of the central nervous system in rodent models of amyotrophic lateral sclerosis and Huntington's disease could be the consequence of: (i) an attenuated heat shock response in neurons, or (ii) the capacity of disease-associated misfolded proteins and aggregates to evade the heat shock response. Chapter 5 investigates each of these aspects through the use of a fluorescent reporter of heat shock response activation in a neuron-like cell line, Neuro-2a (HSE:EGFP) cells. Live cell fluorescence imaging of Neuro-2a (HSE:EGFP) showed that, not only do differentiated cells have a competent heat shock response, but also that heat shock response induction after treatment with heat shock or $CdCl_2$ is significantly greater in magnitude in differentiated compared to non-differentiated cells.

The ability of a range of pathogenic and non-pathogenic proteins to induce a heat shock response was also quantified using Neuro-2a (HSE:EGFP) cells. The extracellular application of soluble or aggregated α-synuclein or superoxide dismutase 1 (G93A mutant) did not induce

a heat shock response. This suggests that in the context of neurodegenerative diseases, the cell-to-cell transfer of aggregates may not elicit a heat shock response. With regard to intracellular aggregation, flow cytometric analysis showed that the expression of mutant superoxide dismutase 1 and huntingtin induced a heat shock response in a low proportion of cells, whereas expression of mutant firefly luciferase induced a heat shock response in a significantly greater proportion of cells. Through the combination of FloIT, flow cytometric analysis of intact cells, and live cell imaging by confocal microscopy, the effect of various factors (*i.e.* relative size of the inclusions, number of inclusions, protein concentration, and rate of inclusion formation) on induction of the heat shock response was investigated. The data presented in Chapter 5 shows that there was a positive relationship between the ability of a cell to induce the heat shock response and (i) the expression levels of aggregation-prone proteins and, (ii) the number of inclusions formed. Lastly, cells expressing mutant firefly luciferase that induced a heat shock response were found to live longer after inclusion formation compared to cells with inclusions that did not induce a heat shock response. This shows that the induction of the heat shock response is cytoprotective, even in the presence of inclusions.

Chronic neuroinflammation is stimulated by the death of neurons and release of protein inclusions, which activates microglia and astrogliosis. For example, activated microglia secrete pro-inflammatory mediators, such as tumour necrosis factor-α and nitric oxide, which exacerbate the degeneration of surrounding neurons. The work described in Chapter 6 investigated the ability of inflammatory stimuli to activate the cytoprotective heat shock response (using Hsp70 and Hsp25 as markers). Primary murine mixed glial cultures were treated with lipopolysaccharide and tumour necrosis factor-α to simulate inflammation. Immunoblot analysis showed that inflammatory stimuli did not increase Hsp70 or Hsp25 expression in these cultures. However, heat shock of spinal cord mixed glial cultures showed that these cells were capable of increasing the proportion of Hsp25-positive cells. Therefore,

these glial cells have a competent heat shock response, however these inflammatory stimuli do not induce the heat shock response.

The focus of the work described in Chapter 6 was to assess whether motor neuron degeneration in the spinal cord in patients with amyotrophic lateral sclerosis is a consequence of differences in cortical and spinal cord glia to activate inflammatory and heat shock responses. This research showed that murine spinal cord glia generated a significantly greater concentrations of nitric oxide compared to cortical glia after treatment with inflammatory stimuli. High concentrations of nitric oxide in the spinal cord could play a significant role in increasing the vulnerability of motor neurons to degeneration. Furthermore, spinal cord cultures showed higher proportions of Hsp25-positive astroglia in the absence of treatment and could up-regulate Hsp25 expression after heat shock, compared to cortical astroglia, which did not. It is hypothesised that in the context of amyotrophic lateral sclerosis, where disease onset and progression occur primarily in the spinal cord, the presence of a higher proportion of Hsp25-positive astroglia could provide a cytoprotective buffer at the onset of disease pathology.

Overall, the work presented in this thesis highlights that neuronal vulnerability in neurodegenerative diseases may the consequence of a failure (or impairment) of neurons and glia to induce a heat shock response in the context of protein aggregates (intra- or extracellular) and inflammatory stimuli. Therefore, two major stress-inducing, pathological hallmarks associated with neurodegenerative diseases do not induce a strong cytoprotective heat shock response in neuron-like cells or primary murine glia. This research also showed that differentiated neuron-like cells are capable of inducing a heat shock response after treatment with classical inducers (heat shock and $CdCl_2$). Furthermore, regional differences in inflammatory pathway activation and heat shock protein expression may increase the susceptibility of neurons to degeneration in neurodegenerative diseases Therefore, future

research should investigate how heat shock proteins can safely be pharmacologically or genetically up-regulated in neurons and astroglia to treat neurodegenerative diseases.

Table of contents

List of figures

List of tables

List of publications and presentations

Refereed publications:

1. D. R. Whiten*, **R. San Gil***, L. McAlary, J. J. Yerbury, H. Ecroyd and M. R. Wilson. Rapid flow cytometric measurement of protein inclusions and nuclear trafficking. *Scientific Reports.* 2016; 6: 31138. * - these two authors contributed equally to this work.

2. **R. San Gil**, T. Berg, and H. Ecroyd. Using bicistronic constructs to evaluate the chaperone activities of heat shock proteins in cells. *Scientific Reports*. 2017; 7: 2387.

3. **R. San Gil**, L. Ooi, J. J. Yerbury, and H. Ecroyd. The heat shock response in neurons and astroglia and its role in neurodegenerative diseases. *Molecular Neurodegeneration.* 2017, 12:65.

4. **R. San Gil,** B. Kalmar, J. Yip, H. Ecroyd, and L. Greensmith. Inflammatory and heat shock responses differ between cortical and spinal cord glia: Can this explain motor neuron death in the spinal cord. 2017 (manuscript in preparation).

5. **R. San Gil,** L. Ooi, J. J. Yerbury, and H. Ecroyd. Investigating the effect of neuronal differentiation and protein aggregates on the induction of the heat shock response in neuron-like cells. 2017 (manuscript in preparation).

6. D. Cox, D. R Whiten, J. Brown, M. H Horrocks, **R. San Gil**, C. M Dobson, D. Klenerman, A. M van Oijen, and H. Ecroyd. The small heat shock protein Hsp27 binds alpha-synuclein fibrils preventing elongation and cytotoxicity. Under review at the *Journal of Biological Chemistry*.

Non-refereed publications:

1. D. Cox, **R. San Gil**, A. Rote, H. Ecroyd (2016). "Molecular chaperones: Guardians of the proteome." *Australian Biochemist Showcase on Research,* August edition, 47: 8-10.

Conference presentations:

2017 **3rd Proteostasis and disease symposium, Australia.** Oral presentation: *Can pathogenic protein aggregation induce the heat shock response in neuron-like cells?* Presentation prize.

2017 **ISN-ESN Neurochemistry Meeting, France.** Poster presentation: *Regional differences in nitric oxide synthesis and Hsp27 expression in spinal cord and cortical glia*.

2017 **42nd Lorne Protein Structure and Function Conference, Australia.** Poster presentation: *Regional differences in stress-responses between spinal cord and cortical glia*. Poster Prize.

2016 **10th FENS Forum of Neuroscience 2016, Denmark.** Poster presentation: *A new tool to evaluate the anti-aggregation activities of heat shock proteins in cells*.

2016 **Queens Square Symposium, United Kingdom.** Poster presentation: *A new tool to evaluate the anti-aggregation activities of heat shock proteins in cells*.

2015 **25th Biennial Meeting for the International Society for Neurochemistry, Australia.** Poster presentation: *Re-examining the chaperone efficacy of heat shock proteins using novel bicistronic expression constructs.*

2015 **East Coast Protein Meeting, Australia.** Oral presentation: *A new method to study ancient proteins.* Presentation Prize.

2014 **2nd International Proteostasis and Disease Symposium, Australia.** Poster presentation: *Developing and validating bicistronic vectors for the study of small heat shock protein function in cells.*

List of abbreviations

αB-c	AlphaB-crystallin
ALS	Amyotrophic lateral sclerosis
ANG	Angiogenin
ANOVA	Analysis of variance
ATP	Adenosine triphosphate
C9ORF72	Chromosome 9 open reading frame 72
CCNF	Cyclin F
CD11b	Cluster of differentiation molecule 11B
ChIP	Chromatin immunoprecipitation
CNS	Central nervous system
CoREST	Repressor element-1 silencing transcription factor corepressor 1
Cx	Cortex
DBD	DNA binding domain
DMEM/F12	Dulbecco’s modified eagle medium/Nutrient mixture F12
DNA	Deoxyribonucleic acid
EGFP	Enhanced green fluorescent protein
$EGFP^{inv}$	Enhanced green fluorescent protein Y66L non-fluorescent mutant
FACS	Fluorescence activated cell sorter
fALS	Familial amyotrophic lateral sclerosis
FCS	Foetal calf serum
FloIT	Flow cytometric measurement of inclusions and trafficking
Fluc	Firefly luciferase
FSC	Forward scatter
FUS	Fused in sarcoma
GFAP	Glial fibrillary acidic protein
GLAST	Glutamate aspartate transporter
GLT-1	Glutamate transporter
HD	Huntington's disease
HRP	Horseradish peroxidase

HSE	Heat shock element
HSF1	Heat shock transcription factor 1
HSF1+	Heat shock transcription factor 1 active mutant
Hsps	Heat shock proteins
HSR	Heat shock response
Htt	Huntingtin
ICC	Immunocytochemistry
IHC	Immunohistochemistry
IFNγ	Interferon γ
IκBα	Nuclear factor-κB inhibitor-α
IL-1β	Interleukin-1β
IPOD	Perivacuolar inclusion bodies
iPop	Inclusion population
IRES	Internal ribosomal entry site
JUNQ	Juxtanuclear compartments
KO	Knock-out
LC-MS	Liquid chromatography – Mass spectrometry
LPS	Lipopolysaccaride
LZD	Leucine zipper domain
mCherry	Monomeric cherry fluorescent protein
mRNA	Messenger ribonucleic acid
mSOD1	Mutant superoxide dismutase 1
NDs	Neurodegenerative diseases
NEDD4	Neural precursor cell expressed developmentally down-regulated protein 4
NeuN	Neuronal nuclei
NF-κB	Nuclear factor-κB
niPop	Non-inclusion population
NMDA	N-methyl-D-aspartate
NO	Nitric oxide
OTPN	Optineurin

PCR	Polymerase chain reaction
PolyQ	Polyglutamine
PulSA	Pulse shape analysis
PVDF	Polyvinylidene difluoride
QBP	Polyglutamine binding peptide
qPCR	Quantitative polymerase chain reaction
RD	Regulatory domain
RFU	Relative fluorescence units
RNA	Ribonucleic acid
Sc	Spinal cord
sHsps	Small heat shock proteins
SOD1	Superoxide dismutase 1
SSC	Side scatter
SUMO	Small ubiquitin like modifier
TAD	Transactivation domain
TDP-43	TAR DNA binding protein
Tg	Transgenic
TGFβ	Transforming growth factor-β
tGFP	Turbo green fluorescent protein
TNFα	Tumour necrosis factor-α
TRAF6	TNF receptor associated factor 6
TRiC/CCT	T-complex protein-1 ring complex/chaperonin containing TCP1
UBQLN2	Ubiquilin 2
WT	Wild type

Chapter 1: Introduction

Portions of this chapter have been previously published in the following work:

R. San Gil, L. Ooi, J. J. Yerbury, and H. Ecroyd. The heat shock response in neurons and astroglia and its role in neurodegenerative diseases. *Molecular Neurodegeneration.* 2017, 12:65.

Author contributions: RSG wrote the initial literature review and constructed the figures. All authors contributed to the editing of the manuscript and approved the final manuscript for submission.

1.1 Introduction

Neurodegenerative diseases (NDs), such as amyotrophic lateral sclerosis (ALS) and Huntington's disease (HD), manifest through either a loss of function of the wild type (WT) protein or toxic gain-of-function as a result of the oligomerisation and aggregation of the protein (Chiti and Dobson 2006). The progression of NDs into late stage is thought to be driven by astroglia and microglia, which are activated by damaged neurons and pathogenic aggregates that subsequently propagate a chronic inflammatory response in the central nervous system (CNS) (Meissner et al. 2010, Roberts et al. 2013, Zhao et al. 2015). The neuron-specific degeneration observed in discrete regions of the brain in NDs suggests that specific neuronal sub-types are particularly vulnerable to protein misfolding and aggregation. This may be the result of: (i) an inability of differentiated neurons to activate stress-inducible mechanisms of proteostasis; (ii) a failure of the proteostasis network to detect pathogenic protein aggregates; (iii) regional variations in glial inflammatory and stress-inducible mechanisms of proteostasis or (iv) a combination of these factors (Verbeke et al. 2001, Douglas and Dillin 2010, Brehme et al. 2014).

The heat shock response (HSR) is a key stress-inducible pathway of the proteostasis network. Little is known about how and/or if an HSR is induced in neuronal and glial cells by pathogenic protein aggregation and inflammatory stimuli. Elucidating whether the HSR is triggered by protein aggregation and inflammation, and the mechanism(s) by which this occurs, is important for future work aimed at developing therapeutics to ameliorate ND pathologies. The objectives of this chapter are to summarise what is currently known about the activation of the HSR in different tissues and cell-types during cellular stress and explore evidence regarding the involvement of the HSR in rescuing neurons and astroglia from protein aggregation and inflammation associated with NDs. In doing so, progress in this field of research is evaluated,

gaps in our knowledge are highlighted, and the need for new methodologies to study Hsp activities in the cell and measure protein aggregation are discussed.

1.2 Proteostasis

The maintenance of a stable and functional proteome is achieved by the combined activities of the proteostasis network (Gidalevitz et al. 2011, Wyatt et al. 2013). To maintain proteostasis, cells sense and respond to extrinsic and intrinsic stimuli (*e.g.*, genetic mutations, biosynthetic errors, energetic deficits, protein damage, environmental insults and aging) via several integrated pathways. The eukaryotic proteostasis network comprises pathways that are either non-inducible ("housekeeping") or inducible ("stress-response"); these pathways are activated by the constitutive or stress-inducible expression of ~800 proteins, 332 of which are molecular chaperones (Brehme et al. 2014, Yerbury et al. 2016). Some examples of stress-inducible pathways include the HSR (Richter et al. 2010, Morimoto 2011), unfolded protein response (Walter and Ron 2011, Hetz 2012), antioxidant responses (Morano et al. 2012, Niforou et al. 2014), the ubiquitin-proteasome system (Varshavsky 2012, Inobe and Matouschek 2014), the mitochondrial unfolded protein response (Haynes and Ron 2010) and autophagy (Boya et al. 2013, Mardones et al. 2015). Stress-responses regulate gene transcription, RNA processing and metabolism, and protein synthesis, folding, translocation, assembly, disassembly, and degradation during periods of cellular stress (Morimoto 2008, Gidalevitz et al. 2011). The induction of these stress pathways acts to maintain cell viability; however, if the proteostasis network deteriorates or becomes overwhelmed, for example by physiological or pathological stress, cell viability can be threatened.

Molecular chaperones are a central component of the proteostasis network as they act to facilitate the correct folding of nascent polypeptides, maintain partially-folded protein intermediates in folding-competent states and re-fold damaged proteins (Hartl et al. 2011,

Wyatt et al. 2013, Balchin et al. 2016, Kampinga and Bergink 2016). A recent comprehensive analysis of the human "chaperome" identified 332 chaperones, 142 of which correspond to the heat shock protein subfamilies [Hsp90, Hsp70, Hsp60, Hsp40 and small Hsps (sHsps)] (Brehme et al. 2014). The Hsps are a family of evolutionarily conserved chaperones with diverse functions in proteostasis. In addition to their well-characterised molecular chaperone functions, Hsps also stabilise the cytoskeleton, regulate stress-responses, mitigate apoptotic signalling and shuttle damaged proteins for degradation by the ubiquitin proteasome system or by autophagy to augment the capacity of a cell to recover from stress-induced damage (Leak 2014, Treweek et al. 2015).

1.3 The HSR

The activation of the HSR is a primary defence mechanism that protects cells from stress conditions that promote protein misfolding, aggregation and cell death. Many insults have a common effect of damaging proteins and inducing the accumulation of partially-folded protein intermediates, which in turn can activate transcription factors and induce the heat shock response. The human genome encodes four heat shock transcription factors (HSF), HSF1 – HSF4, which have unique as well as overlapping functions (Åkerfelt et al. 2010). For example, HSF1 is the prime integrator of transcriptional responses during stress; HSF2 can form hetero-oligomers with HSF1 and modulate stress-responses but is also involved in corticogeneis (Wu 1995); HSF3 may be involved in heat shock responses; HSF4 regulates lens and olfactory epithelium development (Åkerfelt et al. 2010). The role of HSF1 in the activation and attenuation of the heat shock response in cells under conditions of cellular stress is examined in this chapter.

1.3.1 Heat shock transcription factor 1

Heat shock transcription factor 1 is constitutively expressed in most tissues and cell types and, apart from its role in the HSR, is involved in a wide range of processes including organismal development, insulin signaling and cancer metastasis [for recent comprehensive reviews see (Anckar and Sistonen 2011, Vihervaara and Sistonen 2014)]. Human HSF1 is characterised by an N-terminal "winged" helix-turn-helix DNA-binding domain (Figure 1.1) adjacent to 3 leucine zipper domains that mediate oligomerisation (Vihervaara and Sistonen 2014). The HSF1 central regulatory domain undergoes extensive post-translational modifications that act upon the C-terminal *trans*-activation domain to regulate the magnitude of HSF1 *trans*-activity (Vihervaara and Sistonen 2014). In addition, a fourth leucine zipper domain in the C-terminus has been implicated in the formation of inhibitory intermolecular contacts with leucine zipper domains 1-3, to allosterically prevent HSF1 activation in the absence of stress (Rabindran et al. 1993).

Post-translational modifications are critical in modulating the activity of HSF1 (Xu et al. 2012); it can be acetylated, SUMOylated and extensively phosphorylated (Velichko et al. 2013) (Figure 1.1). The type and site of each post-translational modification have been predominantly identified by proteomic mass spectrometry and site-directed mutagenesis experiments (Anckar and Sistonen 2011, Xu et al. 2012, Zheng et al. 2016). Whilst the activation of HSF1 is complex and only partially understood, previous studies highlight the importance of post-translational modifications in stabilising, activating and inhibiting the transcriptional activity of HSF1 (Zheng et al. 2016). For example, conversion of HSF1 into a transcriptionally active trimer occurs concurrently with extensive post-translational modifications including stress-inducible hyperphosphorylation of S230, S326 and T142 (Holmberg et al. 2001, Soncin et al. 2003, Guettouche et al. 2005), such that hyperphosphorylated HSF1 is used as a marker of HSF1 activation (Mathur et al. 1994, Yang et al. 2008, Chafekar and Duennwald 2012, Raychaudhuri

et al. 2014). Aside from (extensive) phosphorylation, acetylation and SUMOylation of HSF1 also play important roles in regulating the strength and duration of the HSR.

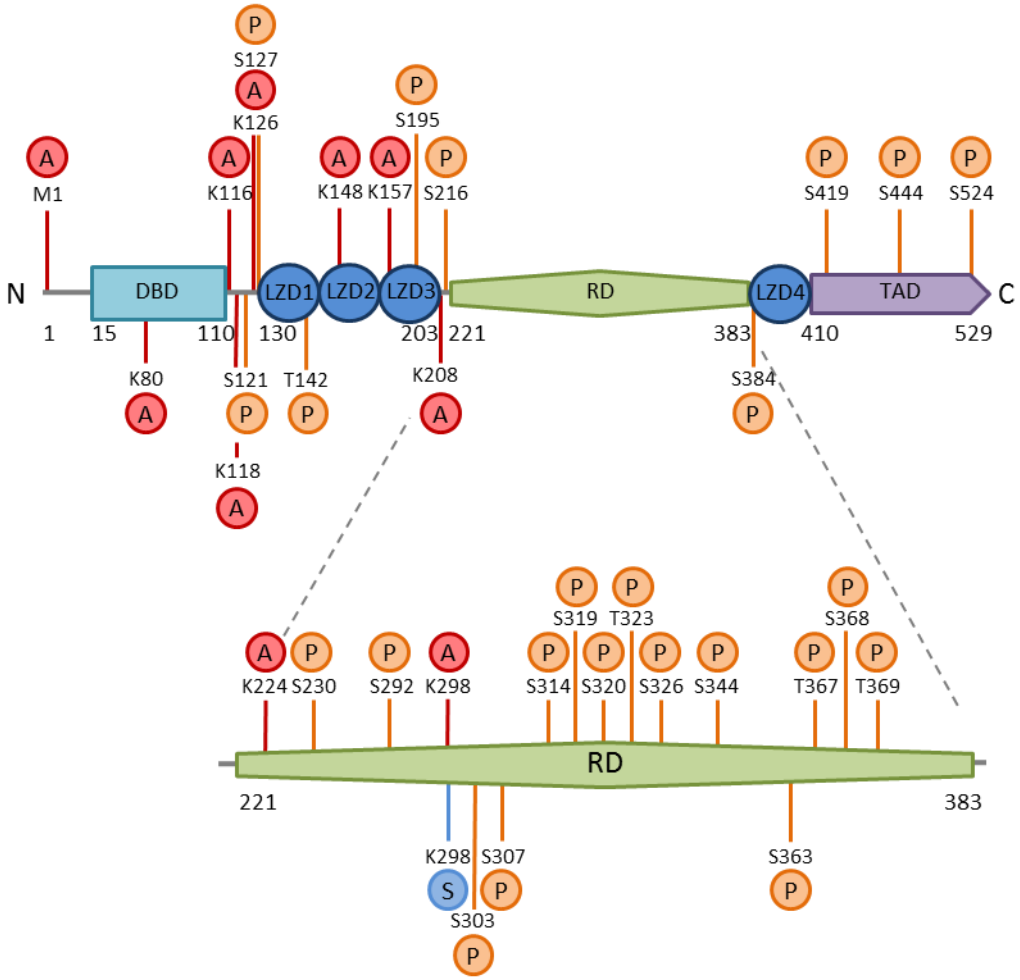

Figure 1.1. Post-translational modifications of HSF1 in relation to the functional domains in the protein. The HSF1 protein consists of a DNA-binding domain (DBD), four leucine zipper domains (LZD), a regulatory domain (RD) and a transactivating domain (TAD). The proposed sites of serine/threonine phosphorylation (P), lysine acetylation (A) and phosphorylation-dependent lysine SUMOylation (S) are marked on the HSF1 amino acid chain. These post-translational modifications are mediated by numerous kinases, acetylases and SUMOylases and act to modulate the stabilisation and activity of HSF1 and thus the strength and duration of the HSR. Figure adapted from (Anckar and Sistonen 2011).

1.3.2 HSF1 activation and DNA-binding

Under conditions of cellular stress, HSF1 monomers form activated homo-trimers and translocate into the nucleus. Trimerisation is mediated through the formation of leucine zippers on adjacent HSF1 oligomerisation domains (Figure 1.2) (Rabindran et al. 1993, Sandqvist et

al. 2009). Activated HSF1 trimers bind to *cis*-regulatory elements on DNA composed of nGAAn pentamers (where n is any base), collectively called heat shock elements (HSEs) (Pelham 1982, Amin et al. 1988, Sorger and Pelham 1988, Xiao and Lis 1988). Each DNA-binding domain of a HSF1 trimer recognises a single HSE. Thus, three alternately oriented HSE pentamers are required for stable binding of a HSF1 trimer in the major groove of the DNA helix (Amin et al. 1988, Littlefield and Nelson 1999, Vihervaara and Sistonen 2014). Recent co-crystal structures of recombinant human HSF1 with DNA showed that the DNA-binding domains of trimeric HSF1 bridge across both strands of DNA, which contains three alternately oriented HSEs (Neudegger et al. 2016). The extent and duration of HSF1-mediated transcription is influenced by the number of HSEs, the exact sequence of nGAAn pentamers in the promoter regions of HSF1 target genes, and post-translational modifications on HSF1 itself (Vihervaara and Sistonen 2014). Transcription of HSF1 target genes is initiated by HSF1-mediated release of the RNA polymerase II elongation complex from a paused to an active state (Figure 1.2). In addition to the rapid upregulation of Hsp expression in response to cellular stress, HSF1 also coordinates the expression of many transcriptional and translational regulators, co-chaperones, ubiquitin, signaling molecules and mitotic regulators (Trinklein et al. 2004a, Trinklein et al. 2004b, Vihervaara and Sistonen 2014).

1.3.3 Negative regulation of HSF1 transcriptional activity

Heat shock factor 1-mediated transcription is attenuated by an auto-regulatory mechanism, whereby HSF1-induced Hsps competitively inhibit HSF1 trimer activity (Anckar and Sistonen 2011, Zheng et al. 2016). The trimerisation of HSF1 is suppressed by interaction of the monomer with a multi-chaperone complex composed of Hsp90, co-chaperone p23 and immunophilin FK506-binding protein 5 (Bharadwaj et al. 1999, Guo et al. 2001). In addition, the chaperonin TRiC/CCT can also interact with HSF1 to inhibit its activation (Neef et al. 2014). Active HSF1 trimers in the nucleus can be inhibited by the binding of Hsp70 and its co-

chaperone Hsp40, possibly through recruitment of the Hsp70-interacting transcriptional co-repressor, CoREST (Shi et al. 1998, Gómez et al. 2008). When the cell is subjected to stress, these HSF1/chaperone complexes, which had formed to attenuate the HSR, dissociate as a result of competition for chaperone binding between damaged misfolded proteins and HSF1 (Zuo et al. 1994, Zuo et al. 1995). This negative feedback loop provides an important mechanism by which cells can regulate the activation and attenuation of an HSR via the presence and concentration of Hsps in the cell. To summarise, the activation of HSF1 and its binding to DNA is regulated by a multi-step pathway that involves nuclear accumulation, intramolecular and intermolecular protein interactions, and post-translational modifications (Figure 1.1 and Figure 1.2) (Velichko et al. 2013, Vihervaara and Sistonen 2014, Zheng et al. 2016).

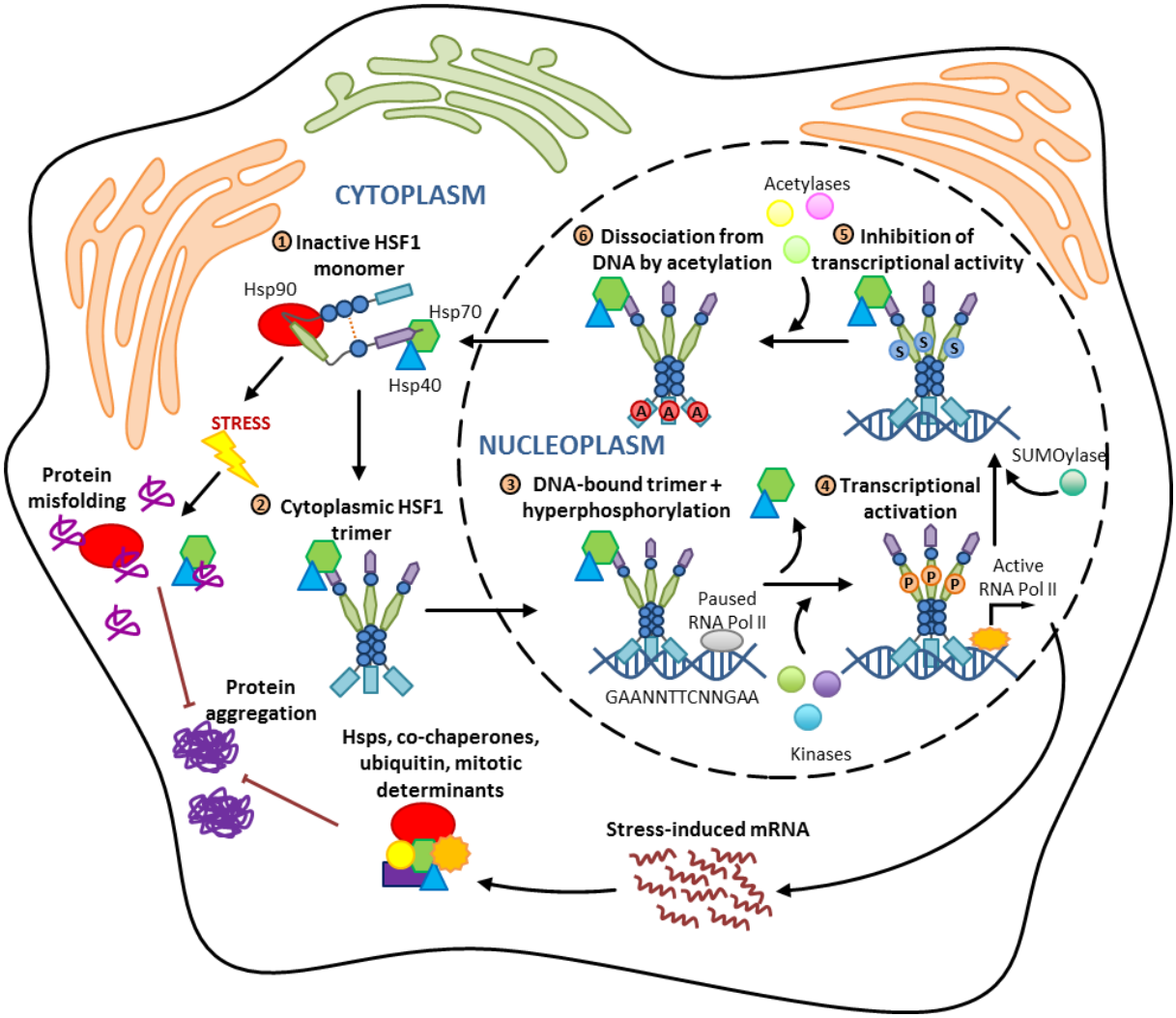

Figure 1.2. The cycle of activation and attenuation of the HSR. (1) In the absence of stress, HSF1 is maintained in a monomeric state through the regulatory actions of several post-translational modifications, intramolecular contacts, and interactions with Hsps in inhibitory complexes. Cellular stress results in the accumulation of misfolded and damaged proteins, which compete with HSF1 for binding to Hsps. (2) HSF1 monomers are released and undergo a conformational change conducive to trimerisation. (3) Concurrent nuclear accumulation, HSE-binding and hyperphosphorylation of trimeric HSF1 occur. (4) This process releases RNA Pol II from a paused to an active state to initiate the transcription of stress-induced genes. (5) SUMOylation at K298 and binding of Hsp40/Hsp70 represses the transcriptional activity of HSF1 trimers. (6) Acetylation at K80 disrupts HSF1 bound to DNA and HSF1 trimers dissociate and re-join the monomeric pool in the cytosol. Stress-inducible Hsps participate in a negative-feedback loop to inhibit further HSF1 activation.

1.4 The HSR in the mammalian CNS

In mammals, the HSR varies both in terms of kinetics (*i.e.* how fast stress-induced transcripts are generated) and magnitude (*i.e.* the fold increase in Hsp levels) between tissues and even between cells in the same tissue (Blake et al. 1990, Nishimura et al. 1991, Sala et al. 2017). Analysis of the human "chaperome" shows that the constitutive expression of housekeeping

chaperones and co-chaperones varies between tissues (Sala et al. 2017). For example, sHsps are overrepresented in skeletal and cardiac muscle compared with the brain (Sala et al. 2017). With regard to stress-inducible mechanisms of proteostasis, whole organism hyperthermia results in an HSR that varies substantially across tissues types (Blake et al. 1990). For example, the kinetics of the response and magnitude of induction were found to vary between the brain, liver and skin when assessed over time by northern blot of Hsp70 and Hsp27 stress-induced mRNA (Blake et al. 1990). Moreover, cells in the same tissue can display different capacities to induce the HSR. For example, cultured astroglia elicit faster and higher levels of Hsp70 expression after heat shock (45°C for 30 min) compared with cultured cortical neurons (Nishimura et al. 1991). These studies strongly suggest that the capacity of a cell to sense stress and elicit an HSR differs in a cell-type dependent manner.

An attenuated HSR may be an intrinsic characteristic of neurons (Manzerra and Brown 1992, Manzerra et al. 1997, Batulan et al. 2003, Pavlik and Aneja 2007, Oza et al. 2008, Yang et al. 2008). Indeed, this hypothesis is supported by several animal studies that have challenged rodents with hyperthermia or ischaemic injury and shown that neurons (*i.e.* cortical neurons, spinal cord motor neurons, differentiated neuroblastoma cell lines) do not induce Hsp70 expression after exposure to these heat stress, whereas astroglial cells do (Nishimura et al. 1991, Manzerra and Brown 1992, Nishimura and Dwyer 1996, Manzerra et al. 1997, Krueger et al. 1999, Pavlik and Aneja 2007, Oza et al. 2008, Yang et al. 2008). For example, spinal cord motor neurons that were studied *in situ* in rabbits and rats failed to transcribe Hsp70 mRNA and, thus Hsp70 protein following acute heat shock (Manzerra and Brown 1992, Brown and Rush 1999). These seminal studies show that under conditions of acute cellular stress, neurons are inherently poor activators of the HSR, whereas astroglia readily activate the HSR. This prompts the question of whether neurons and astroglia respond to chronic ND-relevant stressors (such as protein aggregation or inflammation) and, if so, whether there is a difference

in the response of neuronal and astroglial cells to this stress. In an attempt to address this question, a portion of this chapter investigates what is known about HSR activation in the context of two NDs, HD and ALS.

1.5 Huntington's disease

Huntington's disease is characterised by the formation of intracellular inclusions composed primarily of the ubiquitous protein huntingtin (Htt) and by the subsequent death of striatal medium spiny neurons and cortical pyramidal neurons (Vonsattel and DiFiglia 1998, Han et al. 2010). The genetic basis for the pathogenesis of HD is a CAG codon repeat expansion in the Huntingtin (*HTT*) gene that leads to a mutant protein that contains an expanded poly-glutamine (polyQ) sequence (MacDonald et al. 1993). Expansions of the polyQ tract beyond 36 glutamines result in an aggregation-prone Htt protein; the length of the polyQ expansion correlates with age of disease onset and severity (*i.e.* the longer the polyQ tract, the earlier the onset of disease and the more rapid the disease progression) (Zoghbi and Orr 2000). Well-characterised cell and transgenic mouse models of HD have been used in investigations into the impact of the HSR on the pathogenicity of polyQ expansions.

PolyQ-expanded Htt may interact differently with the proteostasis network compared with other disease-associated proteins. Evidence for this comes from studies that have shown that polyQ-expanded Htt^{103Q} (*i.e.* Htt with a polyQ stretch of 103 glutamines) partitions exclusively into perivacuolar inclusion bodies (IPODs: Insoluble PrOtein Deposits) that store terminally aggregated proteins (Kaganovich et al. 2008). Fluorescence recovery after photobleaching experiments showed that Htt^{103Q} proteins sequestered into IPODs are immobile (Kayatekin et al. 2014) indicating that sequestration into IPODs prevents possible interactions of the aggregated protein with components of the proteostasis network, exacerbating the formation of inclusions in cells (Kaganovich et al. 2008, Polling et al. 2014). Recent evidence also

suggests that Htt inclusion body formation deactivates apoptosis and results in slow necrotic cell death (Ramdzan et al. 2017). Partitioning of Htt into IPODs contrasts with quality control of other aggregation-prone disease-associated proteins, such as SOD1, which have been shown to accumulate in juxtanuclear compartments in yeast and immortalised cell lines (JUNQ: JUxtaNuclear Quality control) for presentation to molecular chaperones for re-folding and/or the ubiquitin proteasome system for degradation (Matsumoto et al. 2006, Kaganovich et al. 2008, Polling et al. 2014, Farrawell et al. 2015). Therefore, findings pertaining to the HSR in the context of HD may uniquely apply to this ND due to the propensity of polyQ-expanded Htt to misfold directly into terminal aggregates and become stored in IPODs (as opposed to the JUNQ).

1.5.1 The HSR in striatal neurons

The expression and cellular accumulation of pathogenic polyQ-expanded Htt is not associated with an induction of an HSR in cell and animal models of HD. The expression of Htt^{91Q} does not induce an HSR (as assessed by an Hsp70 promoter driven EGFP expression construct) (Bersuker et al. 2013). Notably, the expression of Htt^{111Q} in striatal cells was not sufficient to up-regulate Hsp expression, nor activate HSF1 (Chafekar and Duennwald 2012). Likewise, primary cultures of rat cortical and striatal neurons expressing Htt^{111Q} showed low levels of Hsp70 mRNA transcripts and protein compared to cerebellar granule cells, which have high levels of Hsp70 and are resistant to degeneration (Tagawa et al. 2007). Studies using transgenic mouse models of HD have demonstrated that there is a reduction in Hsp70 (and other molecular chaperones) in the brain as the disease progresses (Table 1-1) (Hay et al. 2004). Taken together, these results suggest that cells expressing polyQ-expanded Htt do not sense or respond to this aggregation-prone protein by inducing an HSR.

The expression of polyQ-expanded Htt sensitises neurons to degenerate after heat stress (Chafekar and Duennwald 2012, Riva et al. 2012). Heat shock (42°C for 6 h) of primary murine striatal neurons expressing pathogenic Htt^{111Q} resulted in a 6-fold increase in caspase activity compared to heat shocked cells expressing non-pathogenic Htt^{7Q} (Chafekar and Duennwald 2012). Furthermore, cells expressing Htt^{111Q} had a reduced capacity to express Hsp70, Hsp25 (the mouse orthologue of Hsp27) and Hsp90 after heat shock compared to those expressing Htt^{7Q} (Chafekar and Duennwald 2012). These findings suggest that expression of polyQ-expanded Htt impairs the capacity of striatal neurons to up-regulate the expression of Hsps after heat shock, which is normally a very strong activator of the HSR.

Based on these findings it is pertinent to question whether the observed inability of striatal neurons to induce a HSR in the context of polyQ Htt is the result of insufficient levels of HSF1, a failure to activate HSF1, a lack of HSF1 binding to DNA, or a combination of these deficiencies (Figure 1.3). Quantification of total HSF1 protein by immunoblot demonstrated that primary striatal neurons expressing Htt^{111Q}, and the striata and cerebella of HD mouse models more generally, have lower total HSF1 levels compared to controls (Chafekar and Duennwald 2012). New evidence implicates CK2α' kinase and Fbxw7 Fbox protein (an E3 ubiquitin ligase) in the enhanced degradation of HSF1 in cells expressing polyQ expanded Htt (Gomez-Pastor et al. 2017). The proposed model suggests that polyQ-expanded Htt up-regulates CK2α′ kinase expression and increases the phosphorylation of HSF1 at S303 and S307. This in turn recruits Fbxw7, which ubiquitinates phospho-HSF1 targeting it for degradation by the ubiquitin proteasome system (Gomez-Pastor et al. 2017). Enhanced degradation of HSF1 by the proteasome has also been implicated in a mouse model and human post-mortem tissues of α-synucleinopathies, whereby elevated levels of the ubiquitin ligase, NEDD4, ubiquitinates HSF1 for degradation (Kim et al. 2016). Whilst expression of Htt^{111Q} is not sufficient to induce HSF1 activation in cerebellar granule cells, heat shock does result in

activated (hyperphosphorylated) HSF1 trimers accumulating in the cell nucleus (Tagawa et al. 2007, Chafekar and Duennwald 2012). Similarly, HSF1 dissociation from Hsp90, hyperphosphorylation, and nuclear translocation are not impaired in HD mice upon treatment with Hsp90 inhibitor, NVP-HSP990, which is able to penetrate the brain (Tagawa et al. 2007). Therefore, there is a reduction in total HSF1 levels in the striatum however, HSF1 is able to become hyperphosphorylated and translocate into the nucleus in HD models.

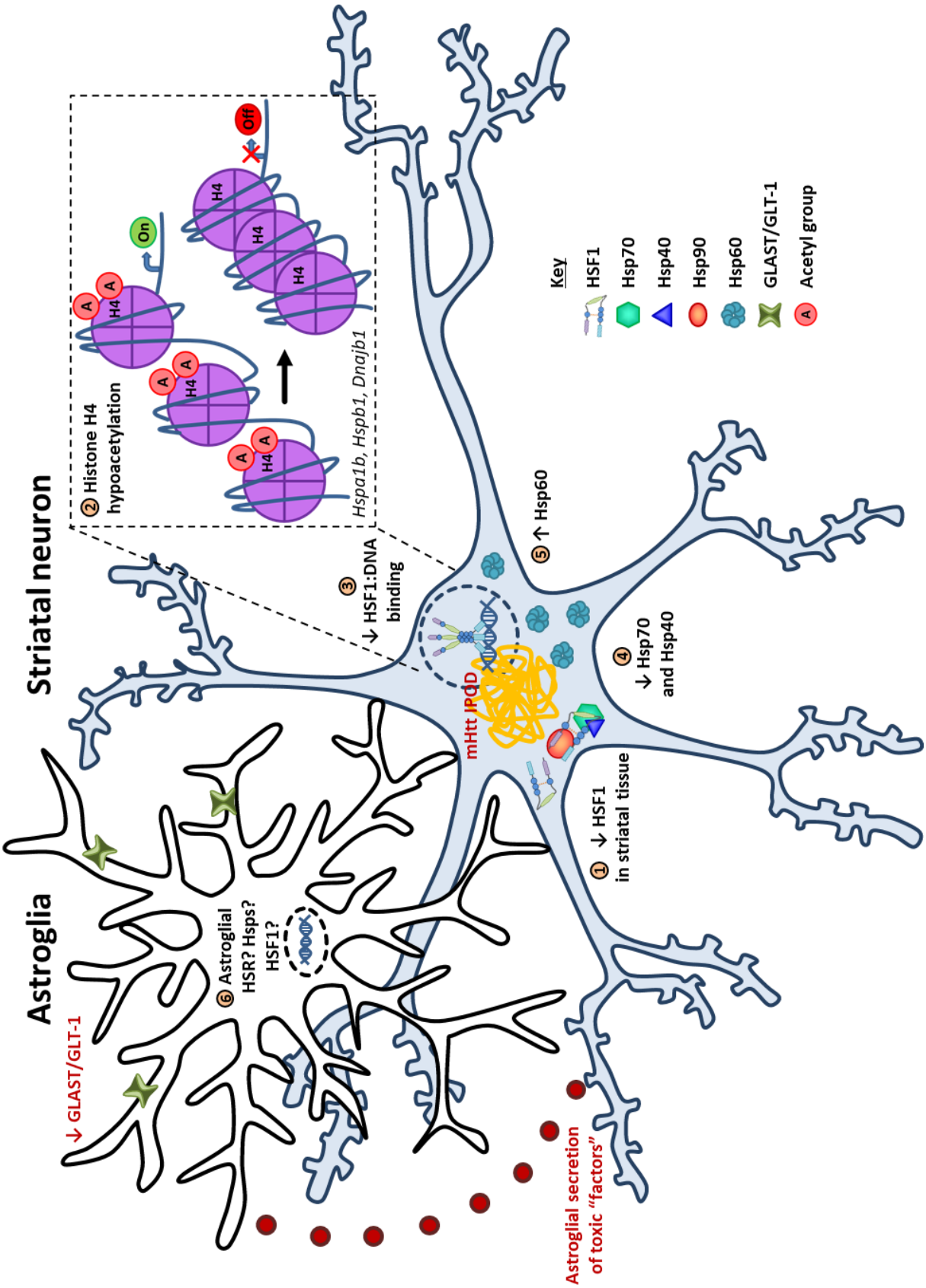
Striatal neuron
Astroglia
Key
HSF1
Hsp70
Hsp40
Hsp90
Hsp60
GLAST/GLT-1
Acetyl group
① ↓ HSF1 in striatal tissue
② Histone H4 hypoacetylation
On
Off
③ ↓ HSF1:DNA binding
Hspa1b, Hspb1, Dnajb1
④ ↓ Hsp70 and Hsp40
⑤ ↑ Hsp60
mHtt /polyQ
⑥ Astroglial HSR? Hsps? HSF1?
↓ GLAST/GLT-1
Astroglial secretion of toxic "factors"

Figure 1.3. Proposed summary of changes in the HSR and its components in polyQ-expanded Htt over-expression models of HD. Huntington's disease onset and progression into late stage is dependent on the molecular pathologies developed in striatal neurons (*e.g.* formation of polyQ-expanded Htt aggregates or IPODs) and astroglia (*e.g.* decline in GLAST/GLT-1 expression and the secretion of unidentified toxic "factors"). The susceptibility of striatal neurons to degeneration from HD-associated stresses could be the result of a polyQ-expanded Htt-mediated attenuation of the HSR. Over-expression of polyQ-expanded Htt in CNS tissues results in a (1) reduction in HSF1 levels. (2) Histone H4 acetylation has been shown to be a strong promoter of HSF1 binding of target genes. However, hypoacetylation of histone H4 at HSF1 targets (*e.g. Hspa1b*, *Hspb1*, and *Dnajb1*) with disease progression can explain (3) the decrease in HSF1 binding to DNA observed in polyQ-expanded Htt expressing striatal neurons. (4) HD disease progression is also associated with a decline in Hsp70 and Hsp40 family members and (5) a striatal-specific increase in Hsp60. (6) There have been few investigations regarding HSF1 activation and DNA-binding in astroglia. Therefore, the capacity of polyQ-expanded Htt over-expressing astroglia to activate HSF1 and induce an HSR is currently unknown.

With regard to the DNA binding capacity of HSF1 in HD models, evidence suggests that the expression of polyQ expanded Htt attenuates HSF1 binding to DNA in striatal cells (Riva et al. 2012). Genome-wide chromatin immunoprecipitation (ChIP) experiments demonstrated that in primary striatal neurons expressing Htt^{111Q} HSF1 is only capable of binding 39% of its target genes after heat shock (1,159 bound genes) compared to cells expressing Htt^{7Q} (2,943 bound genes) (Riva et al. 2012). Microarray data show that the reduced binding of HSF1 to DNA in heat shocked cells expressing Htt^{111Q} corresponds with a decline in the transcription of several Hsps (*Dnajb5*, *Dnajb12* and *Hspb6*). Furthermore, mRNA levels of Hsp70, Hsp40 and Hsp25 were reduced in the cerebral cortices of HD mouse models compared to controls following treatment with NVP-HSP990 (Labbadia et al. 2011). Therefore, since HSF1 activation appears to be unimpaired, low levels of HSF1 and a compromised ability to bind DNA could account for the observed inability of cells expressing polyQ-expanded Htt to elicit an HSR. This dysregulation of chaperone gene expression likely plays a key role in the pathology of HD.

Altered chromatin architecture in HD may explain the reduced capacity of HSF1 to bind to target genes in striatal neurons under stress (Zuccato et al. 2007, Guertin and Lis 2010, Jackrel and Shorter 2011, Labbadia et al. 2011). Quantitative PCR coupled with ChIP analysis after NVP-HSP990 treatment demonstrated significant hypoacetylation of histone H4 at *Hspa1b*,

Hspb1, *Dnajb1* genes in Htt^{111Q} expressing primary striatal neurons compared to those expressing Htt^{7Q} (Labbadia et al. 2011). Hypoacetylation of these Hsp genes may change the chromatin landscape sufficiently to interfere with HSF1 binding to DNA (Figure 1.3). Stress-inducible binding of HSF1 to DNA is associated with histone acetylation, H3K4 trimethylation, RNA polymerase II and other co-activators (Guertin and Lis 2010). Furthermore, tetra-acetyl histone H4 has previously been suggested to be a strong modulator of HSF1 binding to DNA (Guertin and Lis 2010). Therefore, it follows that histone H4 hypoacetylation in HD models may reduce chromatin accessibility of HSF1 at heat shock genes, consequently impairing the HSR (Figure 1.3).

At the tissue level, there are several studies that have investigated Hsp expression, and therefore HSR activation, in affected and non-affected tissues in mouse models of HD (Table 1-1). Immunoblot analysis of whole brain or spinal cord homogenates from HD mice have shown that overall there is no change in the total protein levels of the sHsps, Hsp25 or αB-crystallin, (αB-c) or Hsp90 family members compared to mice expressing non-pathogenic Htt (Hay et al. 2004, Wang et al. 2008). Whole tissue homogenates from HD mice showed a reduction in HSF1, Hsp70, and two Hsp40 family members (Hdj1 and Hdj2; Figure 1.3) (Hay et al. 2004, Chafekar and Duennwald 2012). Conversely, striatal homogenates from HD mice were found to have a 4-fold increase in Hsp60 levels compared to control mice (Liu et al. 2007). A lack of immunohistochemistry in these studies makes it impossible to determine (i) where changes occur at the cellular level and (ii), whether small cell populations or specific cell-types induce an HSR, which is undetectable in bulk cell analyses. Employing immunohistochemistry in parallel to this work, or more powerful omics-based single-cell analyses, such as the proteomics approach undertaken by Sharma et al. (2015) (Sharma et al. 2015a), has the potential to resolve cell-type and brain-region specific differences in the presence or absence of disease. In this way, cell-type specific differences in the ability to induce a pro-survival HSR will be identified.

Table 1-1. List of Hsps and whether their expression is up-regulated (↑), down-regulated (↓), or not changed (No Δ) across rodent models of HD compared to transgenic WT or non-transgenic mouse controls. These results are from immunoblot (IB), or liquid chromatography coupled with quantitative mass spectrometry (LC-MS) of affected CNS regions.

Hsps	Transgenic disease models	Tissue or cell type	Reference
HSF1	STHdh(Q111) knock-in mice	IB: 80% ↓striatal and cerebellar tissue homogenates	(Chafekar and Duennwald 2012, Gomez-Pastor et al. 2017)
αB-c	R6/2	IB: No Δ whole brain homogenates	(Hay et al. 2004)
	Htt-N171-82Q	IB: No Δ spinal cord homogenates	(Wang et al. 2008)
Hsp25	R6/2	IB: No Δ whole brain homogenates	(Hay et al. 2004)
	Htt-N171-82Q	IB: No Δ spinal cord homogenates	(Wang et al. 2008)
Hsp40	R6/2	IB: 60% ↓Hdj1 whole brain homogenates IB: 25% ↓Hdj2 whole brain homogenates	(Hay et al. 2004)
Hsp60	R6/2	LC-MS: 4-fold ↓ in protein abundance in the cortex LC-MS: 4-fold ↑ in protein abundance in the striatum	(Liu et al. 2007)
Hsp70	STHdh(Q111) knock-in mice	IB: 80% ↓striatal and cerebellar tissue homogenates	(Chafekar and Duennwald 2012)
	R6/2	IB: ↓ whole brain homogenates IB: No Δ Hsc70 whole brain homogenates	(Hay et al. 2004)
Hsp90	R6/2	IB: No Δ Hsp90 whole brain homogenates IB: No Δ Hsp84 whole brain homogenates	(Hay et al. 2004)
Hsp105	-	-	-

1.5.2 The role of glial cells in HD

There is evidence that the onset and progression of HD requires both cell-autonomous and non-cell autonomous processes. One study showed that a transgenic mouse with pan-neuronal expression of Htt^{103Q} developed pathologies associated with end-stage disease, including astrogliosis, motor deficits and neurodegeneration (Gu et al. 2005, Gu et al. 2007). However, when Htt^{103Q} expression was restricted to either striatal neurons or cortical pyramidal neurons, pathologies associated with end-stage disease did not develop despite these cells having nuclear polyQ-expanded Htt aggregates and alterations in NMDA receptor function (Gu et al. 2005,

Gu et al. 2007). These studies showed, for the first time, that HD pathogenesis and propagation depends on interactions between neurons. Neuron-astroglia interactions have also been implicated in the non-cell autonomous progression of HD. A study that investigated transgenic mice that expressed Htt^{98Q} in both neurons and astroglia observed that these mice displayed more severe neurological symptoms and earlier death compared to mice in which Htt^{98Q} expression was restricted to either neurons or astroglia alone (Bradford et al. 2010). Therefore, it seems likely that both neuron-neuron and neuron-astroglia interactions are responsible for the onset and progression of HD.

The combination of molecular pathologies that develop in neurons and astroglia work in tandem to progress HD (Figure 1.3). However, the mechanisms that underlie astroglial-mediated toxicity in HD are only partially understood. Astroglia expressing polyQ-expanded Htt secrete neurotoxic factors and decrease the expression of the glutamate transporters, GLAST and GLT-1 (Bradford et al. 2009, Faideau et al. 2010, Liddelow et al. 2017). Indeed, polyQ-expanded Htt-expressing astroglia have been shown to increase the vulnerability of striatal and cortical neurons in co-culture to excitotoxic stresses (Shin et al. 2005). Conversely, in co-culture experiments, astroglia expressing non-pathogenic Htt^{23Q} protected 78% of the Htt^{130Q}-expressing cortical neurons from glutamate toxicity (Shin et al. 2005). Furthermore, conditioned medium derived from WT astroglial cultures protects Htt^{111Q}-expressing striatal neuronal progenitor cells from neurotoxic insults (*e.g.* H_2O_2, glutamate, 3-nitropropionic acid) (Ruiz et al. 2012).

With respect to neurotoxic factors secreted by astroglia, an elegant study by Liddelow et al. (2017), demonstrated that reactive microglia (*i.e.* pro-inflammatory microglia) can activate a neurotoxic phenotype in astroglia (defined in the work as A1 astroglia). They showed that A1 astroglia formation is a pathological response of the CNS in mice treated with systemic injections of lipopolysaccharide (LPS) and acute CNS injury, and in patients with NDs

(Liddelow et al. 2017). The proportion of neurotoxic (A1) astroglia in the caudate nucleus of HD patients was significantly greater that in controls (60% in HD tissue compared to 25% in the control) (Liddelow et al. 2017). Furthermore, qPCR of A1 astroglia-associated transcripts showed a 60-fold increase in the caudate nucleus of HD patients compared to controls (Liddelow et al. 2017). Thus, cell-cell interactions and dysfunctions of striatal or cortical pyramidal neurons and astroglia are likely to work synergistically to progress HD into late-stages. Therefore, maintaining striatal astroglia in a healthy and neurotrophic condition may be a novel approach to minimise neurodegeneration in the striatum.

1.5.3 The HSR in striatal astroglia

Studies investigating HSR-inducing compounds have provided valuable insights into the capacity of different cell populations to induce an HSR in the absence of the expression of polyQ-expanded Htt. Primary striatal astroglia derived from WT mice showed a stronger induction of HSR compared to striatal projection neurons after treatment with the Hsp90 inhibitor, NVP-HSP990. Treated striatal astroglia showed an 18-fold increase in Hsp70 and 4-fold increase in Hsp25 mRNA levels (Carnemolla et al. 2015). In contrast, NVP-HSP990 treated striatal projection neurons only showed an 8-fold increase in Hsp70, 3-fold increase in Hsp40, and no change in Hsp25 mRNA levels (Carnemolla et al. 2015). In the vehicle treated mice, there were no significant differences in the synthesis of any of the Hsp mRNAs investigated (Hsp70, Hsp40, Hsp90 or HSF1), with the exception of Hsp25, which showed a 7-fold increase in astroglia compared to striatal projection neurons (Carnemolla et al. 2015). Together these findings suggest that, in the absence of polyQ-expanded Htt expression, striatal astroglia are “pre-loaded” with greater levels of Hsp25 mRNA and are capable of inducing a stronger HSR compared to striatal projection neurons.

Determining the mechanisms that maintain astroglia in a healthy and neurotrophic state should be a priority in future HD research, given that polyQ-expanded Htt expression decreases the levels of glutamate transporters and induces a neurotoxic phenotype of astroglia. Indeed, a recent study demonstrated that the over-expression of the sHsp, αB-c, in astroglia ameliorates the pathologies associated with HD in transgenic mice that express full-length Htt^{97Q} (Oliveira et al. 2016). Over-expression of αB-c in astroglia significantly reduced the number of large (>1 μm) Htt^{97Q} inclusions in the striatum and cortex, and resulted in a 12.5% increase in the number of NeuN-positive neurons in the striatum (Oliveira et al. 2016). This provides an elegant example of how increasing Hsps in astroglia can ameliorate HD neuropathologies in a non-cell autonomous manner and provides support for increased investigation into the HSR in astroglia in the context of HD.

1.5.4 Summary of the HSR in HD

It has been demonstrated, using a range of cell and animal models of HD, that striatal neurons do not sense or respond to polyQ-expanded Htt expression by up-regulating Hsps. Moreover, striatal neurons expressing polyQ-expanded Htt have an attenuated capacity to induce an HSR after heat shock. This could be due to decreased levels of HSF1 in striatal tissue observed in HD models. In addition, the altered chromatin landscape caused by histone H4 hypoacetylation at Hsp genes observed in a HD mouse model, may also lead to decreased binding of HSF1 to DNA, and down-regulation of Hsp70 and Hsp40. In the absence of polyQ-expanded Htt expression, striatal astroglia, compared to striatal projection neurons, have greater levels of Hsp25 mRNA and are capable of inducing a stronger HSR. However, the effect of polyQ-expanded Htt on HSR induction in astroglia remains to be elucidated.

Previous research has demonstrated that a variety of Hsps can inhibit polyQ-expanded Htt protein aggregation. However, the affected neurons in HD appear not to sense the initial stages

of pathogenic protein misfolding as a cellular stress and therefore do not activate an HSR. As the neurons and surrounding astroglia in the CNS appear to be incapable of activating an HSR in the context of HD, therapeutics that can induce Hsp expression in early stages of disease may prove beneficial.

1.6 Amyotrophic lateral sclerosis

Amyotrophic lateral sclerosis is characterised by a loss of motor neurons in the primary motor cortex, corticospinal tracts, brainstem and spinal cord. Only 5-10% of ALS cases are familial (fALS) and some of these arise from mutations in one of 13 (or more) genes leading to the expression of aberrant aggregation-prone proteins. Mutations in *SOD1* (copper/zinc ion-binding superoxide dismutase), *C9ORF72* (chromosome 9 open reading frame 72), *FUS* (fused in sarcoma), *TDP-43* (TAR DNA binding protein), *CCNF* (cyclin F) (Williams et al. 2016), *OPTN* (optineurin), *ANG* (angiogenin, ribonuclease, RNase A family, 5), *UBQLN2* (ubiquitin-like ubiquilin2), and others are all associated with fALS [recently reviewed by (Chen et al. 2013, Iguchi et al. 2013)]. The remaining 90-95% of ALS cases are idiopathic and sporadic.

In ALS, motor neurons are preferentially susceptible to degeneration despite the ubiquitous expression of disease-associated mutant proteins in neuronal and non-neuronal cells (Asea and Brown 2008). Motor neurons have functional and morphological characteristics that may make them particularly vulnerable to toxic protein misfolding and aggregation, neuroinflammation, and subsequent degeneration in ALS (Asea and Brown 2008). For example, motor neurons have a high metabolic load, high energy demands, long axons, rely on rapid signaling of neurotransmitters to other neurons and muscle tissue, and are long-lived due to their terminal differentiation. Malfunction of each of these characteristics of motor neurons has been associated with ALS pathology (for reviews see (Bruijn et al. 2004, Boillée et al. 2006a, Rothstein 2009)).

Recent findings have shown that multiple housekeeping and stress-response pathways involved in maintaining proteostasis (*e.g.* the ubiquitin proteasome system and endoplasmic reticulum unfolded protein response) are dysregulated in ALS-affected motor neurons, which would further exacerbate their degeneration (Kabashi et al. 2004, Asea and Brown 2008, Kabashi et al. 2008a, Nishitoh et al. 2008, Cheroni et al. 2009, Ferrucci et al. 2011, Prell et al. 2012, Tashiro et al. 2012, Taylor et al. 2016). However, it remains to be established whether affected cell-types in the CNS are capable of inducing an HSR as a result of pathogenic protein aggregation associated with ALS as a protective response to this chronic stress.

1.6.1 The HSR in motor neurons

Motor neurons may have a relatively high threshold for HSR induction compared to surrounding non-neuronal cells. Batulan et al. (2003) investigated the endogenous expression of HSF1 in motor neurons and their capacity to activate the HSR. In these studies, immunohistochemistry of motor neurons in spinal cord cultures demonstrated the presence of HSF1, but not the inducible Hsp70 isoform, in these cells. The capacity of motor neurons to induce an HSR was assessed following heat shock (42°C for 1 h) by monitoring the stress-inducible expression of an Hsp70 promoter driven EGFP construct. The lack of EGFP fluorescence in motor neurons after heat shock suggested that HSF1 was not activated and thus did not bind to the promoter used in this reporter construct (Batulan et al. 2003). Other studies have also shown that spinal cord motor neurons *in situ* fail to transcribe and express Hsp70 following heat shock (Manzerra and Brown 1992, Brown and Rush 1999). However, it is not clear from this work whether HSF1 was (i) not activated and therefore not capable of binding DNA and/or (ii) not present at sufficient levels in these cells to induce an HSR.

To determine which of these possibilities was responsible for these observations, WT HSF1 ($HSF1^{WT}$) and a constitutively active mutant of HSF1 ($HSF1^{+}$) were over-expressed in primary

murine motor neurons (Batulan et al. 2003). Simply increasing the level of $HSF1^{WT}$ in cells was not sufficient to enhance their capacity to express Hsp70 (Batulan et al. 2003). Conversely, over-expression of $HSF1^{+}$ resulted in an upregulation of Hsp70, Hsp40, and Hsp25 levels in 96.1 ± 3.4%, 100 ± 0%, and 14.6 ± 7.3% in motor neurons, respectively (Batulan et al. 2003, Batulan et al. 2006). Furthermore, expression of $HSF1^{+}$ in motor neurons expressing pathogenic $SOD1^{G93A}$ significantly reduced the formation of inclusions and conferred cytoprotection, compared to $HSF1^{WT}$ (Batulan et al. 2006). Together, these findings suggest that the attenuated capacity of motor neurons to induce an HSR in the context of heat shock is due to their inability to activate HSF1, not insufficient levels of HSF1 in these cells (Figure 1.4).

The over expression and aggregation of mutant SOD1 (mSOD1) in mouse models may not be sufficient to induce an HSR in motor neurons. Primary murine motor neurons expressing mSOD1 demonstrate no change in expression levels of Hsp70, Hsp105, Hsp90, Hsp60, or Hsp40 compared to those expressing $SOD1^{WT}$ and non-transgenic control motor neurons (Table 1-2). Furthermore, a reduction in Hsp105 levels was observed in spinal cord tissue homogenates of $SOD1^{G93A}$ mice (Yamashita et al. 2007). Hsp105 is a chaperone expressed in neurons and glia in the CNS and can inhibit the aggregation of mSOD1 in cell-based models (Yamashita et al. 2007). Therefore, the decline in Hsp105 expression, combined with the inability of rodent motor neurons to upregulate Hsp70, Hsp90, Hsp60, or Hsp40, suggests that the HSR is either unable to be activated or is impaired in these models of ALS (Figure 1.4).

In the absence of disease, the endogenous and constitutive expression of Hsp27 in motor neurons of the spinal cord plays an important role in the housekeeping of proteostasis. Hsp27 is a well characterised molecular chaperone that also has potent anti-apoptotic functions (Charette et al. 2000). Hsp27 can inhibit the release of mitochondrial cytochrome c and associate with Daxx, thereby inhibiting a motor neuron-specific apoptosis pathway that is

mediated by Fas-Ask1-p38 (Raoul et al. 1999, Charette et al. 2000, Raoul et al. 2002, Raoul et al. 2005). However, in transgenic mouse models of ALS, Hsp25 levels become dysregulated and decline in motor neurons during disease progression (Table 1-2). Studies have shown that pre-symptomatic mSOD1 mice have Hsp25 levels comparable to age-matched controls (Maatkamp et al. 2004, Strey et al. 2004). However, immediately prior to the onset of disease symptoms, Hsp25 levels decline in spinal cord motor neurons as demonstrated by immunohistochemistry of spinal cord sections (Maatkamp et al. 2004, Strey et al. 2004). In contrast, by the late stages of the disease, both Hsp25 and αB-c are up-regulated in spinal cord astroglia, a finding consistent in numerous studies (Vleminckx et al. 2002, Maatkamp et al. 2004, Strey et al. 2004, Wang et al. 2005, Wang et al. 2008). The decrease in Hsp25 in motor neurons during the later stages of ALS in these transgenic mouse models may increase their susceptibility to neurodegeneration as a consequence of toxic protein accumulation and other ALS-related stresses (Figure 1.4).

Table 1-2. List of Hsps and whether their expression is up-regulated (↑), down-regulated (↓), or not changed (No Δ) in rodent models of ALS at the late-stage of disease compared to age-matched transgenic WT or non-transgenic mouse controls. These results are from immunoblot (IB) or immunohistochemical (IHC) staining and microscopy of different CNS regions.

Hsps	Transgenic disease models	Tissue or cell type	References
HSF1	TDP-43$^{WT\times Q331K}$	IB: ↓ spinal cord tissue homogenates	(Chen et al. 2016)
	SOD1^{G93A}	IB: ↓ spinal cord tissue homogenates	(Mimoto et al. 2012)

αB-c (HSPB5)	$SOD1^{L126Z}$	IHC: ↑ spinal cord astroglia IHC: ↓ spinal cord oligodendrocytes	(Wang et al. 2005)
	$SOD1^{G93A}$	IHC: ↑ spinal cord astroglia	(Vleminckx et al. 2002, Zinkie et al. 2013)
	$SOD1^{G37R}$	IHC: ↑ spinal cord astroglia	(Vleminckx et al. 2002)
Hsp22 (HSPB8)	$SOD1^{G93A}$	IHC: ↑ spinal cord motor neurons	(Crippa et al. 2010, Marino et al. 2015)
Hsp25 (HSPB1)	$SOD1^{G93A}$	IHC: ↑ spinal cord astroglia IHC: ↓ spinal cord oligodendrocytes	(Vleminckx et al. 2002, Batulan et al. 2003, Maatkamp et al. 2004, Strey et al. 2004)
	$SOD1^{G37R}$	IHC: ↑ astroglia in the inferior colliculus, cerebellar white matter, brain stem, spinal cord	(Wang et al. 2008)
	$SOD1^{L126Z}$	IHC: ↓ spinal cord motor neurons	(Wang et al. 2005)
	$SOD1^{G93A}$, $SOD1^{G85R}$, $SOD1^{G37R}$, $SOD1^{H46R/H48Q}$	IHC: ↑ spinal cord astroglia IHC: ↑ spinal cord undefined neurons	(Wang et al. 2003)
Hsp40	$SOD1^{G93A}$	IHC: No Δ spinal cord	(Wang et al. 2008)
	$SOD1^{G93A}$, $SOD1^{G85R}$, $SOD1^{G37R}$, $SOD1^{H46R/H48Q}$	IB: No Δ spinal cord tissue homogenates	(Wang et al. 2003)
	$TDP\text{-}43^{WT\times Q331K}$	IB: No Δ spinal cord tissue homogenates	(Chen et al. 2016)
Hsp60	$SOD1^{G93A}$	IHC: No Δ spinal cord	(Wang et al. 2008)
	$SOD1^{G93A}$, $SOD1^{G85R}$, $SOD1^{G37R}$, $SOD1^{H46R/H48Q}$	IB: No Δ spinal cord tissue homogenates	(Wang et al. 2003)
Hsp70	$SOD1^{G93A}$, $SOD1^{G85R}$, $SOD1^{G37R}$, $SOD1^{H46R/H48Q}$	IB: No Δ spinal cord tissue homogenates	(Batulan et al. 2003, Wang et al. 2003, Wang et al. 2005, Wang et al. 2008)
	$SOD1^{G93A}$	IHC: ↑ "sick-appearing" spinal cord motor neurons	(Vlug et al. 2005)
	$SOD1^{G85R}$	IB: ↑ spinal cord tissue homogenates	(Liu et al. 2005)
Hsp90	$SOD1^{G93A}$	IHC: No Δ spinal cord	(Wang et al. 2008)
	$SOD1^{G93A}$, $SOD1^{G85R}$, $SOD1^{G37R}$, $SOD1^{H46R/H48Q}$	IB: No Δ spinal cord tissue homogenates	(Wang et al. 2003)
Hsp105	$SOD1^{G93A}$	IB: ↓ in spinal cord tissue homogenates	(Yamashita et al. 2007)

With regard to ALS in humans, immunohistochemistry of human motor neurons in cervical spinal cord sections obtained at autopsy showed no change in Hsp70 or Hsp27 levels compared to age-matched controls (Batulan et al. 2003). The combined evidence suggests that the toxicity of mSOD1 in spinal cord motor neurons is not sufficient to elicit the stress-inducible expression of Hsps in rodents or humans. In contrast, Hsp70 (but not Hsp27 or αB-c) immunoreactivity

was occasionally observed to be higher in neighbouring glial cells in fALS or sporadic ALS patients (Batulan et al. 2003). This suggests that astroglia in humans and rodents are capable of up-regulating certain Hsps in response to stresses associated with ALS. This further supports the hypothesis that motor neurons intrinsically have a high threshold for induction of the HSR and also suggests that misfolded mSOD1 can go undetected by this inducible arm of the proteostasis network in these cells.

There is a lack of diversity in the models that have been used in work investigating the HSR in association with ALS. Data regarding neuronal and glial Hsp expression in ALS is derived primarily from mSOD1 rodent models, with the exception of one study that used the TDP-$43^{WT\times Q331K}$ transgenic mouse model of ALS (Chen et al. 2016). Therefore, it remains to be determined whether these findings also apply to other fALS-associated mutations (*e.g. FUS*). This is of particular relevance if each aggregation-prone protein engages a specific set of Hsps, as has been previously proposed (Kakkar et al. 2014). Therefore, additional research is required in other rodent models of ALS to advance our understanding of the HSR in this disease.

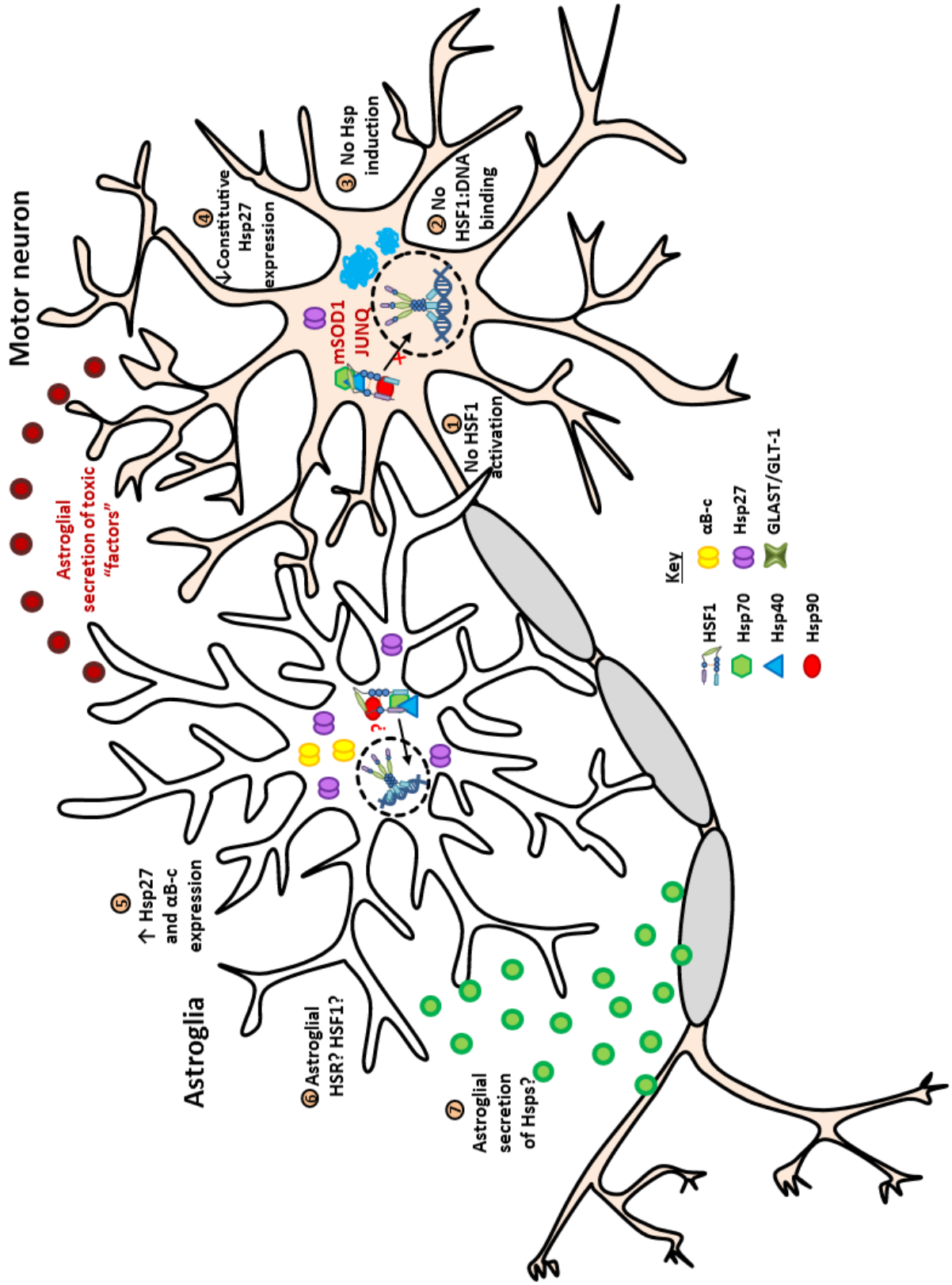
Motor neuron
Astroglial secretion of toxic "factors"
4 ↓Constitutive Hsp27 expression
3 No Hsp induction
2 No HSF1:DNA binding
mSOD1
JUNQ
1 No HSF1 activation
Key
αB-c
Hsp27
GLAST/GLT-1
HSF1
Hsp70
Hsp40
Hsp90
?
5 ↑ Hsp27 and αB-c expression
Astroglia
6 Astroglial HSR? HSF1?
7 Astroglial secretion of Hsps?

Figure 1.4. Proposed mechanism of the HSR and its components in motor neurons and astroglia of mSOD1 over-expressing models of ALS. Motor neuron disease initiation and progression is dependent on the molecular pathologies developed in motor neurons (*e.g.* formation of mSOD1 aggregates or JUNQ) and astroglia (*e.g.* secretion of unidentified toxic "factors"). The susceptibility of motor neurons to degeneration is likely due to an inability of motor neurons and astroglia to induce a cytoprotective HSR in response to increasing quantities of misfolded proteins (*e.g.* mSOD1) and neuroinflammation. (1 and 2) HSF1 in motor neurons has a relatively high threshold for activation and the over-expression of mSOD1 and subsequent molecular pathologies do not activate HSF1 nor induce the binding of HSF1 to DNA. (3) There is no detectable basal expression or upregulation of Hsps in mSOD1 over-expressing motor neurons, with the exception of (4) Hsp27, which gradually declines with disease progression. (5) Astroglia in mSOD1 over-expressing mice have increased amounts of Hsp27 and αB-c with disease progression; however, the levels of other Hsps are not changed. (6) There have been few investigations regarding HSF1 activation and DNA-binding in astroglia in the context of ALS. Therefore, the capacity of mSOD1 over-expressing astroglia to activate HSF1 and induce an HSR remains unknown. (7) There is increasing evidence that extracellular vesicles containing Hsps are secreted by astroglia, and these vesicles are endocytosed by motor neurons and facilitate transfer of Hsps.

1.6.2 The role of glial cells in ALS

There is strong evidence that ALS can be characterised as a non-cell autonomous disease (Boillée et al. 2006a, Lee et al. 2016). As such, ALS initiation and progression depends on both the molecular pathologies developed within motor neurons, and the subsequent pro-inflammatory activities of surrounding non-neuronal cell populations such as astroglia and microglia. For example, transgenic mice expressing $SOD1^{G37R}$ specifically in motor neurons in the ventral horn of spinal cords remained healthy for up to 1.5 years of age compared to mice that ubiquitously express this mSOD1 isoform, which die at 4 months of age (Wong et al. 1995, Pramatarova et al. 2001). Moreover, knock out of $SOD1^{G37R}$ expression in motor and dorsal root ganglion neuron progenitors of transgenic mice results in an 18 day delay to disease onset and 31 day delay to early disease progression compared to controls (Boillée et al. 2006b). Together, these findings demonstrate that mSOD1 expression in motor neurons plays a role in early disease initiation. Selective deletion of $SOD1^{G37R}$ expression from glial fibrillary acidic protein (GFAP)-positive spinal cord astroglia or cluster of differentiation molecule 11B (CD11b)-positive microglia significantly delayed late disease progression resulting in an overall extension of survival by 60 and 99 days, respectively (Boillée et al. 2006b, Yamanaka et al. 2008). These two studies demonstrate that mSOD1 expression in astroglia and microglia plays a significant role in late disease progression and overall survival. This work and the work

of many others emphasises the importance of astroglia and microglia in the pathogenic cascade associated with ALS [for in-depth reviews examining the non-cell-autonomous nature of ALS see (Boillée et al. 2006a, Ilieva et al. 2009, Lee et al. 2016)]. The non-cell-autonomous progression of ALS by glial cells has also recently been demonstrated in a mutant TDP-43 model of ALS (Tong et al. 2013, Huang et al. 2014, Ditsworth et al. 2017), suggesting that the non-cell-autonomous progression of ALS is not confined to mSOD1-expressing mouse models, but may represent a generic mode of ALS progression. Furthermore, the vulnerability of spinal cord motor neurons in ALS may be explained by regional variations in the ability of surrounding glia to provide cytoprotective support during disease onset.

Glia are thought to exert their neurotoxicity in NDs through the activation of inflammatory pathways that propagate from the site of onset in the CNS and manifest as chronic neuroinflammation. At the molecular level, neuroinflammation is driven by the transcription factor nuclear factor-κB (NF-κB). In the absence of stress, the NF-κB-mediated inflammatory pathway is maintained in an inhibitory complex with IκBα. Previous work has suggested that cellular stress, for example the expression and aggregation of mSOD1, causes Iκ kinase to phosphorylate IκBα that signals for its polyubiquitination by ubiquitin ligases (*e.g.*, Skp1/Cullin/F-box protein FWD1), which tags IκBα for degradation at the proteasome (Chen et al. 1995, Hatakeyama et al. 1999, Israël 2010, Meissner et al. 2010, Roberts et al. 2013). NF-κB released from this inhibitory complex becomes activated, and translocates into the nucleus to induce the transcription of pro-inflammatory (*e.g.*, TNF-α and IL-1β) or anti-inflammatory genes (*e.g.*, IL-13) (Tak and Firestein 2001, Israël 2010).

The spectrum of inflammatory mediators that are up-regulated as a consequence of NF-κB activation are cell-type dependent. For example, mSOD1 expressing, reactive spinal cord astroglia have been shown to release interferon-γ (IFNγ), transforming growth factor-β (TGFβ), nerve growth factor (NGF) and nitric oxide (NO) (Pehar et al. 2004, Aebischer et al.

2011, Phatnani et al. 2013). Furthermore, mSOD1 expressing microglia have been shown to release anti-inflammatory cytokines and neurotrophins in early disease and the pro-inflammatory mediators tumour necrosis factor-α (TNFα), interleukin-1β (IL-1β) and NO in late disease (Weydt et al. 2004, Xiao et al. 2007, Meissner et al. 2010). In these previous studies, activated astroglia and microglia expressing mSOD1 led to increased motor neuron toxicity and reduced motor neuron viability in co-culture experiments (Pehar et al. 2004, Aebischer et al. 2011, Phatnani et al. 2013). The microglia examined in these studies were derived from cortical preparations. However, regional variations in inflammatory pathway activation may exist. Thus, it is necessary to investigate inflammatory responses in spinal cord glia in research that is focused on spinal cord motor neurons. A lower threshold for activation and a stronger inflammatory response in spinal cord glia could sensitise motor neurons to degeneration over neuronal populations in other regions of the CNS. Therefore, future research should investigate whether regional differences in the ability of glia to activate the inflammatory pathway can be linked to the degeneration of neurons in discrete population of the CNS.

The ubiquitous expression of mutant ALS-associated proteins in the CNS may not alone facilitate the transition of astroglia from a neurotrophic to neurotoxic phenotype in ALS. Co-culture with A1 astroglia induces the rapid death of a range of neurons, including spinal cord α-motor neurons (Liddelow et al. 2017). Interestingly, there was a significant increase in the proportion of A1 astroglia in the motor cortex of patients with ALS (40% of ALS astroglia were A1 compared to 15% in controls) (Liddelow et al. 2017). Likewise, there was a 60-fold increase in A1-related transcripts in the motor cortex of ALS patients compared to controls (Liddelow et al. 2017). The mechanism by which these A1 astroglia induce toxicity was proposed to be through the secretion of a ‘toxic factor’ (Liddelow et al. 2017). Other studies have also suggested that mSOD1-expressing astroglia release a soluble ‘toxic factor’, which

significantly reduces the viability of motor neurons in co-culture (Di Giorgio et al. 2007, Nagai et al. 2007, Bilsland et al. 2008, Cassina et al. 2008). The identity of this neurotoxic factor is currently unknown and additional research is required to determine its mode of action. In any case, it is important to consider cytoprotective mechanisms that maintain the neurotrophic functions of glia in ALS, such as the HSR, which leads to Hsp expression.

1.6.3 The HSR in astroglia

It is generally regarded that astroglia can activate an HSR in response to stress, including whole animal hyperthermia (Nishimura et al. 1991, Manzerra and Brown 1992, Manzerra et al. 1997, Krueger et al. 1999). In the context of ALS, astroglia have higher levels of the sHsps, αB-c and Hsp25, compared to WT controls at the end-stage of disease, but not Hsp90, Hsp70, Hsp60 or Hsp40 (Table 1-2, Figure 1.4). Interestingly, these findings suggest that the over-expression of unstable and misfolded mSOD1 species at the onset and early-stage of ALS fails to activate the HSR in the CNS. Chronic neuroinflammation in the CNS may upregulate these sHsps at the end-stage of disease in rodent models of ALS.

There is a scarcity of published work investigating HSF1-activation and HSR induction in astroglia at the molecular level using biochemical techniques (Figure 1.4). However, the discord between sHsps being up-regulated and other Hsps not being affected in astroglia in the context of ALS suggests that there are additional layers of regulation of the HSR in these cells that are either HSF1-mediated or post-translational. In recent work, Zheng et al. (2016) hypothesised that the phosphorylation of HSF1 at serine and threonine residues serves to fine-tune HSF1 transcription at promoter regions, rather than act as an on/off switch. Thus, HSF1 phosphorylation could serve to regulate the kinetics and magnitude of the HSR in a cell-type dependent manner. Additional unidentified mechanisms of HSF1 regulation, including those that are cell-type specific, could explain the complete absence of HSR induction in motor

neurons compared to astroglia in mSOD1-expressing transgenic mice. In fact, the HSF1-mediated HSR in the different cell-types that comprise the CNS is likely to be much more complex than our current models of HSR induction and attenuation (Figure 1.2), which are based primarily on findings from S*accharomyces cerevisiae*, *Drosophila melanogaster*, cell-lines or studies using recombinant human HSF1 in solution (Peteranderl and Nelson 1992, Rabindran et al. 1993, Westwood and Wu 1993, Neudegger et al. 2016). Future research should elucidate the mechanisms of HSR induction in astroglia, with a focus on investigating astroglia derived from affected and not affected regions of the CNS (*e.g.*, spinal cord compared to cortical glia).

Upregulation of cytoprotective Hsps in astroglia could maintain astroglia in a healthy neurotrophic state to support motor neuronal viability and prevent conversion of astroglia to a neurotoxic (A1) phenotype. One mechanism by which astroglia may provide cytoprotection to motor neurons is through the exchange of extracellular vesicles containing Hsps (Frühbeis et al. 2013). Extracellular vesicles derived from chick spinal cord primary astroglial cultures, following heat shock, contain Hsp70 and Hsc70 (Taylor et al. 2007). In another study investigating glial-neuronal interactions, T98G glioma cells were shown to secrete Hsp70 into the culture medium and LA-N-5 neuroblastoma cells took up this Hsp70 (Guzhova et al. 2001). The Hsp70 uptake increased the stress tolerance of the LA-N-5 cells to heat shock and staurosporine-induced apoptosis (Guzhova et al. 2001). The mechanisms of astroglial exocytosis and neuronal endocytosis used to traffic Hsps are also yet to be elucidated. The non-cell-autonomous mechanism(s) by which astroglia provide products of the HSR to neurons could be exploited to increase Hsp levels in motor neurons. This strategy could enhance the stress tolerance of motor neurons and decrease degeneration in the spinal cord in ALS (Figure 1.4).

1.6.4 Summary of the HSR in ALS

Spinal cord motor neurons from primary cell or animal models of ALS are unable to activate HSF1 and hence lack stress-induced expression of Hsps. The endogenous levels of Hsp27 in motor neurons decline with disease progression. Motor neurons have an inherently high threshold for the activation of the HSR and the expression and accumulation of mSOD1 in the cell is not sufficient to activate the HSR. In contrast, spinal cord astroglia have elevated levels of αB-c and Hsp25 (rodent) or Hsp70 (human) at the end-stage of disease. However, the precise mechanisms by which these Hsps are up-regulated are unknown. Overall, there is a distinct lack of research into the HSR in spinal cord astroglia and its potential role in ALS.

Due to the non-cell-autonomous nature of ALS, future research should focus on maintaining affected spinal cord astroglia in a neurotrophic state to support motor neuron viability. Furthermore, investigation of Hsp70 (and other Hsp) transfer between astroglia and motor neurons could represent an exciting new mechanism to target for the development of therapeutics that target the proteostasis network in ALS.

1.7 Studying the therapeutic effects of increasing HSR components

Plaques and inclusion bodies associated with NDs are co-localised with various components of the proteostasis network, which may represent an irreversible sequestration, and subsequent loss of function, of these vital housekeeping components (Muchowski and Wacker 2005). The sequestration of these chaperones, in conjunction with the possibility that toxic misfolded proteins do not induce an HSR in the CNS, are likely to be important molecular mechanisms that lead to neurodegeneration in these diseases. The absence of a stress-induced upregulation of Hsps in early disease allows the formation of toxic protein species, which precede a cascade of cellular dysfunctions in NDs. Therefore, in the absence of an HSR in affected neurons and

surrounding glia in the CNS, boosting the HSR pharmacologically represents a promising therapeutic intervention for the treatment of these diseases at an early stage.

Investigations into the therapeutic benefit of pharmacological activation of the HSR in the context of NDs are currently in progress. There are two classes of therapeutics under investigation, each targets different aspects of the HSR pathway. One class of therapeutics targets the HSF1 inhibitory complex composed of Hsp90, co-chaperone p23 and immunophilin FK506-binding protein 5. Since, Hsp90 activities are ATP-dependent, this complex can be targeted by small molecules that compete with ATP for binding to Hsp90. Radicicol, NVP-HSP990, geldanamycin and geldanamycin-derived 17-allylaminogeldanamycin are Hsp90 inhibitors that act in this way and are currently under investigation for the treatment of NDs (Sittler et al. 2001, Hay et al. 2004, Labbadia et al. 2011, Ortega et al. 2014). In addition, the interaction between HSF1 and TRiC/CCT, which inhibits HSF1 activation, can be inhibited with the compound HSF1A *in vitro* (Neef et al. 2014). An important limiting factor of the Hsp90-inhibiting compounds is that they are cytotoxic at low concentrations and therefore, not strong candidates to pursue for clinical trials. The other class of therapeutics that targets the HSR pathway activate HSF1 and/or up-regulate downstream products of the HSR (predominantly via unknown mechanisms). These include celastrol, arimoclomol, withaferin A, acetyl-L-carnitine and pyrrolidine dithiocarbamate (DeMeester et al. 1998, Abdul et al. 2006, Khan et al. 2012, Kalmar et al. 2014, Sharma et al. 2015b). Thus far, arimoclomol is the most promising HSR-mediating therapeutic. Administration of arimoclomol to mouse models of ALS (10 mg/kg/day), spinal and bulbar muscular atrophy (120 mg/kg/day) and inclusion body myositis (120 mg/kg/day) ameliorated neuropathologies associated with each disease, and arimoclomol has progressed to Phase II/III human clinical trials (Kieran et al. 2004, Kalmar et al. 2008, Malik et al. 2013, Ahmed et al. 2016).

A significant amount of work has investigated the effects of over-expressing individual Hsps or activating an HSF1-mediated HSR in rodent models of NDs [for comprehensive reviews see (Muchowski and Wacker 2005, Leak 2014, Duncan et al. 2015, Pratt et al. 2015, Bose and Cho 2017)]. Over-expression of individual chaperones in mSOD1 mouse models of ALS has resulted in modest effects with regard to a reduction in the amount of insoluble protein and increased motor neuron survival (Table 1-3) (Liu et al. 2005, Gifondorwa et al. 2007, Krishnan et al. 2008, Sharp et al. 2008, Novoselov et al. 2013, Watanabe et al. 2014). However, this does not correlate with an increase in overall survival of the double transgenic animals (Table 1-3). Conversely, upregulation of the HSR by treatment with withaferin A, celastrol or arimoclomol results in an increase in the number of surviving motor neurons and the lifespan of mSOD1 expressing mice (Kieran et al. 2004, Kiaei et al. 2005, Lin et al. 2013, Patel et al. 2014). This same trend was observed in mouse models of HD, whereby over-expression of HSJ1a and Hsp70 has no effect on overall survival but over-expression of an active mutant of HSF1 extended survival by 15 days (Table 1-4) (Fujimoto et al. 2005). Therefore, increasing the expression of a broad range of stress-related proteins appears to be more efficacious in reducing protein aggregate load, preventing neurodegeneration and increasing lifespan of mouse models of NDs compared to upregulation of individual chaperones. The exceptions to this are DNAJB1, DNAJB6 and polyQ binding peptide (QBP)-Hsc70 binding motif which, when over-expressed, reduced insoluble Htt and extended survival by 17, 21 and 32 days, respectively (Bauer et al. 2010, Popiel et al. 2012, Gillis et al. 2013, Kakkar et al. 2016). These findings illustrate how specific sets of Hsps may be more efficacious against aggregating proteins associated with HD, thus, ongoing investigations that evaluate the activities of a range of Hsps are warranted.

Table 1-3. The effect of the over-expression of Hsps and upregulation of the HSR on the molecular pathologies developed in rodent models of ALS.
Double transgenic (Tg) mice were bred for the over-expression of an Hsp and a SOD1 mutant associated with ALS. Alternatively, mice that over-express mutant SOD1 were treated with a therapeutic compound for the activation of the HSR. The fold increase in Hsp levels (and, if reported, the tissue-type in which this occurs), number of extended days of life, percent increase (↑) or decrease (↓) in spinal cord motor neurons, and percent ↑ or ↓ in the levels of inclusions is reported for each study.

Transgenic model/ Therapeutic compound	ALS model	Increase in Hsp in Tg mouse	Extended lifespan	% ↑/↓ in surviving motor neurons	% ↑/↓ in levels of inclusions	References
Hsp27 Tg	$SOD1^{G93A}$	40-fold ↑spinal cord 25-fold ↑ cortex, cerebellum, hippocampus Expressed in MN + $GFAP^{+ve}$ astroglia	No Δ (prolonged 4.2 days)	-	No Δ	(Krishnan et al. 2008)
	$SOD1^{G93A}$	-	No Δ (died 6 days sooner)	24% ↑	No Δ	(Sharp et al. 2008)
HSJ1a Tg	$SOD1^{G93A}$	7-fold ↑	No Δ	61% ↑	No Δ	(Novoselov et al. 2013)
Hsp70 Tg	$SOD1^{G93A}$	10-fold ↑	No Δ (prolonged 1.4 days)	-	-	(Liu et al. 2005)
	$SOD1^{G85R}$	10-fold ↑ spinal cord	No Δ	-	-	
	$SOD1^{G37R}$	10-fold ↑	No Δ	-	-	
Hsp70 administered exogenously	$SOD1^{G93A}$	rhHsp70 injected 3x weekly (20ug)- detected in muscle not CNS	9 days	12.5% ↑	-	(Gifondorwa et al. 2007)
HSF1 Tg	$SOD1^{H46R/H48Q}$	3-fold ↑	No Δ	-	34% ↓	(Lin et al. 2013)
SIRT1 Tg	$SOD1^{G93A}$	3-fold ↑	15 days	-	40% ↓	(Watanabe et al. 2014)
Withaferin A	$SOD1^{G93A}$	2.6-fold ↑ Hsp25 2.2-fold ↑ Hsp70 Phosphorylated HSF1	8 days	30% ↑	39% ↓	(Patel et al. 2014)
	$SOD1^{G37R}$	-	18 days	-	-	
Celastrol	$SOD1^{G93A}$	-	16 days	30% ↑	-	(Kiaei et al. 2005)
Arimoclomol	$SOD1^{G93A}$	3-fold ↑ Hsp70 2.5-fold ↑ Hsp90 Phosphorylated HSF1	28 days	74% ↑	-	(Kieran et al. 2004)

Table 1-4. The effect of the over-expression of Hsps and upregulation of the HSR on the molecular pathologies developed in rodent models of HD.
Double transgenic (Tg) mice were bred for the over-expression of an Hsp and polyQ-expanded Htt associated with HD. Alternatively, HSF1 and HSF2 genes were knocked-out (KO) of HD mouse models. Lentiviral vectors for the expression of QBP1-Hsc70 binding motif and DNAJB1 were injected directly into the striatum of R6/2 mice. In one case, mice that over-express polyQ-expanded Htt were treated with NVP-HSP990, a therapeutic compound for the activation of the HSR. The fold increase in Hsp levels (and, if reported, the tissue-type in which this occurs), number of extended days of life, percent increase (↑) or decrease (↓) in spinal cord motor neurons, and percent ↑ or ↓ in the levels of inclusions is reported for each study.

Transgenic model/ Therapeutic compound	HD model	Increase in Hsp in Tg mouse	Extended lifespan	% ↑/↓ in surviving neurons	% ↑/↓ in levels of inclusions	References
αB-c Tg (astroglia only)	BACHD	-	-	12.5% ↑	50% ↓	(Oliveira et al. 2016)
Hsp27 Tg	R6/2	12-fold ↑	-	-	No Δ	(Zourlidou et al. 2007)
Hsp70 Tg	R6/2	Rat Hsp70	-	-	No Δ	(Hay et al. 2004)
	R6/2	5-15-fold ↑ human Hsp70	No Δ	No Δ	No Δ	(Hansson et al. 2003)
rAAV-QBP1-Hsc70 binding motif	R6/2	Injected into the striatum	32 days	-	90.8% ↓	(Bauer et al. 2010)
rAAV-DNAJB1	R6/2	Injected into the striatum	17 days	-	39.2% ↓	(Popiel et al. 2012)
DNAJB6 Tg	R6/2	Brain-specific upregulation (nestin promoter)	21 days	-	33% ↓	(Kakkar et al. 2016)
HSJa Tg	R6/2	Brain specific upregulation	No Δ	No Δ	35% ↓	(Labbadia et al. 2012)
Hsp104	N171-82Q HD	"Strongly" expressed in the brain, heart kidneys, testis	-	-	No Δ	(Vacher et al. 2005)
HSF1^{Active} Tg	R6/2	Expressed in skeletal muscle, heart and testes	15 days	No Δ	79% ↓	(Fujimoto et al. 2005)
NVP-HSP990 treatment	R6/2	2.7-fold ↑ Hsp70 3.8-fold ↑ Hsp25 1.6-fold ↑ Hsp40	No Δ	-	20% ↓	(Labbadia et al. 2011)
HSF1 KO	R6/2	-	105 day decrease in lifespan	-	15% ↑	(Hayashida et al. 2010)
HSF2 KO	R6/2	-	91 day decrease in lifespan	-	20% ↑	(Shinkawa et al. 2011)

1.7.1 Studying the activities of Hsps in cells

Determining which of the HSR components are the most efficacious in preventing protein aggregation and subsequent neurotoxicity is an important step in elucidating targets for the development of therapeutics that ameliorate NDs. Previous work has demonstrated that Hsps can prevent the disease-associated aggregation of proteins and the toxicity associated with this process in cells. For example, Ormsby *et al.* (2013) showed, by flow cytometric pulse shape analysis, that Hsp40 inhibited the aggregation of pathogenic polyglutamine-expanded Htt. In contrast, whilst Hsp70 reduced cell death in this model, it had no effect on inclusion body formation (Ormsby et al. 2013). However, the relative co-transfection efficiencies and levels of the Hsp in cells cannot be easily determined when the expressed Hsps are not fluorescently tagged. In particular, this confounds efforts to compare the effect of different Hsps on cellular functions. Vos *et al.* (2010) performed a systematic comparison of the chaperone efficacy of human sHsp family members in inhibiting polyglutamine-expanded Htt in cells, in which immunoblotting was performed to determine the relative expression levels of each sHsp in HEK293 cells (each sHsp had a C-terminal V5-tag to enable detection with the same anti-V5-antibody) (Vos et al. 2010). In this work, the expression levels of HspB7 and HspB9 were significantly lower than the expression levels of the other sHsps investigated. However, immunoblotting did not reveal whether the differences in expression levels were attributable to a lower rate of expression, a lower transfection efficiency of the HspB7 and HspB9-encoding constructs compared to the other constructs used, or higher turn-over rate of HspB7 and HspB9 in these cells (Vos et al. 2010). Moreover, such techniques do not provide any information regarding the levels of the expressed protein in individual cells. Thus, it is advantageous to be able to account for transfection efficiencies and the levels of Hsps in cell-based assays, particularly when the aim is to compare the activities of different Hsps.

The chaperone activities and diverse range of cellular roles of Hsps are only partially understood. This is the consequence of their dynamic (in some cases, polydisperse and oligomeric) structure and transient interactions with client proteins and co-chaperones (Treweek et al. 2015, Balchin et al. 2016). The functions of Hsps have historically been investigated by fusing their N- or C-termini with fluorescent proteins. However, fusion of fluorescent proteins to Hsps is likely to interfere with their dynamic structures, protein interactions, and thus, function. In the case of the sHsps, for example Hsp27, whose monomeric molecular weight is 27 kDa, fusion of a fluorescent protein (*e.g.* green fluorescent protein; 25 kDa) would double its molecular weight. Indeed, recombinant Hsp27 that has been C-terminally tagged with enhanced yellow fluorescent protein demonstrates an altered ability to form large oligomers (a conformation necessary for sHsp function) and increased chaperone activity (Datskevich and Gusev 2014). Therefore, to elucidate the diverse roles of a range of Hsps in cell-based assays, new approaches for the expression of Hsps and a fluorescent reporter protein that negate the need for N- or C-terminal fusion are important to develop in future research.

1.7.2 Quantifying inclusion body formation in cell-based models of NDs

The role of Hsps in inhibiting protein aggregation associated with NDs in cell-based models is an intensely investigated area of research. Despite this, there is still a scarcity of techniques that can rapidly and reproducibly quantify inclusion bodies formed from a range of different proteins. Interestingly, there is no consistency in the reporting of the effect of over-expressing Hsps or drug treatment on protein inclusion formation in the transgenic animal models of ALS and HD in Table 1-3 and Table 1-4. Measurement of inclusion body load in the tissues of these transgenic mice is important due to the strong correlation between inclusion body formation, cellular dysfunction and degeneration in NDs.

Detecting and quantifying inclusion bodies has traditionally been performed by fluorescence microscopy, immunoblot and filter trap analysis of soluble and insoluble protein fractions Fluorescence microscopy enables the visualisation and localisation of fluorescently-tagged protein aggregates in the cell, however, it is limited in terms of high-throughput and quantitative analysis. Recent advances in high-content image screening and self-learning algorithms have addressed these limitations and significantly facilitated the temporal and spatial resolution of fluorescently-tagged proteins within individual cells (Daub et al. 2009). Furthermore, the automation of this process has eliminated the subjectivity and bias typically associated with image analysis (Danuser 2011). Despite these computational advancements, high content image screening is still plagued by several pitfalls; these include an inability to distinguish individual cells and aggregates when in clumps and relatively poor performance on images with high background noise (Sommer and Gerlich 2013). In addition, access to this type of image processing is limited as a consequence of the need for specialised instruments, training on complicated data-mining software or code-writing capabilities (Daub et al. 2009, De Vos et al. 2010, Sommer and Gerlich 2013).

Immunoblotting of SDS-soluble and SDS-insoluble fractions of whole cell lysates is a commonly used method for determining the chaperone activities of Hsps in the context of protein aggregation associated with NDs (Vos et al. 2010, Gillis et al. 2013). However, the shortcomings of this approach include that it is qualitative, low throughput, and transfection efficiencies and protein expression levels cannot be taken into account. In an attempt to address these shortcomings, Ramdzan et al. (2013) developed a flow cytometric technique based on the differences in pulse shapes of cells with and without inclusion bodies called PulSA (pulse shape analysis). However, PulSA was only able to accurately quantify the proportions of cells with inclusion bodies formed from Htt but is not as amenable to the quantification of cells with SOD1 or TDP-43 inclusions, suggesting that this technique is primarily amenable to the

physical properties of cells with Htt inclusions (Ramdzan et al. 2013). Therefore, future techniques should be developed to rapidly quantify inclusion bodies formed from a range of proteins, take into account differences in transfection efficiencies across samples, with the capacity for high-throughput analysis of samples.

1.8 Summary and aims

Regulation of the HSR and its downstream products are of particular relevance to the cells that comprise the CNS, where protein inclusion formation and inflammation associated with NDs occurs. Evidence from cell lines and rodent models of NDs, and human post mortem tissues, suggests that protein aggregation and inflammation are undetected by the HSR in affected neurons and astroglia. However, further research is warranted to identify the role of the HSR in responding to protein aggregation and inflammation, and whether its impairment contributes to neuronal vulnerability in NDs, therefore, the objectives of this PhD project were to:

1. Generate bicistronic constructs for the expression of Hsps to study their intracellular activities in cells without the need for N- or C-terminal fusion to a fluorescent reporter protein.
2. Develop a novel method for the rapid and high throughput quantification of inclusions in cells to overcome the limitations of the current methodologies.
3. Assess whether differentiated neuron-like cells can induce the HSR, and determine whether intra- and extracellular protein aggregates associated with NDs can induce an HSR in a neuron-like cell line.
4. Compare the inflammatory response and HSR in cortical and spinal cord primary mixed glial cells to establish a link between regional variations in glial support and neurodegeneration in the spinal cord in ALS.

Chapter 2: General materials and methods

The general methods used in this research are outlined in this chapter. Methods specifically pertaining to work presented in Chapters 3 – 6 are provided in the relevant chapters.

2.1 Materials

All reagents used for this work were obtained from Sigma-Aldrich (St Louis, MO, USA) or Amresco (Solon, OH, USA) unless otherwise stated. Halt^{TM} Protease and Phosphatase Inhibitor Cocktail (100 ×) and all restriction enzymes were acquired from Thermo Fisher Scientific (Scoresby, VIC, Australia). The transfection reagent Lipofectamine LTX/PLUS reagent, 0.025% trypsin-EDTA, Dulbecco's Modified Eagle Medium/Ham's F12 media (DMEM/F12), and L-glutamine (100 ×) were purchased from Invitrogen (Carlsbad, CA, USA). Foetal calf serum (FCS) was obtained from Bovogen Biologicals (Keilor, VIC, Australia).

2.2 Plasmids

Lists of plasmids appear in each of the relevant chapters in this thesis.

2.3 Antibodies

Lists of antibodies and their dilutions appear in each of the relevant chapters in this thesis.

2.4 Molecular cloning, construct verification and storage

2.4.1 Molecular cloning

Details of the methods undertaken for the generation of the constructs used in this thesis appear in the relevant chapters.

2.4.2 Agarose gel electrophoresis

DNA samples were prepared for agarose gel electrophoresis by mixing the sample with an appropriate amount of loading buffer (final concentrations: 30% (v/v) glycerol, 0.25% (w/v) bromophenol blue in H_2O). The molecular weight markers, Hyperladder I (200 – 10037 bp) or

Hyperladder II (50-2000 bp) were run on each gel. DNA samples were electrophoresed using 0.8 or 1% (w/v) TAE agarose gels. Gels were submerged in 1 × TAE buffer in a MiniSub Cell GT electrophoresis tank (Bio-Rad) and electrophoresis was performed at 85 V until the bromophenol blue dye front had migrated to the end of the agarose gel. Gels were stained in a 0.005% (w/v) ethidium bromide solution for 15 min and destained in dH2O for 5 min. Ethidium bromide stained DNA bands were visualised and images were captured by a 0.5 s exposure to UV light using a Gel Logic 2200 Pro Imaging System (Carestream Health, Rochester, NY, USA).

2.4.3 Preparation of chemically competent Escherichia coli

Chemically competent DH5α *E. coli* were prepared by inoculating 10 mL of lysogeny broth [LB; 5% (w/v) yeast, 10% (w/v) NaCl, 10% (w/v) tryptone, pH 7.4] with a single colony. The culture was incubated overnight at 37°C on an orbital shaker at 180 rpm. The following day, the cells were centrifuged (5 min/ 5,000 × *g*) and washed in ice-cold 100 mM $CaCl_2$. The cells were centrifuged again (5 min/ 5,000 × *g*) and washed in ice-cold 100 mM $CaCl_2$ with 15% (v/v) glycerol and snap frozen in liquid nitrogen for storage at -80°C.

2.4.4 Transforming E. coli

To transform cells, plasmid DNA was mixed with 100 µL of chemically competent DH5α *E. coli* and incubated on ice for 1 h. Cells were then heat shocked at 42°C for 30 s. LB was added to the transformation mixture and incubated at 37˚C for 1 h on an orbital shaker (180 rpm). Transformation cultures were then plated onto LB agar media (LB with 15% (w/v) agar) supplemented with ampicillin (100 µg/mL) or kanamycin (50 µg/mL) and incubated at 37˚C overnight.

Successfully transformed *E. coli* colonies were screened for the gene of interest by PCR using their respective cloning primers. One colony that was positive for the gene insert was chosen

and the plasmid was extracted using the Wizard® Plus SV Miniprep DNA Purification System according to the manufacturer's instructions. The purity (A260/280) and concentration (A260) of plasmid DNA recovered from DH5α *E. coli* was assessed using a NanoDrop 2000c Spectrophotometer (Thermo Fisher Scientific).

2.4.5 Construct verification by sequencing

Extracted and purified cloned constructs were prepared for sequencing using the BigDye® Terminator v3.1 Cycle Sequencing Kit according to the manufacturer's instructions. The 10 µL reaction mix contained 1 × BigDye® buffer, 1.6 µM primer, 1 × BigDye® Ready Reaction Premix, and an appropriate concentration of plasmid DNA. PCR was performed using a Mastercycler ProS (Eppendorf) and consisted of 35 cycles (denaturation at 96°C for 10 s, annealing at 50°C for 5 s, and extension at 60˚C for 4 min). DNA was precipitated by incubation with 100% ethanol, 125 mM EDTA (pH 8.0) and 3 M sodium acetate for 2 h at room temperature (RT). Precipitated DNA was washed with ice-cold 70% (v/v) ethanol (30 min/ 21 000 × *g*/ 4°C) and dried. Constructs were sequenced using a Hitachi 3130xl Genetic Analyser (Applied Biosystems, Mulgrave, Australia) by Ms. Margaret Phillips (University of Wollongong, Australia).

2.4.6 Generation of glycerol stocks of transformed E. coli

Plasmids were stored as glycerol stocks at -80°C. Briefly, 5 mL of LB supplemented with ampicillin (100 µg/mL) or kanamycin (50 µg/mL), was inoculated with a single colony of DH5α *E. coli* transformed with the construct. This was incubated overnight at 37°C on an orbital shaker (180 rpm) and 1 mL of culture was mixed with 1 mL of sterile glycerol in a cryovial for storage at -80°C.

2.5 Bacterial culture and plasmid extraction for mammalian cell transfections

Transfection-quality purified plasmid DNA was extracted from DH5α *E. coli* containing the plasmid of interest using the PureYield™ Plasmid Midiprep System, according to the manufacturer's instructions. Briefly, 100 mL of LB supplemented with either ampicillin (100 µg/mL) or kanamycin (50 µg/mL) and DH5α *E. coli* transformed with the plasmid of interest was incubated overnight at 37°C on an orbital shaker (180 rpm). The cells were pelleted by centrifugation (10 min/ 5,000 × *g*), resuspended in Cell Resuspension solution and lysed in Cell Lysis solution. Neutralisation solution was added to the cell lysate and incubated for 3 min at RT. The flocculant was removed by passing the cell lysate through the PureYield Clearing column (3 min/ 1,500 × *g*), and the cleared lysate was applied to a PureYield Binding column, incubated for 1 min and eluted by centrifugation (3 min/ 1,500 × *g*).

2.6 Cell culture

The murine neuroblastoma cell line, Neuro-2a, and human embryonic kidney cell line, HEK293, were both obtained from the American Type Culture Collection (Manassas, VA, USA). Neuro-2a cells were used in this PhD research because they have a neuronal origin, are able to be transfected to relatively high efficiencies using standard lipid-based protocols (see Figure 3.1), and they can be differentiated into neuron-like cells (Tremblay et al. 2010). Neuro-2a, HEK293 and the HSE:EGFP stable cell lines (see section 5.2.6) were cultured in DMEM/F-12 supplemented with 2.5 mM L-glutamine and 10% FCS (10% FCS-DMEM/F-12) at 37°C under 5% CO_2/95% air in a Heracell 150i CO_2 incubator (Thermo Fisher Scientific). Cells were passaged every 2 days or once they had reached 80% confluency. Details regarding the transfection of established cells lines are explained in the relevant sections of this thesis.

2.7 Immunoblotting

2.7.1 Cellular protein extraction and protein quantification

In some experiments, following transfection, cells were harvested, washed twice with PBS (5 min/ 300 × *g*/ RT) and total cellular protein was extracted by lysis with SDS extraction buffer [2% (w/v) SDS in 0.5 M Tris-HCl, pH 6.8, supplemented with 1 × Halt protease and phosphatase inhibitors] and heating at 95˚C for 5 min. Whole cell lysates were centrifuged (5 min/ 20,000 × *g*) to pellet the insoluble protein.

Bicinchoninic acid assays were performed to determine the protein concentrations of the soluble cell extracts using a standard 96-well plate format as described elsewhere (Redinbaugh and Turley 1986). Protein concentrations were adjusted with PBS (pH 7.4) so that equal quantities of total protein were loaded onto SDS-PAGE gels for subsequent immunoblotting.

2.7.2 SDS-PAGE

Protein samples were prepared in an appropriate volume of 3 × loading buffer [final concentrations: 2% (w/v) SDS, 0.5 M Tris-HCl, 25% (w/v) glycerol, 0.01% (w/v) bromophenol blue, 5% (v/v) β-mercaptoethanol]. Reduced samples were denatured by heating at 95°C for 5 min. Precision Plus Protein™ dual colour molecular weight standards (10-250 kDa; Bio-Rad) were run on each gel. SDS-PAGE was conducted using a 12% (v/v) polyacrylamide resolving gel overlaid with a 4% (v/v) polyacrylamide stacking gel following standard procedures (Laemmli 1970) using a Mini-Protean Tetra cell system (Bio-Rad). Samples were electrophoresed at 150 V until the bromophenol blue dye front had migrated to the bottom of the gel. SDS-PAGE gels were stained with Coomassie blue staining solution and destained in destaining solution.

2.7.3 Immunoblotting and detection

SDS protein extracts were electroblotted onto an ImmunoBlot™ polyvinylidene difluoride membrane (PVDF; Bio-Rad) using a standard technique (Towbin et al. 1979). Briefly, protein transfer to the PVDF membrane was performed in ice-cold immunoblotting transfer buffer (0.192 M glycine, 25 mM Tris, 20% (v/v) methanol, pH 8.6) at 100 V for 90 min. Membranes were blocked with 5% (w/v) non-fat milk in Tris-buffered saline (TBS; 50 mM Tris and 150 mM NaCl, pH 7.5) supplemented with 0.05% (v/v) Tween-20 (TBS-T) for 1 h at RT. Membranes were incubated at 4˚C overnight with 5% (w/v) non-fat dry milk in TBS-T and primary antibodies. The blots were washed four times for 10 min with TBS-T, incubated in 5% (w/v) non-fat dry milk in TBS-T with the corresponding horseradish peroxidase (HRP)-conjugated secondary antibody for 1 h at RT, and washed again in TBS-T four times for 10 min. The labelled proteins were detected using SuperSignal® West Pico Chemiluminescent Substrate or SuperSignal® West Dura Extended Duration Chemiluminescent Substrate according to the manufacturer's instructions (Thermo Fisher Scientific). The membrane was exposed to Amersham Hyperfilm ECL (GE Healthcare Life Sciences) and developed according to a standard technique or imaged using the Amersham GelImager600 (GE Healthcare Life Sciences).

2.8 Immunocytochemistry

2.8.1 Fixing, permeabilisation, and immunolabelling

Cells were fixed in 4% (w/v) paraformaldehyde for 15 min either in suspension for flow cytometry or in a monolayer on a coverslip for epifluorescence and confocal microscopy. Cells were washed twice in PBS (pH 7.4) and then permeabilised and blocked in 5% (v/v) normal goat or donkey serum (or BSA) and 0.1% (v/v) TritonX-100 in PBS (PBS-T) for 1 h at RT. Cells were then incubated with primary antibodies diluted in 5% (v/v) normal goat or donkey

serum or BSA in PBS-T for 16 h at 4°C. The cells were washed three times in PBS for 5 min, incubated with secondary antibodies for 1 h at room temperature, and washed three times with PBS for 5 min. Cells destined for epifluorescence or confocal microscopy were counterstained with DAPI or Hoescht 33342 (where indicated), 1:1000 dilution in PBS for 10 min at room temperature and washed three times in PBS for 5 mins. Coverslips were mounted onto 26 × 76 mm glass slides (Thermo Fisher Scientific) using Citifluor™ Anti-Fadent Mounting Solutions (ProSciTech) for epifluorescence or confocal microscopy.

2.8.2 Microscopy

The slides were analysed using a Leica TCS SP5 confocal microscope using the 63× oil-immersion objective lens (Leica Microsystems, Wetzlar, Germany). Fluorescence was excited at 488 nm, 561 nm and 633 nm by argon, DPS 561 and He633 lasers, respectively. Fluorescent emissions from fluorophore-conjugated secondary antibodies were acquired by sequential scanning using the Leica Application Suite – Advanced Fluorescence (LAS-AF) software (version 3, Leica Microsystems, Wetzlar, Germany).

2.9 Flow cytometry

Flow cytometry was performed using an LSR Fortessa X-20 cell analyser equipped with 405 nm, 488 nm, 561 nm and 640 nm lasers (BD Biosciences). A minimum of 20,000 events per sample were collected at a high flow rate. Forward scatter was collected using a linear scale and side scatter in a log scale. Fluorescent emissions were collected as area (log scale), pulse height (log scale), and pulse width (linear scale) for each channel. The acquisition parameters (*i.e.* excitation laser and filter) for the fluorescence emissions of each fluorophore or fluorescent protein analysed in this research are listed in Table 2-1.

Table 2-1. Table of fluorophores and fluorescent proteins and the lasers and filters used to excite and collect their respective fluorescent emission.

Fluorophore/ Fluorescent protein	Laser (nm)	Filter (nm)
Cerulean	405	450/50
GFP EGFP tGFP DyLight 488	488	525/50
mCherry tdTomato	561	586/15
DyLight 650 RedDot1 RedDot2	640	670/30

Spectral compensation, gating and data analysis of events acquired by flow cytometry was performed using Flow Jo software (Tree Star).

2.9.1 Pulse shape analysis (PulSA)

PulSA was performed as previously described (Ramdzan et al. 2013). Briefly, area, height and width fluorescent emissions for the fluorescently-tagged protein were collected using the excitation lasers and bandpass filters outlined in Table 2-1. Plotting fluorescence height against width allows (in some cases) the identification of a population of cells with inclusions in the upper left portion of the cytogram.

2.10 Statistics

Results shown are the mean ± S.E.M. of three independent experiments unless otherwise indicated. Evaluation of differences in means was determined by a student's t-test, a one-way analysis of variance (ANOVA) or two-way ANOVA for multiple comparisons. The F-statistic from the ANOVA test and its associated degrees of freedom (between groups and within groups, respectively) are reported in parentheses. The *P*-value from the ANOVA test is also stated. Post hoc testing of differences between means was done using Dunnett's, Tukey's or Bonferroni's test, where appropriate, using GraphPad Prism 5 (GraphPad Software, Inc., La Jolla, CA, USA).

Chapter 3: Using bicistronic constructs to evaluate the chaperone activities of heat shock proteins in cells

Portions of this chapter have been previously published in the following work:

R. San Gil, T. Berg, and H. Ecroyd. Using bicistronic constructs to evaluate the chaperone activities of heat shock proteins in cells. *Scientific Reports*. 2017; 7: 2387.

Author contributions: RSG designed and performed experiments and analysed the data. TB contributed to the construct generation and validation experiments. HE developed the original idea to use bicistronic constructs to study Hsps, designed experiments, oversaw their implementation, and analysed the data. RSG wrote the manuscript and generated the figures; and all authors edited the manuscript for submission.

3.1 Introduction

The functions of many proteins have been studied by tagging them to a fluorescent protein. Hsps are dynamic (and often oligomeric) proteins that interact with various co-factors and client proteins. For example, some sHsps, such as αB-c and Hsp27, form large and polydisperse homo- and hetero-oligomers with other sHsps, and undergo dynamic subunit exchange, features that are thought to be fundamental to their chaperone activity (Haslbeck et al. 2005, Houck and Clark 2010). There is evidence to show that the addition of a fluorescent tag can compromise Hsp activity (Datskevich et al. 2012, Datskevich and Gusev 2014, Datskevich et al. 2015). Since fluorescently labelled Hsps can show aberrant structure and function compared to the non-tagged protein, an alternative technique is needed for studying Hsp function in cells.

There is a clear need to develop strategies to evaluate and compare Hsp functions in cells that take into account differences in transfection efficiencies, and avoid the use of bulky fluorescent proteins to label them. With this in mind, bicistronic vectors were exploited to develop a suite of mammalian expression constructs for the correlated expression of non-labelled Hsps and a fluorescent reporter protein (*e.g.* enhanced green fluorescent protein, EGFP, or mCherry). The Hsp-encoding constructs generate bicistronic mRNA with an internal ribosomal entry site (IRES) between the multiple cloning site and the fluorescent reporter gene (Jespersen et al. 1999). Translation of this mRNA results in the expression of two separate proteins, the Hsp of interest and the fluorescent reporter.

Using these Hsp-encoding bicistronic constructs, the capacity of a range of Hsps (Hsp90, Hsp70, Hsp40, Hsp27, and αB-c) to inhibit protein aggregation in a cell-based model was evaluated. The development of these bicistronic constructs provides a useful new tool to evaluate both the role of Hsps in the proteostasis network and their capacity to modulate a range of key cellular processes. This strategy also has applications beyond the field of

proteostasis, for example, the study of proteins in cells in which labeling with a fluorescent protein is not a viable option.

3.2 Methods

3.2.1 Antibodies

Dilutions and concentrations used for immunoblotting (IB) and immunocytochemistry (ICC) are included in parentheses. Mouse monoclonal anti-Hsp40 (ab78437; IB 1:5000, ICC 2 mg/mL), anti-Hsp90 (ab13492; IB 1:5000, ICC 1 mg/mL), anti-Hsp27 (ab2790; IB 1:2500, ICC 2 mg/mL), anti-αB-c (ab13496; IB 1:5000, ICC 1 mg/mL), anti-mCherry (ab125096; IB 1:2000) and IgG1-isotype control (ab91353; ICC 2 mg/mL) primary antibodies, and goat anti-mouse IgG DyLight 488 (ab96871; ICC 1:200) and goat anti-mouse IgG DyLight 650 (ab96874; ICC 1:200) conjugated secondary antibodies were obtained from Abcam (Cambridge, MA, USA). Mouse monoclonal anti-Hsp70 primary antibody (ADI-SPA-810-F; IB 1:1000, ICC 1 mg/mL) was from Enzo Life Sciences (Farmingdale, NY, USA). Mouse monoclonal anti-α-tubulin primary antibody (T8203; IB 1:5000) and rabbit polyclonal anti-mouse IgG-HRP conjugated secondary antibody (SAB3701084; IB 1:5000) were obtained from Sigma Aldrich.

3.2.2 Plasmids and cloning of Hsp-encoding bicistronic constructs

The pIRES2-EGFP plasmid was obtained from Clontech (Palo Alto, CA, USA). A series of constructs were generated from the pIRES2-EGFP plasmid that transcribes bicistronic mRNA consisting of an IRES flanked by an upstream Hsp and downstream fluorescent reporter. The mCherry gene (GenBank AY678264) was synthesised by GenScript with flanking 5′ *Bst*XI and 3′ *Not*I restriction sites to allow replacement of the EGFP in pIRES2-EGFP with mCherry to generate pIRES2-mCherry. Primers were designed to amplify genes encoding Hsps (with flanking restriction sites) from existing plasmid constructs for sub-cloning upstream of the IRES site of the pIRES2 plasmids; αB-c (*CRYAB*; GenBank NM_001885) with *Nhe*I/*Sal*I, HSP27 (*HSPB1*; GenBank BT019888.1) with *Bgl*II/*Sal*I, HSP70 (*HSPA1A*; GenBank

AK291295.1; gifted by Prof Sophie Jackson, Cambridge University, UK) with *Nhe*I/*Bam*HI. Genes encoding HSP40 (*DNAJ1*; GenBank NM_001539.2) with *Nhe*I/*Bam*HI sites, and HSP90 (HSP90AA1; GenBank NM_001017963.2) with *Sal*I/*Not*I sites, were synthesised by GenScript, prior to their digestion from the supplied pUC57 constructs and sub-cloning into pIRES2-mCherry. In addition to the Hsp-encoding bicistronic constructs, a plasmid was constructed with flanking *Bgl*II/*Eco*RI sites to encode for $EGFP^{inv}$ (Olshina et al. 2010), a non-fluorescent Y66L mutant of GFP, which was used in place of a Hsp in a bicistronic construct and acted as a chaperone-negative control. All the constructs synthesised in this work were verified by sequencing using a Hitachi 3130xl Genetic Analyser (Applied Biosystems, Mulgrave, Australia).

Mammalian expression constructs containing sequences encoding WT and the conformationally destabilised double mutant of firefly luciferase-EGFP ($Fluc^{WT}$-EGFP, pcDNA4-TO-myc-hisA-$Fluc^{WT}$; $Fluc^{DM}$-EGFP, pcDNA4-TO-myc-hisA-Fluc R188Q/R261Q respectively) were kind gifts from Prof Mark Wilson (University of Wollongong, Australia).

3.2.3 Neuro-2a cell culture and transfection

Neuro-2a cells were cultured as described in Section 2.6.

For transfections, 7.5×10^4 cells/mL were seeded (unless otherwise stated) into a 6-well plate and cultured in 2 mL of 10% FCS DMEM/F-12 overnight. These cells were transiently transfected with the bicistronic vectors using Lipofectamine LTX/PLUS reagent. Cells were transfected with DNA:lipid complexes (2 μg/well of DNA, 6 μL/well of Lipofectamine LTX and 2 μL/well PLUS reagent) and incubated for 48 h at 37˚C under 5% CO_2/95% air. The cells were harvested with trypsin 48 h post-transfection, washed twice with PBS (pH 7.4) and either fixed in 4% (w/v) paraformaldehyde in PBS at room temperature (RT) for 30 min, or live transfected cells were purified by fluorescence-activated cell-sorting for subsequent analyses.

To confirm that cells in the inclusion population (iPop), which were resolved by PulSA, did contain inclusions, cells were transfected to express $Fluc^{DM}$-EGFP and fixed in 1% (w/v) PFA in PBS (pH 7.4) for 30 min on ice. Samples were washed twice in PBS (5 min/ 300 × *g*) and resuspended in FACS buffer. Cells were sorted on a FACSAriaII equipped with a 488-nm laser (BD Biosciences, San Jose, CA, USA) at the MWAC BRIL Flow Cytometry Facility, University of New South Wales (Sydney, Australia).

3.2.4 Immunocytochemistry and confocal microscopy

A 12-well plate containing sterile 19 mm coverslips (ProSciTech, Thuringowa, Australia) was seeded with 4.0×10^4 cells/well and cultured in 10% FCS-DMEM/F-12 overnight at 37˚C under 5% CO_2/95% air. Cells were transfected with 1 µg/well of pIRES2-EGFP-αB-c DNA and 1.5 µLLipofectamine LTX with 0.5 µL PLUS reagent, and incubated for 48 h at 37˚C under 5% CO_2/95% air. Cell culture media was removed 48 h post-transfection and coverslips were washed twice with PBS (pH 7.4). Cells were fixed, permeabilised, immunolabelled and mounted for microscopy as described in Chapter 2, section 2.8.1.

3.2.5 Cell preparation for sorting

To purify $mCherry^{+ve}$ cells for subsequent immunoblotting, cells transfected with the Hsp-encoding bicistronic constructs were harvested with trypsin 48 h post-transfection. Samples were washed twice in PBS (pH 7.4; 5 min/ 300 × *g*) and resuspended in fluorescence-activated cell sorting (FACS) buffer (25mM HEPES, 1 mM EDTA, 0.5% w/v bovine serum albumin in PBS, pH 7.0). Cell clumps were removed by straining through a 40 µm nylon mesh before analysis on an S3e Cell Sorter equipped with a 561-nm laser (Bio-Rad Laboratories, Hercules, CA, USA). $mCherry^{+ve}$ cells were sorted such that 300,000 cells were recovered.

3.2.6 Immunoblotting

FACS-purified populations of mCherry^{+ve} cells were collected (10 min/ 1000 × *g*) and subsequently immunoblotted for Hsp, mCherry and α-tubulin expression in samples transfected with each of the Hsp-encoding bicistronic constructs. Whole cell lysates were prepared as described in section 2.7.1 for separation by SDS-PAGE (section 2.7.2). Proteins resolved by SDS-PAGE were subsequently immunoblotted (section 2.7.3).

3.2.7 Immunolabelling of Hsps in transfected Neuro-2a cells for flow cytometry

Cells were immunolabelled as described in section 2.8.1. Immunolabelled cells were resuspended in an appropriate volume of PBS for flow cytometry, section 2.9.

3.2.8 Image J single cell analysis

Fixed and immunolabelled cells were imaged by confocal microscopy and the fluorescent intensities of individual cells were analysed using Image J to determine the relative levels of the Hsp and fluorescent reporter protein. Images were converted into greyscale, 8-bit image and a threshold of 10 was applied. Images were further processed to remove speckles (despeckle tool) and separate cell clumps to identify individual cells (watershed tool). This sequence of processing events defines the cell outlines of individual cells. The same original image is opened again and converted into a greyscale, 32-bit image and the fluorescence intensity of single cells was measured (analyse particle tool; cell size, 100 – infinity; circularity, 0-1). This sequence of processing events was repeated for images taken in the green and red channel. To determine whether the level of fluorescent reporter expression (in this case EGFP) correlated with Hsp expression, a bivariate blot of EGFP and DyLight 650 mean fluorescence intensity was used.

3.2.9 Cell-based model of protein aggregation: Mutant firefly luciferase ($Fluc^{DM}$-EGFP)

A 6-well plate was seeded with 2.0×10^6 Neuro-2a cells/well and maintained in 10% FCS-DMEM/F-12 overnight at 37˚C under 5% CO_2/95% air. Cells were co-transfected with the $Fluc^{DM}$-EGFP encoding constructs (1.25 µg) and one of the Hsp-encoding (or $EGFP^{inv}$) pIRES2-mCherry constructs (0.25 µg), such that cells were transfected with a 5:1 ($Fluc^{DM}$-EGFP:Hsp) ratio of each construct. Each DNA construct was incubated in separate tubes with Lipofectamine LTX/PLUS reagent according to the manufacturer's instructions. The DNA:lipid complexes were sequentially applied to the cells. Cells were harvested with trypsin 48 h post-transfection, washed twice in ice-cold PBS (5 min/ 300 × *g*/ 4°C) and resuspended in 500 µL ice-cold PBS for analysis by flow cytometry.

Some cells were left untransfected or only transfected with $Fluc^{DM}$-EGFP- or $EGFP^{inv}$ encoding constructs. These samples were used to set gates and to determine the spectral overlap that occurs between mCherry and DyLight 488 fluorescence emissions in this experiment using the compensation matrix in Flow Jo (version 10.0.8, Tree Star, Ashland, OR, USA). The spectral overlap was negligible (0.0028% spectral overlap) in these experiments.

The relative EGFP fluorescence was used to represent $Fluc^{DM}$ levels in the cell. The data presented was analysed using equation 3.1:

$$Relative\ EGFP\ fluorescence = \frac{EGFP\ fluorescent\ median\ of\ Hsp\ sample}{EGFP\ fluorescent\ median\ of\ EGFPinv\ sample} \qquad (3.1)$$

The percent of cells in the iPop gate in each sample was normalised to the relative EGFP fluorescence in that sample. In this way, differences in the relative levels of $Fluc^{DM}$-EGFP expression were taken into account and data was analysed using equation 3.2:

$$\%\ cells\ in\ iPop\ normalised\ to\ mFluc\ levels\ = \frac{\%\ cells\ in\ iPop\ of\ sample\ x}{Relative\ EGFP\ fluorescence\ of\ sample\ x} \quad (3.2)$$

The data presented in Figure 3.8 is presented as a fold change compared to the average result for the EGFP^{inv} negative control sample across all three independent repeats of the experiment using equation 3.3:

$$Fold\ \Delta\ (\%\ cells\ with\ inclusions) = \frac{\%\ cells\ in\ iPop\ normalised\ to\ mFluc\ in\ sample\ x}{Average\ \%\ cells\ in\ iPop\ in\ EGFPinv\ (n=3)} \quad (3.3)$$

This method of normalising data maintains the standard error in the EGFPinv control samples such that the dataset is normally distributed and satisfies the criteria of a one-way ANOVA for statistical analysis.

3.2.10 Flow cytometry

See section 2.9 and 2.9.1 for methods relating to standard flow cytometry and PulSA of cells.

3.2.11 Statistics

See section 2.10. With respect to binning of mCherry fluorescence into 16 bins of equal relative fluorescence intensity (40 RFU), bins containing less than 100 cells were excluded from subsequent analysis.

3.3 Results

3.3.1 Validation of correlated Hsp and fluorescent reporter expression from bicistronic constructs

A new approach was developed to study the ability of Hsps to prevent protein aggregation in live cells that avoided some of the limitations of previous work (*i.e.* tagging Hsps with fluorescent proteins which can affect structure, dynamics and function; inability to take into account differences in co-transfection efficiencies between plasmids; lack of information regarding the expression levels of the Hsps in individual cells). An experimental set-up where the Hsp and a fluorescent reporter protein are expressed from two separate plasmids is one possible approach. Figure 3.1 shows that cells co-transfected to express mCherry and EGFP have correlated expression of both proteins. However, to simplify the experimental design, the use of bicistronic vectors was considered for the simultaneous expression of an Hsp and fluorescent reporter from a single construct. Since both proteins are translated from the same mRNA transcript, the transcription of which is driven by a single promoter, this approach has the potential to overcome the need to transfect cells with an additional plasmid.

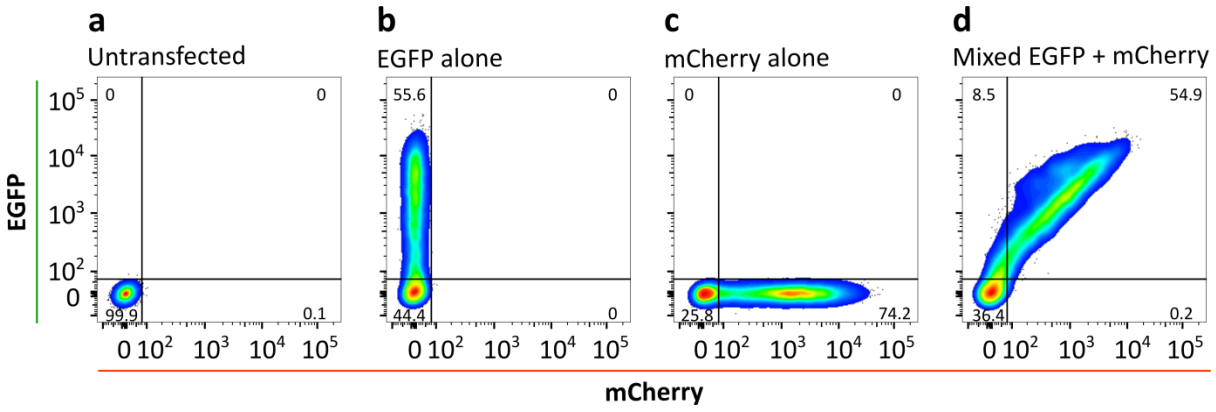

Figure 3.1. Co-transfection of cells with two constructs as an alternative approach to using bicistronic constructs. Neuro-2a cells were either (a) untransfected or transfected with (b) pIRES2-EGFP^{inv}-EGFP or (c) pIRES2-EGFP^{inv}-mCherry, or (d) co-transfected by mixing the two constructs together with transfection reagent. The co-transfected cells (54.9%) showed a high correlation between EGFP and mCherry expression (*e.g.* cells with high expression levels of EGFP also show high mCherry fluorescence).

Immunoblot analysis was performed to confirm the over-expression of the Hsp of interest and fluorescent reporter (in this case mCherry) in Neuro-2a cells transfected with one of the Hsp-encoding pIRES2-mCherry constructs. Immunoblot analysis of cells transfected with each of the pIRES2-mCherry constructs encoding Hsp40, Hsp70, Hsp90, Hsp27 and αB-c showed that the Hsp and mCherry were expressed in these cells (Figure 3.2). With the exception of Hsp40 and Hsp90, no endogenous Hsp expression was detected in untransfected Neuro-2a lysates (Figure 3.2).

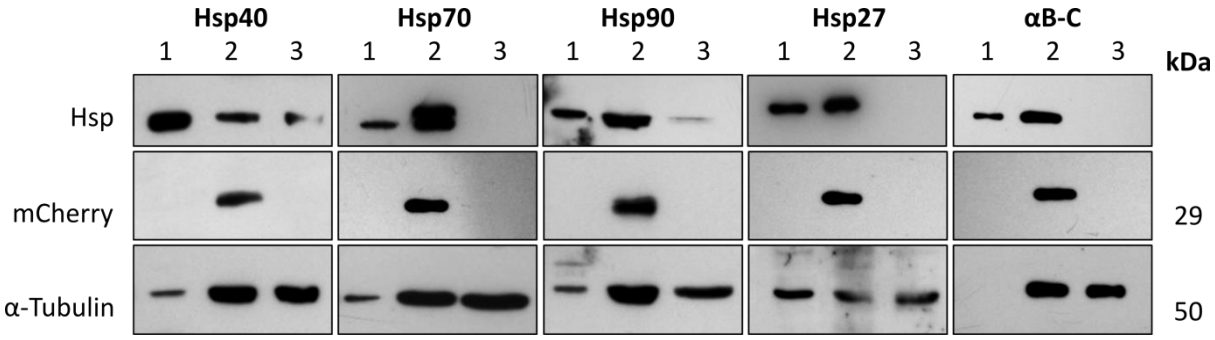

Figure 3.2. Immunoblot analysis of Hsp and mCherry expression in Neuro-2a cells transfected with one of the Hsp-encoding pIRES2-mCherry bicistronic constructs. Neuro-2a cells transfected with one of the Hsp-encoding bicistronic constructs were sorted by FACS such that a population of mCherry^{+ve} cells were purified and whole cell lysates, equivalent to 100,000 cells, were loaded into each well. The membranes were probed for α-tubulin (50 kDa), mCherry (29 kDa) and Hsp40, Hsp70, Hsp90, Hsp27, and αB-c. Protein samples analysed were (1) positive control sample consisting of either 10 µg of heat-shocked HeLa cell lysate (42°C, 2 h with a 37°C, 3 h recovery period) or 5 ng purified recombinant αB-c for blots probing for αB-c, (2) whole cell lysates from cells transfected with the corresponding Hsp-encoding bicistronic construct, and (3) untransfected cells.

The correlated expression of the non-labeled Hsp and fluorescent reporter was tested in cells transfected with the bicistronic constructs, since this would enable the fluorescence intensity of the fluorescent protein to be used as a reporter of intracellular Hsp levels. Neuro-2a cells were transfected with an Hsp-encoding bicistronic construct and intracellular Hsps were immunolabelled with specific primary and DyLight 488 (or in the case of the pIRES2-EGFP-Hsp constructs DyLight 650)-conjugated secondary antibodies and subsequently analysed by flow cytometry and confocal microscopy (Figure 3.3).

To exclude cellular debris and cell clumps from the flow cytometric analysis, a polygonal gate was used to identify viable cells based on a plot of forward and side scatter (Figure 3.3a). Quadrant gating based on the untransfected and unlabeled sample (*i.e.* DyLight 488^{-ve}: mCherry^{-ve}) was used to establish background fluorescence (Figure 3.3b). Low levels of DyLight 488 fluorescence were observed in untransfected cells immunolabelled for αB-c, indicating that these cells express low levels of endogenous αB-c (Figure 3.3c). Samples incubated with an isotype (IgG) species-matched control primary antibody exhibited no DyLight 488 fluorescence, confirming no non-specific binding had occurred in the labeling process (Figure 3.3d). Cells transfected with the pIRES2-mCherry-αB-c construct were positive for both DyLight 488 and mCherry fluorescence and there was a strong correlation in the expression of these two proteins (Figure 3.3e). Likewise, levels of Hsp27 and Hsp70 correlated well with levels of mCherry fluorescence in transfected cells (Figure 3.4). Whilst the levels of Hsp40 and Hsp90 and fluorescent reporter were correlated in cells, this correlation was weaker than for the other Hsps tested (Figure 3.4). This may be due to Hsp40 and Hsp90 both being endogenously expressed in Neuro-2a cells, whereas Hsp27, αB-c and Hsp70 are not expressed at levels detectable by immunoblotting in untransfected Neuro-2a cells (see Figure 3.2 and Figure 3.4a). Similarly, confocal microscopy of Neuro-2a transfected with pIRES2-EGFP-αB-c also demonstrated a strong correlation between the expression of αB-c and EGFP reporter protein (Figure 3.3f-i). Confocal microscopy also showed that αB-c and EGFP were not fused because EGFP was localized in the nucleus and cytoplasm, whereas αB-c was only observed in the cytoplasm.

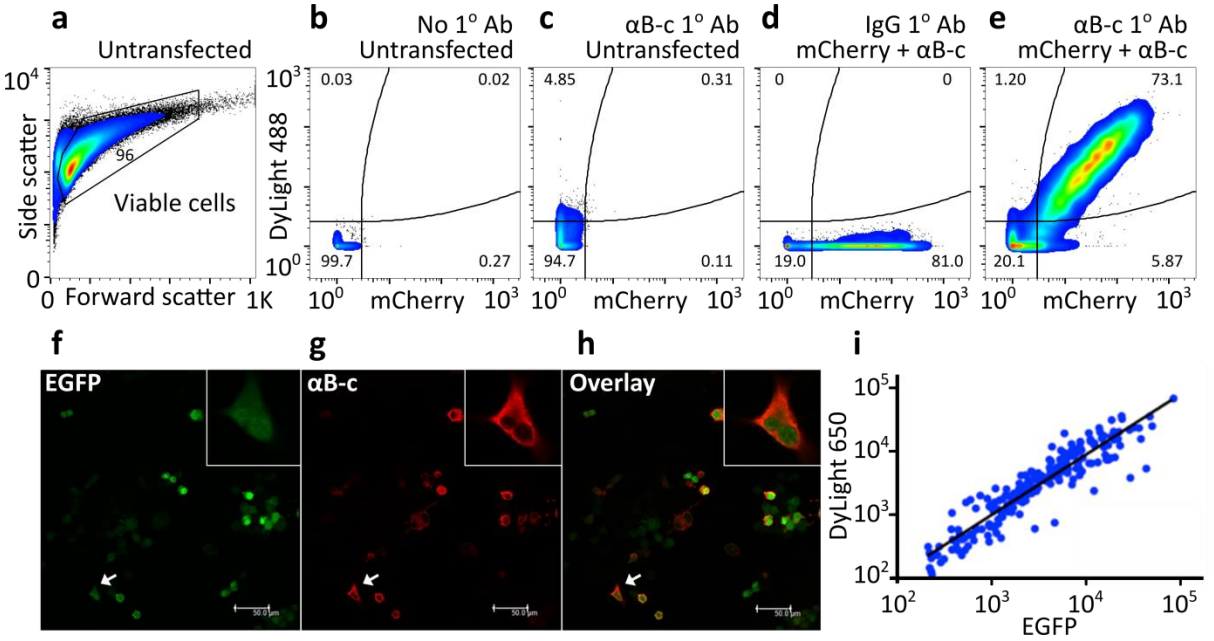

Figure 3.3. Validating the correlated expression of an Hsp and fluorescent reporter protein in transfected Neuro-2a cells. (a)-(e) Flow cytometric analysis of αB-c and mCherry protein expression in pIRES2-mCherry-αB-c transfected Neuro-2a cells. Data are presented as pseudo-colour plots where blue depicts – low, green – medium and red – high frequency of cells. Outliers are shown as black dots. (a) The untransfected sample was used to set gates for the viable cell population to exclude cellular debris and cell clumps. (b) Quadrant gating of DyLight 488 and mCherry fluorescence was based on untransfected and unlabeled cells. (c) Untransfected cells were immunolabelled with anti-αB-c and DyLight 488-conjugated secondary antibodies. Cells transfected with pIRES2-mCherry-αB-c were immunolabelled with (d) species-matched IgG isotype control antibody to determine background staining and (e) anti-αB-c and DyLight 488 conjugated secondary antibodies. (f)-(i) Immunofluorescence microscopy to analyse the expression of αB-c and EGFP following transfection of Neuro-2a cells with pIRES2-EGFP-αB-c. Intracellular αB-c was immunolabelled using anti-αB-c primary and anti-mouse IgG DyLight 650 conjugated secondary antibodies. Coverslips were mounted onto glass slides and emissions from (f) EGFP and (g) DyLight 650 were acquired. (h) The overlay of EGFP and DyLight 650 emissions is also presented. Insets show magnification of the cell identified by the arrow. Scale bar = 50 µm. (i) EGFP and DyLight 650 fluorescence levels of individual cells based on the confocal data.

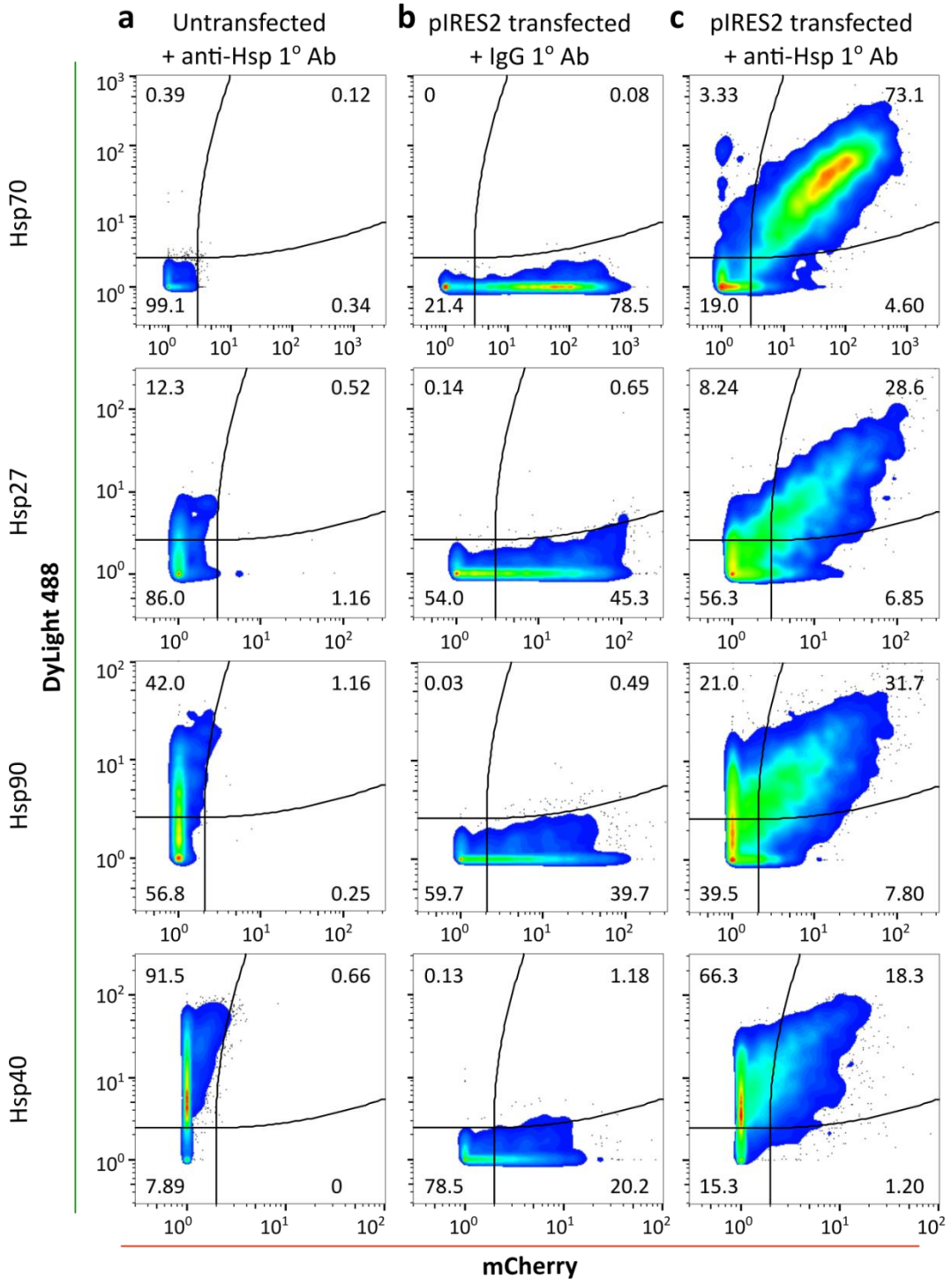

Figure 3.4. Flow cytometric verification of the correlated expression of mCherry and each of the Hsps in individual cells following transfection of cells with each of the Hsp-encoding bicistronic constructs. Cellular debris and cell clumps were excluded based on forward and side scatter (see Figure 3.3a) such that subsequent analysis was only performed on viable cells. Quadrant gating of DyLight 488 and mCherry fluorescence was based on untransfected and unlabelled cells (see Figure 3.3b). (a) Untransfected cells were immunolabelled with anti-Hsp40/Hsp70/Hsp90/Hsp27/αB-c primary (1°) antibody and DyLight 488 conjugated secondary antibody. (b) Cells were transfected with each of the Hsp-encoding bicistronic constructs and immunolabelled with species-matched IgG control to account for background primary antibody staining. (c) Cells were transfected with each of the Hsp-encoding bicistronic constructs and subsequently immunolabelled with the respective anti-Hsp40/Hsp70/Hsp90/Hsp27/αB-c primary antibody and DyLight 488 conjugated secondary antibody. Note the scale across the cytograms in this figure varies between panels.

3.3.2 Cell-based Fluc^{DM}-EGFP aggregation assay

To assess the relative ability of each Hsp to prevent the aggregation of proteins into inclusions in cells, a conformationally destabilised form of firefly luciferase, C-terminally tagged with EGFP (R188Q/R261Q; Fluc^{DM}-EGFP), was used as an aggregation-prone protein (Gupta et al. 2011b). This isoform of firefly luciferase has previously been shown to form cytosolic inclusion bodies in HeLa cells when cultured at 37°C (Gupta et al. 2011b). Importantly, in these co-transfection experiments, the Fluc^{DM}-EGFP-encoding plasmid and the Hsp-encoding IRES plasmid were added separately to cells (*i.e.* each DNA:lipid complex was made up separately and then added to the cells, instead of mixing the two plasmids together prior to making the DNA:lipid complexes). This is because when the plasmids are first mixed and then DNA:lipid complexes are made and applied to cells there is a very strong correlation in the expression of proteins from both plasmids (Figure 3.1d) such that the majority of cells that express high levels of Fluc^{DM}-EGFP also express high levels of the Hsp. Making separate DNA:lipid complexes for both plasmids and then adding these to cells resulted in a greater range in the relative expression of proteins from both plasmids in the population (*i.e.* a range of levels of Hsp expression at a given level of Fluc^{DM}-EGFP expression; Figure 3.5). In this way, cells were randomly either singly transfected, co-transfected, or untransfected, and co-transfected cells have low, medium and high levels of a given Hsp.

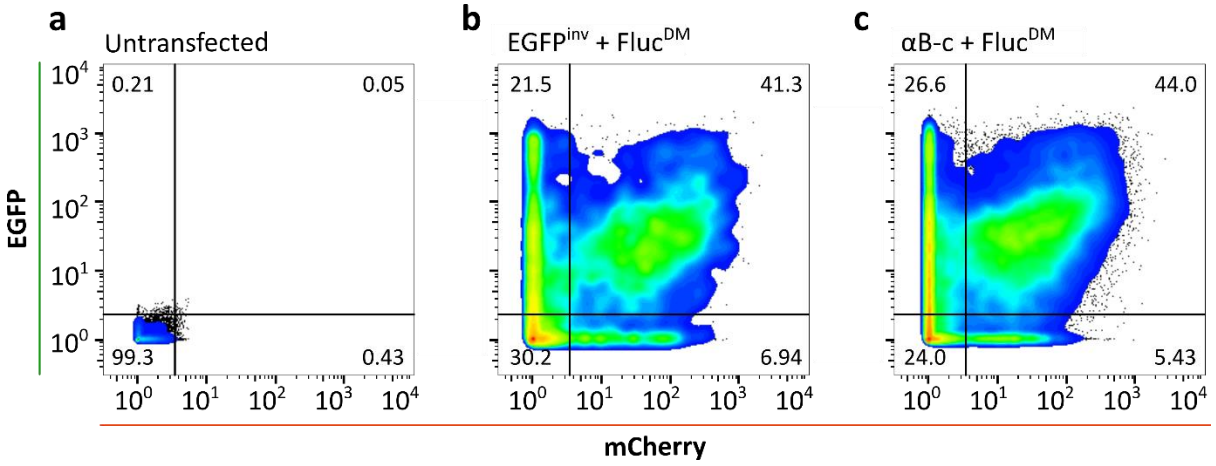

Figure 3.5. Co-transfections in Neuro-2a cells for the Fluc^{DM}-EGFP cell-based model of protein aggregation. With regard to analyses involving mCherry binning, we attempted to overcome the likelihood that cells expressing high levels of Hsp also express high levels of Fluc^{DM} by preparing the constructs separately for transfection and applying them to the cells sequentially. In this way, cells were randomly either, singly transfected, co-transfected, or untransfected. Whilst this methodology for the co-transfections still resulted in a weak correlation between Hsp and Fluc^{DM} expression, it resulted in a greater range in the expression levels of both proteins compared to the method involving mixing the plasmids prior to making the DNA:lipid complexes (see Figure 3.1). Representative cytograms are shown of Neuro-2a cells that were either (a) untransfected, or co-transfected to express (b) EGFPinv with mCherry and Fluc^{DM}-EGFP and (c) αB-c with mCherry and Fluc^{DM}-EGFP. Quadrant gating was based on the untransfected sample and the proportion of cells in each quadrant is shown.

Neuro-2a cells were co-transfected with one of the Hsp-encoding bicistronic constructs and the Fluc^{DM}-EGFP-encoding construct, and the cells incubated for 48 h prior to analysis by flow cytometry. Cellular debris and cell clumps were excluded from subsequent analyses using forward and side scatter signals (as in Figure 3.3a). The untransfected sample was used as an EGFP^{-ve} and mCherry^{-ve} population to identify EGFP^{+ve} and mCherry^{+ve} cells (Figure 3.6a-b). Sub-populations of cells with Fluc^{DM}-EGFP inclusion bodies (iPop) were detected using flow cytometry-based PulSA. PulSA can resolve populations of cells with fluorescent inclusions when this leads to a change in the fluorescent pulse-shape of the cell (reduced fluorescent pulse width and increased fluorescent pulse height) compared to cells lacking inclusions. It was confirmed by cell sorting and imaging that a higher proportion of cells in the iPop contained Fluc^{DM}-EGFP inclusions compared to those in the non-inclusion population (niPop), which did not contain inclusions (Figure 3.7). Cells with inclusions were defined by bright fluorescent EGFP puncta and cells without inclusions were identified by their diffuse distribution of EGFP.

Analysing cells via PulSA demonstrated that only a minor (2%) proportion of cells expressing the stable Fluc^{WT}-EGFP isoform contained inclusions (Figure 3.6c), whereas the proportion of cells containing inclusions increased (to > 10%) when they expressed Fluc^{DM}-EGFP (Figure 3.6d).

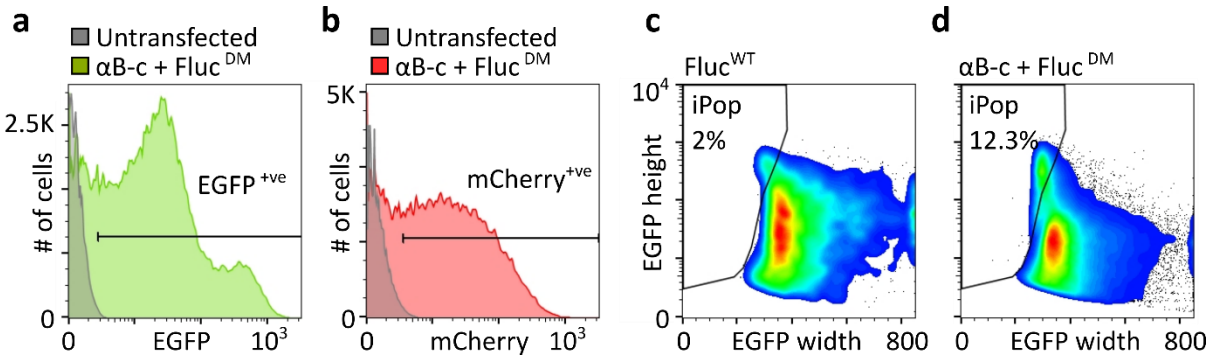

Figure 3.6. Gating strategy used to examine the effect of Hsp over-expression on Fluc^{DM}-EGFP inclusion body formation in cells. (a)-(d) Gating strategy employed to analyse flow cytometric data from Neuro-2a cells co-transfected to express Fluc^{DM}-EGFP and one of the Hsps (or a control protein, EGFPinv) with a mCherry reporter. Untransfected cells were used to set gates for (a) EGFP^{+ve} and (b) mCherry^{+ve} cells. Representative samples co-transfected with the pIRES2-mCherry-αB-c and Fluc^{DM}-EGFP constructs are shown in the histogram overlays with the untransfected sample in (a) and (b). Cells expressing Fluc^{WT}-EGFP (c) were used to set the iPop gate and (d) the population of viable, EGFP^{+ve} and mCherry^{+ve} cells with Fluc^{DM}-EGFP inclusions (iPop) was resolved by PulSA using plots of EGFP fluorescence height versus width.

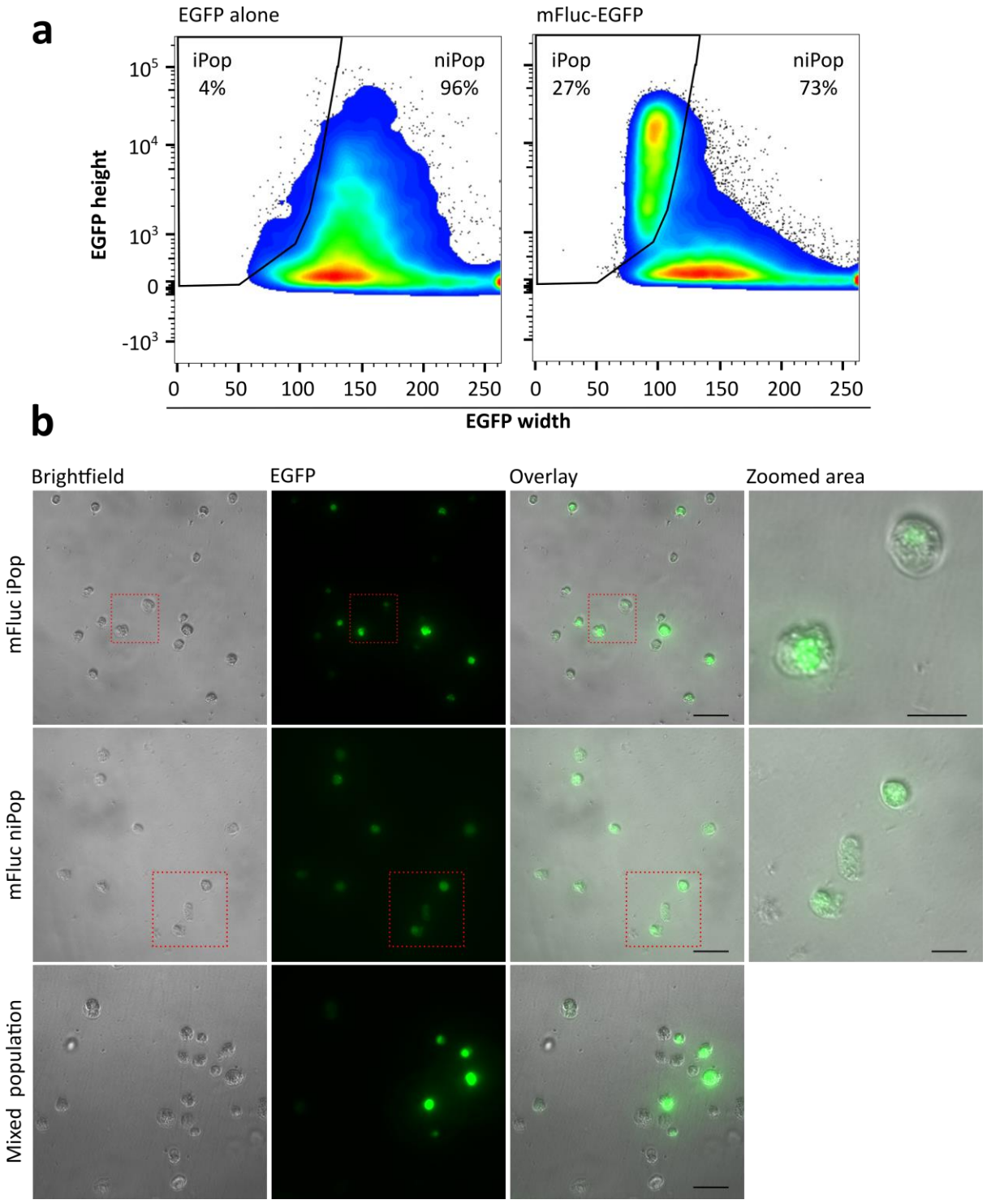

Figure 3.7. Fluorescence activated cell sorted iPop and niPop populations. Neuro-2a cells were transfected to express either EGFP alone or Fluc^{DM}-EGFP, fixed 48-hours post-transfection and sorted for fluorescence microscopy. (a) PulSA of cells expressing EGFP alone (left) and Fluc^{DM}-EGFP (right). Cells expressing EGFP alone were used to set the iPop polygonal gate. (b) Representative images are shown of the sorted iPop, niPop and the mixed cell population prior to FACS. Left – right: brightfield images, EGFP fluorescence, the overlay and a zoomed region of interest denoted by the red dashed square. Scale bar = 50 µm and 20 µm in the zoomed images.

To assess the impact Hsps had on the proportion of cells with inclusions, three methods were employed to analyse the data (Figure 3.8). First, only cells expressing Fluc^{DM}-EGFP were taken into account (Figure 3.8a and c), a strategy that is indicative of the type of data analysis that is performed in assays where the Hsp is not fluorescently labeled. This approach demonstrated that there was no significant effect of over-expressing different Hsps on the proportion of cells with Fluc^{DM}-EGFP inclusions [F (6, 14) = 1.631, P = 0.2109]. There was a small reduction in the proportion of cells with Fluc^{DM}-EGFP inclusions that were co-transfected to express Hsp40, Hsp70 or Hsp40 + Hsp70, compared to those cells co-transfected to express EGFP^{inv}, however, post hoc comparisons using Dunnett's test showed that these differences were not statistically significant. In contrast, expression of Hsp90, Hsp27 or αB-c had a negligible effect on the proportion of cells with Fluc^{DM}-EGFP inclusions (Figure 3.8c). When an alternative analysis strategy that takes into account differences in co-transfection efficiencies between the Hsp-encoding constructs was applied (*i.e.* analysis of EGFP^{+ve} and mCherry^{+ve} cells; Figure 3.8b and d), one-way ANOVA indicated that there is a significant effect of Hsp expression on Fluc^{DM}-EGFP inclusion formation [F (6, 12) = 12.43, P = 0.0002]. There was a significant increase in the fold change of cells with Fluc^{DM}-EGFP inclusions in samples co-expressing Hsp90, compared to those co-expressing EGFP^{inv}. The expression of Hsp40, Hsp70, or Hsp40 + Hsp70 resulted in a small (but not statistically significant) decrease in the proportion of cells with Fluc^{DM}-EGFP inclusions, compared to those expressing EGFP^{inv}. Expression of Hsp27 or αB-c had a negligible effect on the proportion of cells with inclusions.

Previous studies have demonstrated that high levels of expression of aggregation-prone proteins are strongly correlated with an increased propensity for inclusion body formation (Arrasate et al. 2004, Ormsby et al. 2013, Ramdzan et al. 2013). Therefore, differences in the levels of Fluc^{DM}-EGFP expressed in cells upon co-transfection with the Hsp-encoding constructs were examined (Figure 3.8e). One-way ANOVA analysis demonstrated that the

median EGFP fluorescence intensity varied significantly between samples co-expressing different Hsps [F (6,12) = 10.72, P = 0.0003]. Co-transfection with the Hsp40 or Hsp90 bicistronic constructs resulted in a significant increase in the levels of Fluc^{DM}-EGFP in co-transfected cells compared to those co-transfected to express EGFP^{inv}. Therefore, higher levels of Fluc^{DM}-EGFP in the Hsp40 and Hsp90 samples could result in higher levels of aggregation in these cells thus, obscuring the effects of the expression of Hsps. Indeed, analysis of cells co-transfected to express Hsp90 and Fluc^{DM}-EGFP show a significant increase in the proportion of cells with inclusions (Figure 3.8d) and this correlates with a significantly higher expression of Fluc^{DM}-EGFP in this sample (Figure 3.8e).

These differences in the relative levels of Fluc^{DM}-EGFP expression were taken into account when analysing the aggregation-propensity of Fluc^{DM} in cells by normalising the percent of cells with inclusions with Fluc^{DM} levels (*i.e.*, EGFP median fluorescence intensity; equation 3.2; Figure 3.8f). There was a significant effect of Hsp expression on the population of cells with Fluc^{DM}-EGFP inclusions [F (6,12) = 7.406, P = 0.0017]. The expression of Hsp40, Hsp70 or Hsp40+Hsp70 significantly reduced the population of cells with Fluc^{DM}-EGFP inclusions compared to the cells expressing EGFP^{inv}. Whilst the expression of Hsp90, Hsp27 or αB-c reduced the population of cells with Fluc^{DM}-EGFP inclusion bodies, this was not statistically significant.

We found that the raw percent of cells with inclusions varied between biological replicates (Appendix B). This could be the result of numerous factors, for example, cell passage number and cell density. Another factor that could lead to variability is that the instability of mFluc-EGFP, which leads to its formation of inclusion bodies, is highly dependent on temperature (Gupta et al. 2011a). Therefore, any temperature fluctuations throughout the post-transfection incubation period could influence inclusion body formation across three experiments. Despite

the differences in the raw percent of cells in the iPop gate, the trends across the Hsp expressing samples remained constant between experiments. Therefore, the data in Figure 3.8 is expressed as a fold change rather than a raw percent to better reflect the chaperone activities of the Hsps in this assay.

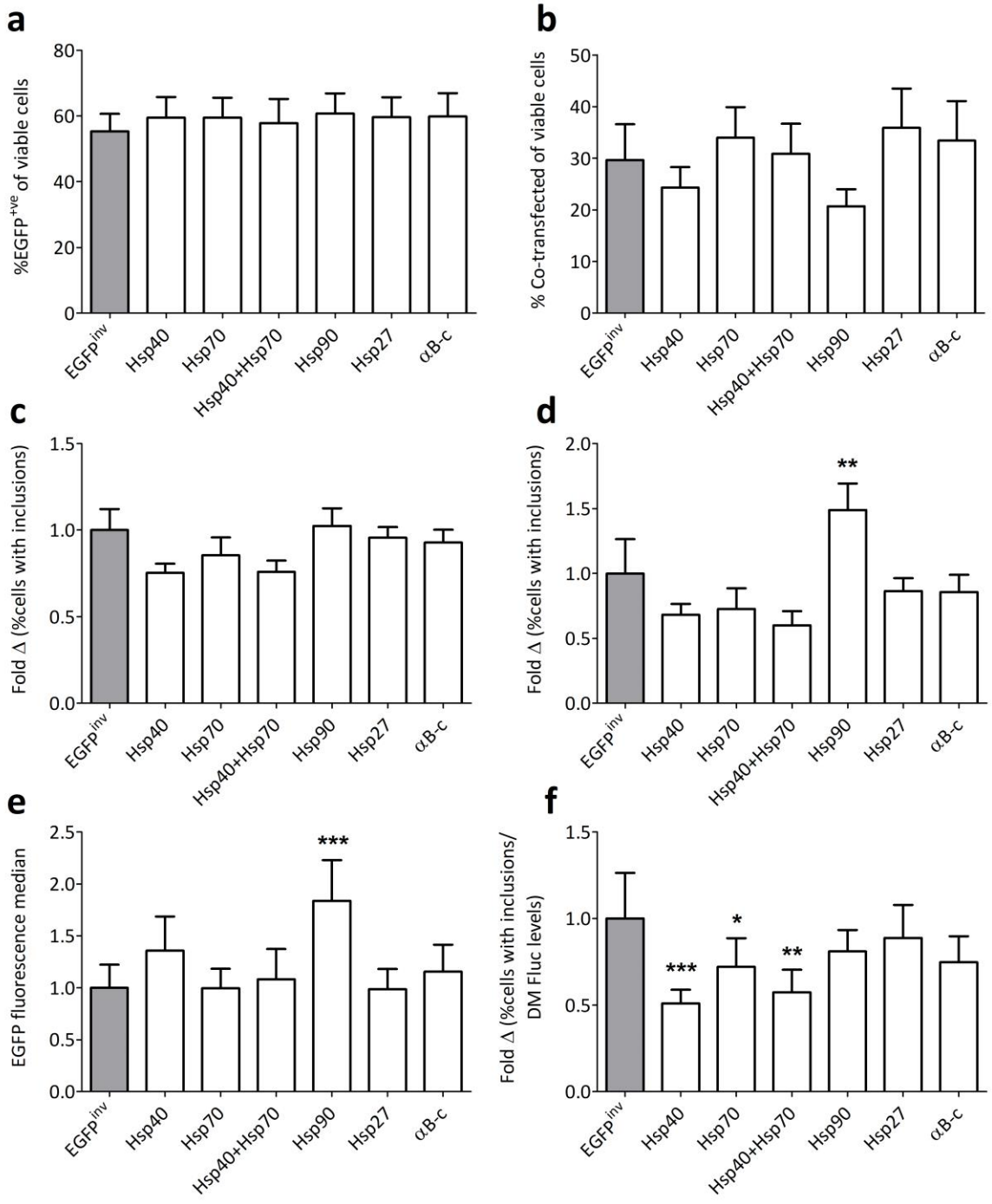

Figure 3.8. Using Hsp-encoding bicistronic constructs to examine the effect of Hsp over-expression on Fluc^{DM}-EGFP inclusion body formation in cells. (a) The percent of EGFP^{+ve} cells of the viable cell population. (b) The percent of co-transfected cells (ie. EGFP^{+ve} and mCherry^{+ve}) of the viable cell population. (c)-(f) show a

comparison of three strategies used to analyse the proportion of cells containing $Fluc^{DM}$-EGFP inclusion bodies in the iPop. (c) The proportion of cells with $Fluc^{DM}$-EGFP inclusions when only viable and $EGFP^{+ve}$ cells were taken into account. (d) The proportion of cells with $Fluc^{DM}$-EGFP inclusions when viable and co-transfected cells (*i.e.* $EGFP^{+ve}$ and $mCherry^{+ve}$) were analysed. (e) The average relative EGFP fluorescence in cells as a measure of $Fluc^{DM}$-EGFP expression levels. (f) The proportion of cells with $Fluc^{DM}$-EGFP inclusions normalised to the levels of $Fluc^{DM}$-EGFP in cells (based on relative EGFP fluorescence levels). In all graphs, data are reported as the fold difference relative to the chaperone-negative control, $EGFP^{inv}$. Data presented are the means + SEM of three independent replicates. Differences between the means were assessed using a one-way ANOVA followed by a Dunnett's post-hoc test, where $P < 0.05$ (*), $P < 0.01$ (**) and $P < 0.001$ (***).

3.3.3 Hsp70 and Hsp70+Hsp40 inhibit protein aggregation in a concentration-dependent manner

The correlation between the levels of Hsps and the fluorescent reporter in cells was exploited in order to investigate the effect of increasing Hsp levels on the proportion of cells with $Fluc^{DM}$-EGFP inclusions. To do so, cells co-expressing an Hsp (or $EGFP^{inv}$ control) and $Fluc^{DM}$-EGFP, were sub-divided into "bins" of equal width (40 RFU) based on the level of mCherry fluorescence (the Hsp reporter; Figure 3.9a). Pulse shape analysis was then used to determine the proportion of cells with inclusions in each of these bins. The relative $Fluc^{DM}$-EGFP expression levels (*i.e.* the EGFP fluorescent median) in each bin was used to normalize for the relative levels of the aggregation-prone protein to determine the proportion of cells in the iPop of each respective mCherry bin (Figure 3.9b). For cells co-transfected to express Hsp70 and $Fluc^{DM}$, increasing levels of Hsp70 resulted in a significant decrease in the proportion of cells with $Fluc^{DM}$-EGFP inclusions compared to cells expressing $EGFP^{inv}$ (Figure 3.9c-d). Similarly, increasing levels of Hsp40+Hsp70 resulted in a significant reduction in the proportion of cells with $Fluc^{DM}$-EGFP inclusions, relative to cells expressing $EGFP^{inv}$ (Figure 3.9e). This indicates that these Hsps work in a concentration-dependent manner. Conversely, increasing concentrations of αB-c and Hsp27 had no effect on the proportion of cells with $Fluc^{DM}$-EGFP inclusions (Figure 3.9f-g). Cells expressing Hsp40 and Hsp90 were excluded from this type of analysis due to the weaker correlation observed between levels of the Hsp and the reporter protein (see Figure 3.4).

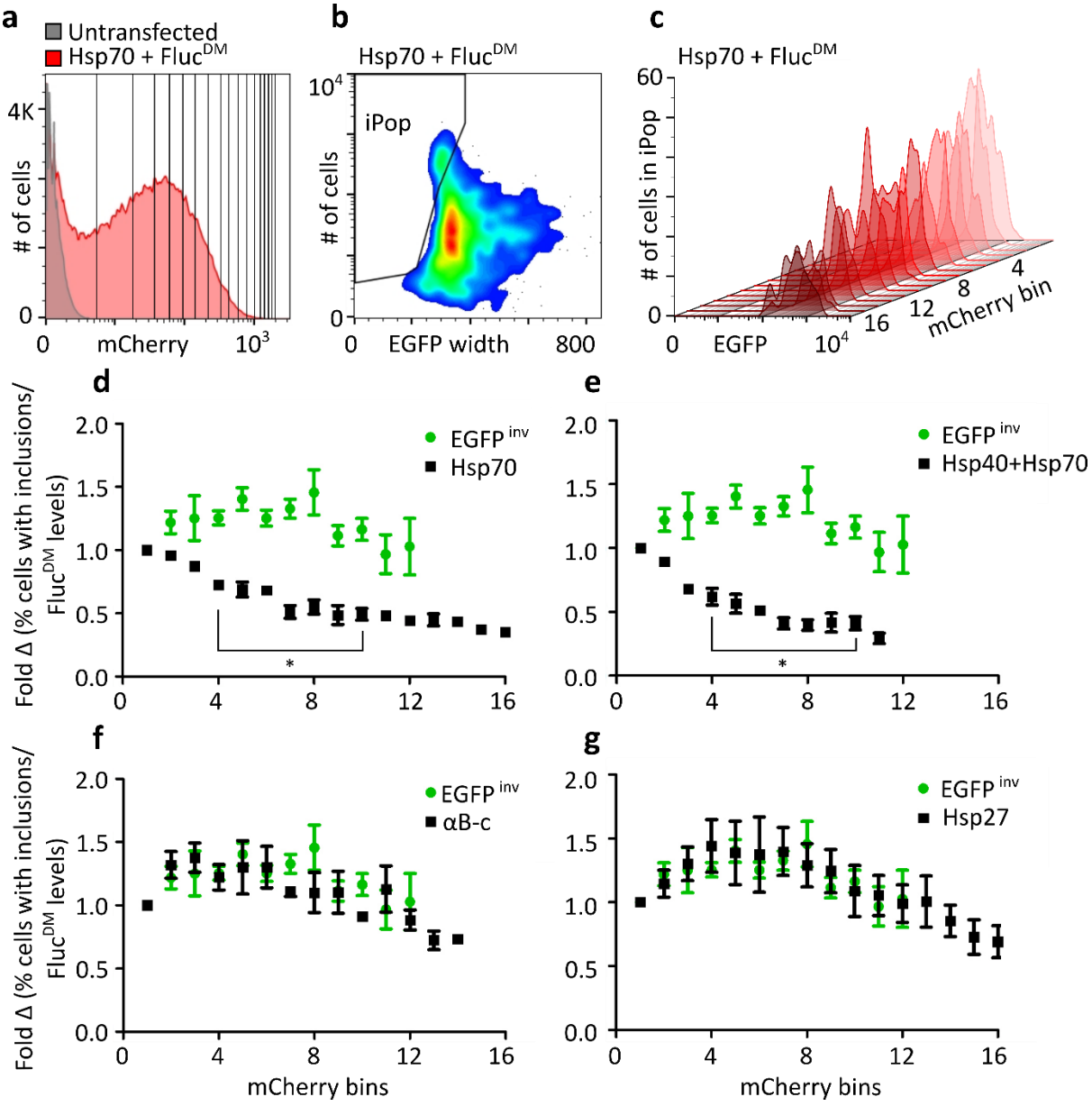

Figure 3.9. Use of bicistronic constructs to determine the effect of increasing Hsp levels on the formation of Fluc^{DM}-EGFP inclusion bodies in cells. (a) Gating strategy used to determine the fraction of cells with inclusion bodies as a function of mCherry (Hsp) expression. The frequency histogram of mCherry fluorescence was subdivided into 16 bins of equal mCherry RFU (40 RFU), where bin 1 represents the lowest, and bin 16 the highest level of mCherry expression. Pulse shape analysis was used to obtain (b) the proportion of cells with inclusions in each mCherry bin. (c) The frequency histogram overlay shows the relative reduction in the number of cells with inclusions with increasing mCherry reporter protein, using the mCherry binning strategy. Neuro-2a co-transfected to express Hsp70 with mCherry and Fluc^{DM}-EGFP are shown in these representative plots. (d) - (g) Fold change in cells with inclusions as a function of mCherry fluorescence (normalised to Fluc^{DM}-EGFP levels) when transfected with EGFP^{inv} and (d) Hsp70, (e) Hsp40 + Hsp70, (f) αB-c, and (g) Hsp27-encoding bicistronic constructs. Mean ± SEM of three independent replicates. Statistically significant differences between the means of cells expressing EGFP^{inv} and Hsp were assessed at each mCherry bin using a student's t-test where $P < 0.05$ (*). mCherry bins with less than 100 events were excluded from subsequent analysis.

3.4 Discussion

The dynamic and complex nature of the interactions Hsps have with themselves and their client proteins presents a barrier to studying them in cells using fluorescent tags. To overcome this, a suite of Hsp-encoding bicistronic constructs for the correlated expression of a non-tagged Hsp and a fluorescent reporter protein were developed. These bicistronic constructs can be used to study and compare the cytoprotective functions and chaperone abilities of Hsps in the physiologically relevant context of the cell.

Before using these bicistronic constructs to evaluate the function of Hsps in cell-based assays, it was established that the Hsp and fluorescent reporter were expressed in a correlated manner. A strong correlation between the Hsps and fluorescent reporter protein was observed in cells transfected with αB-c, Hsp27 or Hsp70-encoding bicistronic constructs, which corresponded to Hsps that were found not to be endogenously expressed in Neuro-2a cells (as determined by immunoblotting of cell lysates). The correlation between the levels of Hsp40 or Hsp90 and the fluorescent reporter protein were not as strong. It is not currently clear why this is the case. It is possible that the endogenous expression of Hsp90 and Hsp40 observed in Neuro-2a, combined with over-expression from the bicistronic construct, may promote a higher turn-over of these Hsps in these cells. Interestingly, the level of the mCherry reporter from the Hsp40-encoding IRES vector was also significantly lower than observed from the other Hsp-encoding constructs (Figure 3.4) suggesting that there are differences in the levels of transcription and translation from these constructs, which is dependent on the genes being expressed. Whatever the reason, through using the bicistronic constructs and monitoring for differences in transfection efficiency, expression levels and correlations in expression between the Hsp and fluorescent reporter, these differences were able to be taken into consideration in downstream analyses. Together, these data emphasise the importance of validating the correlated expression

of proteins expressed from bicistronic constructs, since relative levels may vary significantly between constructs.

In previous studies that have expressed Hsps without a fluorescent tag in cells, differences in transfection and co-transfection efficiencies between samples could not easily be taken into account in downstream analyses. In contrast, the use of Hsp-encoding bicistronic constructs enables transfection efficiencies to be determined and accounted for between samples. The analyses presented in this study, which investigated the effect of Hsp expression on the number of cells with protein inclusions, highlight how differences in transfection efficiency between constructs can affect interpretation of the data. Moreover, the Hsp-encoding bicistronic constructs can simultaneously quantify transfection efficiencies and the relative levels of Hsps in live cells by measuring the levels of fluorescence using techniques such as flow cytometry. The fluorescent reporter also provides the option of purifying the transfected cell population by fluorescence-activated cell sorting for subsequent biochemical analyses (*i.e.* immunoblot, filter-trap, or generation of stable cell lines).

Three different approaches were compared to investigate the effect Hsps have on the formation of intracellular inclusions, namely analyses that take into account (i) only cells expressing $Fluc^{DM}$-EGFP (Figure 3.8c); (ii) only co-transfected cells (Figure 3.8d); and (iii) only co-transfected cells and the levels of $Fluc^{DM}$ in those cells (Figure 3.8e-f). The latter approach enables assessment of the chaperone efficacy of each Hsp, taking into account the amount of the aggregation-prone protein (in this case $Fluc^{DM}$-EGFP) expressed in cells. This is advantageous as there is a strong correlation between the amount of protein expressed in a cell and its propensity to form inclusions (Arrasate et al. 2004, Ormsby et al. 2013, Ramdzan et al. 2013, Ciryam et al. 2015). Moreover, in this work, $Fluc^{DM}$-EGFP expression levels were influenced by the level of expression from the co-transfected bicistronic construct, whereby reduced expression from one construct resulted in the elevated expression of protein from the

co-transfected construct. For example, lower relative levels of expression from the Hsp40- and Hsp90-encoding constructs resulted in significantly higher levels of $Fluc^{DM}$ in cells (Figure 3.8e). This could be reflective of the relative stability of bicistronic mRNA, such that some mRNA are degraded more readily (in this case Hsp40 and Hsp90), which facilitates increased translation of the co-transfected plasmid (in this case $Fluc^{DM}$). Thus, differences in the levels of $Fluc^{DM}$-EGFP expression were taken into account in the comparative analyses between samples.

By taking into account the level of $Fluc^{DM}$ in cells co-transfected to express Hsps, the data show that the expression of Hsp70 and/or Hsp40 significantly reduced the proportion of cells with $Fluc^{DM}$-EGFP inclusions (Figure 3.8f). Whilst the over-expression of Hsps may influence the levels of aggregation-prone proteins in cells (*e.g.* via promoting their degradation) a decrease in $Fluc^{DM}$-EGFP levels compared to the $EGFP^{inv}$ control in any of the Hsp-expressing samples was not observed (Figure 3.8e). Therefore, the reductions observed in the proportion of cells with $Fluc^{DM}$-EGFP inclusions can be attributed to Hsps stabilising $Fluc^{DM}$ to prevent its aggregation, rather than stimulating the degradation of $Fluc^{DM}$. Our findings extend on previous studies that demonstrated the ability of Hsp40 and Hsp70 to refold and resolubilise heat denatured firefly luciferase in simple solution-based assays (Minami et al. 1996, Ballinger et al. 1999, Cashikar et al. 2005). Furthermore, studies investigating the aggregation of pathogenic proteins such as polyglutamine-expanded huntingtin (Ormsby et al. 2013), human androgen receptor (Howarth et al. 2009), α-synuclein (Klucken et al. 2004), and TAR DNA binding protein-43 (Chen et al. 2016), showed that over-expression of Hsp40 or Hsp70 (and other proteins in these subfamilies) inhibited inclusion formation of each of these client proteins.

Hsp40 acts to inhibit protein aggregation by binding misfolded proteins to maintain them in a folding-competent state, delivering the misfolded protein to Hsp70 for active refolding (Chen

et al. 2016). In addition to actively re-folding misfolded proteins, Hsp70 can interact with components of the ubiquitin-proteasome system or autophagy to degrade aggregation-prone proteins (Rosser et al. 2007, Gamerdinger et al. 2011). Therefore, it would be of great interest to re-evaluate the chaperone activities, particularly the anti-aggregation and cytoprotective roles, of Hsp40 and Hsp70 in the context of disease-associated aggregating proteins using the bicistronic expression constructs developed for this work. Furthermore, the data show that increasing levels of Hsp70 or Hsp40+Hsp70 in cells results in a concentration-dependent decrease in the proportion of cells with $Fluc^{DM}$-EGFP inclusions. These findings support the concept of boosting the activity or amount of Hsps in cells as a therapeutic approach to inhibit protein aggregation associated with neurodegenerative diseases (Kilpatrick et al. 2013, Kalmar et al. 2014, Chen et al. 2016).

Interestingly, whilst the sHsps, Hsp27 and αB-c, have been shown to inhibit the aggregation of client proteins and promote re-folding of heat denatured firefly luciferase in solution-based assays, often at sub-stoichiometric levels (Ito et al. 2001, Lee et al. 2006, Bryantsev et al. 2007, Ecroyd et al. 2007, Kulig and Ecroyd 2012), they did not significantly reduce the proportion of cells with $Fluc^{DM}$-based inclusions in this study. A possible reason for this is that these sHsps do not interact with this particular client protein in the cellular context. It is well-known that the sHsps show some specificity with regard to client proteins with which they can interact. For example, over-expression of Hsp27 had no effect on inclusion body formation of the huntingtin exon 1 fragment (Firdaus et al. 2006), but its over-expression significantly reduced the aggregation of α-synuclein (Outeiro et al. 2006, Cox and Ecroyd 2017). Furthermore, the molecular mechanism by which αB-c inhibits the aggregation of client proteins can vary depending on the stability of the precursor to aggregation (Kulig and Ecroyd 2012). The complexity of sHsp chaperone activity combined with the substantial evidence showing co-localisation between sHsps and protein aggregates in post-mortem brains with ND, indicates

that further research is required to establish the roles sHsps play in NDs with regard to cytoprotection and inhibition of protein aggregation in cells (Gai et al. 1999, Gordon 2003, Dabir et al. 2004, Pountney et al. 2005, Iwahashi et al. 2006). Bicistronic constructs such as those used here should be useful in such studies.

Studies of Hsp cellular function have typically relied on over-expressing non-labelled Hsps, a strategy generally adopted to minimise any possible adverse effects of tagging a fluorescent protein to these dynamic proteins. In this work, Hsp-encoding bicistronic constructs that provide the correlated expression of a non-labelled Hsp and fluorescent reporter protein were developed and validated. This strategy enables differences in transfection efficiencies and Hsp expression levels (down to the level of individual cells) to be taken into account when performing cell-based assays to investigate and compare the functions of Hsps. This approach can be used in future work to investigate the ability of a range of Hsps to mitigate the underlying molecular mechanisms that characterise a range of neurodegenerative diseases. Moreover, this approach can also be applied to study other proteins whose structure and function are perturbed by fluorescent protein tagging.

Chapter 4: Developing and applying a novel flow cytometric technique to quantify inclusions and protein trafficking

This chapter has been previously published in the following work:

D. R. Whiten*, **R. San Gil***, L. McAlary, J. J. Yerbury, H. Ecroyd and M. R. Wilson. Rapid flow cytometric measurement of protein inclusions and nuclear trafficking. *Scientific Reports.* 2016; 6: 31138. * - these two authors contributed equally to this work.

Author contributions: DRW and RSG were co-first authors of this manuscript. DRW, RSG and LM performed experiments and analysed the data. RSG performed the experiments to generate the data shown in Fig 4.1, 4.2, 4.3, 4.4, 4.5a-c, 4.7c, and 4.8a. HE and MRW designed experiments and oversaw their implementation. MRW and DRW jointly developed the original method. DRW, RSG, JJY and HE contributed to authoring of the manuscript; MRW was the co-ordinating author.

4.1 Introduction

There is a strong correlation between inclusion body formation, impairment of the proteostasis network, (in some cases) mislocalisation of proteins into subcellular compartments, and subsequent neuron-specific cell death, which results in the onset of NDs (Hipp et al. 2014). Therefore, research in this field would greatly benefit from the development of sensitive, high-throughput techniques for the quantification of inclusion bodies and protein trafficking in cell-based models of ND-like protein aggregation. Such techniques would be invaluable in evaluating the capacity of the proteostasis network to mitigate protein misfolding and in elucidating the effects of novel therapeutics on the quantity, population distributions, relative sizes of inclusion bodies, and subcellular localisation of pathogenic proteins in cells.

In a recent development, inclusion bodies formed by the aggregation of polyQ-expanded Htt were detected using a novel, high-throughput flow cytometry-based, pulse shape analysis (PulSA) (Ramdzan et al. 2013). Pulse shape analysis provides quantitative information on shifts in fluorescently-tagged aggregation-prone proteins from a diffuse cytosolic distribution into punctate or dispersed aggregates by tracking the formation of inclusion bodies based on differences in their fluorescent pulse shapes (Ramdzan et al. 2013). Cells containing Htt inclusion bodies have a reduced pulse width and increased pulse height compared to cells with diffuse protein. Thus, cells can be separated into two populations, those with and without inclusions, by gates on a plot of pulse height versus pulse width (Ramdzan et al. 2013). This method of quantitating the so-called inclusion population (iPop) can reproducibly report on the formation of inclusion bodies within whole cells, specifically in cells over-expressing polyQ-expanded Htt (Bersuker et al. 2013, Ormsby et al. 2013) and an aggregation-prone mutant of firefly luciferase (section 3.3.2). However, over expression of ND-associated proteins, such as SOD1 and TDP-43, cannot be reliably distinguished using PulSA (our unpublished data). Thus, although PulSA is a powerful technique for high-throughput tracking of some protein

aggregates, it lacks the sensitivity required to accurately detect a wide range of protein aggregates that are associated with NDs.

Aggregates formed in heat shocked yeast cell cultures are able to be quantified by flow cytometry of cell lysates (Shiber et al. 2014). Therefore, the objective of this study was to develop a method to quantify the formation of aggregates in mammalian cell-based models of ND-associated protein aggregation. Herein, the use of FloIT (flow cytometric quantification of inclusions and trafficking) is described, a sensitive technique for the quantification of inclusion bodies in cells over-expressing aggregation-prone proteins, Htt, SOD1, TDP-43, or firefly luciferase. This technique offers the following advantages over existing methods to quantify inclusion formation: (i) the number of inclusion bodies in each sample can be normalised to the number of nuclei (stained with a nuclear dye) for quantitative comparisons across samples, (ii) sensitive detection of inclusion bodies that cannot be distinguished by microscopy or PulSA, (iii) the ability to determine the range and average size of aggregates (through the use of sizing bead standards), (iv) non-biased, (v) monitor protein trafficking between subcellular compartments, and (vi) FloIT is compatible with standard flow cytometry instrumentation.

4.2 Methods

4.2.1 Plasmids and cloning

The human M337V mutant of TDP-43 was cloned into pCMV6-AC-GFP (Origene) to generate a mutant of TDP-43 C-terminally tagged with turbo GFP (TDP-43^{M337V}-tGFP) (Farrawell et al. 2015). HA-NFAT1(4-460)-GFP was a gift from Anjana Rao (Addgene plasmid #11107). Huntingtin protein-encoding constructs, pT-Rex-Htt^{46Q}-Tc1-mCherry and pT-Rex-Htt^{25Q}-Tc1-mCherry, were gifts from Dr Danny Hatters (University of Melbourne, Australia) (Ramdzan et al. 2013). pEGFP-SOD1^{WT}, pEGFP-SOD1^{A4V}, pEGFP-SOD1^{G93A} were gifts from Dr Brad Turner (The Florey Institute of Neuroscience and Mental Health, Australia) (Turner et al. 2005). SOD1-tdTomato constructs were created by replacing the GFP sequences in the SOD1-GFP plasmids with tdTomato (Genscript) (Farrawell et al. 2015). The expression vector pCMV6-AC-GFP containing FUS was obtained from Origene and site directed mutagenesis was performed by Genscript to create an R495X mutant (Farrawell et al. 2015). Plasmids containing sequences encoding EGFP-tagged firefly luciferase WT (pcDNA4-TO-myc-hisA-EGFP-Fluc^{WT}) and a temperature-sensitive double mutant (R188Q, R261Q; DM; pcDNA4-TO-myc-hisA-EGFP-Fluc^{DM}) were kind gifts of Prof Mark Wilson (University of Wollongong).

4.2.2 Tissue culture, transfections and treatments

See section 2.6 for details regarding the cell culture of Neuro-2a and HEK293 cells.

Cells were transfected 24 h after plating using Lipofectamine LTX/PLUS (Life Technologies) according to the manufacturer's instructions. Briefly, 1 µg plasmid DNA, 1 µL PLUS and 3 µL lipofectamine LTX, per well of a 12-well plate, was used to transfect cells. In some experiments, cells transfected to express WT and mutant SOD1, Htt, TDP-43 and Fluc proteins were analysed by flow cytometry 48 h post-transfection.

In experiments investigating TDP-43 translocation from the nucleus, Neuro-2a cells were transfected to express TDP-43^{M337V}-tGFP and 48 h post-transfection were treated with 0 or 10 µg/mL MG132. Treatment with MG132, as previously described (Walker et al. 2013), inhibits proteasomal function and subsequently induces the cytoplasmic accumulation and aggregation of mutant TDP-43. The percent of TDP-43^{M337V}-tGFP-positive nuclei were quantified by FloIT after 0, 2, 5, 10 and 16 h of MG132 treatment. A second model of nucleo-cytoplasmic shuttling, independent of protein aggregation, was also investigated by FloIT. In these experiments, FloIT was used to investigate the well-characterised translocation of nuclear factor of activated T-cells (NFAT-EGFP), from the nucleus to the cytoplasm following induction of calcium dyshomeostasis in HEK293 cells (Jia et al. 2014, Vihma et al. 2016). HEK293 cells were transfected to express NFAT-EGFP and 48 h post-transfection, cells were treated with 0, 0.25, and 1 µM ionomycin (a calcium ionophore used to induce calcium dyshomeostasis) for 30 min. The percent of NFAT-EGFP-positive nuclei was quantified by FloIT at each dose of ionomycin. For imaging of whole cells, the cells were grown directly in an 8 well µSlide (Ibidi), and following treatment were fixed with 4% (w/v) PFA in PBS for 15 min at RT, permeabilised by incubation with 0.5% (v/v) TritonX-100 in PBS supplemented with RedDot2 (1:1000) for 20 min at RT and then imaged by confocal microscopy.

4.2.3 Flow cytometry

Flow cytometry was used to analyse the transfection efficiency of intact cells in each sample prior to analysis by FloIT. Flow cytometric analysis of whole cells was performed as described in section 2.9.

4.2.3.1 Flow cytometric quantification of inclusions and trafficking (FloIT)

Cells to be analysed were grown and transfected in 24-well plates. After the indicated treatments, the cells were harvested using 0.025% (v/v) trypsin/EDTA (Life Technologies),

then diluted with 1% FCS (v/v) DMEM/F12 and centrifuged (5 min/ 300 × *g*/ RT), washed in PBS and resuspended in 500 µL of PBS. An aliquot of the cell suspension (150 µL) was taken and the transfection efficiency (γ) determined using untransfected cells as a negative control sample. Flow cytometry was performed using a BD Biosciences LSR Fortessa X-20 analytical flow cytometer; excitation wavelengths and emission collection windows were, respectively, EGFP and tGFP (488 nm, 525/50 nm) and mCherry and tdTomato (561 nm, 586/15 nm). The remaining 350 µL of cell suspension was centrifuged as above and resuspended in lysis buffer, comprised of PBS containing 0.5% (v/v) TritonX-100 and 1 × Halt protease and phosphatase inhibitors. Except in control samples used to set gates, RedDot2 (Biotium) was diluted 1:1000 into lysis buffer prior to adding to cells. After a 2 min incubation at RT to lyse cells, the lysate was analysed by flow cytometry measuring forward and side scatter, together with RedDot2 fluorescence (640 nm excitation, 670/30 nm collection) and EGFP/tGFP and/or mCherry/tdTomato fluorescence as above. The FSC threshold was set to 200 (minimum possible) to minimize exclusion of small inclusions from the analyses. Acquisitions were performed with all axes set to $\log_{10}$, and 100,000 events were acquired in all cases. Unless otherwise indicated, voltages of 418 (FSC), 199 (SSC), 410 (E/tGFP), 538 (RedDot2) and 412 (mCherry/tdTomato) were used in all experiments. Nuclei were identified and counted based on RedDot2 fluorescence and FSC and then excluded from further analysis. The remaining particles were analysed for the presence of inclusions based on fluorescence and FSC and compared to untransfected or vector only controls. Analysis of all events was performed using Flow Jo (version 10.0.8, Tree Star, Ashland OR, USA). The number of inclusions in each sample was normalised to the number of nuclei in the same sample using equation 4.1:

$$i = 100\left(\frac{n_i}{y.n_{nuc}}\right) \qquad (4.1)$$

where *i* represents the number of inclusions per 100 nuclei, n_i is the number of inclusions detected, *y* is the transfection efficiency, and n_{nuc} is the number of nuclei counted. The transfection efficiency of Neuro-2a cells in these studies ranged from 75-85%.

4.2.3.2 Pulse shape analysis (PulSA)

See section 2.9.1.

4.2.4 Fluorescence activated sorting of inclusions and nuclei

Neuro-2a cells grown in 24-well plates were transfected to express TDP-43^{M337V}-tGFP, treated with 10 µg/mL MG132 for 16 h, harvested and lysed as described above. The lysate was passed through a 40 µm nylon mesh and analysed on an S3e Cell Sorter (Bio-Rad Laboratories) equipped with 488 nm and 561 nm lasers. Nuclei were collected based on FSC area and SSC area instead of RedDot2 (since the S3e cytometer used lacked a 640 nm laser); the accuracy of this gate was separately confirmed using propidium iodide (1 µg/mL, excitation 488 nm, emission 586/25 nm). Inclusions were collected based on FSC area and GFP-fluorescence area (excitation 488 nm, emission 525/30 nm). Particles were collected in 5 mL FACS tubes containing 50 µL of PBS for subsequent imaging by confocal microscopy.

4.2.5 Confocal microscopy and manual counting of inclusion bodies

Confocal microscopy of cells and cell lysates was performed as described in section 2.8.2. Manual counting of inclusions was performed by counting the number of inclusions present in three sets of images from a randomly selected field of view to count inclusions in ~100 transfected cells.

4.2.6 Statistics

See section 2.10.

4.3 Results

4.3.1 Developing FloIT for the quantification of inclusion bodies

To initially develop the FloIT technique, cultured Neuro-2a cells were transfected to express $SOD1^{G93A}$, C-terminally tagged with EGFP ($SOD1^{G93A}$-EGFP). The cells were lysed in 0.5% (v/v) TritonX-100 in PBS, supplemented with RedDot2 nuclear stain, for flow cytometric analysis. Nuclei were identified and quantified using FSC and RedDot2 fluorescence (cell lysates not stained with RedDot2 were used as a negative control to set the gates; Figure 4.1a-b). To detect small fluorescent inclusion bodies, the sensitivity of the flow cytometer was increased by decreasing the threshold of detection to 200 (the lowest possible setting). Lysates from Neuro-2a cells transfected with the empty vector (pEGFP-N1 for the expression of EGFP only) were used as an inclusion body-negative control to set the square gate on plots of FSC and EGFP fluorescence (Figure 4.1c). Therefore, fluorescent $SOD1^{G93A}$ inclusion bodies in the cell lysates could be resolved and subsequently quantified on plots of FSC and EGFP fluorescence (Figure 4.1d). The remainder of the lysate was comprised of non-fluorescent cellular debris that was gated out of the analysis and not further characterised.

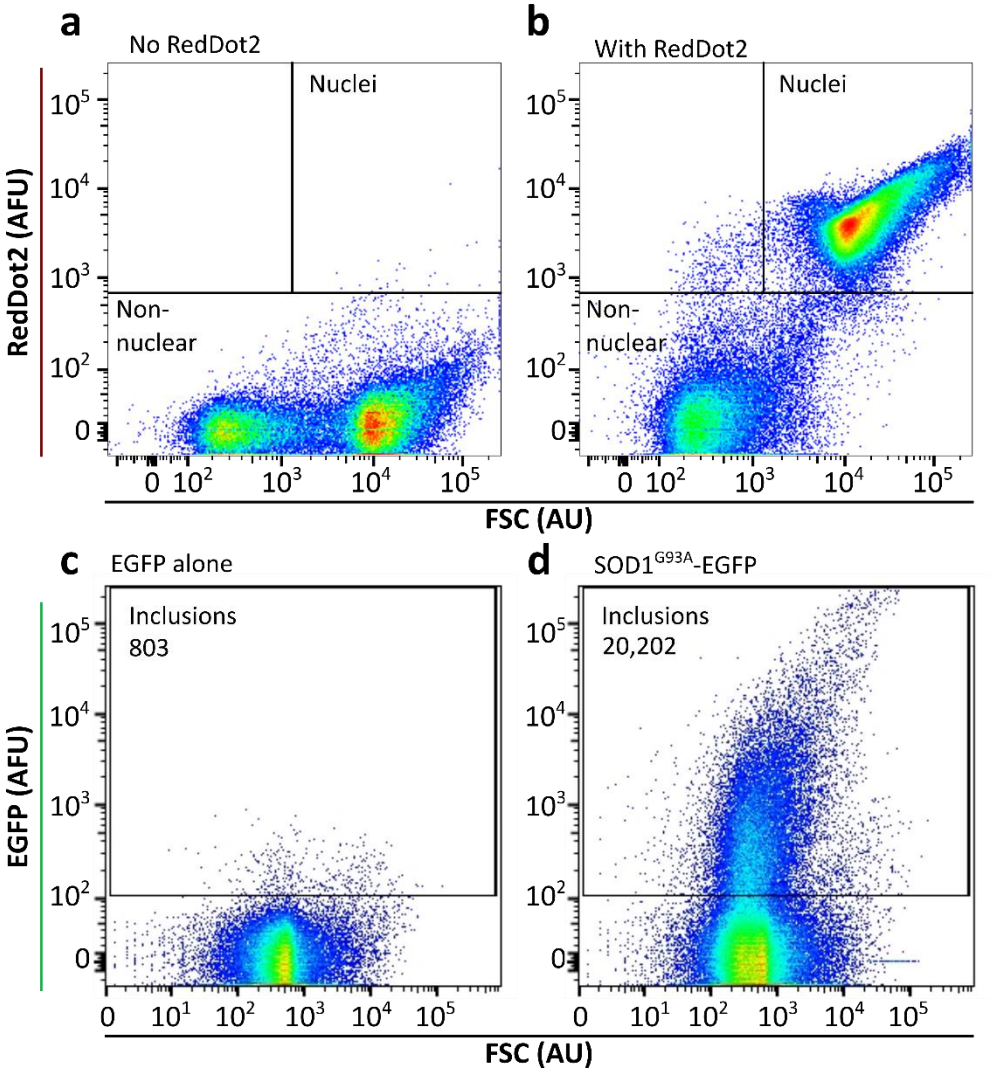

Figure 4.1. FloIT detects inclusion bodies formed by fluorescently-tagged aggregation-prone proteins. Neuro-2a cells were transfected to express EGFP alone or SOD1^{G93A}-EGFP, 48 h post-transfection cells were lysed with 0.5% (v/v) TritonX-100 in PBS and analysed by flow cytometry. (a) Neuro-2a lysates without a nuclear dye and (b) lysates incubated with RedDot2 (1:1000) nuclear dye on plots of FSC and RedDot2 fluorescence. (c) Lysates of cells transfected to express EGFP (a non-aggregating control protein) were used to apply a square gate to resolve fluorescent inclusions on plots of FSC and EGFP fluorescence. (d) Lysates of cells transfected to express SOD1^{G93A}-EGFP, an aggregation-prone mutant. The number of events acquired in the inclusion square gate is reported.

To confirm that the events that were resolved by adopting this approach were indeed nuclei and inclusion bodies, Neuro-2a cells transfected to express TDP-43^{M337V}-tGFP were treated with MG132 to induce cytoplasmic aggregation and lysed. RedDot2-positive nuclei and tGFP-positive protein inclusions were sorted using the same flow cytometric parameters on a fluorescence activated cell sorter (FACS) and imaged by confocal microscopy. Representative

micrographs are shown of a RedDot2-positive nucleus and tGFP^{+ve} TDP-43^{M337V} particles (Figure 4.2). Therefore, the parameters used on the flow cytometer were able to resolve nuclei and fluorescent protein aggregates.

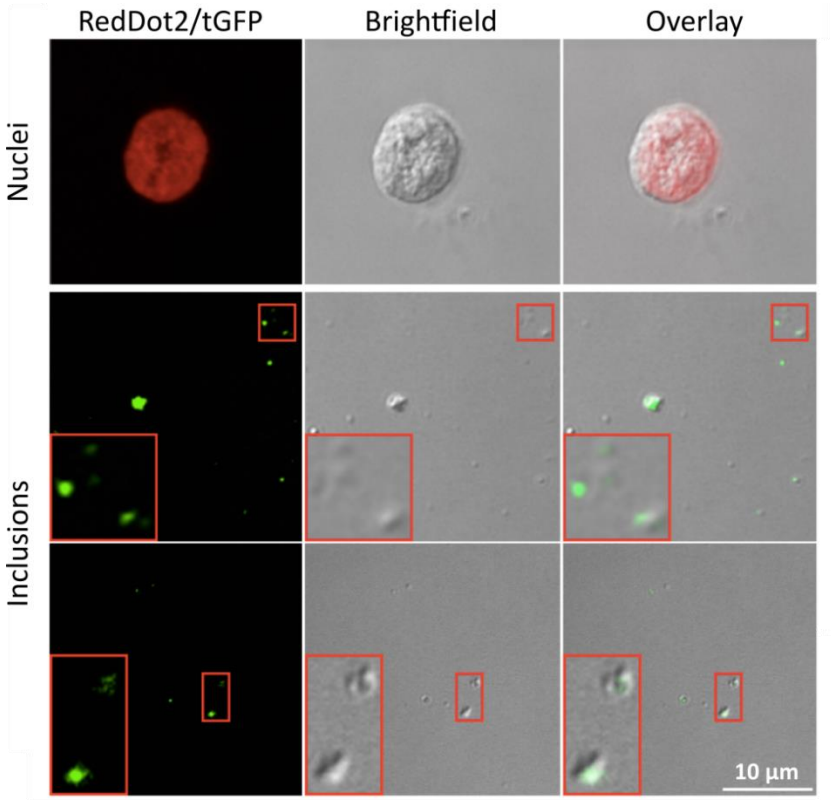

Figure 4.2. Fluorescence activated sorting of nuclei and inclusions from Neuro-2a lysates. Neuro-2a cells were transfected to express TDP-43^{M337V}-tGFP, treated for 16 h with 10 µg/mL MG132, and lysed before analysis by flow cytometry. Inclusions and nuclei were collected using a cell sorter and subsequently imaged by confocal microscopy. *Left-right:* RedDot2 or tGFP emissions, brightfield, and overlay images. *Top-bottom*: Images of a nucleus and two representative images of TDP-43^{M337V}-tGFP inclusions. The insets at the bottom left of the inclusion images represent a 3× zoom of the area indicated by the small red box at the upper right. Scale bar = 10 µm. Results shown are representative of two independent experiments.

One of the shortcomings of a previously published flow cytometric method for the quantification of cells with inclusion bodies (PulSA) was its inability to be applied to a range of aggregation-prone proteins. Therefore, to demonstrate that FloIT can quantify inclusion bodies formed from different proteins, this initial work was extended to encompass a variety of protein aggregation models including SOD1^{WT}, SOD1^{A4V}, Htt^{25Q} and polyQ-expanded Htt^{46Q}, aggregation prone mutant of TDP-43^{M337V}, and Fluc^{WT} and Fluc^{DM}. In comparison to

PulSA, FloIT was able to quantify inclusions in all cases as is demonstrated in the representative PulSA and FloIT cytograms for each protein in Figure 4.3.

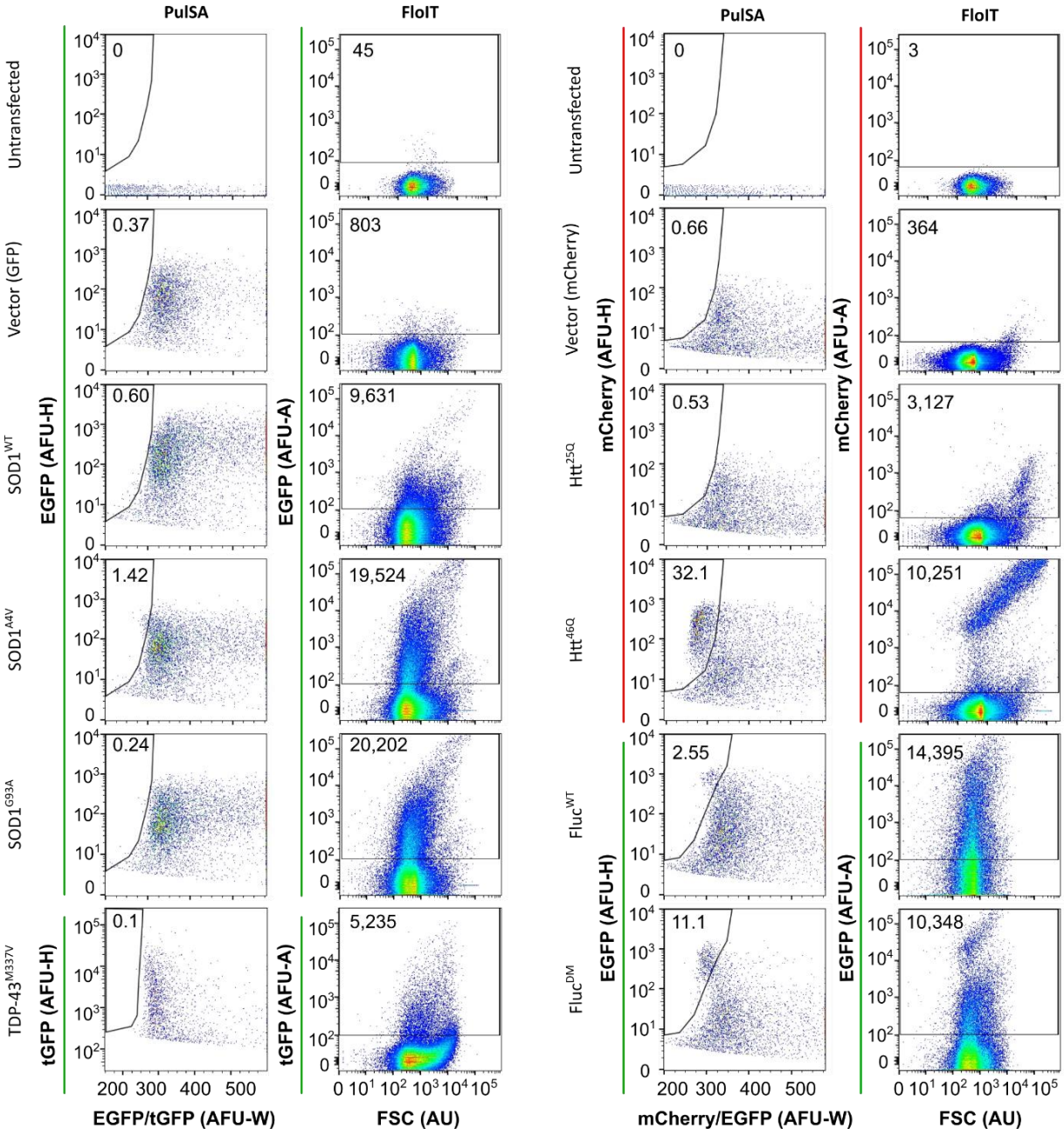

Figure 4.3. Example flow cytometry gates for PulSA (cells with inclusions gated) and FloIT (inclusions from cell lysates gated) for each protein used in this study. Neuro-2a cells were transfected to express $SOD1^{WT}$, $SOD1^{A4V}$, $SOD1^{G93A}$, $TDP\text{-}43^{M337V}$, Htt^{25Q}, Htt^{46Q}, $Fluc^{WT}$ or $Fluc^{DM}$. Cells transfected with the empty vector to express (diffuse) GFP or mCherry were used as controls to set the PulSA and FloIT gates. Numbers on the PulSA plots denote the percentage of cells in the inclusion population (iPop), whereas numbers on the FloIT plots denote the actual number of events within the gates.

In practice, PulSA is limited to detecting fluorescent inclusions that endow the host cells with, relative to cells lacking inclusions, a reduced fluorescence pulse width and increased fluorescence pulse height. These requirements are met by cells expressing polyQ-expanded Htt and to some extent $Fluc^{DM}$ (Figure 4.3 and Figure 4.4a). However, Neuro-2a cells transfected to express $SOD1^{A4V}$ and $SOD1^{G93A}$ demonstrated an increased pulse width and no change or slight increase in pulse height relative to empty vector control (Figure 4.4b). Furthermore, Neuro-2a cells transfected to express $Fluc^{DM}$ demonstrated no change in pulse width and a decrease in pulse height (Figure 4.4c). Therefore, not all cells containing protein inclusions conform to the decreased pulse width and increased pulse height paradigm required for identification by PulSA. In fact, the pulse shapes of cells containing inclusions were dependent on the protein being expressed. These findings explain why PulSA cannot detect inclusions in cells formed from a range of proteins, whereas FloIT is a more broadly applicable technique for the quantification of inclusion bodies in cell-based models of protein aggregation.

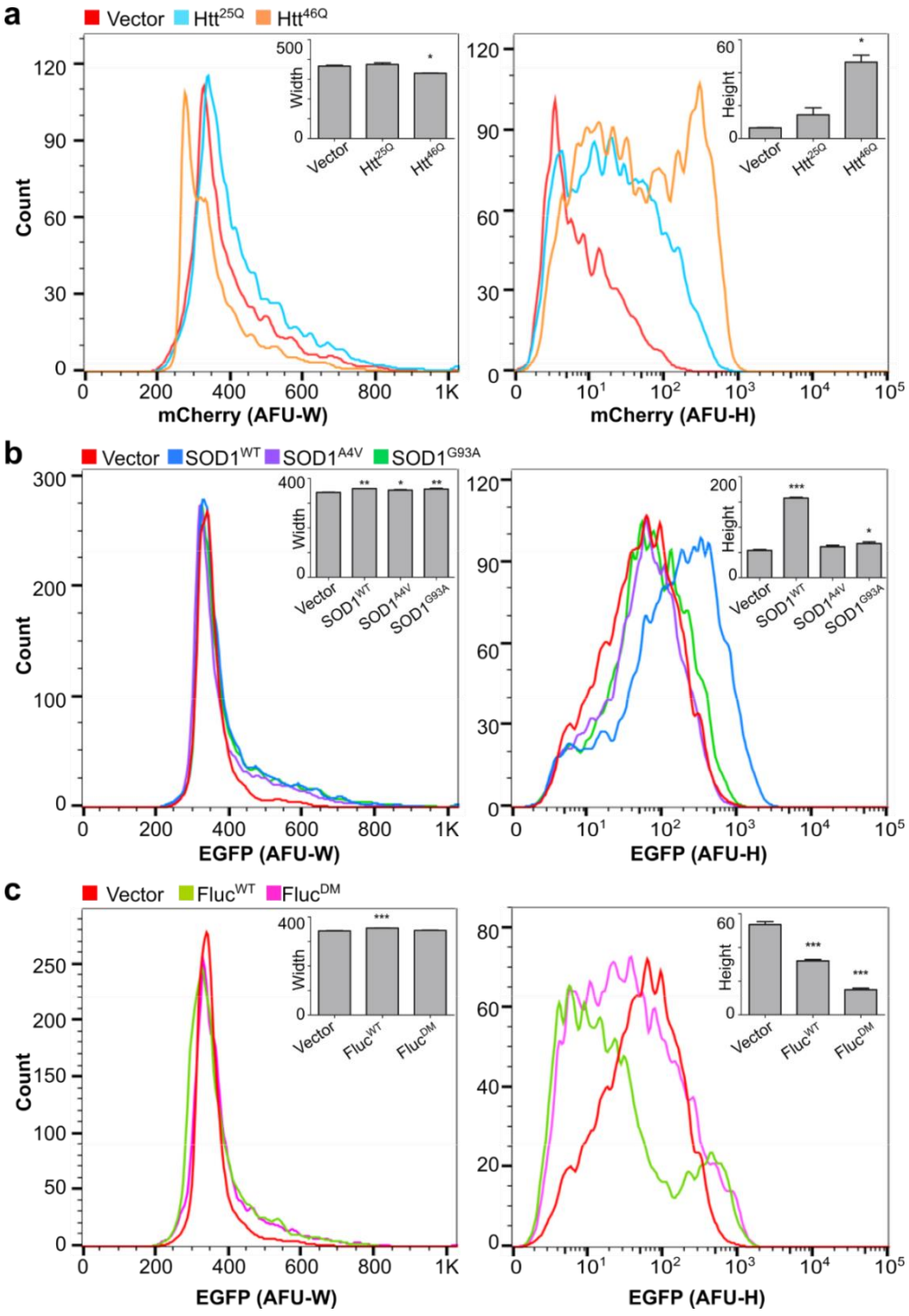

Figure 4.4 Pulse width and height profiles of cells over-expressing a range of aggregation-prone proteins. Overlay frequency histograms of fluorescence pulse width (left panels) and pulse height (right panels) of cells expressing WT and aggregation-prone mutants of Htt, SOD1 and Fluc (10,000 events acquired in all cases). Cells transfected with vector alone to express diffuse GFP or mCherry were used as controls. **(a)** Cells expressing Htt^{46Q} demonstrated a reduced pulse width and increased pulse height compared to the vector alone control. **(b)** Cells expressing $SOD1^{A4V}$ or $SOD1^{G93A}$ showed an increased pulse width and height compared to the vector control. Lastly, **(c)** relative to the vector control, cells expressing $Fluc^{WT}$ or $Fluc^{DM}$ showed little change in pulse width but showed a decreased pulse height. Insets present a summary of the median fluorescence pulse width and height data. All experiments were performed in Neuro-2a cells; values are mean triplicate measurements + SEM. Differences between the means were assessed using a one-way ANOVA followed by a Dunnet's post-hoc comparison to vector control, using an alpha level of 0.5, where $P < 0.05$ (*), $P < 0.005$ (**), and $P < 0.0001$ (***).

To calculate the average number of inclusions per transfected cell in the population analysed, the number of inclusions acquired was divided by the transfection efficiency multiplied by the corresponding number of nuclei counted (equation 4.1, where the fraction of transfected cells was separately quantified by flow cytometry of whole cells). FloIT was able to quantify 60 ± 5 and 70 ± 3.5 inclusions per 100 transfected nuclei in cells transfected to express $SOD1^{A4V}$ and $SOD1^{G93A}$, respectively (Figure 4.5a). However, PulSA detected 0.7 – 1.26% of cells with $SOD1^{A4V}$ or $SOD1^{G93A}$ inclusions (Figure 4.5b). These data again demonstrate that FloIT can quantify inclusion bodies formed from a range of aggregation-prone proteins, whereas PulSA cannot.

With regard to Htt^{46Q} and $Fluc^{DM}$, FloIT quantified 43 ± 5.4 and 84 ± 1.0 inclusions per 100 transfected cells, respectively (Figure 4.5c). These findings in Htt^{46Q} and $Fluc^{DM}$ lysates were compared to manual counts of inclusion bodies in micrographs from epifluorescence microscopy and there were no significant differences in the means suggesting that FloIT can accurately quantify the number of inclusions in these samples (Figure 4.5c). A similar comparison was performed using Neuro-2a cells transfected to express $TDP\text{-}43^{M337V}$ and treated with MG132 over 16 h to enhance nuclear efflux and cytoplasmic aggregation of the protein (Figure 4.5d). FloIT detected 26 ± 0.5 inclusions per 100 transfected cells at 0 h, and more than 90 ± 4.8 inclusions per 100 transfected cells after 16 h of MG132 treatment. After 10 h and 16 h of MG132 treatment, FloIT detected a significantly greater number of $TDP\text{-}43^{M337V}$ inclusions compared to manual counting [$F(1, 20) = 28.71$, $P < 0.0001$]. Several factors are likely to account for these differences, for example, multiple inclusions that align in the Z-axis are not distinguishable when counting inclusions in a 2D image and FloIT may detect very small inclusions that are not resolved by fluorescence microscopy.

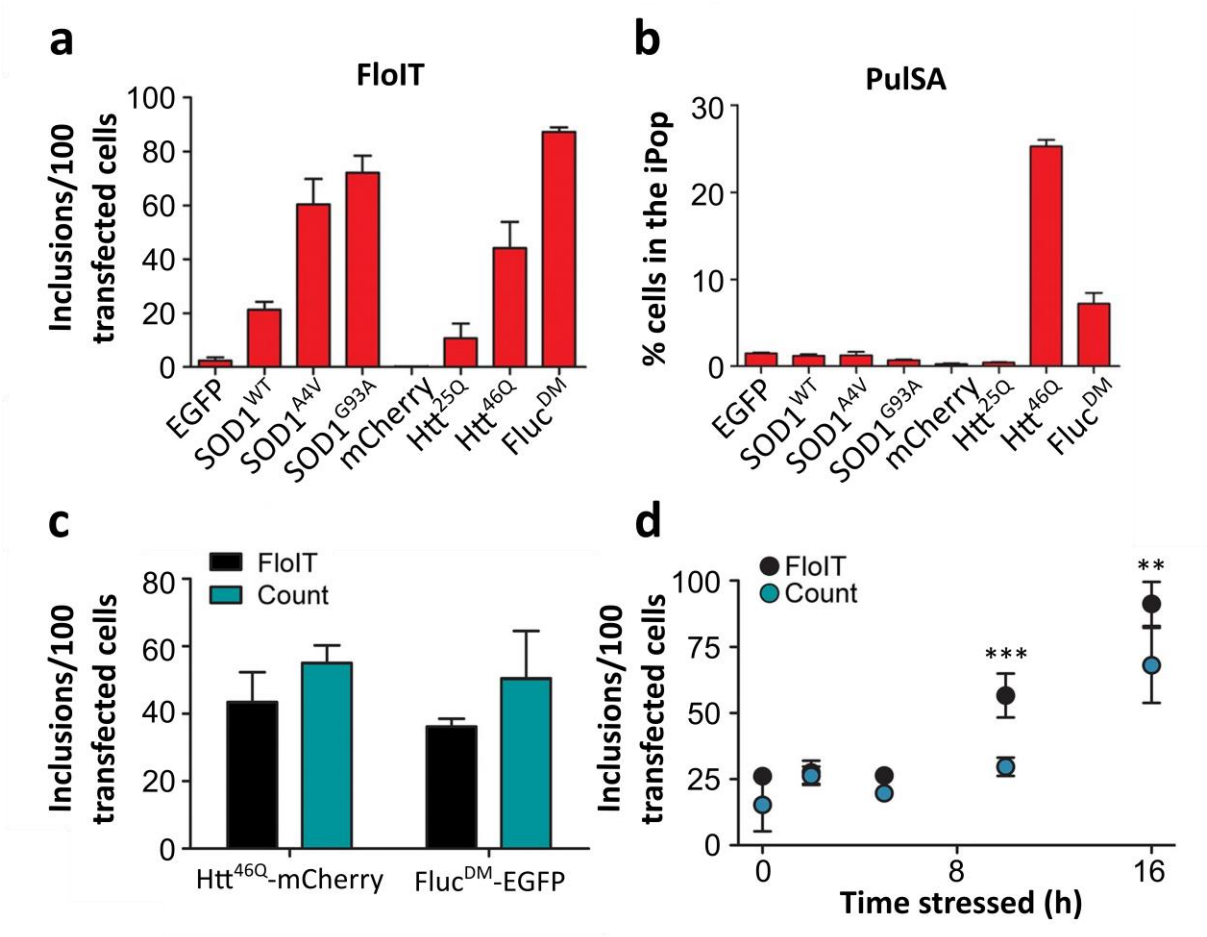

Figure 4.5. FloIT is a sensitive and unbiased method for the detection of inclusion bodies formed from a range of proteins. Neuro-2a cells were transfected to express $SOD1^{WT}$, $SOD1^{A4V}$, $SOD1^{G93A}$, $TDP\text{-}43^{M337V}$, Htt^{25Q}, Htt^{46Q}, $Fluc^{WT}$ or $Fluc^{DM}$. Cells transfected with vector alone to express (diffuse) GFP or mCherry were used as non-aggregation prone negative controls. (a) The number of inclusions detected by FloIT of cell lysates normalised to 100 transfected cells. (b) The percent of cells in the iPop resolved by PulSA of whole cells. (c) A comparison of the number of inclusions per 100 transfected cells quantified by FloIT or by manual counting of confocal microscopy images. Representative data is shown for cells transfected to express Htt^{46Q}-mCherry and $Fluc^{DM}$-EGFP. (d) The number of $TDP\text{-}43^{M337V}$-tGFP inclusions per 100 transfected cells at time points after treatment with 10 µg/mL MG132 quantified by FloIT compared to manual counts. Data are the means ± SEM of two or three independent experiments. Differences between the means were determined using a two-way ANOVA followed by Bonferroni's post-hoc test where $P < 0.001$ (**) and $P < 0.0001$ (***).

4.3.2 Protein inclusions remain insoluble in FloIT lysis buffer

Mammalian cell inclusions, which are comprised of extensively misfolded proteins, are well known to be highly resistant to detergents. Therefore, it was confirmed that incubation with 0.5% (v/v) TritonX-100 rapidly lysed cells but left inclusions intact (Figure 4.6a). Representative images from a time-lapse of cell lysis are shown of Neuro-2a cells transfected to express $SOD1^{G93A}$. The release of soluble $SOD1^{G93A}$ from the newly lysed cell is visible at 30 s while the inclusions remained unchanged for at least 10 min. When lysates were produced

at a density of approximately 150,000 cells/mL, lysates from cells expressing Htt^{46Q}, $SOD1^{G93A}$ and $TDP\text{-}43^{M337V}$, gave the same FloIT results when analysed up to 3 h post-lysis (Figure 4.6b). Therefore, under the experimental conditions used to conduct FloIT, protein inclusions remain insoluble in the lysis buffer and FloIT analyses can be performed up to several hours post-lysis without detectable changes in the samples.

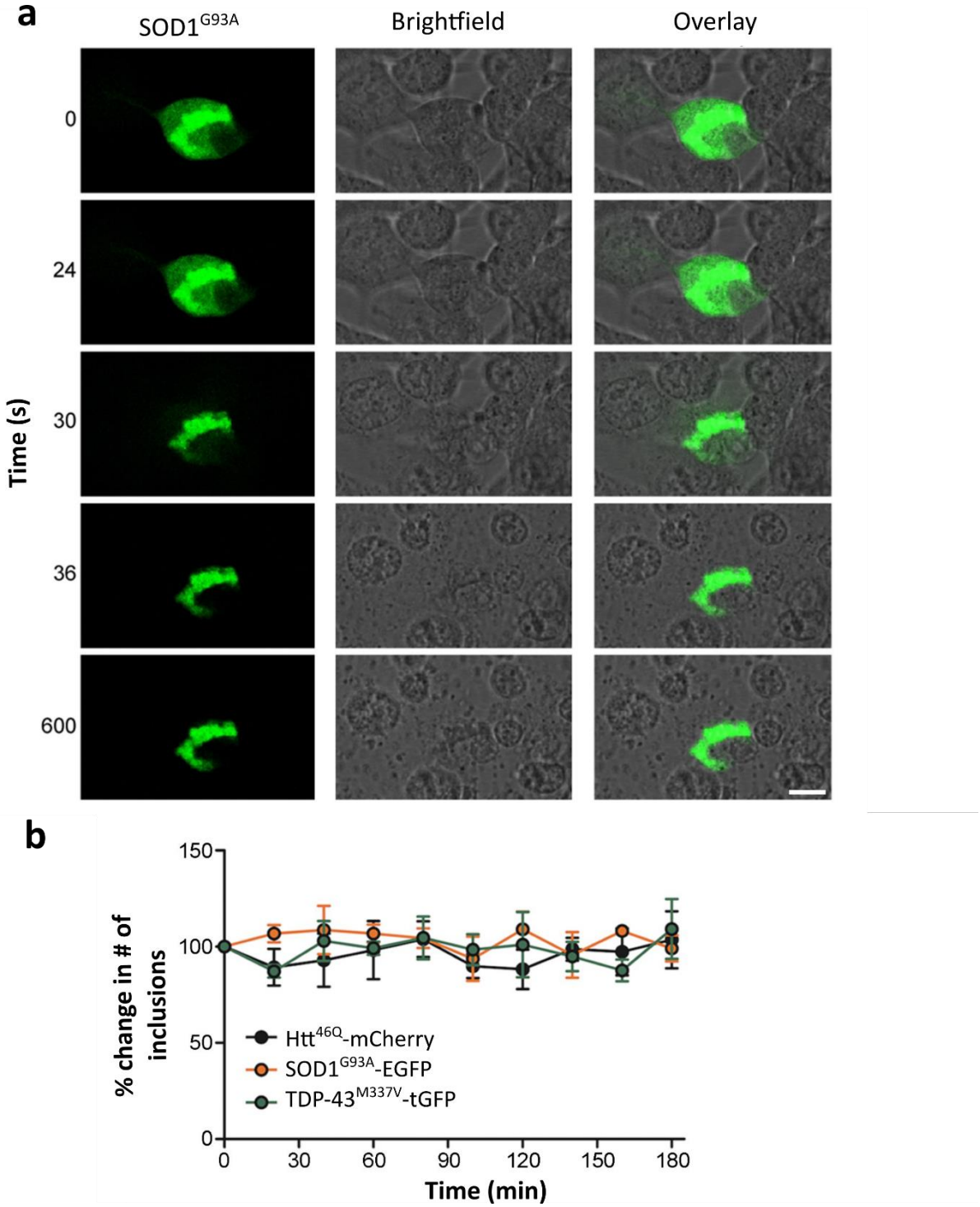

Figure 4.6. Protein inclusions remain insoluble in lysis buffer and FloIT analyses can be performed up to several hours post-lysis. Neuro-2a cells were transfected to express Htt^{46Q}-mCherry, $SOD1^{G93A}$-EGFP, or TDP-43^{M337V}-tGFP and lysed 48 h post-transfection. (a) Images were taken of cells expressing $SOD1^{G93A}$-EGFP at time intervals between 0-600 s by confocal microscopy. Scale bar represents 5 µm. (b) Time course of the percent change in the number of inclusions quantified by FloIT. Transfected Neuro-2a cells were lysed and kept on ice for the duration of the experiment and mixed briefly prior to flow cytometric analysis. Data are plotted as the percent of the time 0 data and are the means ± SEM of triplicate measurements of the samples. Data are representative of two independent experiments.

4.3.3 Using FSC calibration microspheres to determine protein inclusion size

To further exploit the data generated by FloIT, a series of microspheres of known diameters were used to calibrate the FSC signal at the gain setting used for FloIT. Over the size range tested (0.56-14.3 µm diameter), the FSC signal showed a linear dependence upon the size of the microspheres, however the ability to use FSC to resolve between the two smallest beads (0.56 and 0.79 µm diameter) is limited (Figure 4.7a-b). This is expected because, using standard flow cytometry instrumentation, the relationship between FSC and size becomes non-linear for particles of diameter less than the wavelength of the excitation laser (generally 488 nm) (Sharpe and Wulff 2005). The data presented in Figure 4.7c for mCherry (vector alone), Htt^{25Q} and Htt^{46Q}, clearly illustrates that FloIT can resolve a broad range of sizes of inclusions, including some less than 500 nm in diameter. Htt^{46Q} inclusions mostly fall in the range of 0.5-10 µm in diameter. However, owing to the technical limitations discussed above, it is not possible to determine the absolute size of these smallest particles using the flow cytometry instrument used here.

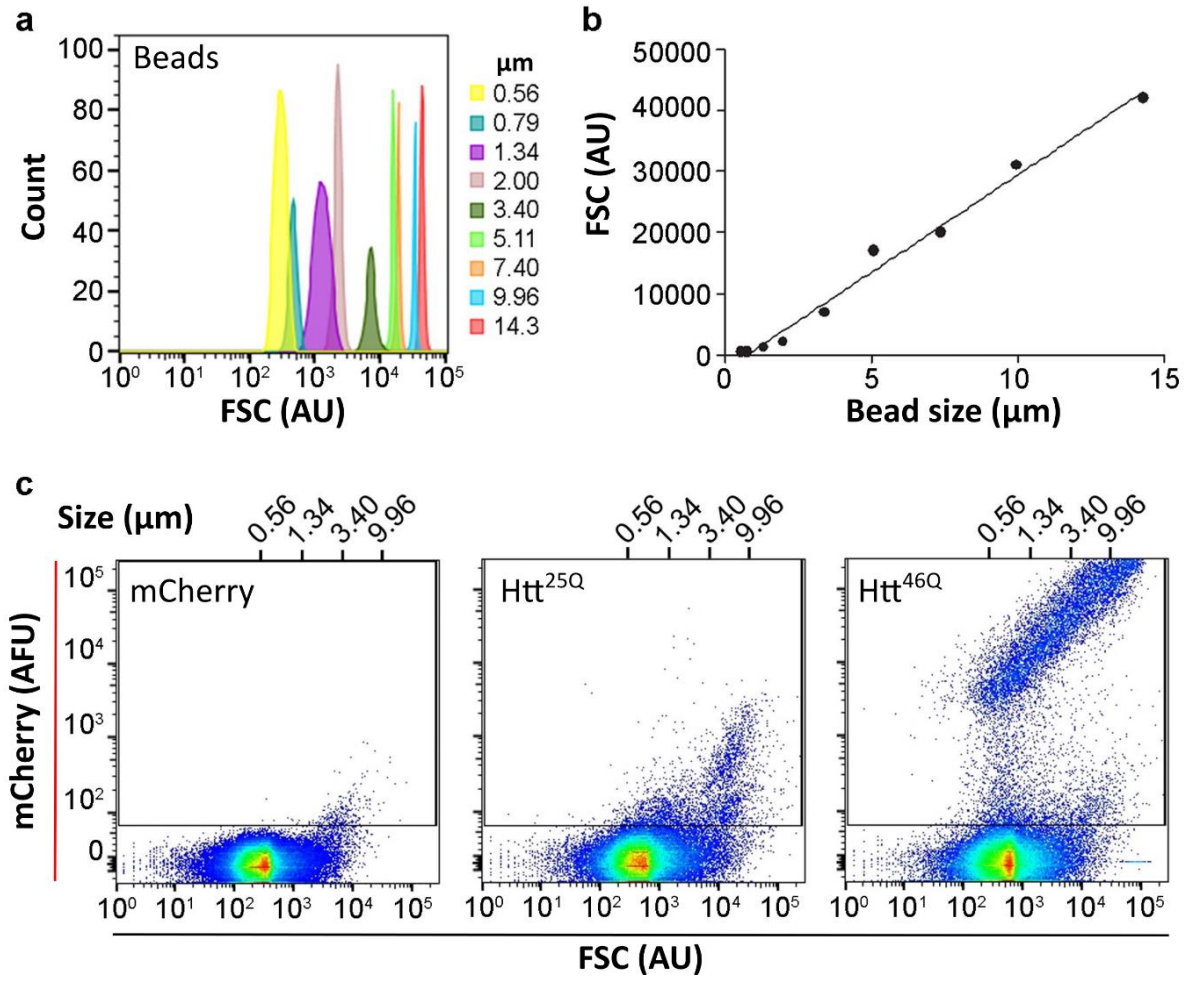

Figure 4.7. FSC calibration microspheres can be used to estimate the sizes of protein inclusions in FloIT analyses. (a) FSC histograms of each of the beads (diameters indicated in the key). (b) Over the size range tested, FSC and bead size displays a linear relationship (r^2=0.99). (c) Pseudocolour plots of analyses of mCherry fluorescence versus FSC for lysates prepared from Neuro-2a cells transfected to express mCherry, Htt^{25Q} and Htt^{46Q}. A range of sizes of inclusions can be resolved, however the absolute sizes of those with diameters less than ~0.5 µm cannot be determined using standard flow cytometers. Results shown are representative of three independent experiments.

4.3.4 FloIT can resolve inclusions of different sizes and two-colour inclusions

As further evidence of the versatility of FloIT, on the basis of FSC and SSC signals (*i.e.* physical parameters of inclusion bodies in cell lysates), this technique can resolve populations of inclusions formed from different proteins (Figure 4.8a). This type of analysis clusters WT and mutant TDP-43, SOD1 and Fluc fluorescent particles together. However, Htt^{46Q} has a higher relative FSC indicating that it forms larger inclusion bodies compared to the other aggregation-prone proteins. Htt^{25Q} particles also demonstrated a relatively high FSC, but also

showed the highest SSC. Further investigation into the nature of these Htt^{25Q} particles is warranted, since this protein is non-pathogenic and has not previously been reported to form aggregates.

On the basis of fluorescence, FloIT can resolve and enumerate inclusions formed from different proteins tagged with two different fluorescent proteins in the same cells. Representative plots are shown for Neuro-2a cells co-transfected to express two aggregation-prone proteins, FUS^{R495X} and Htt^{46Q} (Figure 4.8b). Previous research investigating the co-expression of these two proteins demonstrated that they can co-aggregate in NSC34 cells (Farrawell et al. 2015). Analysis of these cell lysates by FloIT was able to replicate and support these findings in Neuro-2a, whereby events in the top right quadrant of Figure 4.8b represent inclusion bodies comprised of both FUS^{R495X} and Htt^{46Q}. Figure 4.8c shows representative cytograms for untransfected, and singly transfected controls that were used to set the quadrant gating.

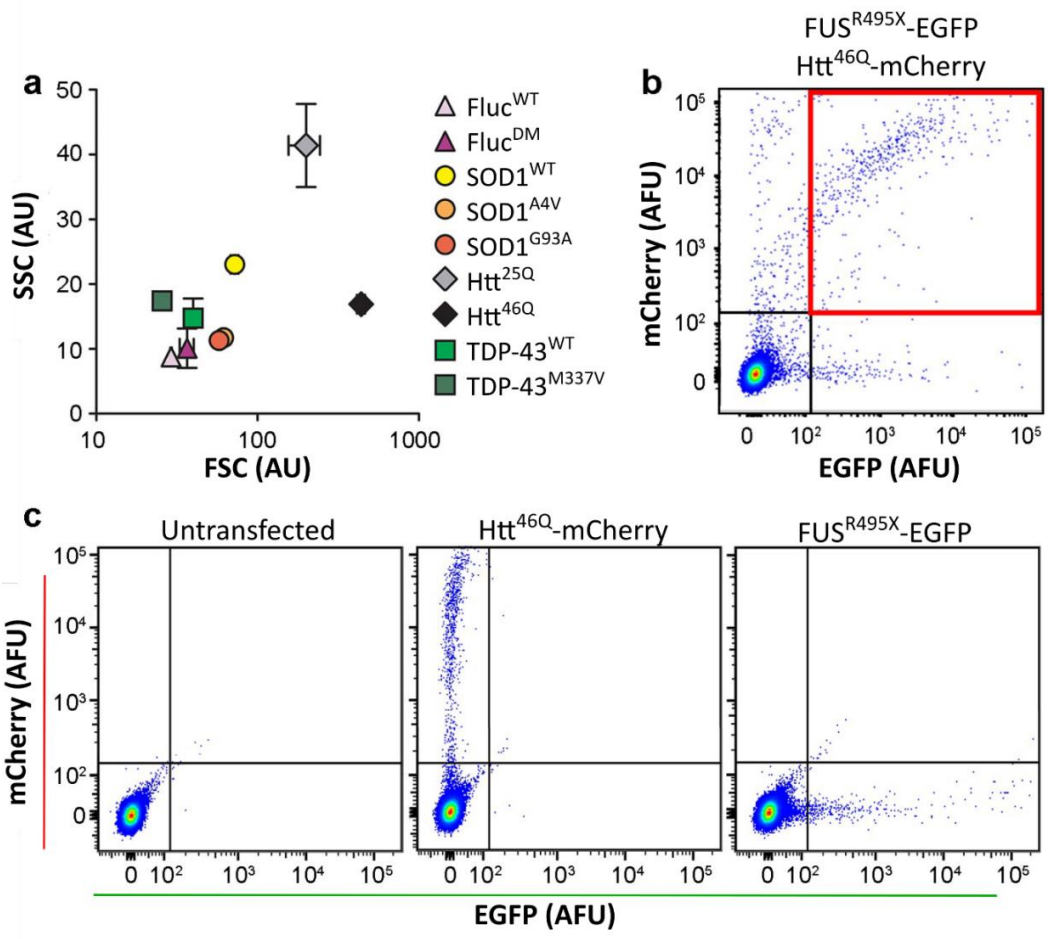

Figure 4.8. FloIT can resolve different types of inclusion bodies. (a) FloIT can resolve inclusion bodies formed by different proteins based on their FSC and SSC. Data shown are means ± SEM of triplicate measurements and are representative of two or three independent repeats. (b) Inclusions containing two different proteins can be detected by FloIT. Data shown are from Neuro-2a cells transfected to co-express FUS^{R495X}-EGFP and Htt^{46Q}-mCherry. Dual colour inclusions containing both fusion proteins are indicated by the red square. (c) Controls for the data shown in (b) *left-right:* Neuro-2a cells were either left untransfected or transfected to express Htt^{46Q}-mCherry or FUS^{R495X}-EGFP alone. Each result shown is representative of two or more independent experiments.

4.3.5 FloIT can quantify nuclear flux of fluorescently tagged proteins

FloIT can also be used to measure the trafficking of fluorescently labelled molecules from one cell compartment to another, providing at least one of these compartments remains intact following cell lysis. Two different nuclear trafficking models were used to demonstrate the feasibility of this application. Firstly, the efflux of TDP-43^{M337V} from the nucleus of transfected Neuro-2a cells induced by MG132 treatment was measured as a time dependent decrease in the proportion of fluorescent nuclei. Approximately 50.7 ± 1.4% of nuclei had tGFP fluorescence at 0 h and this decreased to 31.5 ± 3.8% after 16 h (Figure 4.9a). Thus, FloIT was

able to successfully detect and quantify the MG132-induced efflux of TDP-43^{M337V} from the nucleus to the cytoplasm.

In a second trafficking model independent of protein aggregation, FloIT was used to measure the movement of a transcription factor, NFAT-EGFP, into the nucleus in response to Ca^{2+} dyshomeostasis induced by ionomycin (a Ca^{2+} ionophore). In this experiment, transfected HEK293 cells expressing NFAT were treated with ionomycin and analysed by FloIT. This showed treatment with ionomycin increased the fraction of fluorescent nuclei from 7.6 ± 2.1 % (0 µM) to 58.5 ± 2.6% (1 µM; Figure 4.9b). This movement of NFAT into the nuclei after ionomycin treatment was confirmed by confocal microscopy (Figure 4.9c).

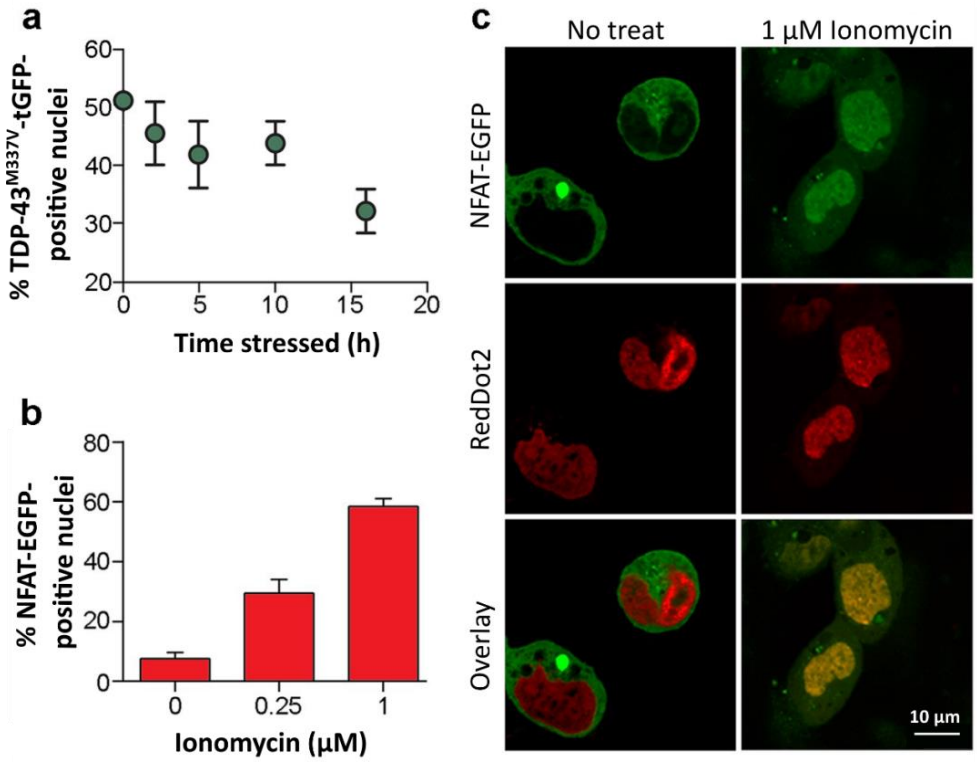

Figure 4.9. FloIT can quantify nuclear flux of fluorescently tagged proteins. (a) Time-dependent efflux of TDP-43^{M337V}-tGFP from the nuclei of Neuro-2a cells treated with 10 µg/mL MG132. Data is shown as the percent change in tGFP-fluorescing nuclei (at t=0, the percent value represents the transfection efficiency). (b) Dose-dependent influx of NFAT-EGFP into ionomycin treated HEK293 cell nuclei. Data is shown as the percent NFAT-EGFP-positive nuclei at the indicated doses. (c) Confocal microscopy images of NFAT-EGFP-expressing HEK293 cells with and without 1 µM ionomycin treatment. Scale bar = 10 µm. Values are means ± SEM of triplicate measurements and each result is representative of two or three independent experiments.

4.4 Discussion

This chapter outlines the development of FloIT, a novel technique that uses standard flow cytometry systems and reagents to quantitatively enumerate and evaluate the physical characteristics of protein inclusions, and protein trafficking. FloIT offers great potential to significantly expand the range and quality of data acquired in the many ongoing studies of proteostasis and neurodegeneration in which inclusions and protein mislocalisation are a focus. The ability of FloIT to discriminate between inclusions formed by a range of different proteins, and by two different proteins in the same cell may find a variety of applications in research. FloIT also provides a platform suitable for medium or high throughput drug screening, to identify small molecules that inhibit the mislocalisation of protein to subcellular compartments, and inhibit the formation of or enhance the clearance of protein inclusions in cells.

By using multiple fluorescent labels, FloIT could be used to track and quantify dynamic interactions between different proteins and cells over time. For example, multi-colour FloIT can be used to investigate the mechanism of the prion-like propagation of protein aggregates in cell-based models of NDs (Jucker and Walker 2013, Hanspal et al. 2017). Recent research using FloIT showed that the internalisation of $SOD1^{G93A}$ aggregates (that were applied extracellularly to NSC-34 cells) promoted the intracellular aggregation of $TDP\text{-}43^{WT}$ (Zeineddine et al. 2017a). Extending on this finding, the same group used two-colour FloIT to show that the cell to cell transfer of an aggregation-prone mutant $TDP\text{-}43^{G294A}$-EGFP co-aggregated with, and increased the aggregation of $TDP\text{-}43^{WT}$-tdTomato in NSC-34 cells (Zeineddine et al. 2017b). Therefore, multi-colour FloIT can be used as a novel approach to monitor the prion like spread of aggregates formed from disease-associated proteins from one cell to another. FloIT can also be used to monitor the incorporation of WT proteins into inclusions formed from mutant aggregation-prone proteins.

FloIT can be used as a platform for the medium-high throughput drug screening of compound libraries that modulate components of the proteostasis network, such as HSF1, the master transcriptional regulator of the HSR. In addition to quantifying changes in the number of inclusions, FloIT can also quantify the effect that these compounds might have on the physical properties of the inclusions (*i.e.* size – FSC, granularity – SSC). In this way, FloIT offers several advantages over other traditional qualitative methods such as filter trap assays, but the basic principle behind these two techniques (*i.e.* analysing the insoluble fraction of cell lysates) is the same.

The applications of FloIT have the potential to be extended to quantify inclusion bodies in brain and spinal cord lysates derived from transgenic mouse models of NDs, and post-mortem patient samples. This can be achieved by using SDS in the lysis buffer, in place of TritonX-100, to digest tissues, which are structurally complex compared to cells in culture. The number of inclusions could then be normalised to total protein content rather than the number of nuclei across each sample. Furthermore, fluorescent dyes that stain amyloid fibrils, such as Thioflavin T (Xue et al. 2017) and tetraphenylethene maleimide (TPE-MI) (Chen et al. 2017), or antibodies specific to a protein of interest directly conjugated to a fluorophore could be used. By using antibodies, inclusions can be identified based on the type of protein of which they are comprised. Alternatively, antibody labelling could be used to identify other proteins that are recruited to the inclusion body, such as chaperones or ubiquitin.

An analysis of studies investigating the effect of different Hsps and upregulation of the HSR in rodent models of ALS and HD highlighted that there is no standard reporting on the development or inhibition of inclusion bodies (see section 1.7, Table 1-3 and Table 1-4). Indeed, in some cases the effect of molecular chaperone upregulation on insoluble protein content is not reported, despite the strong correlation between inclusion body formation and neurodegeneration. This makes the efficacy of different Hsps or drugs that induce the HSR (or

indeed, therapeutic modulation of any mechanism of proteostasis) difficult to compare across multiple studies and decades of research. Therefore, further development of FloIT for its use in CNS tissues would represent an important step towards standardising the quantification of inclusion bodies before and after therapeutic intervention in transgenic mouse models of NDs.

Figure 4.2 shows that fluorescent aggregates and nuclei can be sorted by FACS. Therefore, it follows that inclusions comprised of fluorescently-tagged proteins, or fluorescent antibody-labelled inclusions can be purified by FACS from cells or tissues and subjected to proteomics analysis to determine their composition. Inclusions isolated from cell-based models or tissues from rodent models of NDs can be used to identify: (i) what types of proteins are incorporated into inclusion bodies formed from a range of disease-causing proteins (ii) how proteostasis modulating compounds influence the types of proteins recruited into inclusion bodies, and (iii) how the protein composition of inclusions changes over the time course of the disease in the animal.

With regard to the characterisation of the physical properties of the inclusions, using a standard flow cytometer, FloIT is able to resolve inclusions within 0.5 – 15 μm in diameter. Future research could investigate methods by which the sensitivity of FloIT can be enhanced to detect smaller aggregates that precede the formation of inclusions. For example, the LSR Fortessa X-20 cell analyser used in this research can be upgraded from a 50 mW 488 nm laser to a 100-300 mW 488 nm laser to increase the sensitivity for small particle detection. A recent study reported a sensitive flow cytometric method for the quantification of physical properties of viral particles (Gaudin and Barteneva 2015). The following modifications were made to their FACSAriaII special order cell sorter, 300 mW 488 nm laser, digital focusing system, and advanced optics using a FSC-photomultiplier tube. Fluorescent latex beads between 40 – 100 nm in diameter were able to be detected (Gaudin and Barteneva 2015). Therefore, FloIT can be performed using a standard flow cytometer, and future research could investigate enhancing

the sensitivity of the cytometer to detect oligomers or small aggregates that precede inclusion body formation.

FloIT can be used to study the transport of proteins into cell nuclei, or other cell organelles or structures that can be released intact from cells and are sufficiently large to be resolved by flow cytometry. For example, hypotonic extraction or specific detergents that selectively permeabilise the plasma membrane can be used an alternative approach to study protein trafficking into other intracellular organelles, such as mitochondria (0.5-10 μm in size). In fact, the mislocalisation of proteins into mitochondria is an established molecular pathology associated with several NDs and represents an important area of future research (Kwong et al. 2006). For example, the mitochondrial mislocalisation of SOD1, Htt, α-synuclein, and many other ND-associated proteins have been implicated in the loss of Ca^{2+} uptake, enhanced reactive oxygen species production, apoptosome activation and/or the loss of ATP synthesis (Kwong et al. 2006, Petrasch-Parwez et al. 2007, Devi et al. 2008, Tafuri et al. 2015). More recently, the mitochondrial mislocalisation of mutant TDP-43 (in TDP-43^{A315T} transgenic mice) has been strongly correlated with the degeneration of cortical and motor neurons *in vivo,* by reducing the expression and activity of complex I in the electron transport chain (Wang et al. 2016). Inhibition of TDP-43^{A315T} import into the mitochondria by treating mice with a peptide (PM1; which mimics and competes for binding to mitochondria with the TDP-43 mitochondrial import signal) reversed neurodegeneration and other ALS-associated disease pathologies in these mice (Wang et al. 2016). Therefore, inhibiting the mislocalisation of disease-associated proteins to mitochondria is a promising avenue of research. Future research could employ FloIT to examine the translocation of a range of disease-associated proteins into mitochondria. Furthermore, FloIT can be used in a medium-high throughput platform to screen the ability of novel compounds to inhibit mitochondrial mislocalisation and inclusion body formation in cell-based models of NDs.

To summarise, FloIT is a simple and powerful technique for the rapid quantification of inclusion bodies and nuclear trafficking. The present study demonstrated several applications of FloIT, including its use in cell-based models of ND-associated protein aggregation (with one and two fluorophores), and the translocation of two different proteins (TDP-43 and NFAT) out of and into the nucleus. FloIT has the potential to be further developed, for example to investigate protein mislocalisation or translocation to mitochondria in cell-based models of NDs. Furthermore, FloIT could also be used to analyse CNS tissues from transgenic mice models of NDs to standardise the quantification of inclusion bodies before and after therapeutic intervention or with and without transgene expression. These additional applications of FloIT are likely to find a very wide range of uses in cell biology, biochemistry and biomedical research.

Chapter 5: Investigating the effect of neuronal differentiation and protein aggregates on the induction of the HSR in neuron-like cells

This chapter has been prepared as a manuscript for publication:

R. San Gil, D. Cox, L. McAlary, L. Ooi, J. J. Yerbury, H. Ecroyd, Investigating the effect of neuronal differentiation and protein aggregates on the induction of the HSR in neuron-like cells. (2018). *Manuscript in preparation.*

Author contributions: RSG performed all the experiments, analysed the data, constructed the figures and wrote the initial manuscript. DC and LM made the recombinant α-synuclein and $SOD1^{G93A}$ protein and provided the protocols used for the *in vitro* aggregation of these proteins. HE, LO, and JJY helped design experiments and oversaw their implementation, and edited the manuscript.

5.1 Introduction

The downstream products of HSR activation, such as Hsps, have been shown to have anti-aggregation and cytoprotective activities in cells. Therefore, the upregulation of Hsp expression in response to ND-associated pathologies, such as protein aggregation (intra- or extracellular) would be beneficial to the cell. However, a systematic review of studies involving rodent models of HD and ALS indicated that there is an absence of an HSR in disease-affected CNS tissues, as determined by immunocytochemistry, liquid chromatography-mass spectrometry, and immunoblot analysis of Hsp levels (see Tables 1.1 and 1.2). The absence of an upregulated expression of Hsps in the CNS prompts the question of whether cells in the CNS respond to chronic protein aggregation associated with NDs by inducing an HSR?

One hypothesis is that neurons have an attenuated capacity to induce an HSR in response to cellular stress relative to other cell types in the CNS (*e.g.* astroglia). This hypothesis originates from seminal studies that have investigated the HSR *in vivo* in response to whole organism hyperthermia; these showed that Hsp70 induction occurs in astroglia, but not in neurons (Manzerra and Brown 1992, Pavlik et al. 2003, Pavlik and Aneja 2007). Likewise, cultured astroglia elicit faster and higher levels of Hsp70 expression after heat shock (45°C/30 min) compared to cultured cortical neurons (Nishimura et al. 1991, Nishimura and Dwyer 1996). Furthermore, studies that have differentiated a range of neuroblastoma and other cell-lines into "neuron-like" cells have shown that differentiation is correlated with a decline in the capacity of these cells to induce an HSR (Dwyer et al. 1996, Hatayama et al. 1997, Oza et al. 2008, Yang et al. 2008).

An alternate explanation for the absence of the HSR in the CNS in mouse models of NDs is that inclusion body formation is insufficient to activate the HSR. This aspect has received relatively less attention. One study demonstrated that the expression of pathogenic, polyQ-expanded Htt was unable to induce an HSR in HEK293 cells (Bersuker et al. 2013). Since Htt

forms terminal protein inclusions, termed IPODs, it may be that the formation of this particular type of inclusion enables it to bypass components of the proteostasis network (Kaganovich et al. 2008). Thus, findings investigating whether inclusions formed by Htt induce an HSR may not be relevant to the formation of aggregates by other disease-associated proteins (such as SOD1), since these are thought to form JUNQ inclusions that do interact with components of the proteostasis network (Matsumoto et al. 2006, Kaganovich et al. 2008, Polling et al. 2014, Farrawell et al. 2015). More research is required to establish whether disease-associated protein aggregates induce an HSR in cells, thus leading to an increase in the expression of Hsps that can prevent further aggregation. Of particular importance is whether induction of the HSR differs depending on the type of inclusions that forms in cells.

There is a growing body of literature, using both cell-based and rodent models of HD, ALS, and Parkinson's disease, that demonstrates that protein aggregates can move between cells via a prion-like propagation mechanism [for reviews see (Jucker and Walker 2013, Zeineddine and Yerbury 2015, Hanspal et al. 2017, Victoria and Zurzolo 2017)]. It has been postulated that this involves the release of misfolded protein seeds from a "donor" cell (*i.e.* through cell death or exocytosis) and the uptake of seeds by an "acceptor" cell. These seeds have been shown to recruit endogenous WT proteins into pathogenic aggregates (Jucker and Walker 2013). Several mechanisms of seed uptake have been proposed. For example, with respect to $SOD1^{G93A}$ and α-synuclein aggregates, there is evidence that the uptake of extracellular aggregates by cells occurs via Rac1-mediated macropinocytosis (Zeineddine et al. 2015). These internalised aggregates are able to rupture macropinosomes to gain entry into the cytosol to seed further aggregation (Zeineddine et al. 2015).

When applied extracellularly, aggregates comprised of ND-associated proteins are taken up into neuron-like cells such as Neuro-2a, NSC-34 and SH-SY5Y cells. For example, it takes 60 min for $SOD1^{H46R}$ aggregates to be taken up by Neuro-2a cells (Munch et al. 2011) and 8 h for

α-synuclein aggregates to be taken up by SH-SY5Y cells (Lee et al. 2008). Most research has focused on the role of the extracellular arm of the proteostasis network with regard to interacting with and preventing cytotoxic protein aggregation in the extracellular space (Wyatt et al. 2013). However, relatively few studies have investigated whether the internalisation of extracellular protein aggregates into the cytosol triggers an HSR in cells.

Assessment of the induction of the HSR in cells and tissues has typically involved qualitative and low throughput techniques, including immunoblotting to assess the levels of Hsp70 and hyperphosphorylated HSF1 in cells. In an attempt to quantify the HSR, reporter constructs composed of a firefly luciferase reporter gene downstream of a Hsp promoter (most commonly the *hspa1a* promoter) have been used, whereby addition of luciferin (substrate of firefly luciferase) emits chemiluminescence that can be quantified within cells. More recently, Bersuker et al. (2013) generated stable U2OS and HEK293 cell lines containing fluorescent reporters of the HSR, whereby EGFP is downstream of a *hspa1a* promoter sequence fragment. The advantage of using fluorescent reporters of the HSR over firefly luciferase reporters is that fluorescence facilitates both quantitative single cell (*e.g.* flow cytometry or microscopy) and bulk cell (*e.g.* fluorescence plate reader) analyses. Furthermore, the HSR is a dynamic pathway that demonstrates cell- and stress-type dependent changes with regard to the kinetics and magnitude of induction. Therefore, investigating the time-resolved changes in HSR induction in single cells is an additional advantage of using fluorescent reporters of the HSR.

To investigate possible reasons for the absence of an HSR in the affected CNS tissues of rodent models of HD and ALS, the objectives of the work described in this chapter were to (i) investigate the effect of neuronal differentiation on the induction of the HSR in the context of classical inducers of the HSR, and (ii) evaluate the effect of intra- and extracellular protein aggregation on the HSR. To do so, Neuro-2a and HEK293 cell lines were stably transfected to express a fluorescent reporter under the control of a promoter comprised of 8 putative HSEs

(Appendix A). These stable cell lines were then used to quantitatively assess the kinetics and magnitude of HSR induction after differentiation or exposure to intra- and extracellular protein aggregates.

5.2 Materials and methods

Celastrol was from AdooQ Biosciences (Irvine, CA, USA). Purified recombinant stocks of α-synuclein, α-synuclein seeds, and $SOD1^{G93A}$ were kind gifts from Dr Luke McAlary and Dr Dezerae Cox, respectively (University of Wollongong, Australia).

5.2.1 Antibodies

Dilutions used for immunoblotting (IB) and immunocytochemistry (ICC) are included in parentheses. Rabbit monoclonal anti-tyrosine hydroxylase (ab75875; IB 1:2500 ICC 1:100), rat monoclonal anti-HSF1 (ab81279, IB 1:1000) and mouse monoclonal anti-βIII-tubulin (ab78078; ICC 1:1000) primary antibodies, and goat anti-mouse IgG DyLight 650 (ab96874; ICC 1:500), goat anti-rabbit IgG DyLight 488 (ab96895; ICC 1:500), and goat anti-rat IgG-HRP (ab6734; IB 1:5000) secondary antibodies were obtained from Abcam (Cambridge, MA, USA). Goat anti-rabbit IgG-HRP (A9044; 1:5000) secondary antibody was obtained from Sigma Aldrich.

5.2.2 Plasmids

To generate Neuro-2a and HEK293 cell lines that stably express mCherry constitutively and stress-inducible EGFP downstream of a minimal Hsp70 promoter (minHsp70p) the following two constructs were generated; pCMV-mCherry and pminHsp70p-EGFP. With respect to pCMV-mCherry, the EGFP gene was excised from pEGFP-N1 (Clontech) with flanking *Eco*RI/*Bsr*GI sites and replaced with the mCherry gene. Regarding pminHsp70p-EGFP, a minimal Hsp70 promoter upstream of an EGFP gene was excised with flanking *Acc*651/*Bam*HI sites (kind gift of Dr Frank Coullidad and Dr Chrit Moonen, University of Bordeaux, France) and subcloned into *Acc*651/*Bam*HI digested pGL4.4 (Thermo Fisher Scientific) containing a hygromycin resistance gene (Appendix A).

The constructs coding for the expression of cerulean-tagged huntingtin exon 1 fragment (Htt) with a non-pathogenic (*i.e.* 25 polyglutamines; pT-Rex-Cerulean-Htt^{25Q}) or pathogenic (*i.e.* 72 polyglutamines; pT-Rex-Cerulean-Htt^{72Q}) were kind gifts from Assoc Prof Danny Hatters (University of Melbourne, Australia). Constructs for the expression of cerulean-tagged SOD1^{WT}, SOD1^{G93A}, WT firefly luciferase (Fluc^{WT}) and a double mutant (R188Q/R261Q) form of Fluc (Fluc^{DM}) were also generated. To do so, the *cerulean* gene was PCR amplified from pT-Rex-Htt^{72Q} using forward: 5′-catggatccaccggtcgccaccatggtgagca-3′ and reverse: 5′-caggattcttacttgtacagctc-3′ primers with flanking *Bam*HI/*Bsr*GI restriction sites to replace the EGFP gene in pEGFP-N1-SOD1^{WT} and pEGFP-N1-SOD1^{G93A} (these constructs were kind gifts of Dr Justin Yerbury, University of Wollongong). The *cerulean* gene was PCR amplified from pT-Rex-Htt^{72Q} using forward 5′-catgggatccaccggccggtcgccaccatggtgagc-3′ and reverse: 5′-caggattcttacttgtacagctc-3′ primers with flanking *Bam*HI/*Bsr*GI restriction sites to replace the EGFP gene in pcDNA4-TO-myc-hisA-EGFP-Fluc^{WT} and pcDNA4-TO-myc-hisA-EGFP-Fluc^{DM} (these constructs were kind gifts of Prof Mark Wilson, University of Wollongong).

All the constructs generated and used in this work were verified by sequencing using a Hitachi 3130xl Genetic Analyser (Applied Biosystems, Mulgrave, Australia). The primers used to sequence each construct are listed in

Table 5-1.

Table 5-1. List of primers used to sequence each of the constructs generated in this work.

Plasmid sequenced	Primer sequence
pCMV-mCherry	Forward: 5′-cgcaaatggggcggtaggcgtg-3′
	Reverse: 5′-caggattcttacttgtacagctc-3′
pminHsp70p-EGFP	Forward: 5′-tgcaggtgccagaacatttc-3′
	Reverse: 5′-caggattcttacttgtacagctc-3′
pT-Rex-Cerulean-Htt^{25Q} pT-Rex-Cerulean-Htt^{72Q}	Forward: 5′-cgcaaatgggcggtaggcgtg-3′
	Reverse: 5′-ctctacaaatgtggtatggc-3′
pCerulean-N1-SOD1^{WT} pCerulean-N1-SOD1^{G93A}	Forward: 5′-cgcaaatggggcggtaggcgtg-3′
	Middle: 5′-cttgcggccgcctagaagaagtcgtgctgc-3′
	Reverse: 5′-ctctacaaatgtggtatggc-3′
pcDNA4-TO-myc-hisA-Cerulean-Fluc^{WT} pcDNA4-TO-myc-hisA-Cerulean-Fluc^{DM}	Forward: 5′-cgcaaatggggcggtaggcgtg-3′
	Reverse: 5′-tagaaggcacagtcgagg-3′

5.2.3 Generation of SOD1^{G93A} and α-synuclein aggregates

5.2.3.1 Thioflavin T-based aggregation assays

The formation of SOD1^{G93A} aggregates was monitored by an *in situ* thioflavin T (ThT) binding assay that has previously been described (McAlary et al. 2016). Briefly, 100 µM purified SOD1^{G93A} was incubated with 20 mM DTT, 5 mM EDTA and 10 µM ThT in PBS (pH 7.4) at 37°C. The reaction mixtures were loaded into a clear-bottomed 384-well plate (Greiner, Germany) and covered with adhesive film. The plate was incubated in a PolarStar Omega Plate Reader (BMG Labtechnologies, Australia) at 37°C for 30 min prior to commencement of the PolarStar protocol. The plate underwent double orbital shaking at 300 rpm for 300 s at the start of a 900 s cycle for at least 200 cycles. The ThT fluorescence was measured by excitation at 450 nm and its emission read at 480 nm using the bottom optic of the plate reader.

The formation of α-synuclein fibrils was determined by an end-point ThT assay as previously described (Buell et al. 2014). Briefly, α-synuclein seeds were produced by incubating 150 µM α-synuclein in 50 mM phosphate buffer (pH 7.4), for 48 h at 40°C under maximal stirring with a magnetic stirrer (WiseStir MSH-20A, Witeg, Wertheim, Germany). The seed fibrils were fragmented by sonication using a microtip probe sonicator (Branson 250 Digital Sonifer, Branson Ultrasonics, CT, USA), using 30% amplification and 75% cycles. The fibrils were

flash frozen in liquid N_2 and stored at -80°C until required. To produce mature fibrils, 100 µM of monomeric α-synuclein was incubated with 1% (w/w) α-synuclein seeds in 50 mM phosphate buffer (pH 7.4) at 37°C for 72 h. A 5 µL aliquot of the α-synuclein fibrils was then loaded into a black clear-bottomed 384-well plate with 25 µL 50 mM phosphate buffer and 10 µM ThT. The ThT fluorescence was measured by excited at 450 nm and its emission read at 480 nm using the bottom optic of the plate reader.

5.2.3.2 Transmission electron microscopy of SOD1^{G93A} and α-synuclein

Transmission electron microscopy (TEM) was employed to visualise the SOD1^{G93A} and α-synuclein aggregates used to treat the cells (Section 5.2.7.2). An 8 µL aliquot of the aggregated protein was applied onto an ultrathin carbon film coated 400 mesh copper TEM grid (ProSciTech, Australia). Samples were then diluted with 2 µL of 0.22 µm filtered milli-Q H_2O and left for 3 min. Grids were dried with lint-free paper by wicking away the H_2O from the side. Grids were washed with 10 µL of milli-Q H_2O, dried again, and 10 µL of 1% (w/v) phosphotungstic acid, the contrast reagent, was added and grids left to incubate for 1 min. The phosphotungstic acid was wicked away and the grids were washed twice with 10 µL of milli-Q H_2O. Grids were air dried and imaged at the Australian Institute of Innovative Materials (University of Wollongong) using a JEOL JEM-2011 TEM (JEOL, Japan). Images were processed using Digital Micrograph (Gatan, USA).

5.2.4 Cell culture of Neuro-2a and HEK293

See section 2.6.

5.2.5 Neuro-2a differentiation

The protocol used for the differentiation of Neuro-2a cells into neuron-like cells has previously been described (Tremblay et al. 2010). Briefly, Neuro-2a cells were seeded at a density of 75,000 cells/mL into 96-well plates. After 24 h, the media was replaced with either 0.1% FCS

DMEM/F12 or 0.1% FCS DMEM/F12 supplemented with 1 mM dibutyryl cyclic adenosine monophosphate (dbcAMP) to induce differentiation. Neuro-2a were incubated in the absence or presence of dbcAMP in reduced serum media for 72 h with a media change after 48 h to refresh dbcAMP levels. Differentiation was assessed by examining expression levels of tyrosine hydroxylase and neurite length.

5.2.6 Generation and maintenance of Neuro-2a and HEK293 stable cell lines

Stable cell lines for the constitutive expression of mCherry and stress-inducible expression of EGFP were generated in Neuro-2a and HEK293 cell lines. Thus, activation of the HSR after treatment with a stressor could be monitored in cells in real time using EGFP as a fluorescent reporter. Neuro-2a cells were used as a neuron-like cell line, which are capable of differentiation. HEK293 cells were used as a non-neuronal, positive control, since previous studies have generated and validated the use of a similar fluorescent stable cell line to report on the induction of the HSR (Bersuker et al. 2013).

Neuro-2a and HEK293 were first transfected with *Vsp*I linearised pCMV-mCherry and transfected cells were grown under selective pressure (300 µg/mL and 400 µg/mL G418, respectively) for 7 days. Monoclonal mCherry-expressing Neuro-2a and HEK293 cell lines were generated by limiting dilution and subsequent monoclonal expansion. Monoclonal mCherry-expressing Neuro-2a and HEK293 cell lines were transfected with *Not*I linearised pminHsp70p-EGFP and transfected cells were grown under selective pressure (300 µg/mL or 400 µg/mL G418, and 100 µg/mL hygromycin) for 7 days.

To obtain a polyclonal Neuro-2a or HEK293 cell population with stress-inducible EGFP expression, cells were heat shocked (42°C/ 2 h with recovery at 37°C/ 6 h), harvested by trypsinisation, washed twice in PBS, and resuspended in FACS buffer, 1 mM EDTA, 25 mM HEPES and 0.5% (w/v) BSA in PBS. These cells were then purified using an S3e Cell Sorter

(Bio-Rad, USA) equipped with 488 nm and 561 nm lasers. For both the Neuro-2a and HEK293 cell lines, $mCherry^{+ve}$ $EGFP^{+ve}$ cells were sorted and collected for sub-culture. These EGFP HSR reporter cell lines are referred to in this work as Neuro-2a (HSE:EGFP) and HEK293 (HSE:EGFP).

Neuro-2a (HSE:EGFP) and HEK293 (HSE:EGFP) cell lines were maintained under the same conditions as the parental cell lines. Constant selection pressure was achieved by supplementing the media used to culture Neuro-2a (HSE:EGFP) with 300 µg/mL G418 and 100 µg/mL hygromycin, and HEK293 (HSE:EGFP) with 400 µg/mL G418 and 100 µg/mL hygromycin.

5.2.7 Cell stress treatments

5.2.7.1 Heat shock and cadmium chloride ($CdCl_2$) assays

Heat shock and $CdCl_2$ were used as classical inducers of the HSR to assess the capacity of Neuro-2a and HEK293 cell lines to induce an HSR. Neuro-2a (HSE:EGFP) and HEK293 (HSE:EGFP) cells were seeded at a density of 200,000 cells/mL into 12-well plates. Optimal concentrations of $CdCl_2$ and celastrol were determined in dose response assays, whereby cells were either treated with log and ½ log concentrations of $CdCl_2$ (0-100 µM) or celastrol (0 – 1 µM) for 24 h. In addition, cells were heat shocked (42°C/ 2 h) and recovered at different time points of recovery at 37°C. After treatment, Neuro-2a (HSE:EGFP) and HEK293 (HSE:EGFP) were imaged every 2 h for 24 h using an IncuCyte Live Cell Analysis System (Essen BioScience, USA) to optimise the $CdCl_2$, celastrol and heat shock treatments, where mCherry and EGFP fluorescence intensities were analysed over the time-course of the experiments. The optimal treatment concentrations and times were determined to be 33 µM/ 6 h or 10 µM/ 24 h for $CdCl_2$, 0.75 µM/ 24 h for celastrol and heat shock at 42°C/ 2 h with recovery at 37°C.

To assess the differential effects of these treatments on the HSR in Neuro-2a (HSE:EGFP) and HEK293 (HSE:EGFP) cell lines, the time taken to reach half of the EGFP maximum intensity was analysed as a means to assess the kinetics of HSR induction with each treatment. In addition, analysis of the EGFP intensity after 24 h of treatment represented the magnitude of HSR induction after treatment with different stresses.

5.2.7.2 Extracellular aggregation stress assays

Pathogenic protein aggregates were applied extracellularly to Neuro-2a (HSE:EGFP) cells and activation of the HSR was assessed. Prior to treatment of cells, soluble non-aggregated α-synuclein and $SOD1^{G93A}$ were centrifuged (14,000 × *g*/ 30 min/ 4°C) to remove any oligomeric seeds that may have spontaneously formed. Aggregated $SOD1^{G93A}$ was pelleted (14,000 × *g*/ 30 min/ 4°C) and resuspended in fresh PBS to eliminate possible cytotoxicity of DTT and EDTA in the assay.

Neuro-2a (HSE:EGFP) cells were seeded at a density of 100,000 cells/mL in a 96-well plate and cultured overnight in 10% FCS DMEM/F12. The following day, cells were either treated with buffer alone (50 mM phosphate buffer for α-synuclein or PBS for $SOD1^{G93A}$) or soluble or aggregated α-synuclein or $SOD1^{G93A}$ (1 µM and 10 µM) diluted in serum-free DMEM/F12. Some cells in each plate were treated with 10 µM $CdCl_2$ as a positive control for HSR induction.

5.2.7.3 Intracellular protein aggregation stress assays

To assess the effect of intracellular protein aggregates on the HSR, Neuro-2a (HSE:EGFP) cells were transfected with cerulean-tagged WT and aggregation-prone mutant proteins. Cells were seeded at a density of 100,000 cells/mL in 12-well plates and cultured in 1 mL of 10% FCS DMEM/F12 media overnight. Cells were transfected with DNA:lipid complexes (1 µg DNA, 1 µL PLUS reagent, and 3 µL Lipofectamine LTX per well) for the expression of cerulean-tagged $SOD1^{WT}$, $SOD1^{G93A}$, Htt^{25Q}, Htt^{72Q}, $Fluc^{WT}$, or $Fluc^{DM}$. Cells were washed

twice with PBS (pH 7.4) 48 h post-transfection, harvested mechanically by aspiration on ice, and resuspended in 500 µL ice-cold PBS for analysis of intact cells or cell lysates by flow cytometry.

Parental Neuro-2a were either untransfected, or singly transfected to express EGFP, mCherry or cerulean fluorescent proteins. These samples were used to set gates for the flow cytometric analysis and to determine the spectral overlap that occurs between these three fluorophores so that spectral compensation could be applied prior to analysis. All analyses of the flow cytometry data were performed using FlowJo (version 10.0.8, Tree Star, OR, USA).

5.2.8 IncuCyte Zoom imaging and image analysis

5.2.8.1 Image analysis of total image fluorescence intensity

Time-resolved fluorescence intensity data from Neuro-2a (HSE:EGFP) and HEK293 (HSE:EGFP) cells were acquired using an IncuCyte Live Cell Analysis System. Phase contrast and fluorescent images were acquired at 2 h intervals with the 10× or 20× objective. The fluorescence intensity of mCherry and stress-inducible EGFP were quantified using the basic analyser algorithm (Table 5-2) from a minimum of 9 images per well at each time point. Spectral overlap from the mCherry (3%) channel was removed from the EGFP channel in these images.

Table 5-2. Cell mask parameters for the analysis of relative fluorescence intensities of EGFP and mCherry using the IncuCyte Zoom basic analyser.

Cell-line	Fluorescent protein	Channel	Exposure (ms)	Background correction	Edge sensitivity	Data presentation
Neuro-2a	EGFP	Green	400	Top-hat (50 µm, 2 GCU)	-15	GCU × μm^2/ image

	mCherry	Red	800	Adaptive (2 RCU)	0	RCU × µm^2/ image
HEK293	EGFP	Green	400	Top-hat (80 µm, 2 GCU)	-6	GCU × µm^2/ image
	mCherry	Red	800	Adaptive (2 RCU)	-21	RCU × µm^2/ image

The mean EGFP relative fluorescence intensity (RFU) was normalised by dividing the EGFP RFU by the mCherry RFU at each time point to account for relative changes in cell density over time (equation 5.1). The normalised EGFP data is presented as the mean fold change (Δ) in the EGFP/ mCherry ratio (± SEM) of three independent repeats as described by equation 5.2, where $EGFP_{Tx}$ represents the EGFP RFU at any time and $EGFP_{T0}$ represents the EGFP RFU at time = 0 h.

$$\left(\frac{EGFP\ (RFU)}{mCherry\ (RFU)}\right) = Normalised\ EGFP \qquad \text{(equation 5.1)}$$

$$\left(\frac{Normalised\ EGFP_{Tx}}{Normalised\ EGFP_{T0}}\right) = Fold\ \Delta\ EGFP \qquad \text{(equation 5.2)}$$

5.2.8.2 Image analysis of single cell fluorescent intensities

Differentiated and non-differentiated Neuro-2a cells were immunolabelled for βIII-tubulin and tyrosine hydroxylase and the neurite length and intensity of tyrosine hydroxylase staining was analysed from confocal images. Total neurite length in each image was analysed using the Neurite Tracer macros in Image J with the following parameters (threshold for neurons: 40, threshold for nuclei: 5, minimum size of nuclei: 500, maximum size of nuclei: 3500). The total neurite length in each image was normalised to the number of nuclei in that image and expressed as a fold change compared to the sample not treated with dbcAMP, according to equations 5.3 and 5.4:

$$\frac{Total\ neurite\ length}{\#\ Nuclei} = Normalised\ neurite\ length \qquad \text{(equation 5.3)}$$

$$\frac{Normalised\ neurite\ length}{Average\ neurite\ length\ of\ non{-}treated\ cells} = Fold\ \Delta\ neurite\ length \qquad \text{(equation 5.4)}$$

The fluorescence intensity of tyrosine hydroxylase (DyLight 488) immunolabelled cells was analysed using CellProfiler 2.2.0 (Broad Institute of Harvard and MIT, USA), using the parameters outlined in Table 5-3 and the following custom-made sequence of processing events:

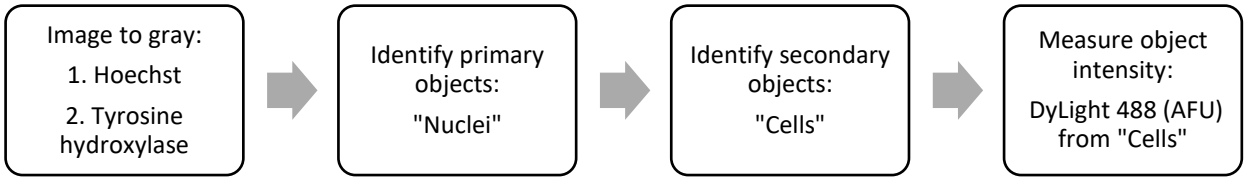

Neuro-2a (HSE:EGFP) were either left untransfected or transfected to express Htt^{72Q} and $Fluc^{DM}$, and imaged on a Leica SP5 confocal microscope at 37˚C under 5% CO_2/ 95% air. Each well was imaged at 8 regions of interest at 1 h intervals for up to 60 h. The images obtained were analysed using CellProfiler 2.2.0 using the following custom-made sequence of image processing events:

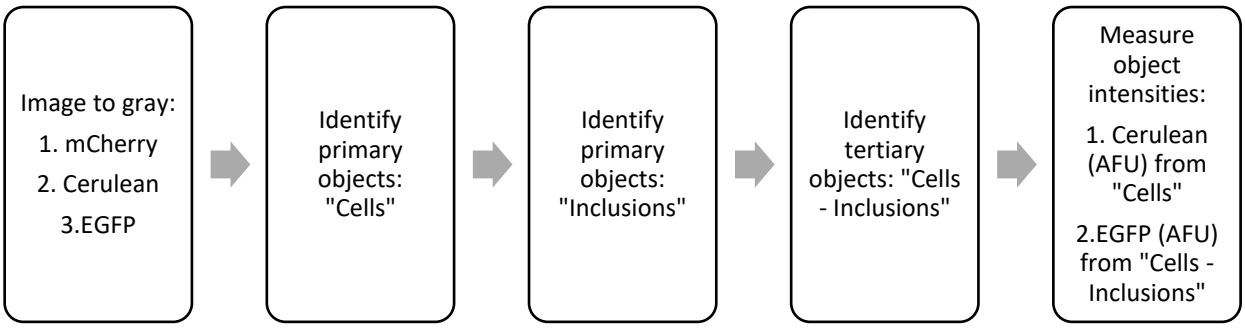

The mask parameters used for the identification of "Cells" and "Inclusions" are outlined in Table 5-3. These parameters were optimised to separate cell clumps and identify individual cells and inclusions. The tertiary objects identified, "Cells – Inclusions", were applied as a primary measure to eliminate the spectral overlap of the cerulean fluorescence signal at the site of inclusions into the EGFP fluorescence signal. Therefore, EGFP fluorescence was measured from an area of the cell that did not contain inclusion bodies (*i.e.* "Cells – Inclusions").

Table 5-3. Mask parameters for the analysis of relative fluorescence intensities of individual cells in confocal imaging experiments using Cell Profiler.

Object identified	Input image	Diameter (pixel units)	Threshold strategy	Thresholding method	Threshold boundaries	Distinguish clumps	Dividing lines in clumps
Nuclei	Hoechst	20-100	Automatic	-	-	Intensity	Shape
Cells	mCherry	20-65	Global	Otsu	0.01-1.0	Intensity	Propagate
	DyLight 488	-	Global	Otsu	0.0-1.0	-	-
Inclusions	Cerulean	15-40	Global	Otsu	0.01-1.0	Intensity	Shape

Spectral compensation was applied to the fluorescence intensity data, whereby 13% of the cerulean signal was removed from the raw EGFP signal (equation 5.5); this was used as a secondary measure to eliminate spectral overlap.

$$Raw\ EGFP - \left(\frac{Raw\ Cerulean}{1} \times \frac{13}{100}\right) = Corrected\ EGFP \qquad \text{(equation 5.5)}$$

Lastly, to count the number of cerulean^{+ve} (or transfected) cells at each time point a threshold of 65 (RFU) was applied. Likewise, to count the number of EGFP^{+ve} (or HSR^{+ve}) cells at each time point a threshold of 15 (RFU) of the corrected EGFP fluorescence intensities was applied. These thresholds were determined from the EGFP RFU and cerulean RFU of cells in the untransfected and untreated samples. With regard to experiments where the HSR was tracked in single cells, membrane permeability was determined by the loss of mCherry fluorescence in cells. In Figure 4.6 (section 4.3.2), membrane permeability after treatment TritonX-100 coincides with the release of soluble fluorescent protein from the cell. Therefore, in this work loss of mCherry fluorescence in a cell was used as an indirect marker of cell death. The raw data analysed in Figure 5.14e and f, were re-analysed by an independent, blinded, third-party and showed the same result.

5.2.9 Flow cytometric analysis

5.2.9.1 Analysis of whole cells

See Chapter 2 section 2.9.

5.2.9.2 Analysis of cell lysates

See Chapter 4 section 4.2.3.1.

Briefly, flow cytometry of the cell lysates was performed using an LSR Fortessa X-20 analytical flow cytometer equipped with a 405 nm and 640 nm laser. Cerulean fluorescence emissions were captured using the 450/50 nm bandpass filter. RedDot1 nuclear stain fluorescence emissions were captured using the 670/30 nm bandpass filter. The forward scatter threshold was reduced to 200 (minimum possible setting) to detect small fluorescent particles. A minimum of 100,000 events were acquired per sample.

5.2.10 Immunoblotting

See section 2.7. The fold change in protein expression was normalised to the total protein loaded, using Mini-Protean, TGX, Stain-Free gels (Bio-Rad). The proportion of hyperphosphorylated HSF1 of the total HSF1 in each sample was determined using equation 5.6.

$$\left(\frac{HSF1_{80\ kDa}\ (AU)}{HSF1_{80\ kDa}\ (AU)+HSF1_{75\ kDa}(AU)}\right) \times 100 = \%\ pHSF1 \qquad \text{(equation 5.6)}$$

5.2.11 Statistics

See section 2.10. The statistical analyses used to determine significant differences between the means are described in the appropriate figure legends. For data showing the fold change in EGFP expression over time in Neuro-2a (HSE:EGFP) and HEK293 (HSE:EGFP), a non-linear fit was applied [log(agonist) vs. response (Variable slope)]. The time taken to reach half maximal EGFP intensity was determined by using the logEC50 value as a measure of the kinetics of the HSR.

5.3 Results

5.3.1 Differentiating Neuro-2a into neuron-like cells

One hypothesis in the field is that the HSR becomes attenuated in terminally differentiated and mature neurons. Therefore, we sought t o investigate whether the capacity of Neuro-2a to induce an HSR was dependent on the differentiation status of the cells.

Neuro-2a cells were differentiated via treatment with 1 mM dbcAMP for 72 h, a protocol that has previously been shown to differentiate Neuro-2a into dopaminergic-like neurons (Tremblay et al. 2010). Immunoblot analysis of whole cell lysates showed that there was significant (6-fold) increase in expression of the dopaminergic neuronal marker tyrosine hydroxylase expression in cells treated with dbcAMP compared to cells cultured in the absence of dbcAMP [$F(2, 9) = 11.39$, $P = 0.0034$] (Figure 5.1a-b). Quantification of the length of neurite extensions of βIII-tubulin immunolabelled cells showed that there was a 3-fold increase in the length of neurite extensions in differentiated cells compared to non-differentiated cells (Figure 5.1c-d). Furthermore, the tyrosine hydroxylase staining was significantly greater in differentiated compared to non-differentiated cells ($P = 0.004$; Figure 5.1c and e). There was no difference in the proportion of tyrosine hydroxylase positive cells between differentiated and non-differentiated cells, as all Neuro-2a cells showed low levels of endogenous tyrosine hydroxylase expression (Figure 5.1c).

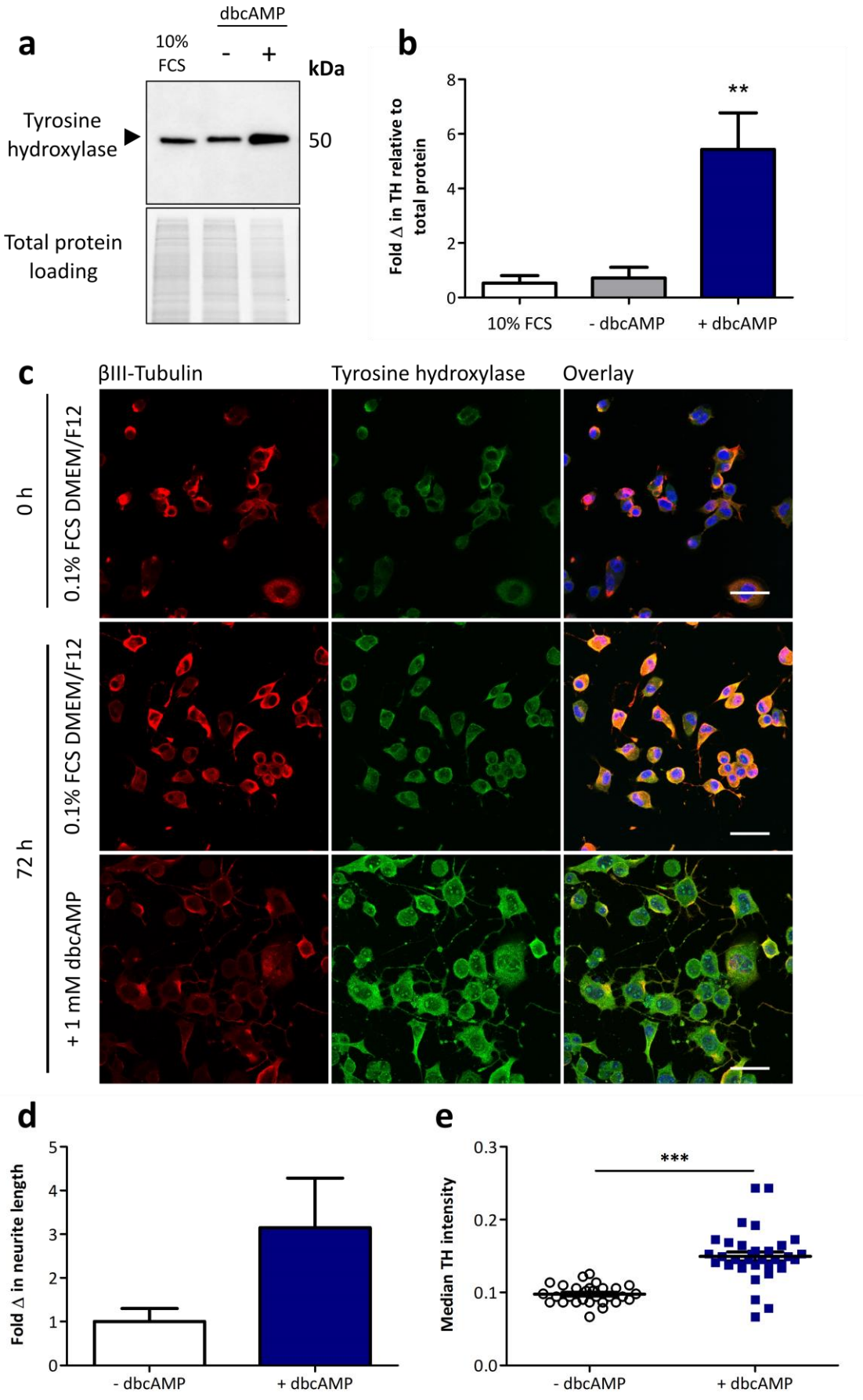
a
dbcAMP
10% FCS
-
+
kDa
Tyrosine hydroxylase
50
Total protein loading
b
Fold Δ in TH relative to total protein
**
10% FCS
- dbcAMP
+ dbcAMP
c
βIII-Tubulin
Tyrosine hydroxylase
Overlay
0 h
0.1% FCS DMEM/F12
72 h
0.1% FCS DMEM/F12
+ 1 mM dbcAMP
d
Fold Δ in neurite length
- dbcAMP
+ dbcAMP
e
Median TH intensity
***
- dbcAMP
+ dbcAMP

Figure 5.1. Characterisation of differentiated Neuro-2a cells. (a) Immunoblot analysis of tyrosine hydroxylase (50 kDa) expression in cells cultured for 72 h with (*left – right*) 10% FCS DMEM/F12, 0.1% FCS DMEM/F12 and 0.1% FCS DMEM/F12 supplemented with 1 mM dbcAMP. Total protein loading was assessed by imaging stain-free gels prior to electroblotting. (b) Fold change in tyrosine hydroxylase expression after 72 h of culture in 10% FCS DMEM/F12, 0.1% FCS DMEM/F12 and 0.1% FCS DMEM/F12 supplemented with 1 mM dbcAMP. Tyrosine hydroxylase band intensity was normalised to total protein loading. Data shown is the mean + SEM of four independent repeats. Statistically significant differences between the means were assessed using a one-way ANOVA followed by a Dunnet post-hoc test, where $P < 0.01$ (**). (c) Immunocytochemistry of Neuro-2a cells at 0 h and 72 h in the presence and absence of the differentiation agent, dbcAMP. *Left- right*: Cells were stained for βIII-tubulin (DyLight 650) and tyrosine hydroxylase (DyLight 488), and overlays are shown with Hoechst 33342 nuclear stain. Scale bar = 50 µm. (d) The fold change in neurite length in the absence and presence of dbcAMP for 72 h. Data represents the total neurite length in three images normalised to the number of nuclei in each image. (e) The median tyrosine hydroxylase (TH)-DyLight 488 fluorescence intensity of cells cultured in the absence or presence of dbcAMP for 72 h. Data shown are the mean of 35 cells imaged by confocal microscopy in each sample group and statistically significant differences between the means were determined using a student's t-test, where $P < 0.001$ (***).

Differentiated and non-differentiated Neuro-2a were treated with classical inducers of the HSR to determine whether HSR induction is impaired after differentiation. Whole cell lysates were subjected to immunoblot analysis probing for the hyperphosphorylation of HSF1 (pHSF1; seen as an upwards shift in migration on the SDS-PAGE) as a marker of HSR activation in these cells.

Treatment of Neuro-2a cells with $CdCl_2$ (33 µM/ 6 h) or heat shock (42°C/ 2 h with no recovery) resulted in an increase in pHSF1 in both differentiated and non-differentiated samples (Figure 5.2a). This indicates that both differentiated and non-differentiated Neuro-2a can induce an HSR. Semi-quantitative analysis of the HSF1 and pHSF1 band densities, followed by two-way ANOVA, demonstrated that there was a significant effect of differentiation on the proportion of pHSF1 (relative to total HSF1) following the treatments [$F(1, 16) = 13.11$, $P = 0.0023$]. Post-hoc analysis indicated that there was a significantly greater proportion of pHSF1 (75 ± 5%) in differentiated Neuro-2a cells treated with $CdCl_2$ compared to non-differentiated cells (38 ± 5%; $P < 0.001$; Figure 5.2b). However, there was no significant difference in the proportion of pHSF1 between differentiated and non-differentiated Neuro-2a after heat shock. After 6 h recovery at 37°C, the HSF1 in heat shocked cells was

dephosphorylated such that there was no pHSF1 detected in differentiated or non-differentiated samples.

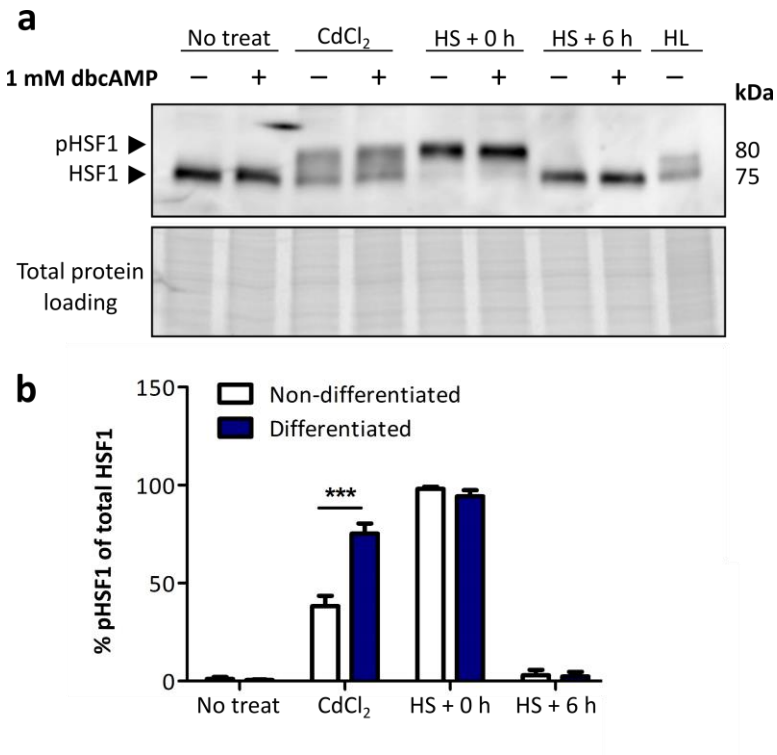

Figure 5.2. The effect of differentiation on the HSR in Neuro-2a cells. Neuro-2a cells were differentiated with 1 mM dbcAMP for 72 h and then stressed by exposure to $CdCl_2$ (33 µM/ 6 h) or heat shock (HS, 42°C/ 2h, with or without recovery at 37°C/ 6 h). (a) Immunoblot analysis of whole cell lysates from cells either differentiated or not and then exposed to stressors. Heat shocked (42°C/ 2 h) HeLa cell (HL) lysate were used as a positive control for pHSF1. Lysates were probed for HSF1 (75 kDa), including hyperphosphorylated isoforms of HSF1 (pHSF1; 80 kDa). Total protein loading was assessed by imaging stain-free gels prior to electroblotting. (b) The proportion of HSF1 that was hyperphosphorylated relative to total HSF1 in each of the samples analysed by immunoblotting. Data shown is the mean + SEM of three independent repeats. Differences between the means were assessed using a two-way ANOVA followed by a Bonferroni post-hoc test, where $P < 0.001$ (***).

5.3.2 Investigating the HSR in Neuro-2a with a fluorescent reporter

To further investigate the activation of the HSR, stable Neuro-2a and HEK293 cell lines were generated in which expression of a fluorescent protein (EGFP) was used to report on HSR induction. The Neuro-2a stable cell line was generated because this would enable induction of the HSR to be investigated in differentiated neuron-like cells and could also be used to investigate the ability of aggregation-prone proteins associated with NDs to induce an HSR in neuron-like cells.

To validate that these stable cell lines report on HSR induction, they were first treated with classical inducers of the HSR, $CdCl_2$, heat shock and celastrol (a compound identified in a drug screen as a potent inducer of the HSR) (Heemskerk et al. 2002, Westerheide et al. 2004). The fluorescent reporter, EGFP, has a half-life of 27 h (Corish and Tyler-Smith 1999), therefore, these experiments needed to be performed in a time-frame that would facilitate the accumulation of EGFP after HSR induction to assess the magnitude of the HSR. Dose-response experiments were conducted to determine the concentration of $CdCl_2$ (0-100 µM) and celastrol (0-1 µM) that induce a maximal HSR (Figure 5.3). Based on these results, the subsequent experiments used 10 µM CdCl2 and 0.75 µM celastrol to induce the HSR in undifferentiated Neuro-2a (HSE:EGFP).

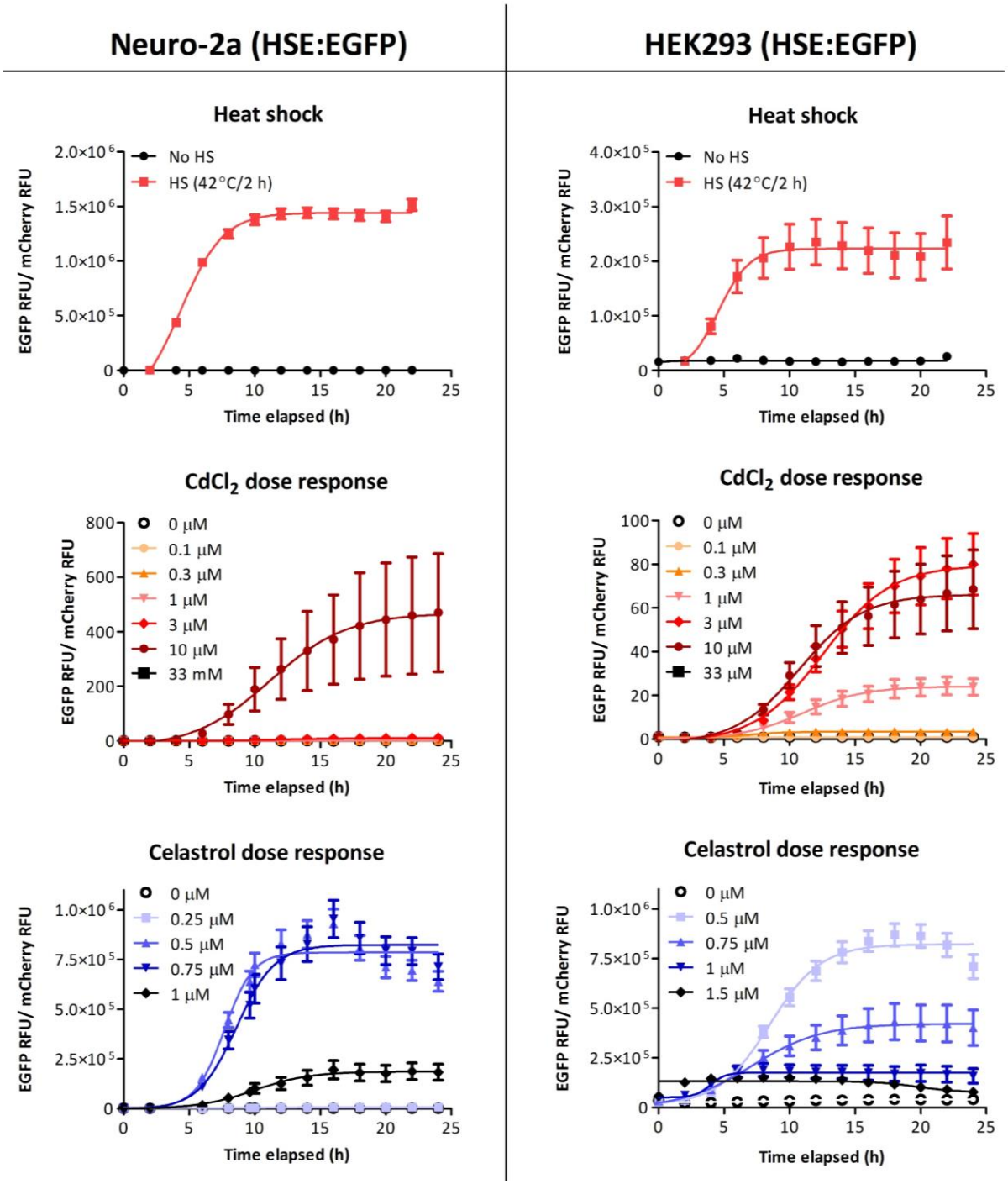

Figure 5.3. Optimisation of heat shock, $CdCl_2$ and celastrol treatments in undifferentiated Neuro-2a (HSE:EGFP) and HEK293 (HSE:EGFP) cells. Cells were plated at a density of 200,000 cells/mL and after 24 h cells were subjected to heat shock (42°C/ 2 h), log and ½ log doses of $CdCl_2$ (0-33 µM) or celastrol (0-1 µM). Cells were imaged every 2 h using an IncuCyte Live Cell Imaging System to monitor the induction of EGFP, a reporter of HSR activation. Data is presented as the fold change in EGFP RFU over time, normalised to mCherry RFU, to account for changes in cell density over the time-course of the experiment. The data shown is the mean ± SEM of three independent repeats. The optimal treatment concentrations and times for IncuCyte live cell imaging experiments were determined to be 10 µM/ 24 h $CdCl_2$, 0.75 µM (Neuro-2a) and 0.5 µM (HEK293)/ 24 h celastrol and heat shock at 42°C/ 2 h with recovery at 37°C over 24 h.

After treatment with 10 µM $CdCl_2$, heat shock (42°C/ 2 h) or 0.75 µM celastrol, there was a time-dependent increase in EGFP fluorescence intensity in Neuro-2a (HSE:EGFP) (Figure 5.4a and b). Fluorescence was first detected 2-4 h following heat shock treatment of Neuro-2a (HSE:EGFP) (Figure 5.4b), reaching a maximum after 10-20 h. The time taken to induce the HSR and to reach maximum EGFP fluorescence varied between treatment types. The expression of EGFP was induced significantly faster after heat shock in Neuro-2a (HSE:EGFP) (5.1 ± 0.2 h) compared to after treatment with $CdCl_2$ or celastrol (11 ± 0.6 h and 8.3 ± 1.5 h, respectively; Figure 5.4d) [$F(2, 6) = 28.28$, $P = 0.0009$] as measured by the time taken to reach half maximal fluorescence. Treatment with each of the classical inducers of the HSR significantly up-regulated EGFP expression in Neuro-2a (HSE:EGFP) compared to no treatment [$F(3,8) = 4.265$, $P = 0.0448$]. However, there were no differences observed between the magnitude of HSR induction between treatment type in Neuro-2a (HSE:EGFP) (Figure 5.4f). Beyond the 24 h time-frame of these experiments, cells treated with $CdCl_2$ or celastrol died as a consequence of the toxicity of these treatments. Heat shocked cells continued to grow and divide during the recovery period, EGFP fluorescence intensity peaked at 10 h and began to slowly decline after 24 h. This is likely representative of EGFP turnover over time.

HEK293 cells that were stably transfected in an identical manner to Neuro-2a (HSE:EGFP) were also generated as a non-neuronal cell line. Treatment of HEK293 (HSE:EGFP) with each of the classical inducers of the HSR also resulted in the induction of EGFP expression over the time course of the experiment, with similar kinetics of HSR induction as the Neuro-2a (HSE:EGFP) cells (Figure 5.4c and e). A direct comparison of the two cell lines was not performed because Neuro-2a (HSE:EGFP) showed a greater fold increase in EGFP fluorescence intensity after each of the treatments compared to HEK293 (HSE:EGFP). For example, following treatment with celastrol, there was a 500-fold increase in EGFP fluorescence in Neuro-2a (HSE:EGFP) cells compared to a 40-fold increase in EGFP in

HEK293 (HSE:EGFP) (Figure 5.4b-c and f-g). There are a number of possibilities that may explain the differences in the fold EGFP induction after treatment between Neuro-2a and HEK293 including: (i) differences in plasmid copy number in the two stable cell lines, (ii) the ability of chromatin to remodel after stress so HSF1 can access target promoter regions, or (iii) differences between the ability of human and mouse derived cell lines to respond to these stresses by inducing an HSR

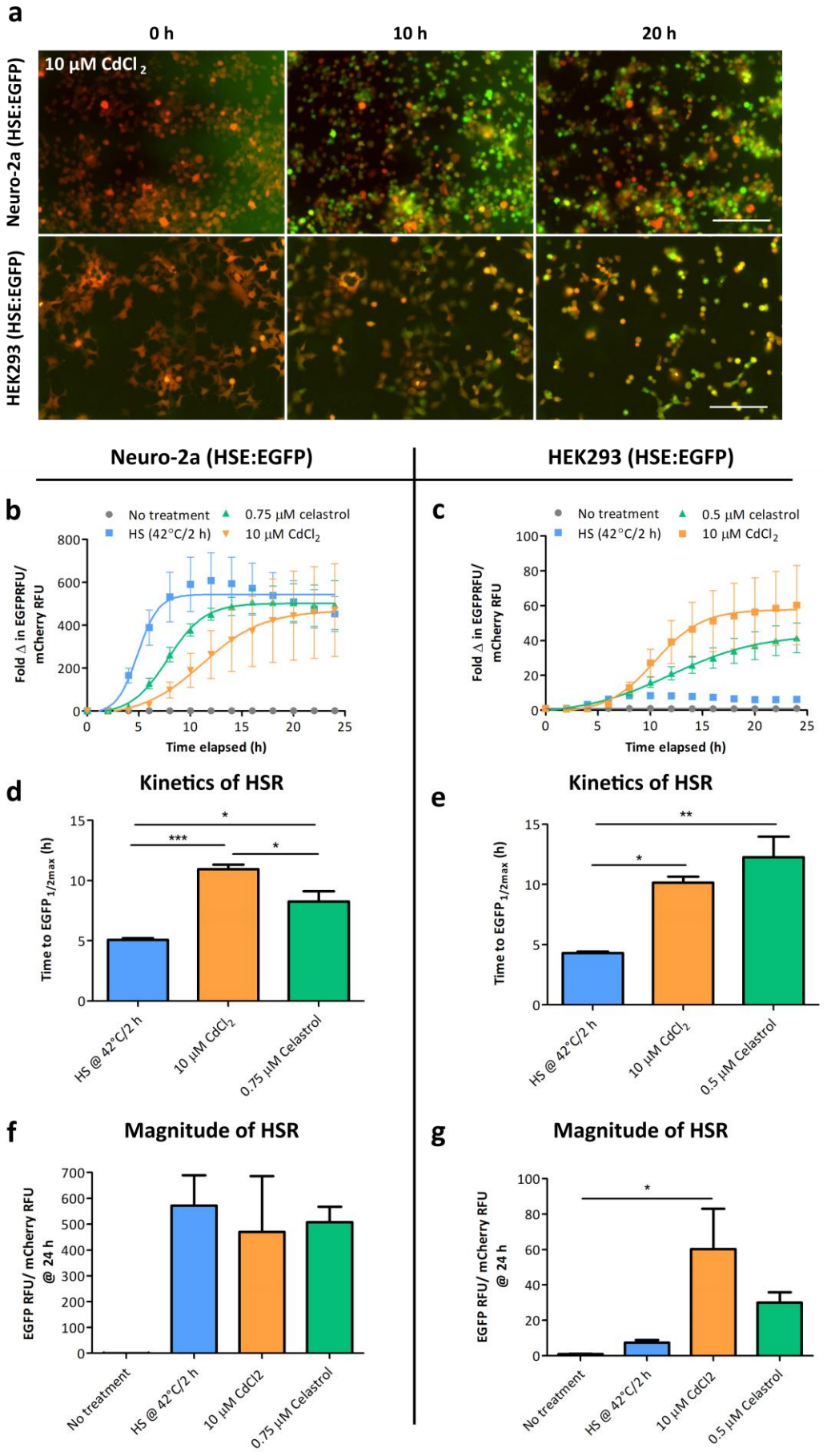
a
0 h
10 h
20 h
10 µM CdCl 2
Neuro-2a (HSE:EGFP)
HEK293 (HSE:EGFP)
Neuro-2a (HSE:EGFP)
HEK293 (HSE:EGFP)
b
No treatment
HS (42°C/2 h)
0.75 µM celastrol
10 µM CdCl2
Fold Δ in EGFPRFU/ mCherry RFU
Time elapsed (h)
c
No treatment
HS (42°C/2 h)
0.5 µM celastrol
10 µM CdCl2
Fold Δ in EGFPRFU/ mCherry RFU
Time elapsed (h)
d
Kinetics of HSR
Time to EGFP 1/2max (h)
HS @ 42°C/2 h
10 µM CdCl2
0.75 µM Celastrol
e
Kinetics of HSR
Time to EGFP 1/2max (h)
HS @ 42°C/2 h
10 µM CdCl2
0.5 µM Celastrol
f
Magnitude of HSR
EGFP RFU/ mCherry RFU @ 24 h
No treatment
HS @ 42°C/2 h
10 µM CdCl2
0.75 µM Celastrol
g
Magnitude of HSR
EGFP RFU/ mCherry RFU @ 24 h
No treatment
HS @ 42°C/2 h
10 µM CdCl2
0.5 µM Celastrol

Figure 5.4. Validating the use of undifferentiated Neuro-2a (HSE:EGFP) and HEK293 (HSE:EGFP) stable cell lines for the quantification of HSR induction. (a) Neuro-2a (HSE:EGFP) and HEK293 (HSE:EGFP) stable cell lines were treated with 10 µM $CdCl_2$ and imaged every 2 h in the IncuCyte to monitor the expression of EGFP, a reporter of HSR induction. Representative overlay images of mCherry and EGFP fluorescence are shown after 0, 10 and 20 h of treatment. (b-c) The fold change in EGFP fluorescence intensity over time normalised to mCherry fluorescence intensity to account for changes in cell density over the time-course of the experiment. The HSR was induced in these cells by heat shock (42°C/ 2 h) or treatment with 0.75 µM (Neuro-2a) or 0.5 µM (HEK293) celastrol or 10 µM $CdCl_2$. (d-e) The kinetics of HSR induction as determined by the time taken to reach half maximal EGFP fluorescence. (f-g) The magnitude of HSR induction as determined by EGFP fluorescence of the HSE:EGFP stable cell lines after 24 h of treatment with each stress. Data shown is the mean ± SEM of three independent repeats. Differences between the means were assessed using a one-way ANOVA followed by Tukey's post-hoc test, where $P < 0.05$ (*), $P < 0.01$(**), and $P < 0.001$ (**).

5.3.3 Evaluating the HSR in differentiated neuron-like cells

Neuro-2a (HSE:EGFP) were used to further evaluate the capacity of differentiated and non-differentiated cells to induce an HSR after treatment with $CdCl_2$ and heat shock. The 3-day differentiation protocol using dbcAMP did not induce an HSR in these cells. This indicated that any responses observed were a result of the stress treatment, not the differentiation process. Heat shock and $CdCl_2$ treatment of undifferentiated and differentiated Neuro-2a (HSE:EGFP) cells resulted in a time-dependent increase in EGFP fluorescence (Figure 5.5a). Analysis by two-way ANOVA indicated that differentiated cells had a significantly increased EGFP fluorescence intensity compared to non-differentiated cells after heat shock [$F(1, 72) = 192.7$, $P < 0.0001$; Figure 5.5b]. Likewise, differentiated cells had a significantly greater EGFP fluorescence intensity compared to non-differentiated cells after $CdCl_2$ treatment [$F(1, 84) = 160.4$, $P < 0.0001$; Figure 5.5c]. Analysis of the time taken to reach half maximal EGFP expression showed that dbcAMP differentiation did not impact the kinetics of HSR induction after heat shock or $CdCl_2$ treatment (Figure 5.5d). There was a significantly greater magnitude of HSR induction at 20 h in differentiated compared to non-differentiated cells after heat shock and $CdCl_2$ treatment ($P < 0.001$; Figure 5.5e).

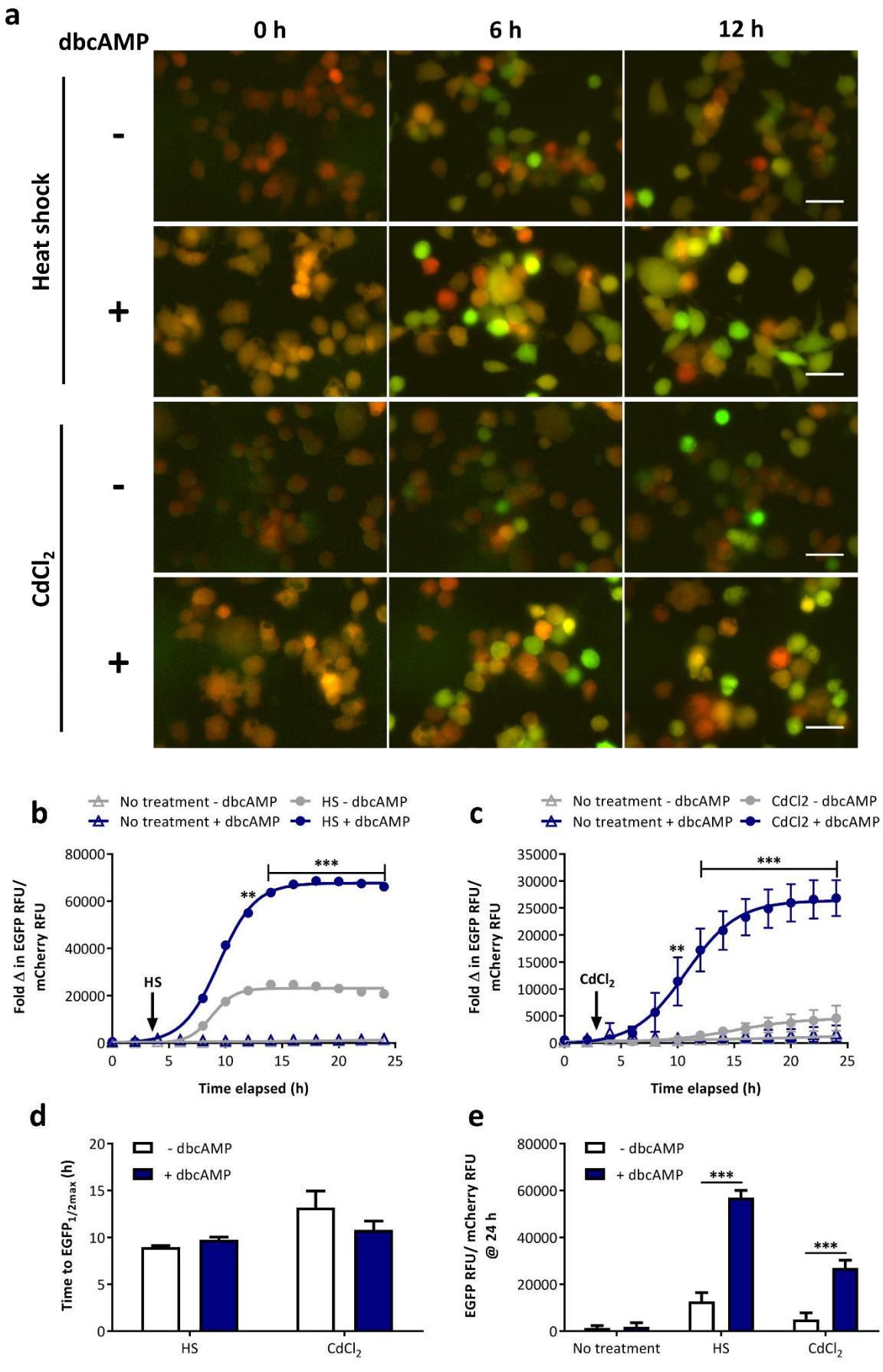
a
dbcAMP
0 h
6 h
12 h
Heat shock
-
+
$CdCl_2$
-
+
b
No treatment - dbcAMP
No treatment + dbcAMP
HS - dbcAMP
HS + dbcAMP
Fold Δ in EGFP RFU/ mCherry RFU
HS
Time elapsed (h)
c
No treatment - dbcAMP
No treatment + dbcAMP
CdCl2 - dbcAMP
CdCl2 + dbcAMP
Fold Δ in EGFP RFU/ mCherry RFU
$CdCl_2$
Time elapsed (h)
d
- dbcAMP
+ dbcAMP
Time to $EGFP_{1/2max}$ (h)
HS
$CdCl_2$
e
- dbcAMP
+ dbcAMP
EGFP RFU/ mCherry RFU @ 24 h
No treatment
HS
$CdCl_2$

Figure 5.5. The effect of differentiation on the HSR in Neuro-2a (HSE:EGFP) following treatment with classical inducers of the HSR. Neuro-2a (HSE:EGFP) were differentiated (or not) with 1 mM dbcAMP for 72 h and then subjected to stress either by treatment with $CdCl_2$ (10 µM) or heat shock (42°C/ 2 h). Cells were monitored over time using the IncuCyte, whereby EGFP fluorescence was used as a reporter of HSR induction. (a) Representative overlays of EGFP and mCherry from the IncuCyte of differentiated and non-differentiated cells over-time after heat shock or $CdCl_2$ treatment. (b) The fold change in EGFP RFU normalised to mCherry RFU over time in heat shocked (or not) cells that were either differentiated (+ dbcAMP) or non-differentiated (- dbcAMP). (c) The fold change in EGFP RFU normalised to mCherry RFU over time in differentiated or non-differentiated cells treated (or not) with $CdCl_2$. Arrows indicate the time at which plates were removed for treatment. (d) The kinetics of HSR induction measured by calculating the time taken to reach half maximal EGFP RFU. (e) The magnitude of HSR induction measured by determining the EGFP RFU after 24 h of treatment. Data shown are the mean ±SEM of three independent repeats. Differences between the means were assessed by a two-way ANOVA followed by post-hoc testing using Bonferroni's test, where $P < 0.01$ (**), and $P < 0.001$ (***).

5.3.4 Extracellular protein aggregates do not induce an HSR in neuron-like cells

There is increasing evidence that misfolded disease-associated proteins propagate through the CNS from the site of onset in a prion-like mechanism. This process likely involves the release of misfolded proteins and inclusion bodies from necrotic neurons into the extracellular matrix and subsequent uptake of these proteins by surrounding cells (Jucker and Walker 2013). However, it remains to be determined whether cells respond to the extracellular application of aggregated protein by inducing an HSR. For the remainder of this chapter, investigations were performed on undifferentiated Neuro-2a (HSE:EGFP) cells.

To test this, recombinant human α-synuclein and $SOD1^{G93A}$ were aggregated *in vitro*. There was a significant increase in ThT fluorescence in the aggregated α-synuclein sample compared to monomeric α-synuclein and buffer alone, indicative of an increase in β-sheet structure with aggregation (Figure 5.6a). Transmission electron microscopy (TEM) indicated that α-synuclein had formed long mature fibrils, > 2 µm in length (Figure 5.6c). The formation of $SOD1^{G93A}$ aggregates was monitored by an *in situ* ThT binding assay; there was a time-dependent increase in ThT fluorescence relative to buffer alone (Figure 5.6b). The $SOD1^{G93A}$ aggregates formed in these assays were imaged by TEM, which indicated that the aggregates had an irregular and amorphous structure, < 80 nm in length (Figure 5.6d). Together, the ThT assay and TEM

images indicate that the $SOD1^{G93A}$ aggregates formed in this study contain an underlying β-sheet structure, but do not assemble into highly-ordered fibrils.

Soluble and aggregated forms of α-synuclein and $SOD1^{G93A}$ were applied extracellularly to Neuro-2a (HSE:EGFP) and the induction of an HSR monitored over the next 72 h by live cell imaging (Figure 5.6e-f). There was no change in EGFP fluorescence in the cells treated with either 1 μM or 10 μM of soluble or aggregated α-synuclein or $SOD1^{G93A}$ compared to cells treated with buffer alone over the 72 h period of these experiments (note: only 0-20 h are displayed in Figure 5.6e-f). Furthermore, analysis of the magnitude of HSR induction based on the EGFP fluorescence at 20 h indicated that there is no difference between treatment with soluble or aggregated α-synuclein or $SOD1^{G93A}$ and buffer alone, except for $CdCl_2$ treated cells (this treatment was used as a positive control in this assay; Figure 5.6g-h). Therefore, these results suggest that the extracellular application of aggregates formed from disease-associated proteins is not sufficient to induce an HSR in cells that have a competent HSR. Therefore, cell-to-cell propagation of misfolded proteins or aggregates, a molecular mechanism by which NDs are thought to spread in the CNS, may not induce an HSR in neurons.

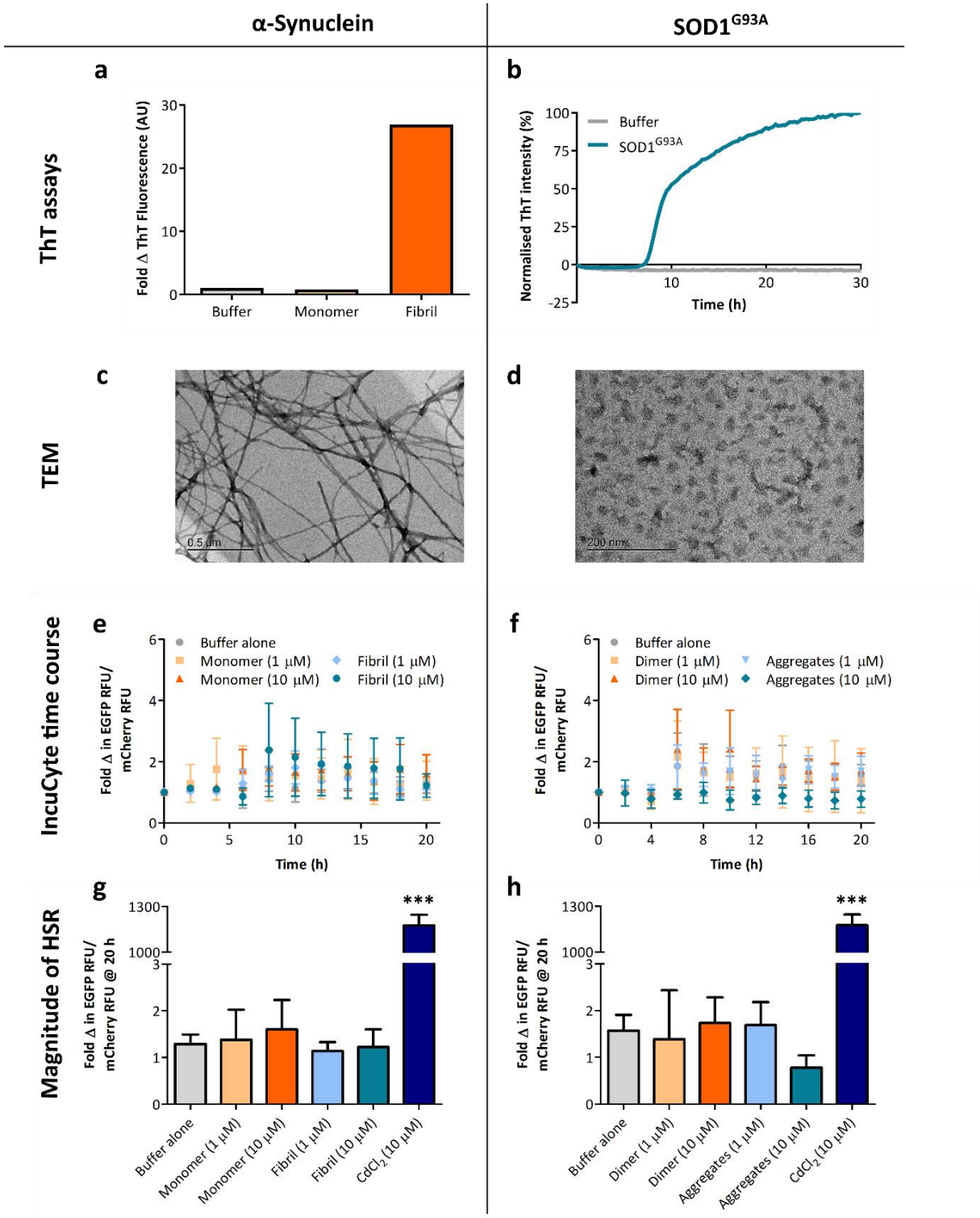

Figure 5.6. The HSR in Neuro-2a (HSE:EGFP) cells treated by applying soluble and aggregated forms of α-synuclein or SOD1^{G93A} extracellularly to cells in culture. (a) α-Synuclein fibrils were generated and tested for β-sheet fibrillar structure by end-point ThT assay. (b) The formation of SOD1^{G93A} aggregates was monitored *in situ* in a ThT time course assay. (c)-(d) TEM micrographs of α-synuclein fibrils and SOD1^{G93A} aggregates. Scale bar = 0.5 µm (c) and 200 nm (d). (e)-(f) Monitoring induction of the HSR using live-cell imaging. Time course of EGFP RFU normalised to mCherry RFU of Neuro-2a (HSE:EGFP) cells treated with (e) monomeric or fibrillar α-synuclein, or (f) dimeric or aggregated SOD1^{G93A}. (g)-(h) The magnitude of HSR activation as determined by the EGFP RFU/ mCherry RFU 20 h after application of the protein aggregates. Data shown is the mean ± SEM of three or four independent repeats. Differences between the means were assessed using a one-way ANOVA followed by Dunnet's post-hoc test (comparing to buffer alone control), where $P < 0.001$ (***).

5.3.5 The impact of protein aggregation on the HSR in neuron-like cells

This study also sought to determine whether Neuro-2a cells elicit an HSR in response to the expression of unstable (aggregation-prone) pathogenic (SOD1 and Htt) and non-pathogenic (Fluc) proteins. To examine this a suite of constructs were generated for the expression of cerulean-tagged $SOD1^{WT}$, $SOD1^{G93A}$, Htt^{25Q}, Htt^{72Q}, $Fluc^{WT}$, and $Fluc^{DM}$. Neuro-2a (HSE:EGFP) were transfected with each of the constructs and harvested for flow cytometric analysis to determine the effect of protein expression on HSR induction.

As a first step, the propensity of each of the cerulean-tagged proteins to aggregate was measured using FloIT, a flow cytometric method for the quantification of inclusions described in Chapter 4. Cells were lysed in the presence of RedDot1 nuclear dye 48 h post-transfection to quantify the number of nuclei in each sample. A sample without RedDot1 was used as a negative control to set the gate that defined nuclei and non-nuclear particles on plots of RedDot1 fluorescence and FSC (Figure 5.7a-b). The nuclei were excluded, and plots of FSC versus cerulean fluorescence resolved protein inclusions comprised of cerulean-tagged proteins. Lysates from cells transfected to express $SOD1^{WT}$, which does not readily form inclusions (McAlary et al. 2016), were used as an inclusion-negative control. Representative plots of non-nuclear particles from cells transfected to express $SOD1^{WT}$ (101 events) and $SOD1^{G93A}$ (933 events) are shown (Figure 5.7c-d).

FloIT analysis of the number of inclusions formed by each of the cerulean-tagged proteins revealed that the total number of inclusions formed by each protein varied. For example, $Fluc^{DM}$ and $SOD1^{G93A}$ formed 27 ± 7 and 3.5 ± 0.6% inclusions per 100 transfected cells, respectively (Figure 5.7e). FloIT analysis also allows the quantification and comparison of physical characteristics (FSC and SSC) of the inclusions formed by each of the cerulean-tagged proteins (Figure 5.7f). This demonstrated that inclusions formed by $Fluc^{DM}$ and $SOD1^{G93A}$ were

significantly smaller (based on the FSC signal) compared to inclusions formed by Htt72Q [$F(2, 4) = 19.22$, $P = 0.0089$].

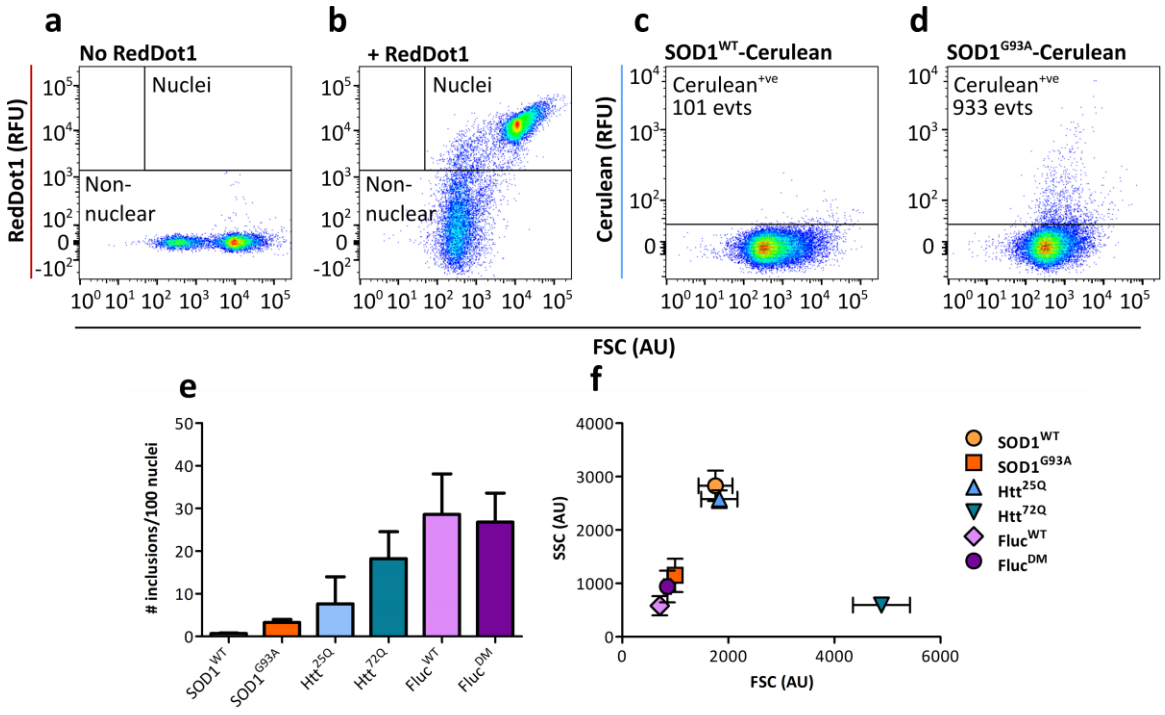

Figure 5.7. Quantification of the number of cerulean-tagged inclusion bodies formed in Neuro-2a (HSE:EGFP) cells by FloIT. Neuro-2a (HSE:EGFP) cells were transfected to express cerulean-tagged $SOD1^{WT}$, $SOD1^{G93A}$, Htt^{25Q}, Htt^{72Q}, $Fluc^{WT}$, or $Fluc^{DM}$ and, 48 h post-transfection, cells were lysed and the lysates analysed by FloIT. (a)-(b) Plots of forward scatter (FSC; size) and RedDot1 nuclear dye fluorescence used to enumerate the nuclei in the cell lysate samples. (a) Cell lysates were lysed in the absence of RedDot1 and used to set square gates to capture $RedDot1^{+ve}$ events and $RedDot^{-ve}$ non-nuclear events. (b) Cells lysed in the presence of RedDot1 are shown as a representative plot. (c)-(d) Plots of FSC and cerulean RFU. Representative plots show events acquired from Neuro-2a (HSE:EGFP) cells transfected to express $SOD1^{WT}$-cerulean and $SOD1^{G93A}$-cerulean. The number of $cerulean^{+ve}$ events are denoted in the gate. (e) The number of cerulean inclusion bodies quantified by FloIT, normalised to the number of transfected nuclei. (f) Bivariate plot of the FSC and side scatter (SSC; granularity) of the cerulean inclusions identified by FloIT. Data shown is the mean ± SEM of three independent repeats. Differences between the means were determined using a one-way ANOVA followed by Tukey's post-hoc test, there were no statistically significant differences in (e).

Following the quantification of the relative levels of inclusion body formation, whole cells were analysed by flow cytometry to assess whether the expression of these proteins induced an HSR in Neuro-2a (HSE:EGFP). The gating strategy that was adopted is outlined in Figure 5.8a-d, such that only single, transfected cells with cerulean fluorescence were included in the analysis when determining the capacity of Neuro-2a (HSE:EGFP) to induce an HSR.

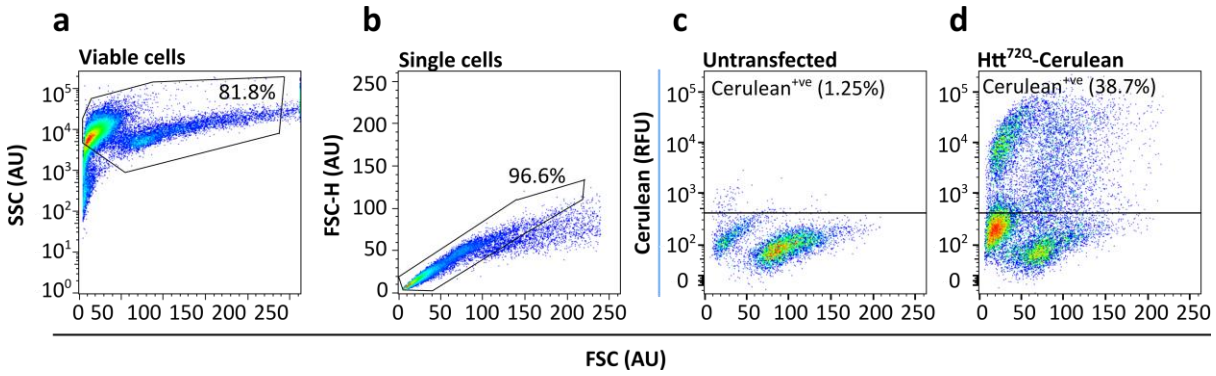

Figure 5.8. Gating strategy adopted for flow cytometric analysis of HSR induction in Neuro-2a (HSE:EGFP). Neuro-2a cells were transfected to express cerulean tagged SOD1^{WT}, SOD1^{G93A}, Htt^{25Q}, Htt^{72Q}, Fluc^{WT}, or Fluc^{DM} proteins and, 48 h post-transfection, cells were analysed by flow cytometry. (a) Plots of FSC and SSC of cells were used to resolve cellular debris and cell clumps. A polygonal gate was set around cells of interest and all downstream analyses was performed on this population. (b) Plots of FSC-height (FSC-H) and FSC-area (FSC-A) were used to resolve singlet and doublet events and a polygonal gate was used to exclude all doublets from downstream analyses. (c) Untransfected cells were used as a cerulean^{-ve} control to identify cerulean^{+ve} events. (d) Representative plot of Neuro-2a (HSE:EGFP) cells transfected to express Htt^{72Q}-cerulean are shown and the percent of cerulean^{+ve} cells in the square gate are denoted. Data shown is representative of three independent repeats.

Some samples were left untreated and were used as an EGFP^{-ve} control to identify EGFP^{+ve} cells (Figure 5.9a). To establish the capacity of Neuro-2a (HSE:EGFP) to report on HSR induction, cells were treated with celastrol (0.75 µM/ 24 h) and this induced EGFP expression in 33.6 ± 1.7% of cells (Figure 5.9b). One-way ANOVA showed that there was a significant effect with regard to the type of protein expressed in Neuro-2a (HSE:EGFP) cells and the induction of an HSR [$F(6, 18) = 101.1$, $P < 0.0001$]. Expression of the two pathogenic proteins, SOD1^{G93A} or Htt^{72Q}, resulted in 1.6 ± 0.4% and 4.0 ± 1.1% of the transfected cells becoming EGFP^{+ve}, respectively (Figure 5.9d). However, this increase in EGFP^{+ve} cells was not significantly greater than the proportion of EGFP^{+ve} cells expressing the non-aggregation prone control, SOD1^{WT}. The expression of Fluc^{DM} resulted in the expression of EGFP in 12.3 ± 1.3% of transfected cells (Figure 5.9c-d). Post-hoc testing showed that the proportion of EGFP^{+ve} cells expressing Fluc^{DM} was significantly greater than in cells expressing Htt^{72Q}, SOD1^{G93A} or SOD1^{WT} ($P < 0.001$). A bivariate plot of the number of inclusions formed by each protein compared to the proportion of EGFP^{+ve} cells showed a positive relationship between number of inclusions formed and induction of an HSR (Figure 5.9e).

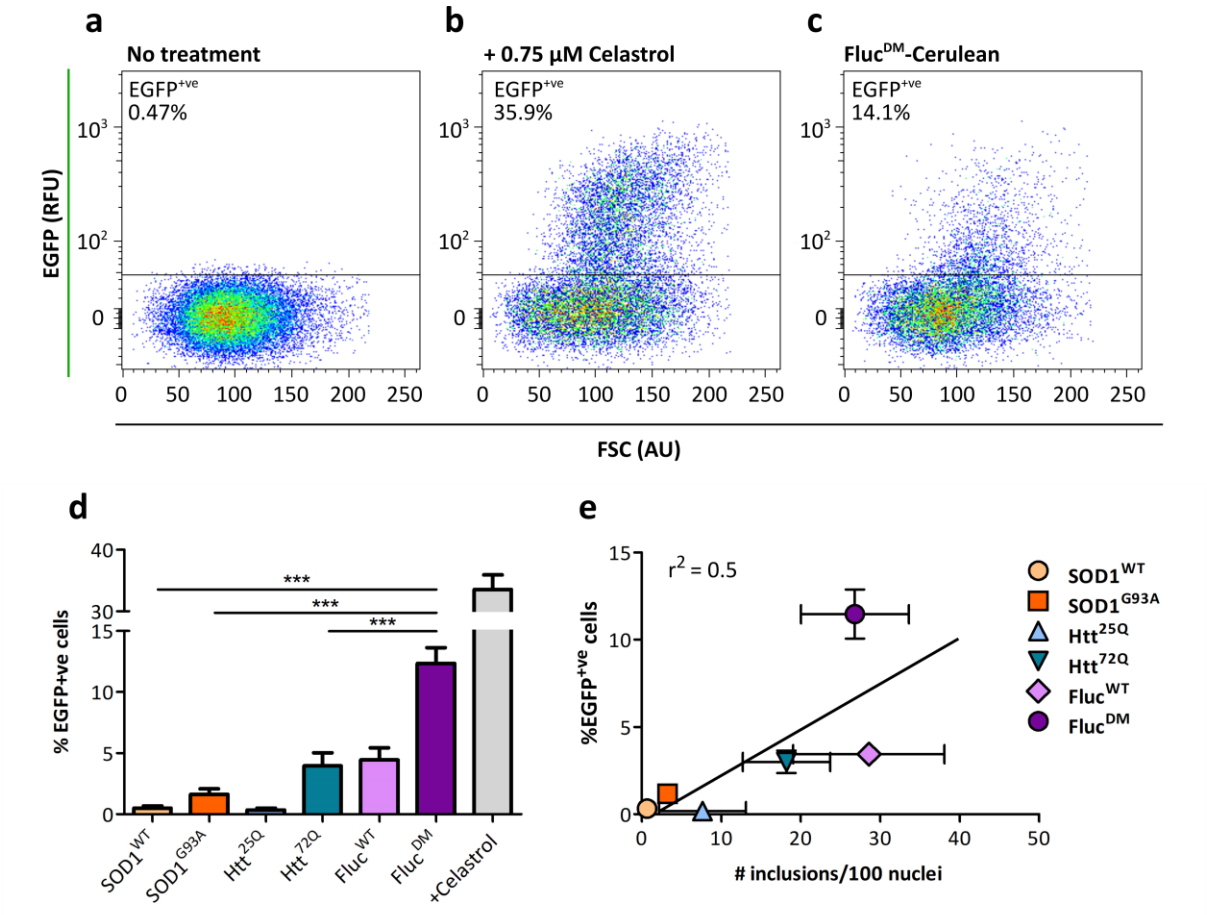

Figure 5.9. Activation of the HSR in Neuro-2a (HSE:EGFP) cells transfected to express cerulean-tagged WT or aggregation-prone mutant proteins. Neuro-2a (HSE:EGFP) cells were transfected to express cerulean tagged $SOD1^{WT}$, $SOD1^{G93A}$, Htt^{25Q}, Htt^{72Q}, $Fluc^{WT}$ or $Fluc^{DM}$ proteins. After 48 h incubation, cells were harvested for analysis by flow cytometry. Cellular debris, cell clumps, doublet events and untransfected cells were excluded from the analysis as described in Figure 5.8a-d. (a)-(c) Representative plots of FSC and EGFP fluorescence of (a) untransfected and untreated cells, (b) cells treated with 0.75 µM celastrol (an inducer of the HSR), and (c) cells transfected to express $Fluc^{DM}$-cerulean. (d) The percent of transfected cells expressing cerulean-tagged WT or mutant proteins which were $EGFP^{+ve}$. (e) The proportion of $EGFP^{+ve}$ cells in each sample compared to the number of inclusions formed by each of the cerulean-tagged proteins. Data shown is the mean ± SEM of three independent repeats. Statistically significant differences between the means were determined by one-way ANOVA and Tukey's multiple comparisons test was used, where $P < 0.001$ (***).

To investigate how the concentration of an aggregation-prone protein effects the activation of the HSR, events from the flow cytometric analysis were binned according to the levels of cerulean expression (5000 RFU per bin; Figure 5.10a), whereby bin 1 represents low levels and bin 10 represents high levels of expression of the aggregation-prone protein in a cell. The proportion of $EGFP^{+ve}$ cells in each cerulean bin was then determined. Representative bivariate plots of EGFP and FSC of cells transfected to express Htt^{72Q} in cerulean bins 5 and 10 are shown in Figure 5.10b. By binning the flow cytometry data in this way two factors can be

assessed: (i) the effect of high and low protein concentration on induction of the HSR, and (ii) the induction of the HSR in cells expressing WT and mutant aggregation-prone proteins (Figure 5.10c-e).

In $SOD1^{G93A}$-cerulean expressing cells, only 0.4 ± 0.2% of cells were $EGFP^{+ve}$ in bin 1 compared to 38.7 ± 7.3% of cells in bin 10 (Figure 5.10c). This same trend is observed in Htt^{72Q}, $Fluc^{WT}$ and $Fluc^{DM}$-cerulean bins, whereby an increasing concentration of these aggregation-prone proteins was correlated with an increase in the percent of $EGFP^{+ve}$ cells, such that cerulean bin 10 had the highest proportion of $EGFP^{+ve}$ cells (23.4 ± 7.6%, 37.1 ± 15.9%, and 57.7 ± 10%, respectively; Figure 5.10d-e). In contrast, cells expressing $SOD1^{WT}$ and Htt^{25Q}, which do not readily form inclusions, did not induce EGFP expression at any level of cerulean expression. Therefore, these data demonstrate that there is a concentration-dependent effect of protein expression on HSR induction in cells expressing an aggregation-prone protein.

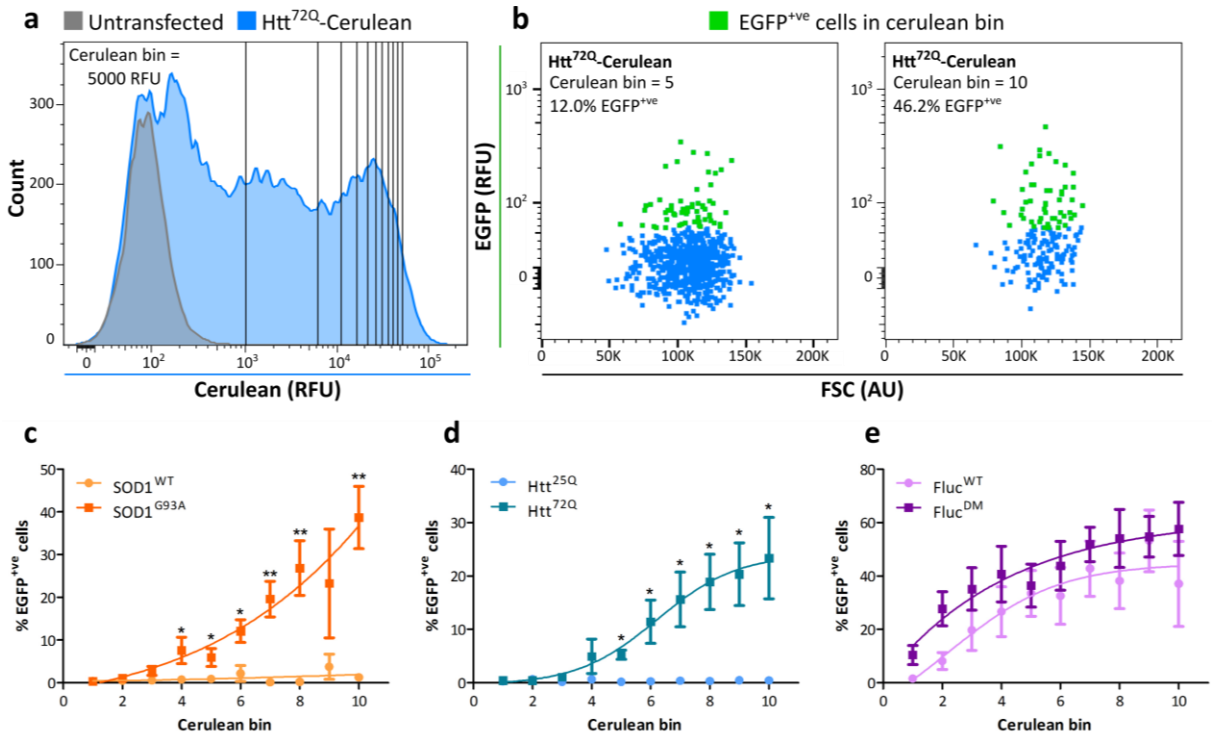

Figure 5.10. High expression levels of aggregation-prone proteins correlate with an increase in the proportion of cells with an activated HSR. (a) Overlay histograms of untransfected and Htt^{72Q}-cerulean transfected Neuro-2a (HSE:EGFP) with 10 cerulean bins corresponding to 5000 AFU. (b) Representative plots of FSC and EGFP fluorescence from samples transfected to express Htt^{72Q}-cerulean from cerulean bin 5 (*left*) and 10 (*right*). The EGFP^{+ve} cells in the indicated cerulean bin (*green*) are highlighted. (c)-(e) The percent of EGFP^{+ve} cells in each cerulean bin for cells expressing (c) SOD1^{WT} or SOD1^{G93A}, (d) Htt^{25Q} or Htt^{72Q}, or (e) Fluc^{WT} or Fluc^{DM}. Data shown is the mean ± SEM of three independent repeats. Differences between the means were determined using a two-way ANOVA followed by Bonferroni's post hoc test, where $P < 0.05$ (*) and $P < 0.01$ (**).

5.3.6 Tracking protein aggregation and HSR induction and over time in neuron-like cells

The induction of the HSR was also investigated over time in Neuro-2a (HSE:EGFP) cells transfected to express Htt^{72Q} or Fluc^{DM}. These two proteins were chosen because they both readily form inclusions and showed differential capacities to induce an HSR in cells (Figure 5.7e and Figure 5.9d). Live cell confocal imaging of Neuro-2a (HSE:EGFP) cells, facilitated the tracking of Htt^{72Q} or Fluc^{DM} expression, inclusion body formation, and HSR induction in single cells. Representative images of Neuro-2a (HSE:EGFP) cells transfected to express cerulean-tagged Htt^{72Q} or Fluc^{DM} show differential induction of the HSR (Figure 5.11). Due to the broad fluorescence emission spectrum of the cerulean protein, spectral overlap was

observed between the channels used to detect EGFP and cerulean fluorescence, particularly in regions containg inclusions.

With regard to cells expressing Htt^{72Q}, over the time course of the experiment there was no diffuse EGFP signal detected at any time point following transfection with Htt^{72Q} (Figure 5.11). This differs from the result shown in Figure 5.9d, which showed that the HSR was induced in 1.1% of cells when analysed by flow cytometry. This difference is most likely attributable to differences between the methods used to detect HSR induction in these experiements; 20,000 transfected cells were analysed by flow cytometry whereas only 40 cells were able to be followed in the live cell imaging experiments. With regard to cells expressing $Fluc^{DM}$, there was an increase in EGFP expression in some cells detected 15 h after transfection and was still able to be detected 25 h after transfection (Figure 5.11). These live cell imaging experiments support findings from the flow cytometric analysis of the same samples 48-h post-transfection, whereby there were a greater proportion of $EGFP^{+ve}$ cells in cells transfected to express $Fluc^{DM}$ compared to those expressing Htt^{72Q}.

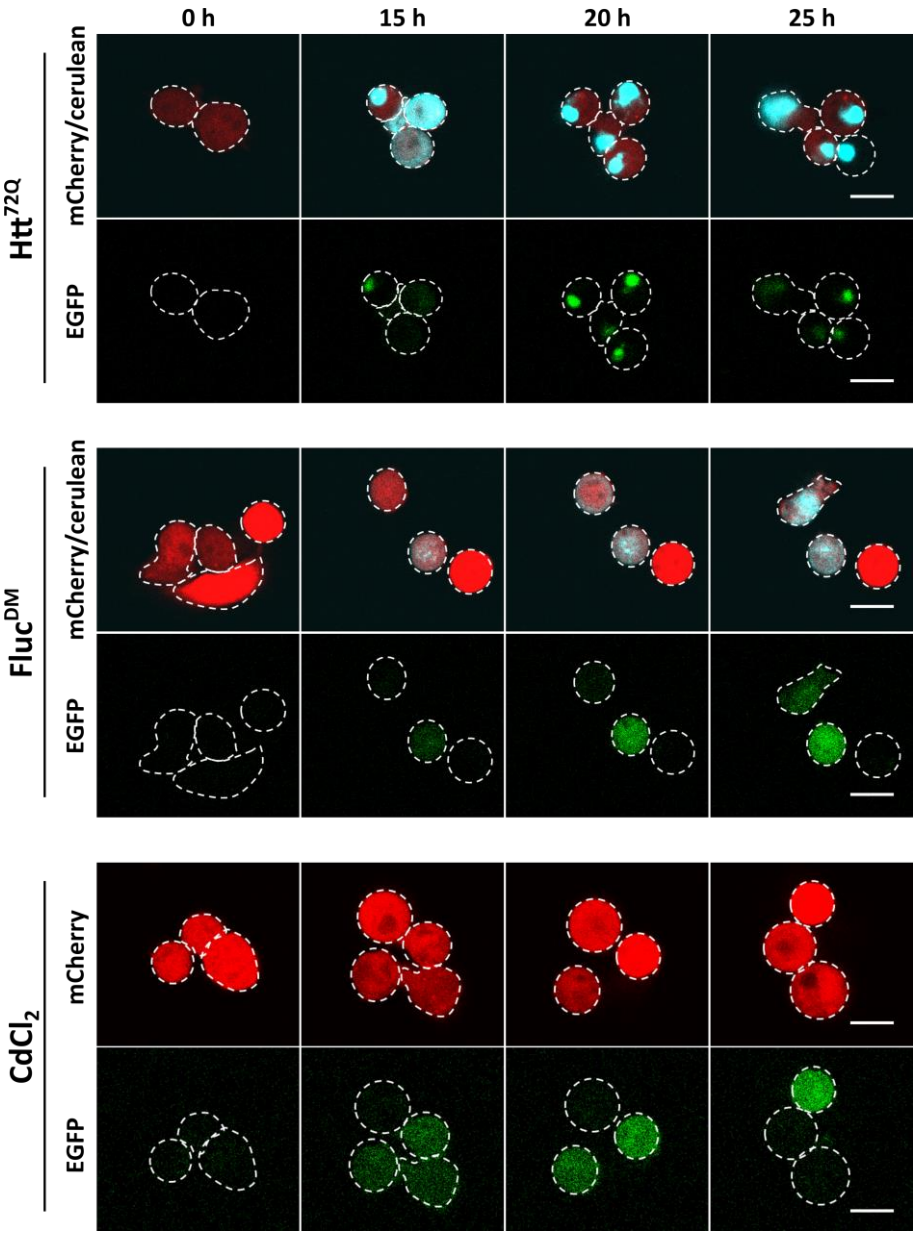

Figure 5.11. Live cell imaging of inclusion body formation and heat shock response activation as a function of time. Neuro-2a (HSE:EGFP) cells were transfected to express Htt^{72Q} (top panel) or $Fluc^{DM}$ (middle panel), or treated with 10µM $CdCl_2$ (bottom panel) and imaged every hour by confocal microscopy. Representative images are shown after 0, 15, 20, and 25 h of imaging. Each image is overlayed by the cell outlines (white dotted line) as defined by the mCherry signal at each time point. Punctate EGFP signal represents spectral overlap from the cerulean signal and diffuse EGFP signal represents the activation of the HSR. Scale bar = 20 µm. Images are representative of three independent experiments.

To minimise spectral overlap, narrow emission windows for detection of cerulean and EGFP fluorescence were applied (462-492 nm and 506-563 nm, respectively; Figure 5.12a). Despite this, an apparent EGFP signal was observed in areas containing inclusion bodies comprised of cerulean-tagged proteins (areas of intense fluorescence; Figure 5.12a inset; white arrowheads), indicative of cerulean fluorescence being detected in the EGFP emission window. Thus, to accurately measure the expression of EGFP over-time, "Cells" and "Inclusions" were identified based on mCherry and cerulean fluorescence, respectively, and EGFP fluorescence intensity was measured from an area in the cell defined as "Cells – Inclusions" (Figure 5.12b). Bivariate plots of the cerulean and EGFP fluorescence intensities derived from regions defined as "Cells – Inclusions" demonstrated a strong correlation suggesting that the cerulean signal was still contributing to the EGFP signal (Figure 5.12c). This spectral overlap was calculated to be 13%. Therefore, spectral compensation was performed on the EGFP data according to equation 5.3.

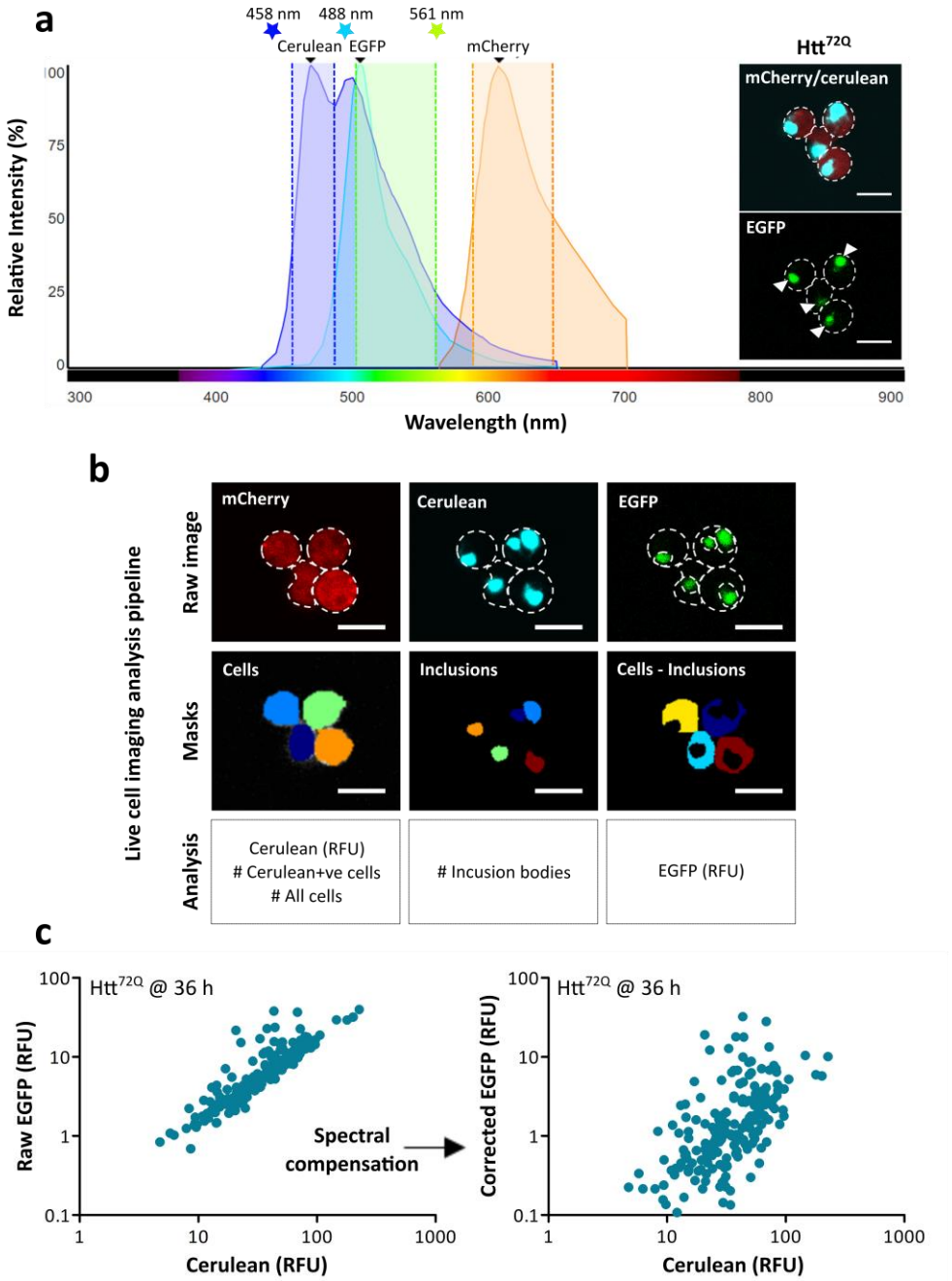

Figure 5.12. Experimental design and analysis of live cell imaging experiments. Neuro-2a (HSE:EGFP) cells were transfected to express Htt^{72Q} or $Fluc^{DM}$ and imaged over time by confocal microscopy. (a) Fluorescence emission spectra of cerulean, EGFP and mCherry fluorescent proteins. The windows for emission collection were set at 462-492 nm (blue dotted lines), 506-563 nm (green dotted lines), and 600-657 nm (orange dotted lines), for cerulean, EGFP and mCherry, respectively. The lasers used to excite each fluorescent protein are depicted by the coloured stars. Inset: A representative image of Neuro-2a (HSE:EGFP) cells transfected to express Htt^{72Q}, demonstrating spectral overlap between the cerulean and EGFP channels (white arrowheads). (b) Analysis pipeline used in Cell Profiler of confocal images acquired during the live cell imaging experiment. The mCherry channel (*left*) was used to define the "Cells", which are masked in different colours, and this region was used to measure cerulean fluorescence intensity, the number of $cerulean^{+ve}$ cells, and the total number of all cells in each image over the time-course. The cerulean channel (*middle*) was used to identify "Inclusions" and this region was used to count the number of inclusions formed in each image over the time-course. The "Inclusions" were subtracted from the "Cells" to generate a third region for measurement defined as "Cells – Inclusions", and this region was used to determine the EGFP fluorescence intensity in this channel. All scale bars = 20 µm. (c) Bivariate plots of cerulean and EGFP fluorescence intensities from the "Cell – Inclusions" region in Htt^{72Q} transfected cells at 36 h, before (left) and after (right) spectral compensation.

Images from these live cell imaging experiments were subjected to the analyses outlined in Figure 5.12, to track the expression of cerulean-tagged proteins, formation of inclusion bodies, and induction of the HSR over time. Treatment of Neuro-2a (HSE:EGFP) with 10 µM $CdCl_2$ (the positive control) resulted in a time-dependent increase in the proportion of cells that were $EGFP^{+ve}$ compared to untreated cells (Figure 5.13a). A two-way ANOVA was conducted to compare the effect of treatment with $CdCl_2$ and time elapsed. Treatment with $CdCl_2$ significantly increased the proportion of $EGFP^{+ve}$ cells compared to no treatment [$F(1, 130) = 369.7$, $P < 0.0001$], and post-hoc analysis using Bonferroni's test showed that this difference was statistically significant 12 h after treatment. Likewise, there was a time-dependent increase in the proportion of $EGFP^{+ve}$ cells in samples transfected to express $Fluc^{DM}$ (Figure 5.13b). In contrast, there was no effect of Htt^{72Q} expression on the proportion of $EGFP^{+ve}$ cells over time (Figure 5.13b). There was a significantly greater proportion of $EGFP^{+ve}$ cells in samples expressing $Fluc^{DM}$ compared to Htt^{72Q} [$F(1, 144) = 33.43$, $P < 0.0001$]. Post-hoc analysis using Bonferroni's test showed that this difference was statistically significant 21 h following transfection.

To determine the rate of $Fluc^{DM}$ and Htt^{72Q} inclusion formation, the proportion of cells with cerulean inclusions was determined in every image over the time-course of the live cell imaging experiment (Figure 5.13c). There was a significant time-dependent increase in the number of inclusions formed in Neuro-2a (HSE:EGFP) by both Htt^{72Q} and $Fluc^{DM}$, with both samples reaching a plateau in the proportion of cells with inclusions after 20 h [$F(12, 143) = 33.43$, $P < 0.0001$]. There was no effect of the type of protein expressed on the mean number of inclusion bodies formed over the time-course of the experiment [$F(1, 143) = 0.09$, $P = 0.7607$]. Both Htt^{72Q} and $Fluc^{DM}$ reached half maximal inclusion body formation by 12.8 ± 2.4 h and 13.9 ± 3.4 h, respectively, indicating that there was no significant difference in the rate of aggregation of either protein. One of the limitations of this type of image analysis was the ability to detect

inclusion bodies of a range of sizes and fluorescence intensities. Consequently, it is likely that the reported maximum proportion of cells with inclusions (75% after 25 h for $Fluc^{DM}$ and Htt^{72Q}) is an underestimate. In fact, visual assessments of these images were unable to identify any transfected cells that did not form inclusions after 36 h.

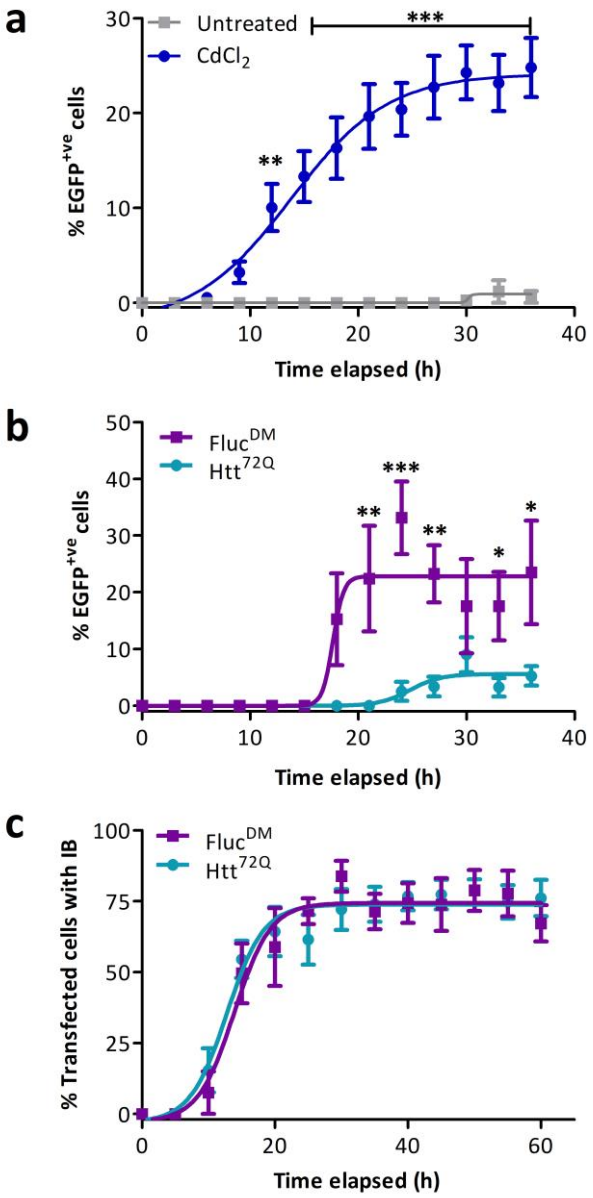

Figure 5.13. Live cell imaging of the heat shock response in Neuro-2a (HSE:EGFP) transfected to express Htt^{72Q} and $Fluc^{DM}$. (a) The proportion of $EGFP^{+ve}$ cells over time after treatment (or not) with 10 µM $CdCl_2$. (b) The proportion of $EGFP^{+ve}$ cells over time after transfection to express Htt^{72Q} or $Fluc^{DM}$. (c) The percent of transfected cells with inclusions over time. Data shown are the mean ± SEM of single cell analyses from 8 fields of view using a 40× dry objective. These findings are representative of three independent live cell imaging experiments. Differences in the means were assessed using a two-way ANOVA followed by post-hoc analysis using Bonferroni's test, where $P < 0.05$ (*), $P < 0.01$ (**), and $P < 0.001$ (***).

These live cell imaging experiments of Neuro-2a (HSE:EGFP) transfected to express Htt^{72Q} and $Fluc^{DM}$ were also used to track the formation of inclusions, the induction of the HSR and cell death in individual cells. Cells transfected to express $Fluc^{DM}$ demonstrated heterogeneity with respect to their capacity to induce an HSR, whereby an increase in EGFP fluorescence over time only occurred in a subset of cells with inclusions. Representative traces of EGFP, cerulean and mCherry fluorescence over time are shown of two individual cells transfected to express $Fluc^{DM}$. In both cells $Fluc^{DM}$ aggregated and formed an inclusion; cell 1 shows no increase in EGFP expression (indicative of an HSR), whereas Cell 2 does (Figure 5.14a-b). In contrast, there was no increase in EGFP over time in any cells expressing Htt^{72Q} (Figure 5.14c-d).

To determine whether HSR induction in cells with $Fluc^{DM}$ inclusions is dependent on the rate of inclusion formation, the time taken for inclusions to form was determined in each transfected cell (Figure 5.14e). There was no difference in the average time taken for cells expressing $Fluc^{DM}$ or Htt^{72Q} to form inclusions, supporting data in Figure 5.13c. Cells were then grouped according to whether they had induced an HSR or not. There was no significant difference in the average time taken for inclusions to form in $Fluc^{DM}$-expressing cells that did (18.2 ± 0.7 h) or did not (18.5 ± 1.5 h) induce an HSR (Figure 5.14e). This suggests that the rate of inclusion formation does not influence whether a cell mounts HSR in response to inclusion formation or not.

To determine whether the induction of the HSR could enhance cell viability in the context of protein aggregation, the time taken for cells to die after inclusion formation was assessed (Figure 5.14f). There was no difference in the time taken for cells with Htt^{72Q} inclusions to die compared to cells with $Fluc^{DM}$ inclusions that did not induce an HSR (Figure 5.14f). This suggests that there is no inherent difference in the cytotoxicity of either of these proteins. However, cells with $Fluc^{DM}$ inclusions that induced an HSR demonstrated a significantly

greater extension in time to cell death (where membrane permeability and loss of mCherry fluorescence was used as a marker of cell death; 30.5 ± 3.6 h) compared to cells that did not induce an HSR (17.6 ± 2.1 h; $P = 0.0049$). This suggests that the induction of the HSR in cells with $Fluc^{DM}$ inclusions enhanced cell viability. Every cell that formed a $Fluc^{DM}$ or Htt^{72Q} inclusion died within the time course (60 h) of the live cell imaging experiment. To summarise, a subset of the cells with $Fluc^{DM}$ inclusions induced an HSR and the induction of the HSR was not influenced by the rate of inclusion formation. However, induction of the HSR in cells correlated with a significantly extended the time taken for the cells to die.

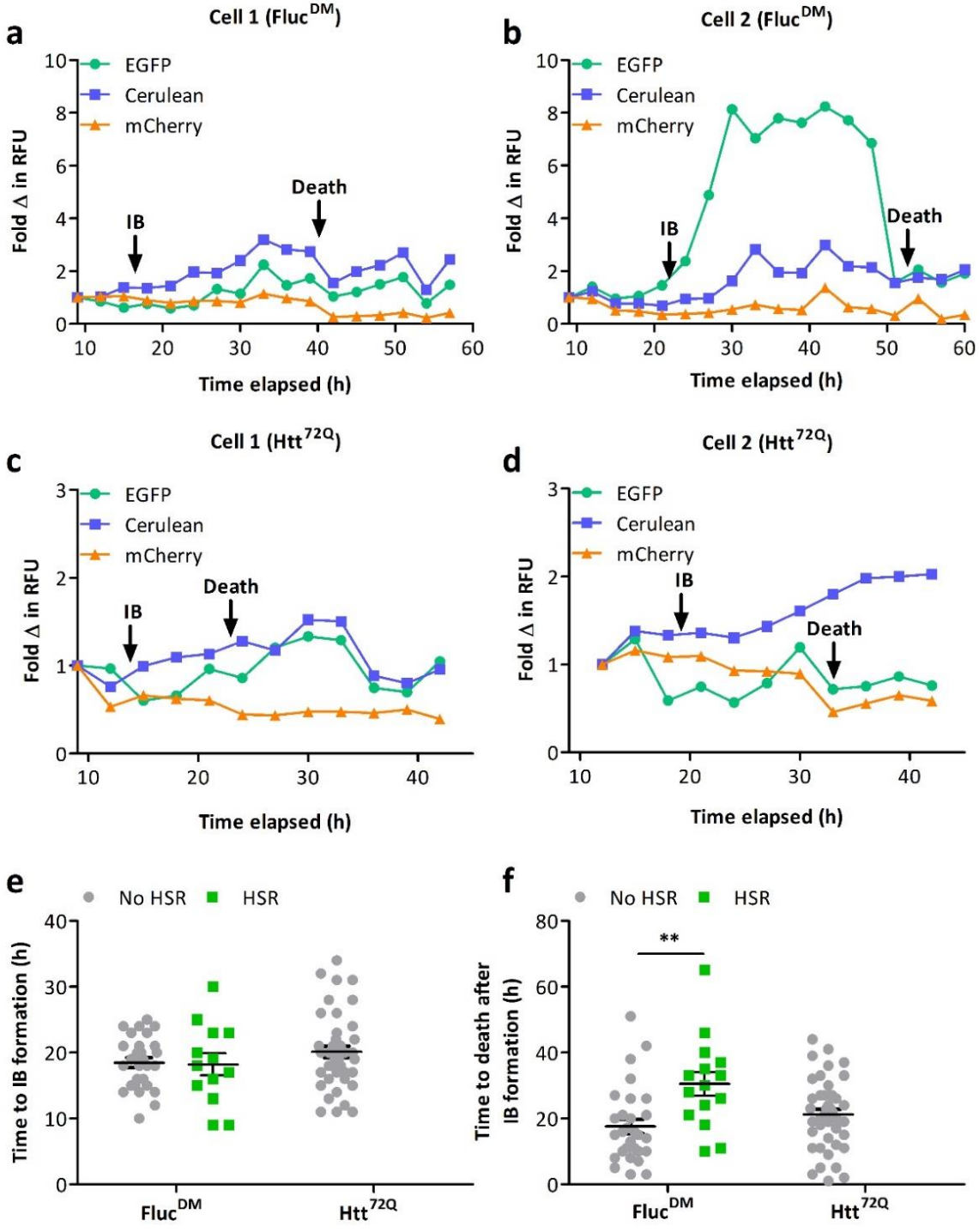

Figure 5.14 Tracking the HSR in individual cells expressing Fluc^{DM} and Htt^{72Q}. Neuro-2a (HSE:EGFP) cells were transfected to express Htt^{72Q} or Fluc^{DM} and imaged over time by confocal microscopy. (a)-(b) The fold change in EGFP, cerulean and mCherry fluorescence intensities (RFU) over time in a single cell expressing Fluc^{DM}. Where EGFP fluorescence was used as a reporter of the HSR, cerulean fluorescence shows Fluc^{DM} expression and a loss of mCherry fluorescence was used to report on cell death over time. (c)-(d) The fold change in EGFP, cerulean and mCherry fluorescence intensities over time in a single cell transfected to express Htt^{72Q}. The times at which inclusion bodies (IB) are formed and cells die are indicated by the arrows. (e) Time taken for transfected cells to form inclusion bodies (IB) in HSR^{-ve} and HSR^{+ve} cells. (f) Time taken for cells to die after to formation of inclusions in HSR^{-ve} and HSR^{+ve} cells. Statistically significant differences between the means were determined using a one-way ANOVA followed by Tukey's post-hoc test, where $P < 0.01$ (**).

5.4 Discussion

In this work, Neuro-2a (HSE:EGFP) cells were used to address whether the absence of the HSR in neurons in the context of NDs is an intrinsic characteristic of differentiated neurons and whether protein aggregates (intra- or extracellular) induce an HSR in neuron-like cells. We showed that Neuro-2a (HSE:EGFP) cells differentiated into neuron-like cells demonstrated a greater magnitude in HSR induction compared to non-differentiated cells. The extracellular application of pathogenic aggregates did not induce an HSR. However, over-expression of the pathogenic proteins Htt^{72Q} and $SOD1^{G93A}$ induced an HSR in a small proportion of cells, whereas the expression of $Fluc^{DM}$ induced an HSR in a significantly greater proportion of cells. This research explored in detail the effect of expression level, number of inclusions formed, inclusion size, and rate of inclusion formation of aggregation-prone proteins to determine which factor/s influence HSR induction in these cells. In doing so, the findings of the present study show that there is a positive relationship between the number of inclusions formed and induction of the HSR, and protein concentration of aggregation-prone proteins and induction of the HSR in cells.

Cell-based studies of the HSR have typically relied on low throughput, qualitative techniques such as, immunocytochemistry and immunoblotting of relative Hsp expression levels, and/or electrophoretic mobility shift assay of HSF1 binding to DNA. A more recent strategy to measure the induction of the HSR in cells has involved the use of *hspa1a* promoter-driven firefly luciferase reporters (Yang et al. 2008, Olzscha et al. 2011). However, there are several disadvantages to using firefly luciferase as a reporter protein, including the requirement of expensive reagents (*e.g.* luciferin to measure firefly luciferase activity), it is not amenable to generating time-resolved data, and it is restricted to bulk cell analysis. The fluorescent reporter stable cell lines developed in the present study help to overcome these limitations and enable quantitative, real-time monitoring of HSR induction in cells, both at the level of single cells

and bulk cell analyses. Importantly for this work, this approach provided a platform to study how cells respond to cellular stresses after differentiation into neuron-like cells or with intra- or extracellular protein aggregates. Furthermore, the kinetics and magnitude of HSR induction could be calculated, which are important parameters when investigating stress-inducible responses, such as the HSR.

5.4.1 Differentiated Neuro-2a have a competent HSR

In the present study, Neuro-2a (HSE:EGFP) cells were differentiated with dbcAMP into neuron-like cells, as indicated by the increased expression of the dopaminergic neuronal marker tyrosine hydroxylase. Immunoblot analysis of heat shocked samples showed 100% of the HSF1 present was phosphorylated after a 2 h heat shock, in both differentiated and non-differentiated cells (Figure 5.2). This finding indicates that differentiation had no effect on the ability to activate an HSR in these cells. Moreover, time-resolved data from the EGFP reporter cell-line showed that there was a significant increase in the magnitude of HSR induction in differentiated compared to non-differentiated cells when they were subjected to heat shock (Figure 5.5). This could be the result of an extended time of HSF1 hyperphosphorylation, which occurs within the 0-6 h period post-heat shock that was not examined by the immunoblot analysis, in differentiated cells. The differences between these two approaches used to determine the capacity of cells to induce an HSR highlight the importance of acquiring quantitative time-resolved data when studying stress-inducible pathways, such as the HSR.

The finding that differentiated Neuro-2a cells showed a greater magnitude of HSR induction than non-differentiated cells contrasts with previous investigations into the effect of differentiation on the capacity of cells to induce an HSR. Heat shock (42°C/ 2 h) of dbcAMP (1 mM) differentiated NG108-15 cells resulted in a significant reduction in the ability of these cells to induce an HSR (measured using a firefly luciferase reporter downstream of the complete *Hspa1a* promoter, immunoblotting and northern blotting) (Oza et al. 2008, Yang et

al. 2008). Indeed, it has been reported in multiple studies that an attenuated induction of Hsp70 expression or *Hspa1a* promoter driven reporter genes is a common feature of neuronal differentiation in the 8 cell lines tested (Dwyer et al. 1996, Hatayama et al. 1997, Yang et al. 2008). Some of these studies used differentiated Neuro-2a (1 mM dbcAMP), PC12 (50 ng/mL nerve growth factor), or NS20 (1 mM dbcAMP) (Dwyer et al. 1996, Hatayama et al. 1997, Yang et al. 2008) cells.

The differences between the findings of the present study and these previous investigations are likely the consequence of differences in the promoter used to drive reporter gene expression and variation in the capacity of different cell lines to induce Hsp70 expression. A screen of the HSR in neuronal cell lines showed that the induc tion of Hsp70 expression after heat shock (43°C/ 90 min) was not observed in 2 (N18TG2 and CL8a5.2) of 9 (SN6.1b, CL8c4.7, NSC-34.4.6, NB-1, GOTO, IMR-32) cell lines (Satoh et al. 1994). This suggests that an upregulation of Hsp70 in response to heat shock is not common to all cell lines (Satoh et al. 1994). With regard to the previous work using Neuro-2a cells, the reporter construct included the complete mouse *Hspa1a* promoter region (position 1–1042 from genbank accession number M76613) (Yang et al. 2008). Therefore, this construct specifically reports on experimental conditions that induce the expression of Hsp70. However, in the present study, a minimal *Hspa1a* promoter with 8 putative HSEs (nGAAn; where 'n' is any nucleotide) was used and thus this promoter reports on HSF1 activation and DNA binding to HSEs. Therefore, the construct used in this work specifically reports on the induction of an HSF1-mediated HSR whereas the *Hspa1a* promoter driven firefly luciferase construct used previously reports on the induction of Hsp70 transcription. This could, at least in part, explain the differences between these two studies.

The increase in HSF1 activity in heat shocked and $CdCl_2$ treated, dbcAMP differentiated cells (Figure 5.5) may be explained by the role of cAMP in the protein kinase A (PKA) signalling

cascade. HSF1 transcriptional activity is highly regulated by the phosphorylation of key serine residues in its regulatory domain (Vihervaara and Sistonen 2014). The cAMP-dependent serine kinases PKA and p38 mitogen activated kinase (MAPK) have been previously shown to bind to HSF1 and phosphorylate key serine residues (S320, S326, S303/307) that activate HSF1 transcription (Choi et al. 1991, Murshid et al. 2010). Therefore, it follows that treating cells with high concentrations of dbcAMP for 72 h is likely to initiate the PKA-dependent signalling cascade, activate kinases that phosphorylate HSF1, and sensitise cells to induce a stronger HSR after treatment by heat shock or $CdCl_2$.

Whilst it has previously been hypothesised that neurons have an attenuated capacity to induce an HSR; this generalisation cannot be applied to all neurons. For example, cerebellar granule neurons and striatal neurons have an intact HSR *in vivo* and in culture (Marini et al. 1990, Carnemolla et al. 2015). In contrast, motor neurons have a high threshold for induction of the HSR (Batulan et al. 2003). The capacity of a neuron to induce an HSR may therefore be dependent on several factors, including neuronal subtype and the specialisation of the neuron, rather than the differentiation of the neuron. These findings highlight the need to move these investigations into models that are more physiologically relevant to neuronal development and NDs, since it is clear that there are distinct differences in the capacity of a range of neuronal subtypes to induce an HSR.

5.4.2 Extracellular protein aggregates evade (or impair) the HSR

SOD1 and α-synuclein aggregates have been shown to be taken up by neuroblastoma cells after 1 h and 8 h, respectively (Lee et al. 2008, Munch et al. 2011). In the present study we showed that the extracellular application of $SOD1^{G93A}$ and α-synuclein aggregates to Neuro-2a (HSE:EGFP) cells did not result in an induction of the HSR up to 72 h post-treatment. Similar studies have shown that treatment of other cell-types in this way elicits other stress-responses, such as inflammatory pathways. For example, treatment of EOC.13 microglial-like cells with

$SOD1^{G93A}$ aggregates resulted in an upregulation of TNFα (Roberts et al. 2013). The absence of an HSR in cells after treatment with protein aggregates in the present study suggests that these pathogenic proteins may evade detection by the components of the HSR that activate this pathway. Thus, the failure of aggregated SOD1 and α-synuclein to activate the HSR may contribute to disease progression in NDs by facilitating the seeding of inclusion formation in neighbouring cells that take up aggregates. Future research could investigate whether the pharmacological induction of the HSR in cells prevents inclusion formation after seeding with aggregates as a potential therapeutic strategy to stop the progression of NDs in the CNS.

Treatment of Neuro-2a (HSE:EGFP) cells with protein aggregates comprised of non-pathogenic proteins would be an interesting comparison to investigate in future studies to determine if the absence of the HSR is specific to aggregates formed from pathogenic proteins. In addition, the internalisation of these aggregates into the cytosol may result in the activation of other stress-inducible arms of the proteostasis network, such as the unfolded protein response. This is another avenue that requires further research.

5.4.3 The effect of intracellular protein aggregation on inducing the HSR

This work showed that the intracellular expression of the pathogenic proteins $SOD1^{G93A}$ and Htt^{72Q} resulted in a low proportion of cells that had induced an HSR 48 h after transfection. In comparison, a significantly greater proportion of cells expressing $Fluc^{DM}$ induced an HSR. Previous research using a HEK293 fluorescent reporter cell line reported that Htt^{91Q} expression did not lead to a detectable induction of the HSR, irrespective of the expression level or aggregation status of the protein in the cell (Bersuker et al. 2013). One possible explanation for the differences observed between these two studies are the design of the promoters in the fluorescent reporter constructs; the promoter used in the previous report was a fragment of the complete *hspa1a* promoter (positon 145-604 from genbank accession number NG_046363).

There also may be differences in the ability of Neuro-2a and HEK293 to respond to polyQ-expanded Htt aggregation.

The differences observed in this study between the effect of pathogenic and non-pathogenic proteins, with regard to inducing an HSR, could be explained by findings that suggest pathogenic protein expression increases the threshold of induction of the HSR. For example, the ability of SH-SY5Y cells to induce the HSR after heat shock (42°C/ 20 min) was significantly reduced after chronic extracellular application of prion protein or amyloid-β (Resenberger et al. 2012). Moreover, synthetic β-sheet forming proteins significantly inhibit the induction of the HSR in MG132-treated HEK293 cells (monitored using a Fluc reporter downstream of the *Hspa1a* promoter) (Olzscha et al. 2011). Furthermore, the HSR is decreased after heat shock in primary striatal neurons expressing Htt^{111Q} compared to those expressing Htt^{7Q} (Chafekar and Duennwald 2012). Together, these findings suggest a possible common underlying pathology in NDs, whereby disease-associated proteins attenuate the HSR and this facilitates inclusion body formation and propagation through the CNS. Future research, which investigates a wide range of disease-causing proteins could establish whether this is a molecular pathology common to all NDs.

Finally, live cell imaging experiments were performed to assess whether the capacity of cells to induce an HSR could be attributed to: (i) the rate of inclusion formation of the protein, (ii) the physical properties of the inclusions formed (*i.e.* size and granularity), and/or (iii) the total number of inclusions formed by each protein. There was no significant difference in the rate of Htt^{72Q} or $Fluc^{DM}$ inclusion formation. $Fluc^{DM}$ formed inclusions that were significantly smaller than those formed by Htt^{72Q} (Figure 5.7f). However, inclusions formed by $SOD1^{G93A}$ were of a similar size to $Fluc^{DM}$ and $SOD1^{G93A}$ expression only induced an HSR in a low proportion of cells. Therefore, the relative difference in the capacity of each of the proteins to

induce an HSR correlates best with the number of inclusions formed by the proteins (*i.e.* $Fluc^{DM}$ > Htt^{72Q} > $SOD1^{G93A}$).

The present study showed that induction of the HSR in cells with $Fluc^{DM}$ inclusions resulted in them having an extended lifespan compared to cells with inclusions that did not induce an HSR. Thus, despite the presence of the inclusion body in the cell, induction of the HSR was sufficient to enhance cell viability. Future research should investigate the differences between the subsets of cells with $Fluc^{DM}$ inclusions that did and did not induce an HSR. For example, these subsets could be cell sorted for proteomic or epigenomic analysis to elucidate the mechanism by which the HSR was induced (or not). Importantly, this finding highlights that inducing the HSR (*e.g.* pharmacologically) may be beneficial to the affected cells of the CNS in patients with NDs, even after inclusion formation has been initiated. Unfortunately, in recent years there has been little development in producing an HSR-inducing compound that is brain permeable and not cytotoxic, with the exception of arimoclomol, a co-inducer of the HSR (see section 1.7). Therefore, future research should investigate mechanisms of HSR induction in the cells that comprise the CNS for the identification of novel targets that can be used in the development of new therapeutics.

5.4.4 Summary

In summary, the findings detailed in this Chapter showed that, contrary to previously published studies, dbcAMP differentiated and non-differentiated Neuro-2a cells have a competent HSR. The magnitude of HSR induction was significantly greater in differentiated compared to non-differentiated cells after treatment with heat shock or $CdCl_2$. This is likely the consequence of treatment of the cells with high concentrations of dbcAMP, that initiates the PKA signalling cascade, which in turn phosphorylates and sensitises cells to activate HSF1 following stress. Future research should investigate the capacity of different neuronal sub-types to induce the HSR, to elucidate the feasibility of inducing the HSR pharmacologically in neurons as a

therapeutic for NDs. Furthermore, these data demonstrate that the extracellular application of aggregated forms of pathogenic proteins does not induce an HSR in neuron-like cells. Likewise, the expression of pathogenic aggregation-prone proteins only induced the HSR in a low proportion of cells (2-4%). This study is unique in that it investigated the effect of a number of different factors on the induction of the HSR, including, the aggregation propensity of pathogenic and non-pathogenic proteins, protein concentration, number of inclusions formed, inclusion size, and the rate of inclusion formation. Based on the flow cytometric and live cell imaging data it is concluded that HSR induction depends on the concentration of aggregation-prone protein, and hence the number of inclusions formed. Induction of the HSR was not dictated by the size of the inclusions nor the rate of inclusion formation.

To conclude, the absence of a strong HSR in cells exposed to intra- and extracellular protein aggregation suggests that pathogenic proteins: (i) do not cause sufficient stress to induce an HSR, (ii) evade detection by the proteins that signal for the induction of HSR, (iii) attenuate the HSR, (iv) active other stress-inducible arms of the proteostasis network, or (v) a combination of these factors. Therefore, future research should extend on this work by investigating the mechanisms by which aggregation prone proteins bypass the HSR in cells. In doing so, this could identify novel pathways to target for the development of HSR modulating therapeutics to treat NDs.

Chapter 6: Regional differences in inflammatory and heat shock responses between spinal cord and cortical glia

The research in this chapter was conducted as part of a 6 month research exchange at the Institute of Neurology, University College London in collaboration with the Graham Watts Laboratory. This chapter has been prepared as a manuscript for publication:

R. San Gil, B. Clarke, J. Yip, B. Kalmar, H. Ecroyd, L. Greensmith, Regional differences in inflammatory and heat shock responses between spinal cord and cortical glia. (2018).

Author contributions: RSG performed the experiments and analysed the data pertaining to Figures 6.1, 6.3, 6.4, 6.5, 6.6, 6.7, 6.8, 6.9, 6.10c, and 6.11. JY performed the experiments and analysed the data pertaining to Figures 6.2 and 6.10a-b. HE, RSG, LG and BK developed the original idea to compare stress-responses in cortical and spinal cord glial cultures, designed experiments, and oversaw their implementation. RSG, BC and BK contributed to the authoring of the manuscript and HE and LG oversaw the editing of the manuscript.

6.1 Introduction

There is strong evidence that suggests that ALS can be characterised as a non-cell autonomous disease (Boillée et al. 2006a, Lee et al. 2016). Glial cells play vital roles in the support and maintenance of neurons. However, in ALS, glia may become toxic to the very cells they usually protect. The initiation and progression of ALS depends on the molecular pathologies developed within motor neurons, and the subsequent reactivity of astroglia and microglia (Yamanaka et al. 2008, Philips and Robberecht 2011, Lee et al. 2016). Evidence for this comes from two studies, which together showed that selective deletion of $SOD1^{G37R}$ expression from GFAP-positive spinal cord astroglia and CD11b-positive microglia does not slow disease onset or early disease progression (Boillée et al. 2006b, Yamanaka et al. 2008). Rather, this astroglial- or microglial-specific deletion of $SOD1^{G37R}$ expression dramatically delays late disease progression, resulting in an overall extension of survival by 60 and 99 days, respectively (Boillée et al. 2006b, Yamanaka et al. 2008). These two studies demonstrate that mutant SOD1 expression in astroglia and microglia plays a significant role in late disease progression and overall survival in ALS.

There is a need to compare differences in astroglial and microglial stress-responses between different regions of the CNS, given the non-cell autonomous progression and specific degeneration of spinal cord and motor cortex motor neurons in ALS. There is a growing body of evidence to demonstrate that there are inter- and intra-regional differences in astroglial and microglial populations in terms of their transcriptome, proteome and subsequent function (de Haas et al. 2008, Hochstim et al. 2008, Farmer et al. 2016, Grabert et al. 2016, Haim and Rowitch 2017). For example, a study that investigated the transcriptome of purified dorsal and ventral horn astroglia of the spinal cord identified significant differences in the expression of 40 genes (Molofsky et al. 2014). Therefore, in the context of ALS, where striking regional differences in neurodegeneration are observed between the cerebral cortex and spinal cord, it

is of importance to investigate how glia differ in the absence and presence of ALS-associated pathologies. In particular, whether pathways that respond to stress, such as inflammation and the HSR, are differentially activated in glia derived from the cortex compared to the spinal cord.

Previous research has shown that cellular stresses propagated from inflammatory pathway activation can subsequently induce the HSR (Santoro et al. 1989, Schett et al. 1998, Ianaro et al. 2001). Induction of the HSR results in the upregulation of Hsps, which possess anti-inflammatory (Kalmar and Greensmith 2009), anti-aggregation (Treweek et al. 2015, Yerbury et al. 2016), and anti-apoptotic (Beere 2004) activities. With respect to the anti-inflammatory effects of the HSR, it has been shown that HSR activation can down-regulate LPS-mediated glial expression of iNOS, which in turn reduces the synthesis of NO (Feinstein et al. 1996, Russo et al. 2006). Furthermore, work in BEAS-2B and A549 cells (both human lung epithelial cell lines) suggests that HSR activation up-regulates the expression of IκBα and IκBβ to increase the cytosolic concentration of these proteins and inhibit NF-κB activation (Wong et al. 1997, Thomas et al. 1998). One of the products of HSR induction, Hsp70, has been shown to inhibit the NF-κB-mediated inflammatory cascade via two independent mechanisms: (i) by binding to the NF-κB-IκBα complex (Zheng et al. 2008) to prevent the activation and nuclear translocation of NFκB, and (2) by binding to and preventing the ubiquitination of TRAF6 and thus, the signal transduction pathway that propagates the NF-κB-mediated inflammatory cascade (Chen et al. 2006). Together, these findings show that Hsps interact with components of the inflammatory pathway and inhibit its activation.

There has been relatively little work investigating the induction of the HSR and Hsp expression in glia in the context of cellular stress associated with ALS. This may be because, historically, research in this area has focused on motor neurons, the degenerating cell-type, rather than the surrounding cells. A recent study showed that the over-expression of the sHsp, αB-c (*Hspb5*),

specifically in the astroglia of a mouse model of HD resulted in a 12.5% increase in motor neuron survival and 50% decrease in insoluble Htt (Oliveira et al. 2016). This finding suggests that further investigation into the mechanisms of HSR induction in glial cells is necessary, since Hsp over-expression in astroglia has been shown to be beneficial to neurons (Oliveira et al. 2016). It prompts the question: can inflammatory stimuli, a significant pathology associated with ALS, up-regulate Hsp expression in glia?

Investigation of inflammatory activation and HSR induction in glial cells of the spinal cord is warranted, as neuroinflammation is a key driver of ALS progression in the spinal cord and ALS is a non-cell autonomous disease. Therefore, the objectives of the current study were to: (i) compare inflammatory responses in cortical and spinal cord glia, (ii) assess whether inflammatory stressors are sufficient to induce an HSR in these cells, and (iii) compare the maximal ability of cortical and spinal cord glia to induce an HSR after heat shock. This research was conducted in cortical and spinal cord mixed glial cultures derived from WT (*i.e.* non-transgenic), $SOD1^{WT}$, and $SOD1^{G93A}$ mice. This type of comparison of glial stress-responses between different regions of the CNS may explain, at least in part, why spinal cord motor neurons in ALS are vulnerable to degeneration over neuronal populations in other regions of the CNS.

6.2 Materials and Methods

6.2.1 Antibodies

The antibody catalogue numbers and the concentrations used for immunoblotting (IB), immunocytochemistry (ICC) and flow cytometry (FC) are provided in parentheses. Rabbit polyclonal anti-iNOS (AB5384; IB 1:1000, ICC 1:100) was from Merck Millipore. Goat polyclonal anti-Hsp27/Hsp25 (sc-1049; IB 1:1000, ICC 1:100, FC 1:100) and mouse monoclonal anti-Hsp70 (sc-24; IB 1:1000) were from Santa Cruz Biotechnology. Rat monoclonal anti-mouse CD11b (MCA74GA, ICC 1:100) was from Bio-Rad. Rabbit polyclonal anti-Iba1 (019-19741, IB 1:5000, ICC 1:500) was from Wako Laboratory Chemicals and rat polyclonal anti-CD11b-APC/Cy7 (101226, FC 1:1000) was from Biolegend. Mouse monoclonal anti-GFAP-Cy3 (C9205, ICC 1:500, FC 1:500) was from Sigma-Aldrich. Donkey anti-rabbit IgG-AlexaFluor488 (A21206, ICC 1:1000), anti-goat IgG-AlexaFluor488 (A11055, ICC 1:1000, FC 1:1000), and anti-rabbit IgG-AlexaFluor633 (A31573, ICC 1:1000, FC 1:1000) secondary antibodies were from Thermo Fisher Scientific. Rabbit anti-mouse IgG-HRP (P0260, IB 1:1000), anti-goat IgG-HRP (P0160, IB 1:2000), and pig anti-rabbit-HRP (P0217, IB 1:2000) secondary antibodies were from Dako-Agilent Technologies.

6.2.2 Breeding and maintenance of (C57BL/6 x SJL) F1 hybrid WT, $SOD1^{WT}$, and $SOD1^{G93A}$ mice

All mice were housed in a controlled temperature and humidity environment and maintained on a 12 h light/dark cycle with access to food and water provided *ad libitum*. All experiments were performed under licence from the UK government in accordance with the Animals (Scientific Procedures) Act 1986 and following approval from the Institute of Neurology Ethical Review Committee.

Non-transgenic, (C57BL/6 x SJL) F1 hybrids, and transgenic mice expressing human $SOD1^{G93A}$ or $SOD1^{WT}$ were used to model ALS and were obtained from Jackson Laboratories (USA). The $SOD1^{G93A}$ mice (TgN[SOD1-G93A]1Gur) have been previously characterised to carry 25 copies of the $SOD1^{G93A}$ transgene (Gurney et al. 1994, Gurney 1994). Therefore, mice that over-express $SOD1^{WT}$ (TgN[SOD1]2Gur) at equivalent protein levels were used as a control transgenic strain in these experiments (Gurney et al. 1994). The mice were maintained at the Institute of Neurology, University College London by breeding heterozygous male carriers with female (C57BL/6×SJL) F1 hybrids.

6.2.3 Genotyping

The mice carrying the $SOD1^{WT}$ or $SOD1^{G93A}$ transgene were identified by polymerase chain reaction (PCR) amplification of the human SOD1 transgene from genomic DNA. DNA was extracted from tail biopsies by incubating the biopsies at 55°C/ 5 min in digest buffer, 10 mM Tris-HCl pH 8.3, 50 M KCl, 0.1 mg/mL gelatin, 0.45% (v/v) Nonidet P-40, 0.45% (v/v) Tween-20, supplemented with 1 U of proteinase K. Samples were then heated at 95°C/ 10 min to inhibit proteinase K activity and centrifuged 23,000 × *g*/ 2 min. The extracted genomic DNA in the supernatant was used to PCR amplify the human SOD1 transgene (forward primer: 5′-catcagccctaatccatctga-3′ and reverse primer: 5′-cgcgactaacaatcaaagtga-3′) and mouse interleukin-2 gene (forward primer: 5′-ctaggccacagaattgaaagatct-3′ and reverse primer: 5′-gtaggtggaaattctagcatcatc-3′) as an internal control.

6.2.4 Primary murine cortical and spinal cord mixed glial cultures

Cortical and spinal cord primary mixed glial cultures were prepared from postnatal day 1-3 new-born (C57BL/6 × SJL) F1 mice using a protocol modified from McCarthy and de Vellis (McCarthy and de Vellis 1980). Briefly, spinal cords and cortices were pooled separately in Ca^{2+}/Mg^{2+} free Hank's balanced salt solution (HBSS), cut into pieces with a scalpel, and

mechanically dissociated by trituration. The tissue was enzymatically dissociated with 0.025% (v/v) trypsin, 0.02% (w/v) DNase I, 0.3% (w/v) BSA, 1% (v/v) penicillin/ streptomycin in HBSS (37˚C/ 10 min) and proteolysis was inhibited with FCS. Cell suspensions were made by triturating 15 times and 5 mL FCS was added prior to centrifugation (400 × *g*/ 5 min). The cell pellet was reconstituted with glial feeding media, 15% (v/v) FCS, 1% (v/v) penicillin/streptomycin in DMEM and filtered through a 100 µm nylon mesh strainer. Cell suspensions were plated at a density of 2.5×10^5 cells/mL into 6-well plates or glass coverslips in 24-well plates coated with poly-D-lysine. The glial feeding media was changed 24 h post-plating and every 3 days thereafter and cultures were maintained at 37°C under 5% CO_2/ 95% air. After 12 days *in vitro*, the monolayer of cells reached 80-90% confluency and the composition of the resulting cortical and spinal cord mixed glial cultures were assessed by immunocytochemistry, and flow cytometry by staining with anti-GFAP (astroglial marker) and anti-CD11b or anti-Iba1 (microglial markers). Biological replicates of cultures for these studies were prepared from separate litters of newborn mice.

6.2.5 Purified primary cortical and spinal cord microglial cultures

Microglia were shaken off the top of the mixed glial cultures after 5 days in culture using a MaxQ 4000 orbital shaker (200 rpm/ 1 h/ 37°C; Thermo Fisher Scientific) and pelleted by centrifugation (400 × *g*/ 5 min). Microglia were resuspended in glial feeding medium and seeded into poly-D-lysine coated plates. Once plated, microglia entered a resting phase and did not proliferate. Therefore, this process was repeated every 5 days using the mixed glial parental culture as a source of proliferating microglia.

6.2.6 Treatment of primary mixed glial cultures

Primary mixed glial cultures were treated after 12 days *in vitro* with inflammatory mediators, LPS or TNFα, or heat shock (42°C/ 30 min with recovery at 37°C/ 6-24 h) as a positive control.

For Griess assays, cells were treated for 24 h with increasing concentrations of LPS (0-100 µg/mL) or TNFα (0-200 ng/mL) diluted in glial feeding media. For all other experiments, cells were treated for 24 h with 80 µg/mL LPS or 100 ng/mL TNFα diluted in glial feeding media, concentrations that were shown to elicit a maximal inflammatory response in cortical and spinal cord primary mixed glial cultures. In experiments that investigated the effect of iNOS inhibition on NO synthesis, mixed glial cultures were pre-treated with 25 µM N-[[3-(aminomethyl)phenyl]methyl]-ethanimidamide, dihydrochloride (1400W) for 2 h prior to treatment with inflammatory mediators. After treatment, cell supernatants were harvested for Griess assays to quantify the concentration of nitrite. Alternatively, cells were either harvested for immunoblot analysis or fixed in 4% (w/v) PFA for immunolabelling and subsequent epifluorescence microscopy or flow cytometry.

6.2.7 Griess assay

The release of NO radicals in the cell culture medium of LPS or TNFα treated cortical and spinal cord mixed glial cultures and was assessed by measuring the accumulation of nitrite (NO_2^-; a stable product of NO breakdown) using the Griess assay. After 24 h of LPS or TNFα treatment, the supernatant from each well was incubated with nitrate reductase (0.028 U/mL) and β-NADPH (100 µM) for 15 min/ 37°C to convert all nitrates in the supernatant to nitrites. Subsequently, lactate dehydrogenase and sodium pyruvate were added for 10 min/ 37°C before the addition of the Griess reagent. The supernatants were mixed with 50 µL Griess reagent in a 96-well plate and incubated for 15 min/ RT and measured using a spectrophotometer at 540 nm. Nitrite concentrations were determined against a standard curve generated from known concentrations of sodium nitrite (0-100 µM). Following assessment of nitrite levels, total protein levels were measured by a DC protein assay (Bio-Rad) and relative colour change was determined using a spectrophotometer at 750 nm. The measurements were converted to µM using the nitrite standard curve and normalised to µM/µg protein to exclude variability in the

initial cell culture plating density. The measurements were also adjusted for background levels of nitrite in the medium.

6.2.8 Protein extraction and quantification

Mixed glial cultures were washed twice with HBSS post-treatment. Whole cell lysates were prepared by adding ice-cold RIPA buffer to each well [50 mM Tris (pH 7.5), 150mM NaCl, 1% (v/v) NP-40, 0.5% (w/v) sodium deoxycholate, 0.1% (w/v) SDS, 1 mM EDTA, 1 mM EGTA, 1 mM PMSF, 1 × protease/phosphatase inhibitor cocktail] and harvesting the lysates on ice. The total protein (mg/mL) concentration of each sample was quantified by DC protein assay (Bio-Rad) according to the manufacturer's instructions. Each sample was adjusted to 1 mg/mL with RIPA buffer to ensure equal protein loading of the SDS-PAGE (see section 2.7.2 for details) for subsequent immunoblotting.

6.2.9 Immunoblotting

See section 2.7. One exception was that detection was determined using Luminata Crescendo Western HRP substrate (Merk-Millipore) and luminescence was captured using the Chemidoc Touch (Bio-Rad) at the Institute of Neurology, UCL.

6.2.10 Immunolabelling

See section 2.8.1.

6.2.11 Epifluorescence microscopy

Mixed glial cortical and spinal cord cultures were plated on 10 mm coverslips and immunolabelled post-treatment. The coverslips were mounted onto 26 × 76 mm glass slides (VWR) using CitiFluor Anti-Fadent Mounting Solutions (ProSciTech). The slides were analysed using a Leica epifluorescence microscope system with Leica Application Suite v.2.8.1 software, using the 20× or 40× objective lens. AlexaFluor488 fluorescence was excited using a mercury lamp with a 488 nm filter and Cy3 fluorescence was excited using a 561 nm filter.

Images were captured using a Nikon colour camera. The proportion of cells that were $Hsp25^{+ve}$ or $iNOS^{+ve}$ were determined using MetaMorph Image Analysis Software (Molecular Devices, CA, USA) and equations 6.1 and 6.2.

$$\left(\frac{\#\ Hsp25\ positive\ of\ GFAP\ positive}{Total\ \#\ GFAP\ positive}\right) \times 100 = \%Hsp25\ positive\ astroglia \quad \text{(equation 6.1)}$$

$$\left(\frac{\#\ iNOS\ positive\ of\ CD11b\ positive}{Total\ \#\ CD11b\ positive}\right) \times 100 = \%\ iNOS\ positive\ microglia \quad \text{(equation 6.2)}$$

6.2.12 Flow cytometry

The entire immunolabelling process was conducted with gentle rocking at each step to ensure appropriate mixing of cells with fixing, permeabilising, blocking, and antibody solutions. Cells were resuspended in 200 µL of PBS for single cell analysis by flow cytometry. Flow cytometry was performed using a FACS Aria II equipped with 488 nm, 561 nm and 633 nm lasers. A minimum of 20,000 events per sample were collected at a high flow rate. Forward scatter and side scatter were collected using a linear scale, and fluorescent emissions were collected as area (log scale) for each channel. For AlexaFluor488 fluorescence, data were collected with the 488 nm laser and 530/30 bandpass filter. For Cy3 fluorescence, data were collected with the 561 nm laser and 582/15 bandpass filter. For APC/Cy7 fluorescence, data were collected with the 633 nm laser and the 670 longpass filter.

6.2.13 Statistics

See section 2.10.

6.3 Results

6.3.1 Characterisation of WT cortical and spinal cord mixed glial cultures

Primary glial cultures were derived from the total cerebral cortex and spinal cords of postnatal day 2-3 mice. Such cultures are typically enriched with fast proliferating astroglia; however, other cell types, such as microglia, oligodendrocytes, and fibroblasts can also grow in these cultures in low quantities (McCarthy and de Vellis 1980, Hansson 1984, Falsig et al. 2006). Therefore, these cultures are described as primary mixed glial cultures. A systematic review of the effect of microglial cells in these cultures showed that microglial-derived effects are often wrongly attributed to astroglia, the predominant cell type in these cultures (Saura 2007). Therefore, to establish that the cortical and spinal cord mixed glial cultures used in this study were composed of comparable proportions of astroglia and microglia, the cultures were analysed by immunolabelling and subsequent fluorescence microscopy or flow cytometry (Figure 6.1).

To determine the proportions of astroglia and microglia present, glial cultures were immunolabelled with GFAP (astroglial marker) and Iba1 (microglial marker) and imaged by fluorescence microscopy (Figure 6.1a). Furthermore, single cell analysis by flow cytometry of GFAP and CD11b (microglial marker) immunolabelled cells demonstrated that approximately 80% of the cells were astroglia (cortical 81.8 ±2.3% and spinal cord 73.0 ±2.8%) and 5-10% were microglia (cortical 4.6±0.7% and spinal cord 11.8±3.0%; Figure 6.1b-d). There were no significant differences between the proportions of astroglia or microglia in the cortical versus spinal cord cultures, and both cultures consistently showed the same cellular composition across independent biological replicates [$F(1, 8) = 0.10$, $P = 0.75$].

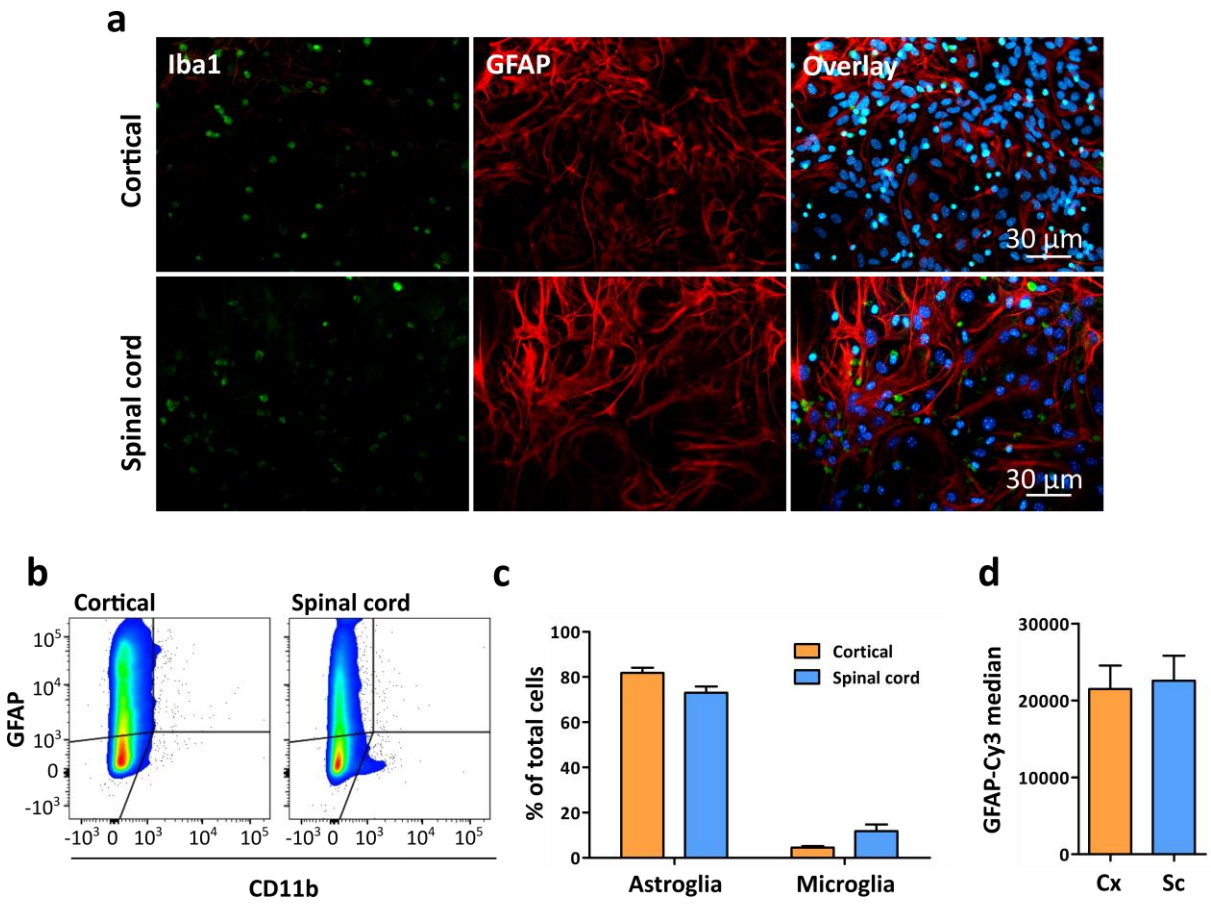

Figure 6.1. Characterisation of cortical and spinal cord mixed glial cultures. The composition of astroglia and microglia in the mixed primary cortical and spinal cord cultures was determined after 12 days *in vitro* by (a) immunocytochemistry and (b)-(d) immunolabelling and single cell analysis by flow cytometry. (a) Mixed primary cortical and spinal cord cultures immunolabelled with Iba1 (*left)*, and GFAP (*middle*). Overlay (*right*) shown with DAPI nuclear stain. Scale bar = 30 µm. (b) Fixed and permeabilised cultures were immunolabelled with GFAP-Cy3 (astroglia marker) and CD11b-APC/Cy7 (microglial marker) and 20,000 events were analysed by flow cytometry. Spider quadrant gating was applied and representative cytograms of immunolabelled cortical (*left*) and spinal cord (*right*) mixed glial cultures are shown. (c) The proportion of astroglia and microglia and (d) the GFAP-Cy3 fluorescence median in cortical (Cx) spinal cord (Sc) cultures determined by flow cytometry. Data shown are the mean + SEM of three biological replicates. Differences between the means were determined using a two-way ANOVA or student's t-test (panel d) and there were no significant differences.

6.3.2 The inflammatory response in WT cortical and spinal cord mixed glial cultures

Neuroinflammation is a characteristic pathological hallmark of ALS (Philips and Robberecht 2011, Hooten et al. 2015). To establish whether the CNS may possess regional differences in the capacity to activate an inflammatory response, NO synthesis was compared in cortical and spinal cord cultures after treatment with the inflammatory mediators, LPS and TNFα (Figure 6.2a-b).

With regard to the LPS dose response, a two-way analysis of variance (ANOVA) indicated that nitrite concentrations were significantly greater in spinal cord glia than cortical glia [$F(1, 36) = 64.01$, $P < 0.0001$] in response to LPS treatment (Figure 6.2a). Likewise, there was a concentration-dependent increase in the concentration of nitrite with increasing LPS concentration [$F(5, 36) = 22.16$, $P < 0.0001$]. Bonferroni post-hoc testing showed that there was a statistically significant difference between the mean nitrite concentration in cortical and spinal cord glial cultures at 10 µg/mL ($P < 0.01$), 80 µg/mL ($P < 0.001$), and 100 µg/mL LPS ($P < 0.001$).

With regard to the TNFα dose response, a two-way ANOVA indicated that spinal cord glia had a significantly greater concentration of nitrite compared to cortical glia following TNFα treatment [$F(1, 24) = 56.38$, $P < 0.0001$] (Figure 6.2b). Increasing the concentration of TNFα also significantly increased the nitrite concentration in both cultures, in a concentration-dependent manner [$F(5, 24) = 5.632$, $P = 0.0014$]. Bonferroni post-hoc testing showed that there were statistically significant differences between the mean nitrite concentration in cortical and spinal cord glial cultures at 40 ng/mL ($P < 0.05$), 80 ng/mL ($P < 0.01$), 100 ng/mL ($P < 0.001$), and 200 ng/mL TNFα treatment ($P < 0.01$).

The data in Figure 6.2a-b demonstrates that the CNS region from which the glial cultures were derived significantly affected the concentration of nitrite in response to each inflammatory mediator, with spinal cord glial cultures generating a 2-4-fold greater concentration of nitrite compared to cortical glia after LPS treatment and 5-12-fold greater concentration after TNFα treatment. Importantly, untreated cortical and spinal cord cultures showed the same basal concentration of nitrite, thus the difference in nitrite concentration between to the two regions was specific to cultures treated with inflammatory stimuli. Spinal cord glia cultures may have a lower threshold for the activation of an inflammatory pathway and have a stronger response

compared to cortical glia. In addition, higher concentrations of nitrite were detected in cultures treated with LPS compared to TNFα.

There are three different NO synthases (NOS) responsible for the production of NO in cells, neuronal NOS (nNOS) and endothelial NOS (eNOS), and the stress-inducible NOS (iNOS) (Murphy 2000). To determine the source of the NO synthesis following activation of the inflammatory pathway, LPS and TNFα treated mixed glial cultures were pre-treated for 2 h with 25 µM 1400W (Figure 6.2c-d), a compound that has previously been shown to selectively and irreversibly inhibit iNOS activity in primary cultures at a range of concentrations (5-400 µM) (Garvey et al. 1997, Saura et al. 2005, Papageorgiou et al. 2016). There was a significant reduction and a complete inhibition of NO synthesis in cortical and spinal cord mixed glial cultures, respectively ($P < 0.05$ for LPS treated cortical and $P < 0.001$ for LPS and TNFα treated spinal cord cultures) following pre-treatment with 1400W. This data demonstrates that NO is synthesised by iNOS in these cultures following treatment with the inflammatory mediators LPS and TNFα.

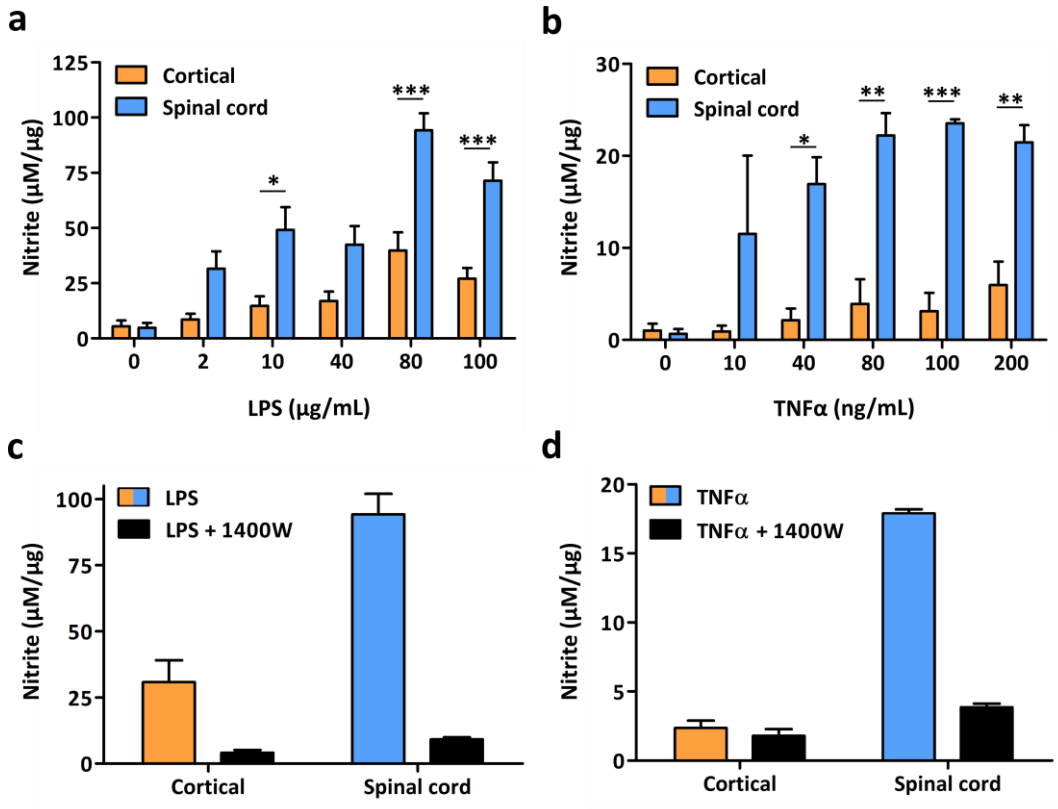

Figure 6.2. Spinal cord mixed glial cultures synthesise more NO in response to LPS and TNFα stimulation compared to cortical glia. Nitrite concentration in cortical and spinal cord mixed glial cultures was determined by Griess assay. (a) LPS dose response with primary cortical and spinal cord mixed glial cultures relative to total protein. (b) TNFα dose response of primary cortical and spinal cord mixed glial cultures with TNFα relative to total protein. (c)-(d) Inhibition of iNOS activity in 80 µg/mL LPS and 100 ng/mL TNFα treated glia pre-treated with 25 µM 1400W for 2 h. Data are the mean + SEM of four biological replicates. Differences between the means were determined using a two-way ANOVA followed by Bonferroni's post-hoc test, where $P < 0.05$ (*), $P < 0.01$ (**), $P < 0.001$ (***).

Subsequent experiments were performed by treating cultures with 80 µg/mL LPS and 100 ng/mL TNFα, since these treatments resulted in maximal concentration of nitrite after 24 h (Figure 6.2). Immunoblot analysis of whole cell lysates from cortical and spinal cord glial cultures was performed to assess iNOS expression after treatment with 80 µg/mL LPS and 100 ng/mL TNFα (Figure 6.3a-b). LPS treated cortical and spinal cord glia showed upregulated iNOS expression, but TNFα treatment did not lead to detectable iNOS expression. The low concentration of NO after TNFα treatment could be the consequence of lower iNOS expression, which may be below the detection limit of the iNOS antibody with the immunoblotting procedure used in this work. A student's t-test was performed to compare iNOS expression in

LPS treated cortical and spinal cord mixed glial cultures (Figure 6.3b) and showed that there was no significant difference in iNOS expression in the whole cell lysates of the cultures (P = 0.737). Since iNOS is similarly upregulated in cortical and spinal cord glia after LPS treatment, this finding suggests that the differences in nitrite concentration observed by Griess assay (Figure 6.2) could be the consequence of higher iNOS activity in spinal cord cultures.

To elucidate which cell type in the mixed glial cultures were expressing iNOS, cells were immunolabelled for GFAP and iNOS and subsequently imaged by fluorescence microscopy (Figure 6.3c). There were no $iNOS^{+ve}$ cells in the untreated samples, however, after treatment with LPS or TNFα, several (<1%) $GFAP^{-ve}$ cells were stained strongly for iNOS. The immunocytochemistry shows that the upregulation of iNOS expression following LPS or TNFα treatment is not due to increased expression by $GFAP^{+ve}$ astroglia; rather, other cell-types in the mixed glial cultures have increased expression of iNOS.

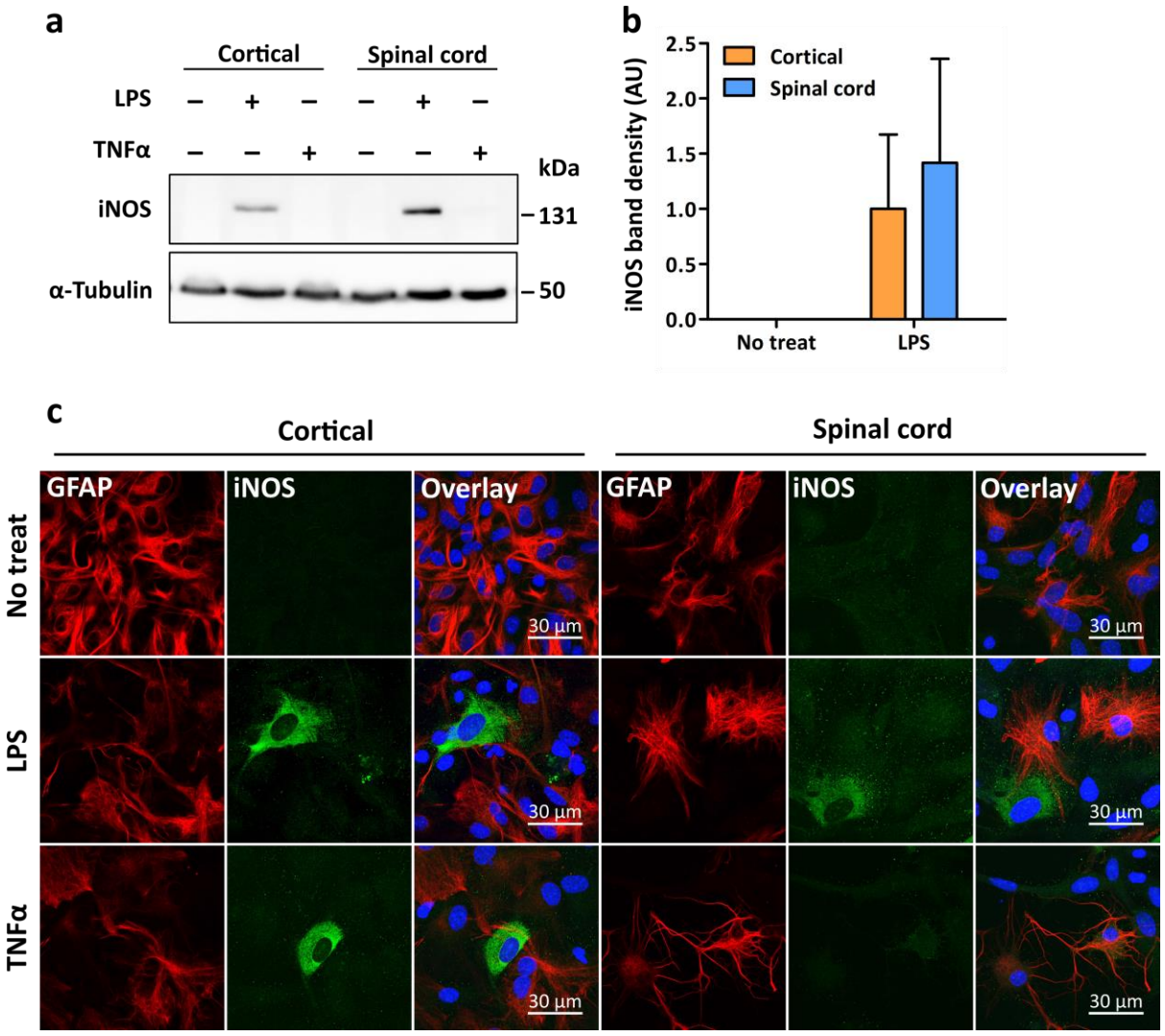

Figure 6.3. Characterisation of iNOS upregulation after treatment with inflammatory mediators in cortical and spinal cord mixed glial cultures. (a) Mixed primary cortical and spinal cord glial cultures treated with either 80 µg/mL LPS or 100 ng/mL TNFα were lysed, 20 µg of total protein immunoblotted, and probed for iNOS (131 kDa) and α-tubulin (loading control; 50 kDa). (b) Fold change in iNOS band density relative to α-tubulin (AU). Data shown are the mean + SEM of three biological replicates. Differences between the means were determined using a student's t-test; there were no significant differences. (c) Cortical and spinal cord mixed glial cultures treated with LPS and TNFα were immunolabelled for GFAP (astroglial marker; *left*) and iNOS (*middle*). Overlay with DAPI nuclear stain (*right*). Scale bar = 30 µm.

A common misconception in studies examining iNOS expression in primary mixed glial cultures is that iNOS is expressed by the astroglia in the culture after LPS treatment (Saura 2007). A review of the literature surrounding LPS-mediated iNOS expression in primary rodent glial cultures showed that only 6 of 16 studies demonstrated evidence for $iNOS^{+ve}$ astroglia (Saura 2007). In most cases it is likely that microglia were the main producers of iNOS.

Therefore, to further investigate the differences observed in nitrite concentration between cortical and spinal cord mixed glial cultures, purified microglia, which were shaken off the mixed glial cultures, were treated with 80 μg/mL LPS or 100 ng/mL TNFα for 24 h, and immunolabelled for CD11b and iNOS for subsequent confocal microscopy (Figure 6.4a). There was no iNOS staining observed in untreated or TNFα treated cultures; however, treatment with LPS resulted in a significant increase in the proportion of $iNOS^{+ve}$ cortical and spinal cord microglia compared to no treatment [$F(2, 6) = 27.04$, $P = 0.001$; Figure 6.4b]. However, there was no significant difference between the proportion of $iNOS^{+ve}$ cells after LPS treatment in microglial cultures derived from the cortex or spinal cord [$F(1,6) = 0.3501$, $P = 0.576$]. Together these findings suggest that cortical and spinal cord microglia similarly up-regulate iNOS expression in response to LPS treatment and that the increased NO observed in LPS treated spinal cord glial cultures may be the result of a higher rate of iNOS activity in microglia from this region compared to those in the cortex.

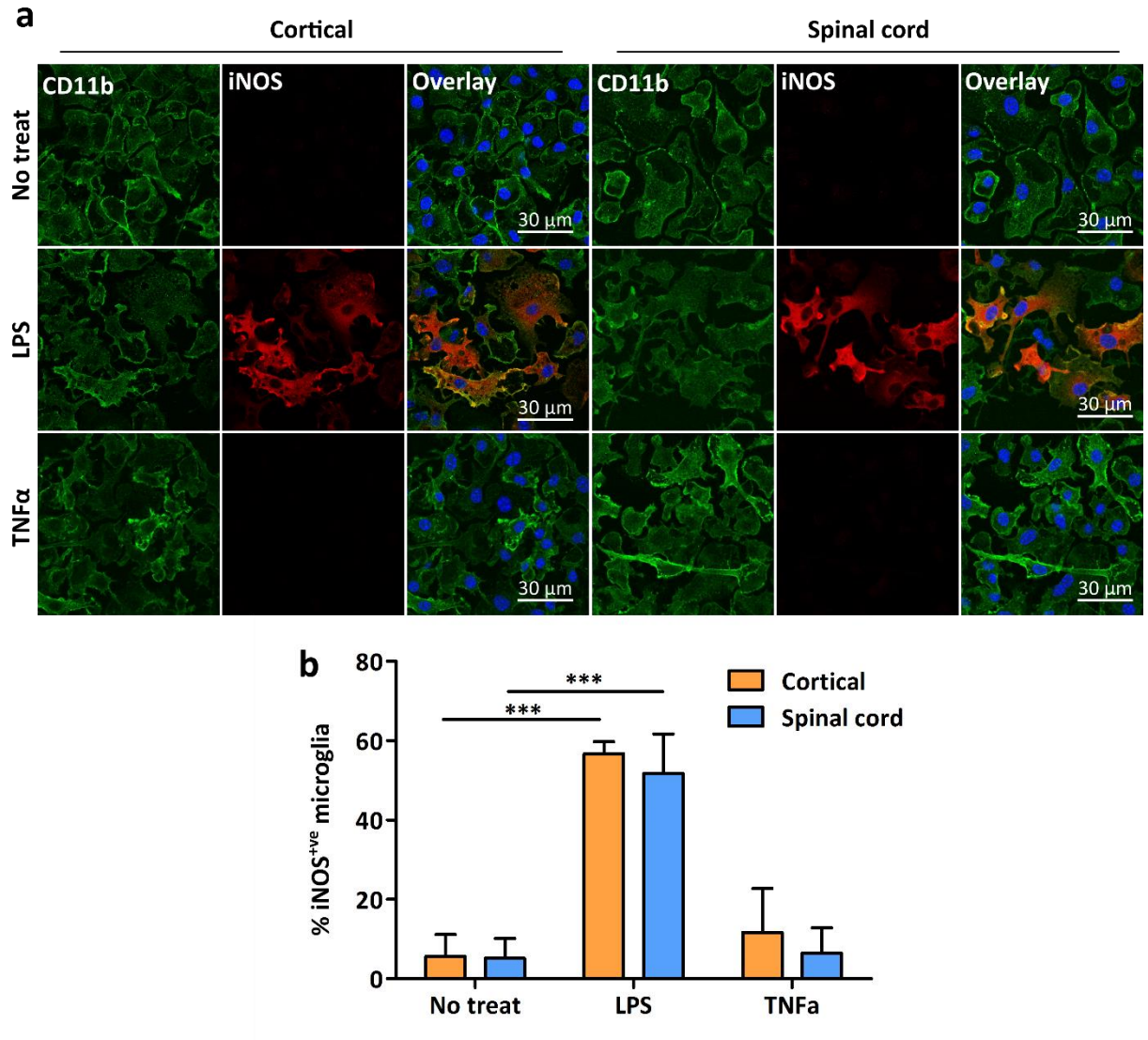

Figure 6.4. iNOS upregulation in LPS and TNFα treated purified cortical and spinal cord microglial cultures. (a) Purified cortical and spinal cord microglial cultures were treated (or not) with LPS or TNFα for 24 h and immunolabelled for CD11b (microglial marker; *left*) and iNOS (*middle*). Overlay with DAPI nuclear stain (*right*). Scale bar = 30 µm. (b) The proportion of $iNOS^{+ve}$ microglia present in cultures in the presence or absence of inflammatory mediators. Data shown are the means + SEM of three biological replicates. Differences between the means were determined using a two-way ANOVA followed by Bonferroni's post-hoc test, where $P < 0.001$ (***).

6.3.3 Comparing Hsp expression in WT cortical and spinal cord mixed glial cultures

The increase in nitrite concentration observed in LPS and TNFα treated spinal cord mixed glial cultures suggests that these cells are also under higher levels of nitrosative stress compared to cortical cultures. It has previously been shown that treatment with NO is capable of inducing an HSR, as determined by increased Hsp70 expression, in rat hepatocytes (Kim et al. 1997),

rat iselts (Scarim et al. 1998), vascular smooth muscle cells (Xu et al. 1997), and primary rat glial cultures (Feinstein et al. 1996, Calabrese et al. 2000). Therefore, to investigate whether the LPS or TNFα treatments could activate the HSR, markers of HSR induction were compared in cortical and spinal cord mixed glial cultures (Figure 6.5a). Heat shock protein 70 is a commonly used marker of the induction of the HSR (Batulan et al. 2003, Kieran et al. 2004, Trinklein et al. 2004b). Immunoblot analysis of Hsp70 expression showed no change in its expression (relative to α-tubulin) following treatment with either LPS or TNFα (Figure 6.5a-b). There was also no significant difference in Hsp70 expression between cortical and spinal cord mixed glial cultures. This data demonstrated that there are no differences in Hsp70 expression between glial cells from each of these CNS regions, nor is Hsp70 expression stress-induced by LPS or TNFα treatment under these experimental conditions.

Heat shock protein 25 (Hsp25; human orthologue is Hsp27) is constitutively expressed in motor neurons of the spinal cord (Plumier et al. 1997, Benn et al. 2002, Kalmar et al. 2002). Since the expression of Hsp25 in the spinal cord is likely to play important "housekeeping" roles in motor neurons, it was also of interest to investigate Hsp25 expression in mixed glial cultures. Immunoblot analysis of Hsp25 showed significant high levels of Hsp25 levels in spinal cord glial cultures compared to cortical cultures in the absence and presence of the inflammatory mediators [$F(1, 6) = 17.07$, $P = 0.006$] (Figure 6.5a and c). However, there was no stress-induced Hsp25 upregulation with either LPS or TNFα treatment in either cortical or spinal cord cultures. Further investigation of Hsp25 expression in cortical and spinal cord mixed glial cultures by immunocytochemistry supported the findings from the immunoblot analysis by showing greater immunoreactivity to Hsp25 in the spinal cord compared to cortical glial cultures, particularly in astroglia (Figure 6.5d). Cell counts of these samples were performed to determine the proportion of $Hsp25^{+ve}$ astroglia in each culture and showed that 30 ± 7% cortical astroglia and 56 ± 6% spinal cord astroglia were $Hsp25^{+ve}$ in the absence of treatment

(Figure 6.5e; $P = 0.0361$). Contrary to the results for Hsp70, this data indicates that there are regional differences in Hsp25 expression between the cortex and spinal cord. Similar to that observed for Hsp70, Hsp25 expression was not increased following treatment with either of the inflammatory mediators.

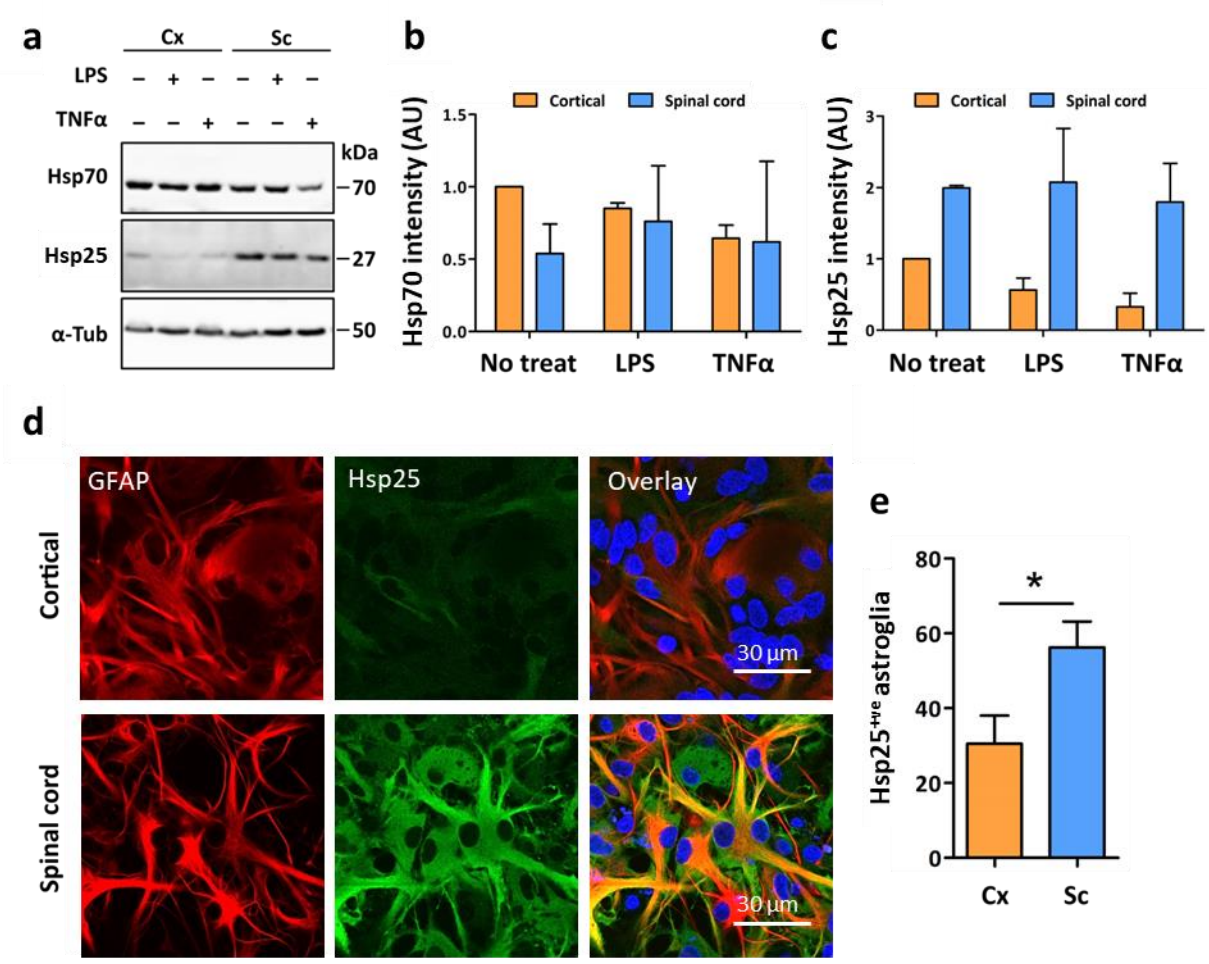

Figure 6.5. Hsp70 and Hsp25 expression in LPS or TNFα-stimulated primary cortical and spinal cord glial cultures. (a) Mixed primary cortical (Cx) and spinal cord (Sc) glia were treated with 80 ug/mL LPS or 100 ng/mL TNFα for 24 h, 30 µg of total protein was immunoblotted, and probed for Hsp70 (70 kDa), Hsp25 (25kDa) and α-tubulin (50 kDa). (b) Fold change in Hsp70 band intensity relative to the untreated cortical sample. (c) Fold change in Hsp25 band intensity relative to the untreated cortical sample. Data in (b) and (c) are mean + SEM from three biological replicates. Differences between the means were determined using a two-way ANOVA followed by Bonferroni's post-hoc test. (d) Representative images of untreated cortical and spinal cord glial cultures immunolabelled for GFAP (astroglial marker; *left*) and Hsp25 (*middle*). Overlay (*right*) is shown with DAPI nuclear stain. Scale bar = 30 µm. (e) The proportion of $Hsp25^{+ve}$ astroglia from cell counts of cortical and spinal cord glial cultures. Data shown are from one biological replicate and are the mean + SEM of >300 cells across five wide field of view images. Statistically significant differences between the means were assessed using a student's t-test where $P < 0.05$ (*).

To further investigate the regional differences in Hsp25 expression between cortical and spinal cord astroglia and microglia, these cultures were immunolabelled for GFAP, CD11b, and Hsp25 for single cell analysis by flow cytometry. Viable cells were gated based on their forward and side scatter to exclude cellular debris and cell clumps (Figure 6.6a). With respect to analysing the $GFAP^{+ve}$ cells, bisected polygonal gates were set using the unlabelled sample as a $GFAP^{-ve}$ and $Hsp25^{-ve}$ control, and two controls that were singly labelled for either GFAP alone or Hsp25 alone (Figure 6.6b-d). Gating the flow cytometry data in this way allowed the proportion of $Hsp25^{+ve}$ cells in the $GFAP^{+ve}$ astroglial population to be determined in both the cortical and spinal cord mixed glial cultures. Similarly, cells were either left unlabelled or immunolabelled for CD11b or Hsp25 alone as single colour controls (Figure 6.6e-g). This gating strategy allowed the proportion of $Hsp25^{+ve}$ cells of the $CD11b^{+ve}$ microglial population to be elucidated in cortical and spinal cord mixed glial cultures.

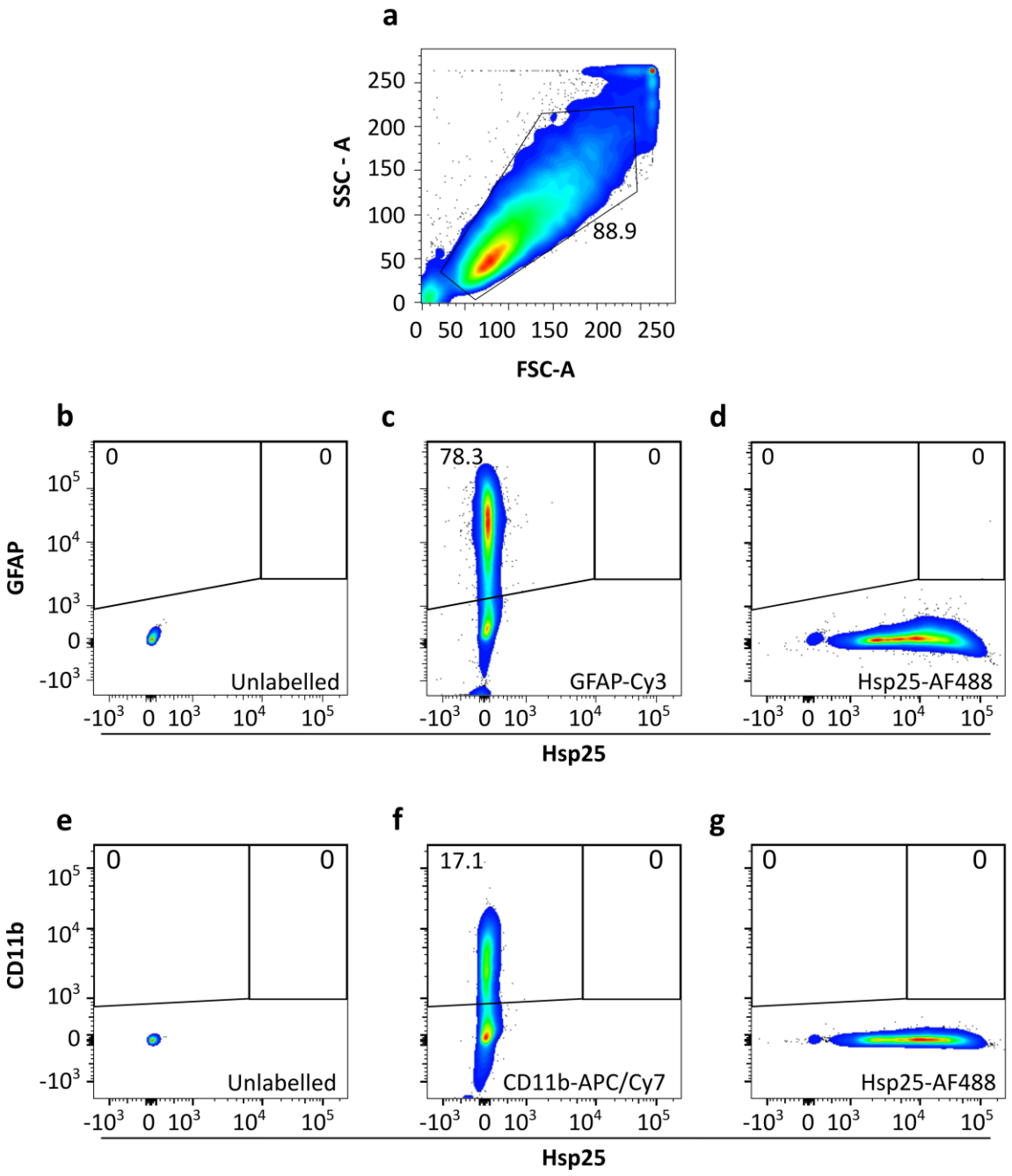

Figure 6.6. Gating strategy for the analysis of Hsp25 expression of astroglia and microglia by flow cytometric data. (a) Viable cells were distinguished based on their forward scatter (area) and side scatter (area) and a polygonal gate was used to exclude cellular debris and cell clumps. Primary glial cultures were fixed, permeabilised and either left (b) unlabelled or singly labelled for (c) GFAP-Cy3 or (d) Hsp25-AF488. These samples were used to set the bisected polygonal gates, which were used to determine the percent of $GFAP^{+ve}$ and $Hsp25^{+ve}$ events in the double labelled samples. Fixed and permeabilised cells were either left (e) unlabelled or singly labelled for (f) CD11b-APC/Cy7 or (g) Hsp25-AF488. These samples were used to set the bisected polygonal gates, which were used to determine the percent of $CD11b^{+ve}$ and $Hsp25^{+ve}$ events in the double labelled samples.

Representative cytograms of GFAP and Hsp25 double immunolabelled cortical and spinal cord mixed glial cultures following 24 h of treatment (or not) with LPS are shown in Figure 6.7a. Comparison between no treatment and LPS treatment in either cortical or spinal cord astroglia did not appear to change the proportion of $Hsp25^{+ve}$ cells in this biological replicate. A two-way ANOVA showed that there was a significant effect of CNS region of the cultures on the percent of $Hsp25^{+ve}$ astroglia [$F(1, 18) = 18.08$, $P = 0.0005$] with an approximately 2-fold increase in the proportion of spinal cord astroglia expressing Hsp25 compared to cortical astroglia (Figure 6.7b). However, treatment of either cortical or spinal cord astroglia with LPS or TNFα did not result in a significant increase in the proportion of cells expressing Hsp25 [$F(2, 18) = 0.018$, $P = 0.9817$]. Moreover, assessment of the levels of Hsp25 expressed in cells positive for Hsp25 expression, using the median of the fluorescent intensity of stained cells, demonstrated that treatment with LPS did not up-regulate Hsp25 expression in the $Hsp25^{+ve}$ cells (Figure 6.7c).

The expression of Hsp25 in cortical and spinal cord microglia was also compared using the same approach. Representative cytograms of CD11b and Hsp25 immunolabelled cortical and spinal cord samples in the presence and absence of LPS treatment are shown (Figure 6.7d) and were used to determine the proportion of $Hsp25^{+ve}$ microglia and the levels of Hsp25 expression in each of the samples (Figure 6.7e-f). There were no differences observed in either the proportion of $Hsp25^{+ve}$ microglia or the fluorescence intensity (corresponding to the levels of Hsp25 expression) between cortical or spinal cord microglia in the absence of treatment. In addition, treatment with LPS or TNFα did not affect Hsp25 expression in either cortical or spinal cord microglia.

Together, this flow cytometry data suggests that higher levels of Hsp25 expression observed in spinal cord mixed glial cultures by immunoblot is primarily due to a higher proportion of $Hsp25^{+ve}$ astroglia in the spinal cord compared to the cortical cultures. This regional difference

in Hsp expression is not observed for Hsp70. This suggests that different regulatory mechanisms control the expression of Hsp25 and Hsp70 in astroglia. This same increase in the proportion of $Hsp25^{+ve}$ cells was not observed in spinal cord microglia and is specific to spinal cord astroglia. Lastly, these findings show that inflammatory stimuli do not up-regulate the expression of Hsp70 or Hsp25 in either microglia or astroglia, suggesting that chronic inflammation in ALS may not activate cytoprotective stress-responses in glial cells.

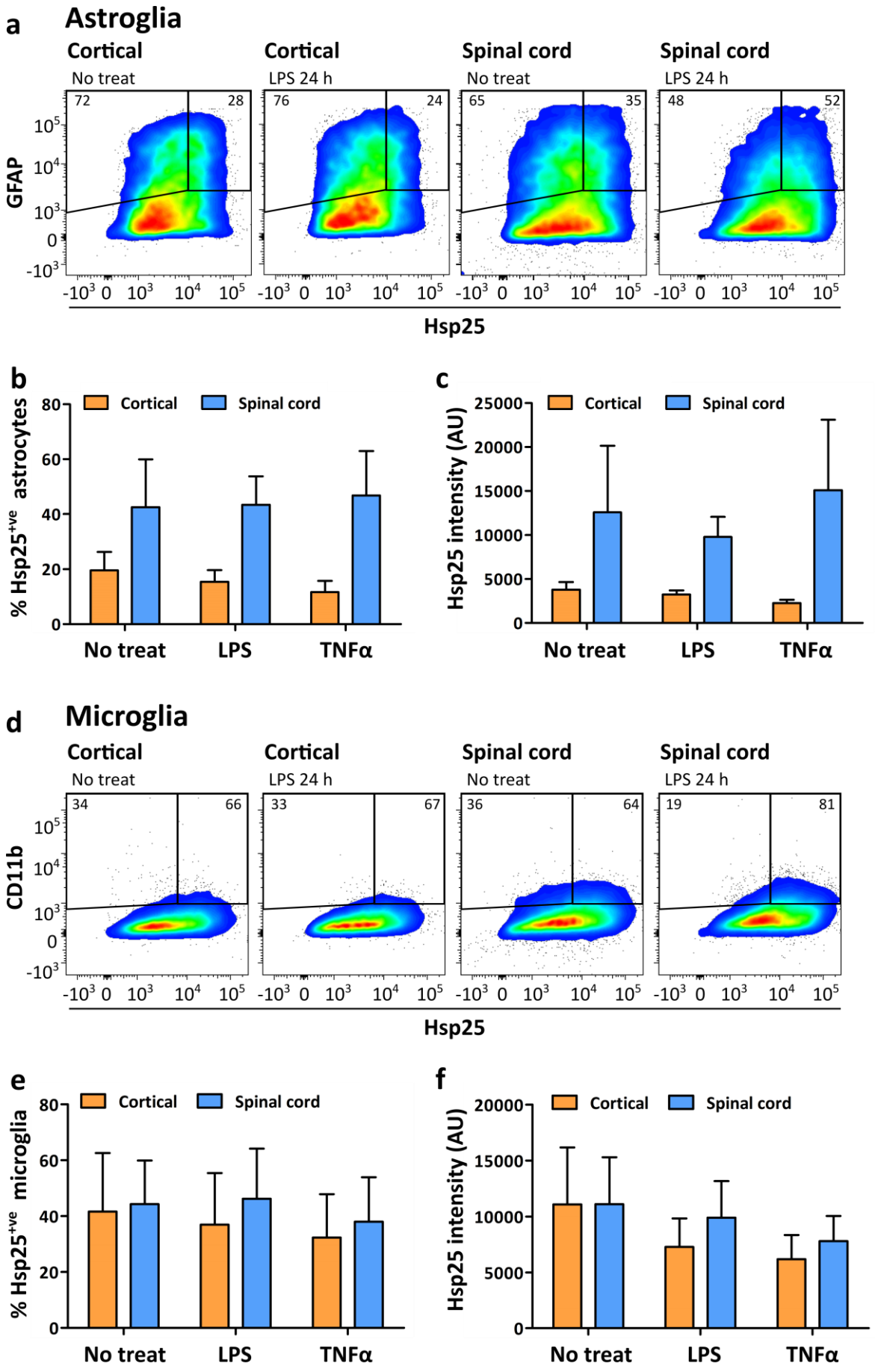
a
Astroglia
Cortical
No treat
Cortical
LPS 24 h
Spinal cord
No treat
Spinal cord
LPS 24 h
72
28
76
24
65
35
48
52
GFAP
Hsp25
b
% Hsp25+ve astrocytes
Cortical
Spinal cord
No treat
LPS
TNFα
c
Hsp25 intensity (AU)
Cortical
Spinal cord
No treat
LPS
TNFα
d
Microglia
Cortical
No treat
Cortical
LPS 24 h
Spinal cord
No treat
Spinal cord
LPS 24 h
34
66
33
67
36
64
19
81
CD11b
Hsp25
e
% Hsp25+ve microglia
Cortical
Spinal cord
No treat
LPS
TNFα
f
Hsp25 intensity (AU)
Cortical
Spinal cord
No treat
LPS
TNFα

Figure 6.7. Flow cytometric analysis of Hsp25 expression in astroglia and microglia after LPS and TNFα treatment. Primary cortical and spinal cord mixed glial cultures were treated with 80 µg/mL LPS or 100 ng/mL TNFα. The cells were fixed, permeabilised and immunolabelled for GFAP-Cy3, CD11b-APC/Cy7 and Hsp25-AF488. (a) and (d) Flow cytometric analysis of cortical and spinal cord glial cultures. *Left – right*: Representative cytograms of untreated and LPS treated cortical glial cultures, and untreated and LPS treated spinal cord cultures. Data are presented as pseudo-colour plots where blue represents low and red represents a high frequency of cells. Outlier events are shown as individual black dots. The percent of $GFAP^{+ve}$ or $CD11b^{+ve}$ cells in each gate is provided. (b) and (e) The percent of $Hsp25^{+ve}$ astroglia or microglia as determined from the flow cytometric analysis. (c) and (f) The Hsp25-AF488 fluorescent median of the astroglial or microglial population. Data shown are means + SEM of three biological replicates. Differences between the means were determined using a two-way ANOVA followed by Bonferroni's post-hoc test.

Since neither astroglia nor microglia demonstrated an induction of Hsp25 expression after treatment with either of the inflammatory mediators, these cells were subjected to heat shock to compare their capacity for Hsp25 upregulation (Figure 6.8). Heat shock (42°C/ 30 min followed by 37°C/ 6 h or 24 h recovery) of cortical astroglia did not induce an increase in the proportion of astroglia expressing Hsp25 (Figure 6.8a-b). The proportion of $Hsp25^{+ve}$ spinal cord astroglia increased from 43 ± 17% in the absence of heat shock to 72 ± 7% after heat shock with a 6 h recovery period at 37°C (Figure 6.8b); however, this difference was not statistically significant. There was no significant effect of time spent recovering following heat shock treatment on the proportion of $Hsp25^{+ve}$ astroglia. Analysis of the levels of Hsp25 in these cells (using the Hsp25-AF488 fluorescence median) demonstrated the same trends, whereby heat shocked spinal cord samples showed a trend towards increased fluorescence, indicating an upregulation in the expression of Hsp25 compared to no treatment, although this was not significant [$F(2, 12) = 0.6076$, $P = 0.5606$; Figure 6.8c].

Together, this data shows trend towards a higher proportion of spinal cord astroglia that are $Hsp25^{+ve}$ compared to cortical astroglia under basal conditions. There is a trend towards an increase in $Hsp25^{+ve}$ spinal cord astroglia following heat shock, whereas there is no increase for cortical astroglia. This data illustrates that there are differences in the capacity of cortical and spinal cord glia to induce Hsp25 expression after heat shock.

With regard to $CD11b^{+ve}$ microglia, a two-way ANOVA showed that there was no significant difference in the proportion of $Hsp25^{+ve}$ microglia derived from the cortex or spinal cord. Moreover, heat shock (42°C/ 30 min followed by 37°C/ 6 h or 24 h recovery) did not increase the proportion of $Hsp25^{+ve}$ microglia in either the cortical or spinal cord samples (Figure 6.8d-e). Analysis of the levels of Hsp25-AF488 fluorescence in heat shocked samples showed that there was no difference between Hsp25 expression levels in cortical or spinal cord microglia. However, spinal cord microglia exposed to heat shock and then allowed to recover for 6 h at 37°C, showed a significant increase in Hsp25-AF488 fluorescence intensity compared to its respective cortical sample and the untreated spinal cord sample (Figure 6.8f; $P < 0.01$). These data indicate that Hsp25 expression levels in $Hsp25^{+ve}$ spinal cord microglia increase after heat shock, but not in cortical microglia.

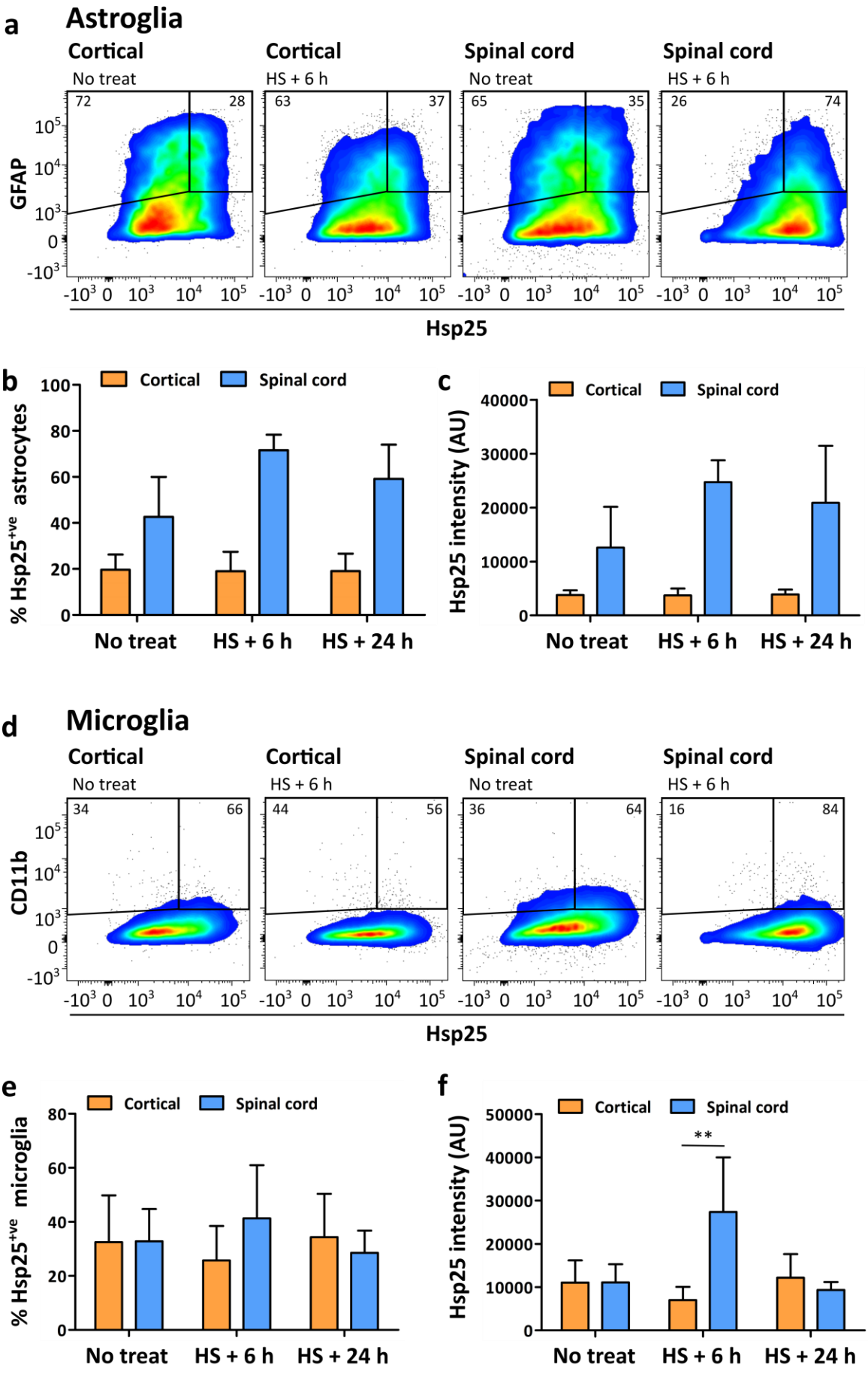
a
Astroglia
Cortical
No treat
Cortical
HS + 6 h
Spinal cord
No treat
Spinal cord
HS + 6 h
72
28
63
37
65
35
26
74
GFAP
Hsp25
b
Cortical
Spinal cord
% Hsp25+ve astrocytes
No treat
HS + 6 h
HS + 24 h
c
Cortical
Spinal cord
Hsp25 intensity (AU)
No treat
HS + 6 h
HS + 24 h
d
Microglia
Cortical
No treat
Cortical
HS + 6 h
Spinal cord
No treat
Spinal cord
HS + 6 h
34
66
44
56
36
64
16
84
CD11b
Hsp25
e
Cortical
Spinal cord
% Hsp25+ve microglia
No treat
HS + 6 h
HS + 24 h
f
Cortical
Spinal cord
**
Hsp25 intensity (AU)
No treat
HS + 6 h
HS + 24 h

Figure 6.8. Flow cytometric analysis of Hsp25 expression in astroglia and microglia after heat shock. Mixed primary cortical and spinal cord glia were heat shocked at 42°C for 30 min and allowed to recover at 37°C for 6 or 24 h. Cells were then fixed, permeabilised, immunolabelled for GFAP-Cy3, CD11b-APC/Cy7 and Hsp25-AF488 and analysed by flow cytometry. (a) and (d) Flow cytometric analysis of cortical and spinal cord glial cultures. *Left – right*: Representative cytograms of untreated and heat shocked cortical glial cultures, and untreated and heat shocked spinal cord cultures. Data are presented as pseudo-colour plots where blue represents low and red represents a high frequency of cells. Outlier events are shown as individual black dots. The percent of $GFAP^{+ve}$ or $CD11b^{+ve}$ cells in each gate is provided. (b) and (e) The percent of $Hsp25^{+ve}$ astroglia or microglia as determined from the flow cytometric analysis. (c) and (f) The median of the Hsp25-AF488 fluorescence intensity of the astroglial or microglial population. Data shown are means + SEM of three biological replicates. Differences were assessed using a two-way ANOVA followed by Bonferroni's post-hoc test, where $P < 0.01$ (**).

6.3.4 Characterisation of $SOD1^{WT}$ and $SOD1^{G93A}$ cortical and spinal cord glial cultures

To determine whether the regional differences in glial stress-responses observed in WT cultures also exist in a model of ALS, cortical and spinal cord cultures derived from $SOD1^{WT}$ and $SOD1^{G93A}$ over-expressing mice were compared. The cellular composition of the cultures was analysed by flow cytometry to determine the proportion of astroglia and microglia in the cortical and spinal cord mixed glial cultures (Figure 6.9a). Flow cytometric analysis of the proportion of astroglia and microglia in each of the cultures showed that $SOD1^{WT}$ cortical and spinal cord cultures contained comparable proportions of microglia (cortex 3.0 ± 0.5%, spinal cord 4.9 ± 0.2%) and astroglia (cortex 82.6 ± 1.3%, spinal cord 70.9 ± 2.2%; Figure 6.9b and c). In contrast, the proportion of microglia was higher in spinal cord cultures from $SOD1^{G93A}$ mice (23.7 ± 8.9%) compared to cortical cultures (12.8 ± 3.9%), however this difference was not statistically significant [$F(1, 6) = 2.032$, $P = 0.204$]. Flow cytometry of $SOD1^{G93A}$ glial cultures showed that there was a significantly lower proportion of astroglia in spinal cord cultures (55 ± 3.6%) compared to cortical cultures (77.1 ± 4.7%; Figure 6.9c) ($P < 0.05$).

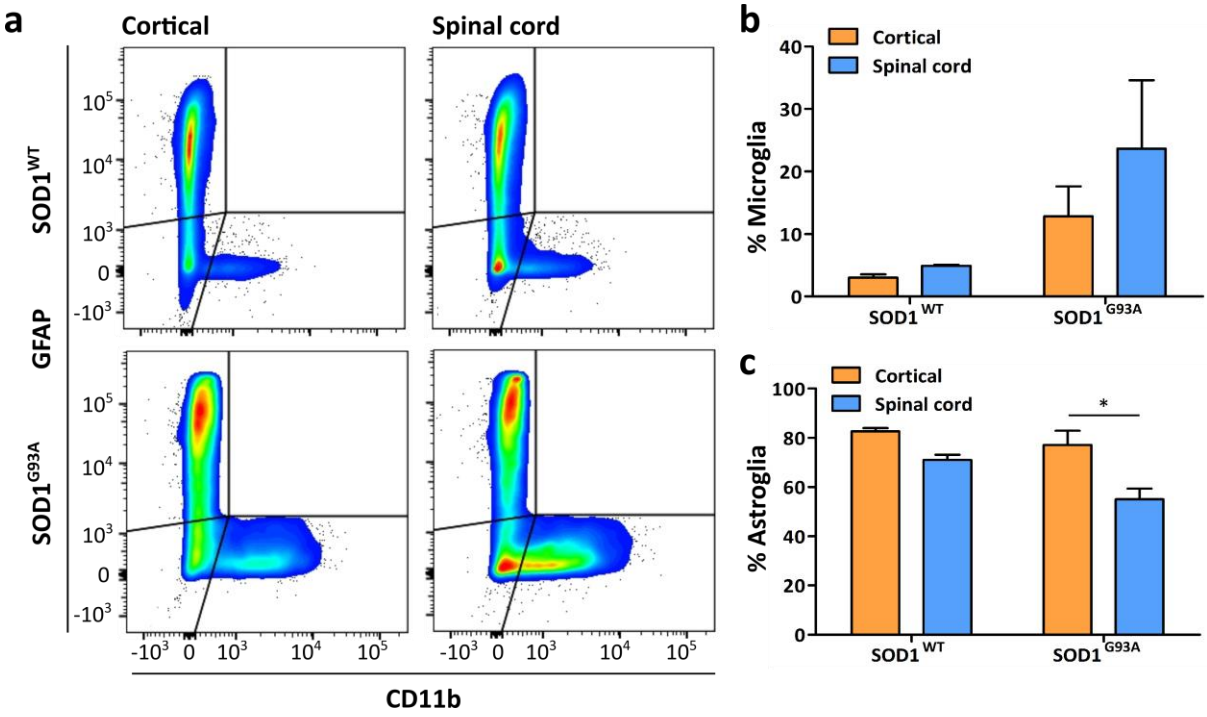

Figure 6.9. Characterisation of cortical and spinal cord mixed glial cultures derived from SOD1^{WT} and SOD1^{G93A} over-expressing mice. The astroglial and microglial composition to the mixed primary cortical and spinal cord cultures was determined after 12 days *in vitro* (a) Fixed and permeabilised cultures were immunolabelled with GFAP-Cy3 (astroglial marker) and CD11b-APC/Cy7 (microglial marker) and 20,000 events were analysed by flow cytometry. Spider quadrant gat ing was applied and representative cytograms of immunolabelled cortical (*left*) and spinal cord (*right*) mixed glial cultures are shown from SOD1^{WT} (*top*) and SOD1^{G93A} (*bottom*) mice. The proportion of (b) microglia and (c) astroglia determined from each sample in the flow cytometry experiments. Data shown are the mean + SEM of three biological replicates. Differences between the means were analysed using a two-way ANOVA followed by Bonferroni's post-hoc test, where $P < 0.05$ (*).

6.3.5 The inflammatory response in SOD1G93A cortical and spinal cord glial cultures

The effect of LPS treatment on NO synthesis was assessed in SOD1^{WT} and SOD1^{G93A} cortical and spinal cord cultures. In both SOD1^{WT} and SOD1^{G93A} cultures, spinal cord glia had a significantly greater nitrite concentration compared to cortical glia [F (1, 8) = 55.21, $P <$ 0.0001; Figure 6.10a]. Similar to the previous findings in WT glial cultures, these data show that the concentration of nitrite is greater in spinal cord cultures compared to cortical cultures for both SOD1^{WT} and SOD1^{G93A} glia.

Pre-treatment of mixed glial cultures with the iNOS inhibitor 1400W, followed by treatment with LPS resulted in the complete inhibition of NO synthesis in each sample [F (3,24) = 26.51,

$P < 0.0001$; Figure 6.10b]. Inducible NOS was detected by immunoblot analysis of whole cell lysates from $SOD1^{WT}$ and $SOD1^{G93A}$ spinal cord cultures treated with LPS. Spinal cord cultures from $SOD1^{G93A}$ mice showed a higher relative level of iNOS in LPS treated samples compared to spinal cord cultures from $SOD1^{WT}$ mice (Figure 6.10c). Inducible NOS was also detected in the untreated spinal cord $SOD1^{WT}$ glial sample (Figure 6.10c), suggesting that there is either a a basal level of inflammation or the culturing protocol has resulted in protease-mediated activation of the inflammatory pathway (Vergnolle et al. 2001). Heat shock of glial cultures did not induce the expression of iNOS in either cortical or spinal cord cultures. Together, these data indicate that, similar to observed for WT mixed glial cultures, iNOS is primarily responsible for NO synthesis in LPS treated SOD^{WT} and $SOD1^{G93A}$ cultures.

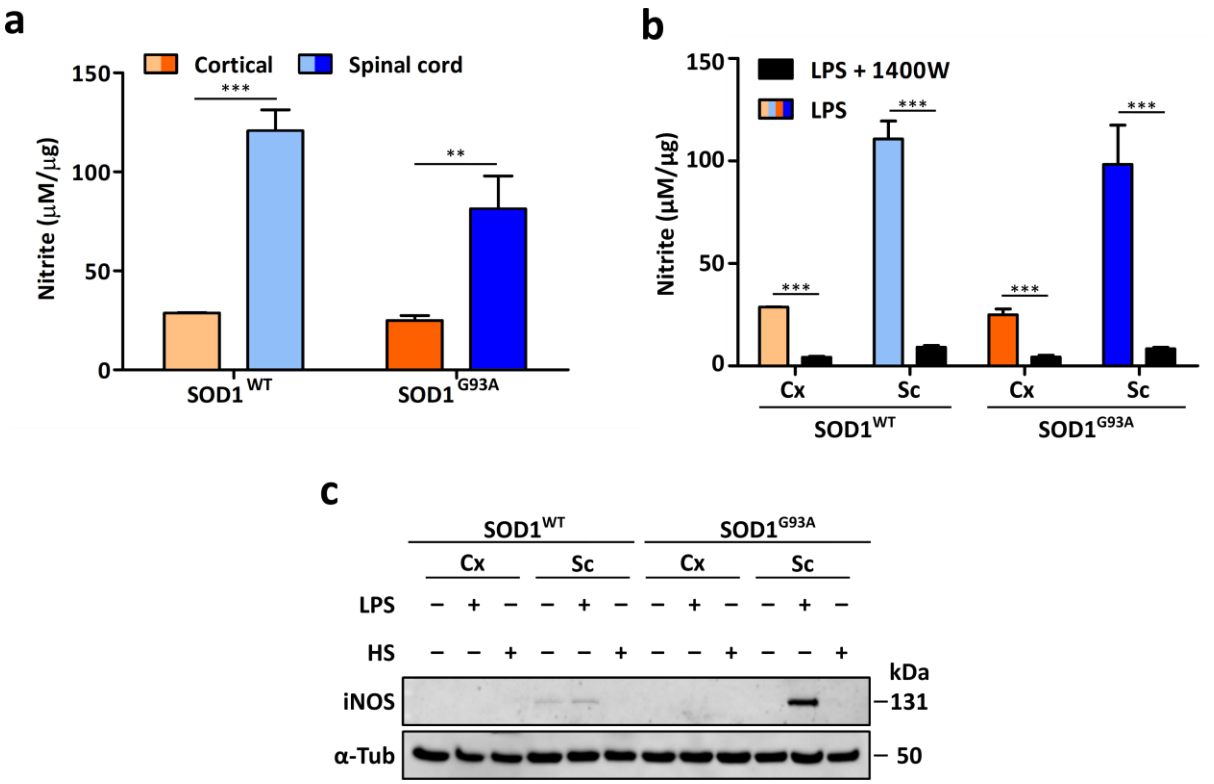

Figure 6.10. Characterisation of NO synthesis and iNOS upregulation in cortical and spinal cord glia cultures derived from SOD1^{WT} and SOD1^{G93A} over-expressing mice. (a) Cortical and spinal cord mixed glial cultures were cultured for 12 days *in vitro* and treated with 80 µg/mL LPS. Levels of NO were determined by measuring nitrite concentrations in each sample 24 h post-treatment by Griess assay. Data shown are the mean + SEM of 2-3 biological repeats. Statistically significant differences were assessed using a two-way ANOVA followed by Bonferroni's post-hoc test, where $P < 0.01$(**) and $P < 0.001$ (***). (b) Mixed glial cultures from the cortex (Cx) or spinal cord (Sc) were either pre-treated with 1400W (iNOS inhibitor) for 2 h or not and then treated with 80 µg/mL LPS for 24 h. Levels of NO were determined by measuring nitrite concentrations in each sample 24 h post-treatment by Griess assay. Data shown are the mean + SEM of 2-3 biological replicates. Differences between the means were assessed by two-way ANOVA followed by Bonferroni's post-hoc test where and $P < 0.001$ (***). (c) Immunoblot analysis of iNOS (131 kDa) expression in mixed glial cultures treated with LPS (80 µg/mL for 24h) or heat shocked (42°C/ 30 min followed by recovery at 37°C for 6 h). α-Tubulin was used as loading control (α-Tub; 50 kDa).

6.3.6 Hsp25 expression in SOD1G93A cortical and spinal cord glial cultures

To determine if SOD1^{G93A} mixed glial cultures from the cortex or spinal cord have different proportions of Hsp25^{+ve} glia, SOD1^{WT} and SOD1^{G93A} mixed glial cultures were immunolabelled for GFAP and Hsp25 and analysed by flow cytometry (Figure 6.11). The effect of LPS treatment and heat shock on Hsp25 expression was also assessed in these experiments. In the absence of treatment, 24.7 ± 7.6% cortical and 53.7 ± 4.0% spinal cord SOD1^{WT} astroglia were Hsp25^{+ve}. This finding aligns with previous data (Figure 6.7b), whereby WT spinal cord astroglia had double the proportion of Hsp25^{+ve} cells compared to

cortical astroglia. Interestingly, cortical and spinal cord astroglia from SOD1^{G93A} showed comparable proportions of Hsp25^{+ve} astroglia (cortex: 56.9 ± 12.1%, spinal cord: 43.6 ± 14.8%). There was an increase in the percent of Hsp25^{+ve} cortical astroglia in untreated SOD1^{G93A} cultures (56.9 ± 12.1%) compared with SOD1^{WT} cultures (24.7 ± 7.6%) however, this difference was not statistically significant ($P < 0.05$).

Treatment with LPS, did not significantly affect the proportion of cells expressing Hsp25 in any of the samples (Figure 6.11a). Heat shock treatment (42°C/ 30 min followed by 6 h recovery at 37°C) increased the proportion of Hsp25^{+ve} spinal cord astroglia in both SOD1^{WT} and SOD1^{G93A} cultures, however this difference was not statistically significant. The overall level of expression of Hsp25 in SOD1^{WT} and SOD1^{G93A} spinal cord astroglia also increased after heat shock, as demonstrated by a significant increase in Hsp25-AF488 fluorescence intensity compared to samples that were not treated [$F(3, 16) = 7.501$, $P = 0.0024$]. In contrast, cortical astroglia did not demonstrate any change in the proportion of Hsp25^{+ve} astroglia or levels of Hsp25 expression after heat shock. There was also a significant increase in the median Hsp25-AF488 fluorescence intensity in heat shocked spinal cord astroglia compared to non-treated samples ($P < 0.05$;Figure 6.11b). There was no increase in Hsp25-AF488 fluorescence intensity in cortical astroglia after heat shock.

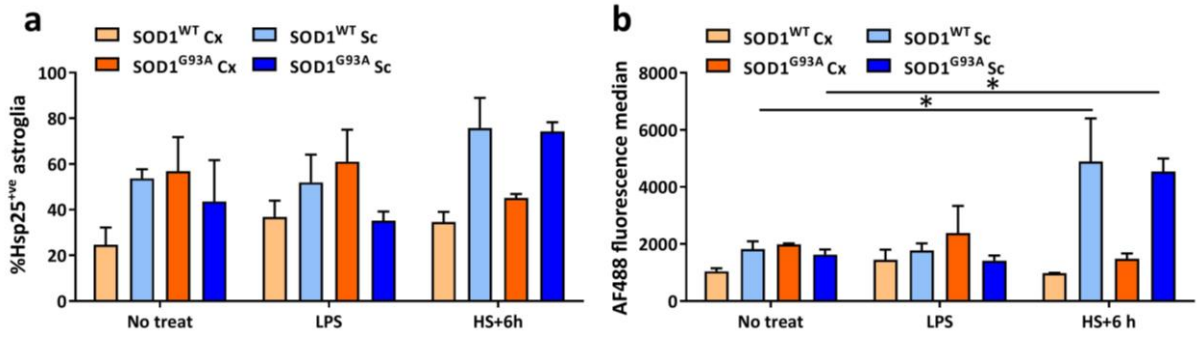

Figure 6.11. Flow cytometric analysis of Hsp25 expression in cortical and spinal cord glia derived from SOD1^{WT} and SOD1^{G93A} over-expressing mice. Mixed primary cortical (Cx) and spinal cord (Sc) glia were either treated with LPS (80 µg/mL) or heat shocked (42°C/ 30 min followed by recovery at 37°C/ 6 h). Cells were then

fixed, permeabilised, immunolabelled for GFAP and Hsp25 and analysed by flow cytometry. (a) The percent of $Hsp25^{+ve}$ astroglia as determined from the flow cytometric analysis. (b) The Hsp25-AF488 fluorescent median of the astroglial or microglial population. Data shown are means + SEM of 2-3 independent experiments. Statistically significant differences between the means were assessed using a two-way ANOVA followed by Bonferroni's post-hoc test, where $P < 0.05$ (*).

6.4 Discussion

ALS disease progression and motor neuron degeneration is exacerbated by reactive astroglia and activated microglia (Weydt et al. 2004, Xiao et al. 2007, Yamanaka et al. 2008, Zurcher et al. 2015). Increasing evidence shows that astroglial and microglial transcriptomes, proteomes, and subsequent functions differ across regions of the CNS. For example, genes involved in the immune response were among the most differentially expressed between microglia derived from the cerebellum, cortex, striatum and hippocampus (*e.g. IL-16*) (Grabert et al. 2016). It follows that the degeneration of motor neurons in the spinal cord in ALS over neurons in other regions of the CNS may be the result of regional variations in the abilities of astroglia and microglia to activate stress-responses and provide cytoprotective support to motor neurons. Therefore, in this study we compared the inflammatory response and HSR activation in primary murine cortical and spinal cord glia. This work establishes that spinal cord microglia from WT, $SOD1^{WT}$ and $SOD1^{G93A}$ mice activate a stronger inflammatory response after treatment with inflammatory mediators compared to cortical microglia. Furthermore, the expression profile of Hsp25, a cytoprotective protein, is increased in WT and $SOD1^{WT}$ spinal cord astroglia compared to cortical astroglia. In contrast, $SOD1^{G93A}$ cortical and spinal cord astroglia have similar proportions of $Hsp25^{+ve}$ cells, which is attributable to an increase in the proportion of $Hsp25^{+ve}$ astroglia in cortical $SOD1^{G93A}$ glial cultures.

6.4.1 Inflammatory pathway activation is stronger in spinal cord glia

The finding that markers of inflammatory pathway activation (*i.e.* nitrite) exist at higher concentrations in spinal cord compared to cortical glia after treatment with inflammatory mediators is supported by studies investigating the inflammatory response in rodent brains and spinal cords (Schnell et al. 1999, Batchelor et al. 2008). These studies showed a significant increase in the number of activated microglia in the spinal cord compared to the brain after mechanical trauma (Schnell et al. 1999, Batchelor et al. 2008). Furthermore, there was

increased astrogliosis in the spinal cord compared to the brain two days after mechanical lesion (Schnell et al. 1999). With respect to tissues derived from sporadic ALS patients, spinal cord sections have 5 times the number of reactive microglia compared to sections from the motor cortex (Kawamata et al. 1992). These data indicate that, at the cellular level, the ability to activate an inflammatory response is stronger in the spinal cord than in the brain.

At the molecular level, there is a large amount of literature regarding NO synthesis and iNOS expression in glia; however, there is a lack of studies that directly compare CNS regions. The results of this work show that spinal cord glial cultures from WT, $SOD1^{WT}$ and $SOD1^{G93A}$ mice have a lower threshold for inflammatory pathway activation and demonstrate higher concentrations of nitrite after LPS and TNFα treatment compared to cortical glia. Nitric oxide was synthesised by iNOS under these experimental conditions in spinal cord and cortical cultures, as demonstrated by a reduction in NO concentration in samples pre-treated with the iNOS inhibitor, 1400W.

Immunoblot analysis showed strong immunoreactivity to iNOS in LPS treated cultures, and there was no significant difference in iNOS protein levels between the cortical and spinal cord glial cultures. This indicates that the increased nitrite levels observed in the spinal cord glial cultures may be attributable to enhanced iNOS activity. The activity of iNOS is regulated, at least in part, by L-arginine and its essential co-factor tetrahydrobiopterin (BH4) (Tzeng et al. 1995, Bogdan 2001, Chaturvedi et al. 2007). Therefore, regional differences in the CNS in the availability, transport, or consumption of arginine or BH4 by other biochemical pathways is likely to play a role in mediating iNOS activity. With regard to L-arginine, previous research has demonstrated that levels of L-arginine are significantly higher in the spinal cord compared to the brain stem in wild-type rats (Jing et al. 2013). Future studies could investigate whether the differences in iNOS activity observed in this PhD research correlates with regional variations in the availability of L-arginine and BH4.

Despite observing 1400W-mediated inhibition of NO synthesis, there was no iNOS detected by immunoblot in TNFα treated cortical and spinal cord glial cultures (Figure 6.3). One possible explanation for the absence of an iNOS band in TNFα treated samples is that the 100 ng/mL TNFα dose resulted in a 2.5-fold lower concentration of nitrite compared to LPS treatment. This reduced NO synthesis could be the consequence of a lower iNOS expression such that it is below the detection limit of the immunoblotting procedure used in this work. Indeed, in all experiments where the nitrite concentration was below 25 μM, iNOS expression was not able to be detected by immunoblotting.

Immunoblot analysis showed higher levels of iNOS expression in LPS treated $SOD1^{G93A}$ spinal cord glia compared to spinal cord $SOD1^{WT}$ glia. This was likely the result of a higher proportion of microglia present in this culture (Figure 6.9b) but could also indicate that spinal cord $SOD1^{G93A}$ glia up-regulated higher levels of iNOS compared to $SOD1^{WT}$ glia. Future studies could support these findings by investigating the proportion of microglia that are iNOS positive in $SOD1^{WT}$ and $SOD1^{G93A}$ mixed glial or microglial cultures by flow cytometric or immunocytochemical analyses.

There are several implications of enhanced NO synthesis in spinal cords with regard to neurotoxicity and neurodegeneration. Nitric oxide is thought to exert its neurotoxic effects by causing DNA damage, glutamate excitotoxicity, mitochondrial damage and subsequent energy depletion (Bolanos 1997). With regard to mitochondrial damage, co-culture of LPS treated, NO-producing, mixed cerebral glial cultures with neurons resulted in an NO-mediated inhibition of mitochondrial complex I, complex II-III, and complex IV (Bolanos et al. 1996). Since motor neurons have relatively high energy demands compared to other neuronal sub-types, inefficient cellular respiration caused by NO-mediated mitochondrial damage could affect cell viability. Indeed, studies have shown that NO causes neuronal death in a concentration-dependent manner (Dawson et al. 1991, Bolanos et al. 1995). This data,

combined with the findings from the present study, suggests that higher concentrations of NO in the spinal cord would result in higher levels of mitochondrial damage and thus, neurotoxicity. Future research should investigate whether different neuronal sub-types across CNS regions are differentially susceptible to NO-mediated mitochondrial damage.

There is also evidence to suggest that motor neurons have a motor neuron-specific cell death pathway, downstream of the Fas death receptor, that requires NO synthesis as a necessary step for its initiation (Raoul et al. 1999). Motor neurons derived from $SOD1^{G93A}$ and $SOD1^{G85R}$ mice have an increased susceptibility to NO-dependent/Fas-mediated apoptosis and decreased viability after NO treatment compared to $SOD1^{WT}$ mice or non-transgenic age-matched littermates (Raoul et al. 2002, Wengenack et al. 2004, Raoul et al. 2006). The enhanced NO synthesis in spinal cord glia observed in this study, combined with evidence for an NO-dependent, motor neuron-specific cell death pathway, may explain the motor neuron-specific degeneration in the spinal cord of ALS patients.

This study showed that iNOS upregulation after LPS treatment occurs in microglia, but not astroglia. In addition, there was no difference in the number of $iNOS^{+ve}$ microglia after LPS treatment between the two CNS regions. These findings suggest that the activity of iNOS is enhanced in spinal cord cultures since the overall levels of expression of iNOS was not significantly different in the WT cultures. The absence of iNOS immunoreactivity in spinal cord astroglia in this study contradicts previous reports of strong iNOS immunolabelling of GFAP positive cells after peroxynitrite treatment in spinal cord cultures (Cassina et al. 2002). However, iNOS upregulation in astroglia is likely to be treatment type dependent. Saura (2007) concluded that NO produced by LPS treated primary rodent glial cultures is mainly derived from microglia. Furthermore, rodent astroglia lack the receptors and downstream signalling components for LPS activation (TLR4 and MYD88), and these are expressed by rodent microglial cells (Liddelow et al. 2017). Similarly, studies of lumbar spinal cord sections from

mSOD1 mouse models of ALS have shown that almost all iNOS-positive cells are Mac2-positive microglia, indicating that the NO synthesised in these mSOD1 mice is likely to be primarily of microglial origin (Yamanaka et al. 2008).

6.4.2 Inflammatory stimuli do not induce an HSR in glial cultures

This work showed that exposing mixed glial cultures to inflammatory mediators to activate the inflammatory pathway did not result in the induction of a heat shock response. Immunoblot and flow cytometric analysis showed that there was no change in Hsp70 or Hsp25 levels following treatment with LPS or TNFα in either cortical or spinal cord glial cultures derived from WT, $SOD1^{WT}$, or $SOD1^{G93A}$. This contradicts the findings of Calabrese et al. (2000), whereby treatment of primary rat mixed glial cells with increasing doses of LPS and IFNγ, in combination, resulted in a concentration-dependent increase of both iNOS and Hsp70 (Calabrese et al. 2000). The difference in expression of Hsp70 between the Calabrese et al. (2000) study and the present study could suggest that astroglia only induce an HSR in response to specific inflammatory mediators. For example, Hsp25 mRNA levels are increased in human cortical astroglia after treatment with a mixture of inflammatory mediators comprised of IL-1β, IFNγ and TNFα (Bajramović et al. 2000). However, Hsp25 mRNA levels did not change when treated with each of these inflammatory mediators individually, suggesting a synergistic mode of action of pro-inflammatory cytokines on the HSR in these cells (Bajramović et al. 2000). The present study showed that LPS, a treatment used to recapitulate inflammatory stresses in the CNS of ALS patients, is not sufficient to induce Hsp70 or Hsp25 expression in astroglia in any of the cultures tested.

6.4.3 Spinal cord glial cultures have a greater proportion of $Hsp25^{+ve}$ astroglia

These data show that there is double the number of $Hsp25^{+ve}$ astroglia in spinal cord compared to cortical glial cultures under basal conditions and that spinal cord astroglia are more heat

shock responsive compared to cortical astroglia. Investigations of Hsp25 expression in astroglia across various regions of the CNS have shown that $Hsp25^{+ve}$ astroglia are found in some hippocampal regions of rats with hyperthermia, CA1, CA3 and the dentate gyrus but not CA1, CA2 or the subiculum (Bechtold and Brown 2000). In another study, excitotoxic lesions resulted in an increase in Hsp25 in cortical astroglia at 3-5 days, and in the thalamus at 5-7 days, suggesting differential regulation of Hsp25 in these two brain regions (Acarin et al. 2002). The findings of the present study and previous investigations suggest that cortical and spinal cord glial populations are heterogeneous with regard to Hsp expression. There are likely to be many other pathways that maintain the neurotrophic functions and viability of glia that are differentially regulated depending on the region of the CNS.

Interestingly, cortical and spinal cord astroglia from $SOD1^{G93A}$ showed comparable proportions of $Hsp25^{+ve}$ astroglia. This indicates that, in the absence of treatment, the proportion of $Hsp25^{+ve}$ cells is elevated in $SOD1^{G93A}$ cortical cultures compared to $SOD1^{WT}$. Additional immunoblotting and immunocytochemistry of these cultures, staining for GFAP and Hsp25, is necessary to confirm this finding. Furthermore, immunohistochemistry of brain and spinal cord slices from $SOD1^{WT}$ and $SOD1^{G93A}$ mice would also contribute to our understanding of the sub-population of $Hsp25^{+ve}$ cells *in vivo* in the CNS.

The functional significance of a greater proportion of $Hsp25^{+ve}$ astroglia in the spinal cord may be related to the cytoprotective chaperone activities of Hsp25. Motor neurons constitutively and stress-inducibly express Hsp25, but not Hsp70 (Plumier et al. 1997, Benn et al. 2002, Kalmar et al. 2002). Therefore, Hsp25 is likely to be an important Hsp in the spinal cord and for motor neuron health (Plumier et al. 1997, Benn et al. 2002, Kalmar et al. 2002). Hsp25 is a well characterised molecular chaperone that can inhibit the protein aggregation of α-synuclein (Cox et al. 2016) and mSOD1 (Yerbury et al. 2013) *in vitro*. Hsp25 is also a potent inhibitor of intrinsic and extrinsic apoptotic pathways downstream of Fas death receptor activation, and

can exert its anti-apoptotic activities at multiple junctures of these pathways (Garrido et al. 1999, Charette et al. 2000, Havasi et al. 2008). Therefore, in the context of ALS, where disease onset and progression occurs primarily in the spinal cord, the presence of a higher proportion of $Hsp25^{+ve}$ astroglia under basal conditions could act to buffer deleterious molecular events that precede disease onset.

Hsp25 has been shown to be up-regulated, compared to control mice, in spinal cord astroglia of $SOD1^{G37R}$ and $SOD1^{G93A}$ mice in late disease stages (Vleminckx et al. 2002, Wang et al. 2003). It would be interesting to extend on this work to investigate whether the same patterns of Hsp25 upregulation also occur in the cortex as was observed in this study. Since treatment with LPS or TNFα were not sufficient to induce an increase in Hsp25 in the present study, it is likely that the cellular stress conditions in these mouse models of ALS act synergistically to induce the HSR and up-regulate Hsp25. Spinal cord astroglia can up-regulate Hsp25 expression after heat shock despite their already high basal level of $Hsp25^{+ve}$ cells. These findings highlight that the HSR in spinal cord astroglia can be targeted pharmacologically to provide support to motor neurons.

Lastly, the practical implications of these findings suggest that the CNS region from which glia are derived should be carefully considered in studies that investigate interactions between spinal cord motor neurons and glia. We have demonstrated that significant differences exist between spinal cord and cortical glial cultures in terms of their inflammatory responses and HSR after treatment with various stresses. There is evidence from previous research describing the inter-regional transcriptomic and proteomic differences of these cell types in the CNS (de Haas et al. 2008, Hochstim et al. 2008, Farmer et al. 2016, Grabert et al. 2016, Haim and Rowitch 2017). For example, there are differences in the ability of astrocytes that are derived from different regions of the mouse brain to support the development of midbrain neurons *in*

vitro (Denis-Donini et al. 1984, Garcia-Abreu et al. 1995). Therefore, in future studies of motor neuronal and glial interactions, spinal cord glia should be used with spinal cord motor neurons.

6.4.4 Summary

In conclusion, the results of this work demonstrates that there are significant differences between glia derived from the cortex and spinal cord with respect to their stress-responses. Spinal cord microglia synthesise high (possibly toxic) levels of NO after stimulation with LPS and TNFα compared to cortical microglia. This could explain the link between a strong microglia-mediated inflammatory response and motor neuron-specific degeneration in the spinal cords of ALS patients. Furthermore, the present study showed that, under basal conditions, double the number of spinal cord astroglia are $Hsp25^{+ve}$ compared to cortical astroglia. The greater numbers of $Hsp25^{+ve}$ astroglia in the spinal cord could play a role in supporting motor neuron growth and maturation or provide a cytoprotective buffer in pathological conditions. Future studies could extend on this work by investigating a range of cytoprotective glial stress-responses in different CNS regions in WT and ALS mouse models. In doing so, this would further establish a link between regional variations in glial stress-responses and motor neuronal vulnerability to degeneration in the spinal cords of ALS patients.

Chapter 7: Research significance and conclusions

7.1 Overview

The purpose of this PhD research was to study the role of the HSR and its downstream products in responding to and preventing the aggregation of pathogenic and non-pathogenic proteins and inflammatory stimuli in cell-based models. In doing so, this research developed a new experimental approach to investigate the activities of Hsps in cells, and validated a new technique for the rapid quantification of inclusion formation and protein trafficking between subcellular compartments. This PhD research also explored the effect of neuronal differentiation on the capacity of neuron-like cells to induce an HSR, evaluated the ability of intra- and extracellular protein aggregates and inflammatory stimuli to induce an HSR in neuron-like cells, and compared inflammatory pathway activation and HSR induction in cortical and spinal cord primary glia. This final chapter summarises the major findings of this PhD research and its significance to the study of the HSR and NDs.

7.1.1 A new approach to study ancient and evolutionarily conserved Hsps

To overcome the problems associated with expressing Hsps with a fluorescent tag (or expressing Hsps without a fluorescent reporter), a suite of Hsp-encoding bicistronic constructs for the expression of a non-tagged Hsp and a fluorescent reporter protein were described in Chapter 3. The use of the Hsp-encoding bicisitronic constructs offers significant advantages, including that they (i) negate the need to tag Hsps with a fluorescent protein, (ii) enable differences in transfection efficiencies and (iii) Hsp expression levels (down to the level of individual cells) across different samples to be taken into account when comparing the functions of a range of Hsps.

As described in Chapter 3, the Hsp-encoding bicistronic constructs were used in a cell-based protein aggregation assay to assess their efficacy in inhibiting the aggregation of $Fluc^{DM}$. Furthermore, the concentration-dependent effects of Hsp expression were elucidated, and it

was shown that increasing levels of Hsp70, and Hsp40 and Hsp70 in combination, were able to inhibit the aggregation of $Fluc^{DM}$ in a concentration-dependent manner. These constructs can now be used in future investigations to quantify the chaperone efficacy of a range of Hsps in inhibiting the aggregation of disease-associated proteins in cell-based models (*e.g.* Htt, SOD1, or TDP-43) by flow cytometry or fluorescence microscopy. Moreover, future studies could use these bicistronic constructs to assess the (concentration-dependent) function of Hsps in the range of cellular processes in which Hsps play an important role (*e.g.* inhibiting inflammation and programmed cell death pathways). In addition to apoptosis, there is new evidence that associates necrosis and necroptosis in the degeneration of neurons in a range NDs (Ramdzan et al. 2017, Zhang et al. 2017). With regard to necroptosis, the RIP1/RIP3 necrosome forms a functional amyloid signalling complex (Li et al. 2012). Previous investigations have reported a role for Hsp90 and its co-chaperone CDC37 in the activation of RIP3 during necroptosis (Li et al. 2015). Thus, there is scope to further characterise the interactions of a range of Hsps and RIP1/RIP3 functional amyloid in the necroptosis programmed cell death pathway.

The generation and validation of these bicistronic constructs represents a significant development in this field of research because they can be used to investigate the role of Hsps in a diverse range of cellular processes in which over-expression of Hsps may have an effect. The strategy of using bicistronic constructs for the correlated expression of a non-labelled protein of interest and a fluorescent reporter protein from bicistronic mRNA can also be applied to other proteins that would otherwise be adversely affected by N- or C- terminal labelling with a fluorescent protein.

7.1.2 A new technique to quantify inclusion bodies and protein trafficking between subcellular compartments

Research in the fields of proteostasis and NDs requires reliable assessment of protein trafficking, protein aggregation and inclusion formation in cells. Current methods to do so,

such as cell imaging, are laborious and subjective. To address this need, a flow cytometric-based technique, termed FloIT, was developed for the rapid quantification of inclusion bodies and protein trafficking between subcellular compartments and is described in Chapter 4. The research presented in Chapter 4 demonstrated several applications of FloIT, including its use in cell-based models of ND-associated protein aggregation ($SOD1^{A4V/G93A}$, Htt^{72Q}, TDP-43^{M337V}), and the translocation of two different proteins (TDP-43^{M337V} and NFAT) out of or into the nucleus. Similar to techniques traditionally used to determine changes in insoluble protein load (*i.e.* slot blot, SDS-PAGE of soluble and insoluble fractions), FloIT also relies on the separation of soluble and insoluble protein fractions from cell lysates. However, FloIT provides a quantitative analysis of the insoluble fraction rather than a qualitative, densitometry-based analysis. Additional advantages of FloIT over existing methods to quantify inclusion formation in cells include: (i) the number of inclusion bodies in each sample can be normalised to the number of nuclei (stained with a nuclear dye) to allow quantitative comparisons across samples, (ii) sensitive detection of inclusion bodies that cannot be distinguished by microscopy or PulSA, (iii) the ability to determine the range and average size of aggregates (through the use of sizing bead standards), (iv) non-biased and (v) compatibility with standard flow cytometry instrumentation.

The rapid detection and quantification of fluorescently tagged inclusions and protein translocation by FloIT has a variety of potential novel applications in research investigating NDs. Future applications of FloIT include the ability to: (i) detect the prion-like transfer of disease-associated proteins (or aggregates) from cell to cell, (ii) monitor the mislocalisation of proteins to subcellular compartments such as mitochondria, (iii) undertake medium to high throughput screens of compounds that modulate inclusion formation in cells, and (iv) determine the aggregate load in CNS tissues from rodent models of NDs with or without treatment or transgene expression. Furthermore, the possibility of upgrading the standard flow cytometer to

increase the sensitivity for the detection of small aggregates in the 100-400 nm range is also feasible. The significance of the development of FloIT stems from its potential to be further developed for a range of additional applications, beyond the fields of proteostasis and NDs, in cell biology, biochemistry and biomedical research.

7.1.3 Differentiated Neuro-2a cells have a competent HSR

The kinetics and magnitude of the induction of the HSR after heat stress has previously been shown to vary depending on cell-type. For example, seminal studies in rodents showed that after whole organism hyperthermia, Hsp70 transcripts and protein expression was observed in astroglia, but not neurons (Nishimura et al. 1991, Manzerra and Brown 1992, Nishimura and Dwyer 1996, Manzerra et al. 1997, Krueger et al. 1999, Pavlik and Aneja 2007, Oza et al. 2008, Yang et al. 2008). This led to the hypothesis that neurons have an attenuated HSR and may explain the absence of the induction of the HSR in the CNS tissues of rodent models of NDs (such as HD and ALS; see Table 1-1 and Table 1-2).

Previous research has demonstrated that neuroblastoma cell lines (*e.g.* NG108-15 and Neuro-2a) differentiated with 1 mM dbcAMP for 72 h results in an attenuation of the cell's ability to induce an HSR (Dwyer et al. 1996, Hatayama et al. 1997, Oza et al. 2008, Yang et al. 2008). The data presented in Chapter 5 contrasts with this previous research and showed that Neuro-2a differentiated with 1 mM dbcAMP for 72 h are able to induce an HSR. In addition, through the use of a fluorescent reporter of the HSR, this work demonstrated that differentiated Neuro-2a cells induced a greater HSR compared to non-differentiated cells in response to stress (heat shock or $CdCl_2$ treatment). The enhanced HSR in differentiated Neuro-2a cells (compared to non-differentiated) observed in this work may be explained by the role of cAMP in activating PKA. Treatment of cells with high concentrations of dbcAMP activates PKA and other kinases, such as p38 MAPK. Both PKA and p38 MAPK have been associated with the phosphorylation of HSF1 at serine residues that switch-on HSF1 transcriptional activities. Therefore,

differentiation of neuroblastoma cell lines with dbcAMP may serve to prime HSF1 by inducing its phosphorylation and thus, sensitise cells to stress, resulting in a greater magnitude of HSR induction compared to non-differentiated cells.

Future studies should extend on this work by testing more physiologically relevant models of neuronal differentiation, due to the limitations of differentiating neuroblastoma cell lines. This is particularly important given that the ability of neurons to induce an HSR *in vivo* is likely to depend upon the neuronal sub-type and ability to alter the chromatin landscape for HSF1 binding to DNA during periods of stress (Marini et al. 1990, Batulan et al. 2003, Tagawa et al. 2007, Carnemolla et al. 2015). It would be interesting to determine whether there are differences with regard to HSR induction in the different neuronal sub-types and cell types that comprise the CNS. This could be achieved by developing a transgenic mouse model containing an HSE:EGFP transgene and treating it with HSR-inducing compounds or whole organism hyperthermia. The identification of these HSR competent cell types would facilitate the development of therapeutics that induce the HSR to ameliorate the molecular pathologies associated with NDs.

7.1.4 Two major pathological hallmarks associated with NDs are poor inducers of the HSR

An alternative hypothesis for the absence of the HSR in affected cells of the CNS in rodent models of NDs is that protein misfolding, oligomerisation and inclusion formation evade the detection of the HSR or impair the induction of the HSR. This absence of the HSR also suggests that the cellular stresses incurred by chronic neuroinflammation do not induce an HSR in these tissues. The objectives of the work described in Chapters 5 and 6 were to explore the induction of the HSR in the context of protein aggregation (both intra- and extracellular) and inflammatory stimuli in neuron-like and primary glial cells. The major findings from the work have been summarised in Figure 7.1.

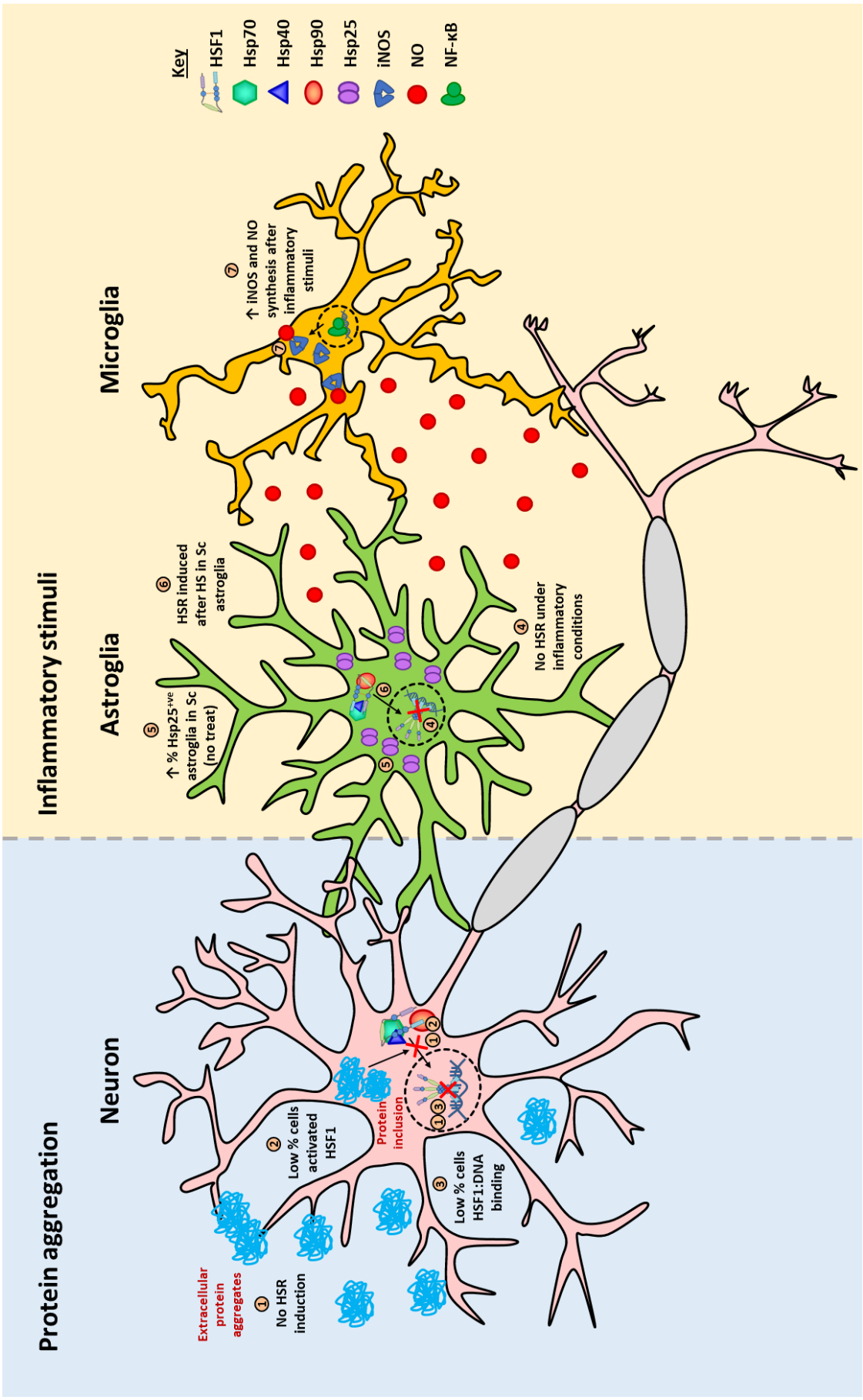
Key
HSF1
Hsp70
Hsp40
Hsp90
Hsp25
iNOS
NO
NF-κB
Inflammatory stimuli
Microglia
⑦ ↑ iNOS and NO synthesis after inflammatory stimuli
Astroglia
⑥ HSR induced after HS in Sc astroglia
⑤ ↑ % Hsp25+ve astroglia in Sc (no treat)
④ No HSR under inflammatory conditions
Protein aggregation
Neuron
Protein inclusion
② Low % cells activated HSF1
③ Low % cells HSF1:DNA binding
Extracellular protein aggregates
① No HSR induction

Figure 7.1. Summary of significant findings from this work with regard to neuron-like cells expressing pathogenic proteins and primary glial cells treated with inflammatory stimuli. Pathogenic aggregates formed from $SOD1^{G93A}$ and α-synuclein applied extracellularly to Neuro-2a (HSE:EGFP) cells do not induce the HSR. Only a low proportion of Neuro-2a (HSE:EGFP) cells transfected to express $SOD1^{G93A}$ and Htt^{72Q} induce an HSR. This is indicative of (2) a low proportion of cells activating HSF1 transcriptional activities, and (3) a low proportion of cells exhibiting HSF1 binding to DNA. Cells expressing $SOD1^{G93A}$ and Htt^{72Q} induce the HSR in a concentration-dependent manner, whereby cells expressing high levels of pathogenic protein are more likely to have an active HSR. (4) The HSR is not induced in either astroglia or microglia after treatment with inflammatory stimuli (LPS or TNFα) suggesting that chronic neuroinflammation associated with NDs is not sufficient to induce an HSR in these cells in the CNS. (5) Under basal conditions (*i.e.* no treatment) spinal cord primary astroglia have a higher proportion of $Hsp25^{+ve}$ cells compared to cortical astroglia. (6) Spinal cord astroglia have a competent HSR when heat shocked and there is an increased proportion of spinal cord astroglia that are $Hsp25^{+ve}$ after 6 h of recovery at 37°C compared to astroglia that have not been heat shocked. (7) Treatment of microglia with inflammatory stimuli results in the up-regulated expression of iNOS and NO is subsequently synthesised.

7.1.5 Neuron-like cells do not induce the HSR after the extracellular application of pathogenic aggregates

The progression of NDs throughout the CNS is thought to occur via the prion-like spread of proteins, where degenerated neurons release misfolded proteins that are taken up by surrounding acceptor cells (Jucker and Walker 2013). The extracellular application of soluble or aggregated $SOD1^{G93A}$ and α-synuclein to the fluorescent reporter Neuro-2a (HSE:EGFP) cell line did not result in induction of the HSR. There is scope to extend on this research by investigating whether the absence of the HSR in response to these extracellular protein aggregates is specific to these pathogenic proteins or also occurs when the cells are exposed to extracellular aggregates formed from non-pathogenic proteins (*e.g.* firefly luciferase). Furthermore, one hypothesis in the field is that the oligomers and protofibrils that preceed the formation of mature fibrils (or aggregates) are the most toxic species (Kirkitadze et al. 2002, Winner et al. 2011). Therefore, investigations into whether toxic oligomers induce an HSR in Neuro-2a (HSE:EGFP) cells could help to establish a link between the structural conformation of the protein and the induction of the HSR.

Future research should also investigate whether other stress-inducible arms of the proteostasis network are up-regulated in cells as a result of exposure to extracellular aggregates, for example the unfolded protein response. This data suggests that protein aggregates, when applied

extracellularly, evade the detection of the HSR and this may facilitate the spread of misfolded proteins throughout the CNS of patients with NDs (Figure 7.1).

7.1.6 The effect of intracellular protein aggregation on the HSR

With regard to the intracellular expression and aggregation of $SOD1^{G93A}$ and Htt^{72Q}, the HSR was only induced in a relatively low proportion of Neuro-2a (HSE:EGFP) cells compared to cells expressing $Fluc^{DM}$. This may suggest that the HSR does not detect early protein misfolding and subsequent inclusion formation in the majority of $SOD1^{G93A}$ or Htt^{72Q} expressing cells (96-98% of total events; Figure 7.1). Structural differences between mutant SOD1 or Htt and $Fluc^{DM}$ may make the cell more susceptible to inducing an HSR in response to $Fluc^{DM}$ expression compared to the expression of these pathogenic proteins. One alternative hypothesis developed from studies examining the effect of polyQ-expanded Htt (Chafekar and Duennwald 2012), amyloid β (Resenberger et al. 2012), and synthetic β-sheet forming proteins (Olzscha et al. 2011) is that pathogenic proteins increase the threshold of HSR activation. Another possibility involves the enhanced ubiquitination and thus, degradation of HSF1, which has been reported in $SOD1^{G93A}$ (Mimoto et al. 2012) and TDP-$43^{WT\times Q331K}$ (Chen et al. 2016) mouse models of ALS, cell-based (Gomez-Pastor et al. 2017) and rodent (Chafekar and Duennwald 2012) models of polyQ-expanded Htt, and rodent models and human patient post-mortem samples of α-synucleinopathies (Kim et al. 2016).

Live cell imaging experiments were undertaken to track the induction of the HSR, inclusion body formation in individual cells and time taken for cells to die. There was no difference in the toxicity of Htt^{72Q} and $Fluc^{DM}$ expression and time taken to form inclusions. However, cells that induced an HSR in $Fluc^{DM}$ expressing cells were viable for approximately two times longer than cells in the same sample that did not switch on the HSR. This is a significant finding, since it provides compelling evidence in support of activating the HSR as a cytoprotective therapy in affected cells of the CNS in NDs, even after inclusions have formed. The Neuro-2a

(HSE:EGFP) fluorescent reporter cell line generated as part of this PhD research could be used in medium-high throughput screening of compound libraries to identify novel HSR-inducing compounds. Combined with FloIT, this cell line can be used to determine which compounds induce the HSR, are cytoprotective, and whether or not this is correlated with a decline in protein aggregation in cell-based models of NDs.

Future research employing Neuro-2a (HSE:EGFP) cells could extend on the work done as part of this PhD by isolating the sub-populations of cells that induced an HSR after expression of $SOD1^{G93A}$, Htt^{72Q} or $Fluc^{DM}$. The use of a new generation of sensitive, cell-permeable dyes that stain misfolded proteins, called TPE-MI (Chen et al. 2017), would help to determine whether the HSR was induced in these cells because they have a higher content of other misfolded protein compared to cells that did not induce an HSR. Furthermore, cells expressing high levels of aggregation-prone protein had the highest proportion of HSR^{+ve} cells. It would be interesting to investigate whether this trend is caused directly by the mutant protein or other indirect processes, such as proteasomal impairment (Bush et al. 1997).

With regard to drugs that require some activation of the HSR in order to work (*e.g.* arimoclomol), this PhD thesis shows that extracellular and intracellular protein aggregation, and inflammatory stimuli are poor inducers of the HSR. However, there are other molecular mechanisms also associated with neurodegenerative diseases, including proteasomal inhibition, that could activate HSF1 in cells of the central nervous system (Bush et al. 1997, Kabashi et al. 2008b). Therefore, investigating compounds such as arimoclomol, which require some induction of the HSR to work, remains a valid line of inquiry.

7.1.6.1 Next generation fluorescent reporters of the HSR

The Neuro-2a (HSE:EGFP) and HEK293 (HSE:EGFP) stable cell lines that were developed in this work represent a first generation design of a fluorescent reporter of HSR induction that can

be improved in future research. For example, artificial promoters comprised of HSEs can be optimised to increase the sensitivity of detection of HSR activation (Ortner et al. 2015). Similar to other HSF1 target genes, *Hspa1a* integrates inputs from various transcription factors that mediate stress-inducible and stress-independent pathways such as nuclear factor-Y, nuclear factor-dB and cAMP response element binding protein (Sasi et al. 2014). Therefore, the complete *hspa1a* promoter is not ideal for selective detection of the induction of the HSR and our research aimed to overcome these shortcomings by using a minimal *Hspa1a* promoter comprised of 8 putative HSEs. In addition to the design of the promoter, it would be of benefit to use reporter genes with short half-lives in order to track the temporal changes in transcription associated with HSR induction (Houser et al. 2012). For example, EGFP has a half-life of 26 h, compared to a novel ubiquitin-N-degron fusion mutant of GFP, which has a half-life of ~ 7 min (Hackett et al. 2006, Houser et al. 2012). These changes to the design of the fluorescent reporters of the HSR used in this study could be applied to develop a second generation of stable cell lines. In this way, the kinetics of HSF1-mediated transcription induction and attenuation can be tracked in real-time in live cells in the absence and presence of stress. The strategy employed in the present study to monitor the HSR and the suggested improvements to the construct design can also be used in the medium-high throughput screening of novel therapeutics that modulate HSF1 and the HSR.

7.1.7 The effect of inflammatory stimuli on the HSR

Chronic neuroinflammation plays a significant role in the progression of NDs from mid-to late-stage disease (Mosher and Wyss-Coray 2014, Lee et al. 2016). Neuroinflammation in NDs is mediated by activated microglia and reactive astroglia, which secrete a range of neurotoxic and pro-inflammatory cytokines (Xiao et al. 2007, Liddelow et al. 2017). Maintaining glia in a neurotrophic condition through the induction of the HSR and Hsps is a potential strategy to prevent neurodegeneration in these diseases (Ianaro et al. 2001, Kalmar and Greensmith 2009).

Therefore, one of the objectives of the work described in Chapter 6 was to investigate whether primary glia treated with inflammatory stimuli can induce a cytoprotective HSR.

Treatment of WT primary murine cortical or spinal cord mixed glial cultures with LPS or TNFα was not able to induce the induction of Hsp70 or Hsp25 after 24 h. However, this treatment was sufficient to activate the inflammatory pathway in these cells such that iNOS was upregulated and NO was synthesised. Therefore, the combined stresses of treatment with inflammatory stimuli and resulting nitrosative stress did not induce the HSR in cortical or spinal cord glial cells. This suggests that inflammatory stimuli are poor inducers of the HSR.

This PhD research has established that two major pathological hallmarks associated with NDs, protein aggregation and neuroinflammation, are poor inducers of the HSR in neuron-like cells and primary murine glia. The vulnerability of affected neurons in the CNS of patients with NDs may stem from the inability of these cells to sense and respond to key pathological cellular stresses. However, the work described in this thesis shows that activation of the HSR in cells, even if they have inclusions, is correlated with an increase in cellular viability (Figure 5.14). Therefore, if affected cells of the CNS in NDs are not capable of inducing an endogenous HSR, it would be beneficial to cellular viability to pharmacologically or genetically up-regulate the HSR. There are currently few HSR-inducing compounds that are not cytotoxic (*e.g.* arimoclomol has progressed to Phase III human clinical trials); therefore, the focus of future research should focus on developing new non-cytotoxic HSR-modulating compounds.

7.1.8 Regional differences in glial stress-responses may explain the vulnerability of discrete neuronal populations in NDs

Striking regional differences in neurodegeneration are observed between the cerebral cortex and spinal cord in ALS, and this may be the consequence of regional variations in glial cells to induce vital stress-responses and provide support to neurons. Therefore, in the work described

in Chapter 6, the activation of the inflammatory response and induction of the HSR were compared in cortical and spinal cord mixed glial cultures derived from WT, $SOD1^{WT}$, and $SOD1^{G93A}$ mice. The major findings regarding inflammatory pathway activation and HSR induction in primary cortical and spinal cord glia presented in Chapter 6 are summarised in Figure 7.2.

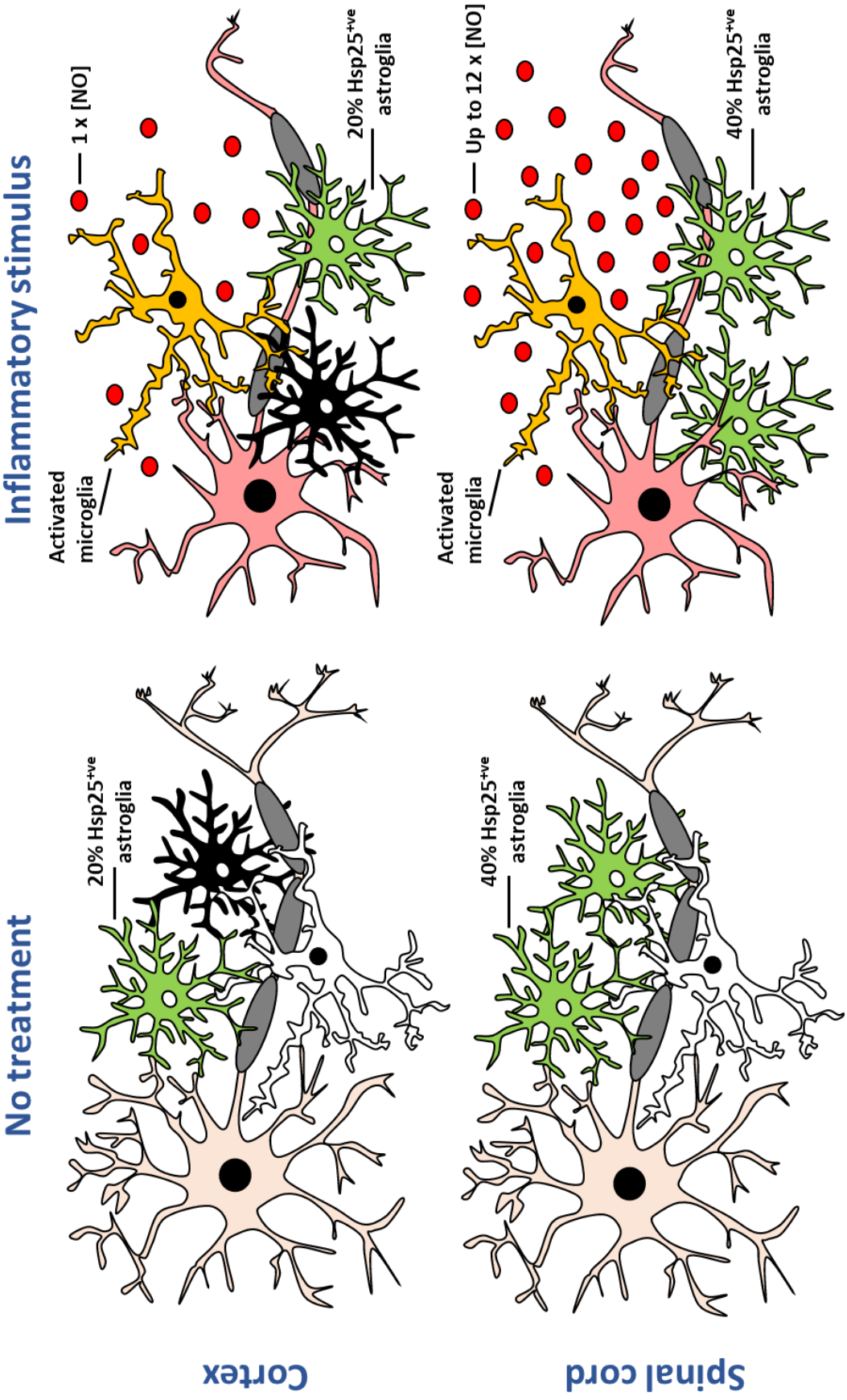
Inflammatory stimulus
No treatment
Activated microglia
1 x [NO]
20% Hsp25+ve astroglia
Up to 12 x [NO]
40% Hsp25+ve astroglia
Cortex
Spinal cord

Figure 7.2. Summary of the findings of this work in relation to regional differences in inflammatory and heat shock responses between cortical and spinal cord glia after treatment with inflammatory stimuli. Mixed glial cultures that were not treated did not demonstrate an upregulation of iNOS or NO in either cortical or spinal cord cultures. Under basal conditions (i.e. not treated) there were double the proportion of $Hsp25^{+ve}$ astroglia in spinal cord cultures (40%) compared to cortical cultures (20%). The higher proportion of $Hsp25^{+ve}$ astroglia in the spinal cord may act to buffer pathological stresses at the onset of disease. Cultures treated with the inflammatory stimuli, LPS and TNFα, demonstrated an increase in NO synthesis that was correlated with iNOS activity in both cortical and spinal cord mixed glial cultures. Spinal cord mixed glial cultures demonstrated a lower threshold for inflammatory pathway activation and higher levels of NO synthesis compared to cortical mixed glial cultures. These findings suggest that inflammation can start earlier and generate neurotoxic levels of NO in the spinal cord, which may explain the vulnerability of spinal cord motor neurons to degenerate in ALS.

This work showed that spinal cord mixed glial cultures synthesise higher levels of NO compared to cortical cultures after treatment with LPS or TNFα (in cultures derived from WT, $SOD1^{WT}$ or $SOD1^{G93A}$ mice). Dose response experiments also demonstrated that spinal cord glial cultures had a lower threshold for inflammatory pathway activation. High concentrations of NO synthesised by spinal cord glia in the CNS is likely to have neurotoxic consequences for surrounding motor neurons. Future experiments should co-culture cortical and spinal cord glia with primary motor neurons after treatment with inflammatory stimuli to determine whether the enhanced inflammatory response in spinal cord glia correlates with greater neurotoxicity.

With regard to the components of the HSR, under basal conditions there were double the proportion of $Hsp25^{+ve}$ astroglia in spinal cord cultures compared to cortical cultures. This may act to buffer pathological events that precede disease onset. Interestingly, $SOD1^{G93A}$ cortical and spinal cord astroglia show the same proportion of $Hsp25^{+ve}$ astroglia suggesting that mutant SOD1 expression does not affect the expression of this Hsp. Future research should investigate whether the higher levels of Hsp25 in astroglia is beneficial to motor neurons in co-culture experiments. Furthermore, seminal research in neuroblastoma and glioblastoma cell lines has shown that Hsps may be transferred via extracellular vesicles from glia to neurons (Guzhova et al. 2001, Frühbeis et al. 2013). It would be interesting to study whether the transfer of Hsps occurs via this mechanism in physiologically relevant cells, such as co-cultures of primary glia and motor neurons.

Chapter 6 describes a targeted approach to examining regional differences in glial support between the cortex and spinal cord, where components of the inflammatory pathway and HSR were examined. These studies can be extended to determine the types of cytokines that are released by WT or $SOD1^{G93A}$ activated microglia and reactive astroglia after treatment with inflammatory stimuli. The ability of glia to induce a range of Hsps (in addition to Hsp25) after treatment with inflammatory stimuli is also of interest. Furthermore, there are likely to be a number of regional differences in the glial cellular mechanisms that are involved in the maintenance of motor neuronal viability. Therefore, it would be interesting to conduct a proteomics-based study to examine the types of proteins that are significantly up- or down-regulated in the spinal cord compared to the cortex. This type of proteomics data can be used to develop a global understanding of how regional differences in the ability of glia to induce cytoprotective responses can influence the vulnerability of surrounding neurons to degeneration.

Lastly, the work described in Chapter 6 focused on the regional differences in motor neuron degeneration relevant to ALS, cortex and spinal cord. Future research could investigate regional differences in glial stress-responses and their ability to provide neurotrophic support to surrounding neurons in brain regions associated with other NDs. For example, comparing glia derived from the frontotemporal cortex with the parietal and occipital lobes in investigations pertaining to Frontotemporal Dementia. In addition, the ability of glia to provide neurotrophic support could be compared in the striatum and cerebral cortex in investigations pertaining to HD. These types of investigations may establish a link between the loss of neurotrophic or gain of neurotoxic function in glia surrounding the neuronal populations that degenerate in these diseases.

7.2 Conclusions

This research aimed to establish the role of the HSR and the primary products of this pathway, namely the Hsps, in processes associated with NDs. The generation of the heat shock protein-encoding bicistronic constructs now allows for the quantification of their intracellular activities at the single cell or bulk cell level through the use of flow cytometry of fluorescence microscopy. Furthermore, FloIT facilitates the quantification of protein inclusions in cell lysates and is a simple technique that can be adopted by most laboratories with standard flow cytometry equipment. FloIT could be adopted as a standard method to screen the efficacy of proteostasis modulating compounds on the number of inclusions in cells, and thus, the development of new therapeutics to treat neurodegenerative diseases. Both strategies described in Chapters 3 and 4 have a wide range of potential applications beyond those presented in this thesis.

Overall, the work presented in this thesis highlights the complexity of HSR activation in the context of different stressors, particularly those associated with NDs (aggregating proteins, inflammatory stimuli). This research showed that disease-associated protein aggregates applied extracellularly to cells do not induce an HSR. The intracellular expression of disease-associated proteins can elicit an HSR, but only in a relatively low proportion of cells. In cells with inclusions formed from the non-pathogenic protein, $Fluc^{DM}$, induction of an HSR resulted in an increase in cell viability. Treatment of spinal cord or cortical glial cultures with inflammatory stimuli does not induce the HSR. Therefore, two major, pathological hallmarks associated with neurodegenerative diseases do not induce a strong cytoprotective HSR in neuron-like cells or primary murine glia. Combined, these findings provide compelling evidence that establishes a link between an evaded (or impaired) HSR in cells of the CNS and neuronal vulnerability to protein aggregation and inflammation associated with NDs. Lastly,

spinal cord glia also demonstrated a lower threshold for the activation of the inflammatory pathway and a greater synthesis of NO, which is neurotoxic at high concentrations in the CNS.

Chapter 8: References

Abdul, H. M., V. Calabrese, M. Calvani and D. A. Butterfield (2006). "Acetyl-L-carnitine-induced up-regulation of heat shock proteins protects cortical neurons against amyloid-beta peptide 1-42-mediated oxidative stress and neurotoxicity: Implications for Alzheimer's disease." J Neurosci Res **84**: 398-408.

Acarin, L., J. Paris, B. Gonzalez and B. Castellano (2002). "Glial expression of small heat shock proteins following an excitotoxic lesion in the immature rat brain." Glia **38**: 1-14.

Aebischer, J., P. Cassina, B. Otsmane, A. Moumen, D. Seilhean, V. Meininger, L. Barbeito, B. Pettmann, et al. (2011). "IFNgamma triggers a LIGHT-dependent selective death of motoneurons contributing to the non-cell-autonomous effects of mutant SOD1." Cell Death Differ **18**: 754-768.

Ahmed, M., P. M. MacHado, A. Miller, C. Spicer, L. Herbelin, J. He, J. Noel, Y. Wang, et al. (2016). "Targeting protein homeostasis in sporadic inclusion body myositis." Sci Transl Med **8**: 331ra341.

Åkerfelt, M., R. I. Morimoto and L. Sistonen (2010). "Heat shock factors: Integrators of cell stress, development and lifespan." Nat Rev Mol Cell Biol **11**: 545-555.

Amin, J., J. Ananthan and R. Voellmy (1988). "Key features of heat shock regulatory elements." Mol Cell Biol **8**: 3761-3769.

Anckar, J. and L. Sistonen (2011). "Regulation of HSF1 function in the heat stress response: Implications in aging and disease." Ann Rev Biochem **80**: 1089-1115.

Arrasate, M., S. Mitra, E. S. Schweitzer, M. R. Segal and S. Finkbeiner (2004). "Inclusion body formation reduces levels of mutant huntingtin and the risk of neuronal death." Nature **431**: 805-810.

Asea, A. A. A. and I. R. Brown (2008). Heat shock proteins and the brain: Implications for neurodegenerative diseases and neuroprotection. Heat shock proteins. A. A. A. Asea and S. K. Calderwood. New York, Springer. **3**.

Bajramović, J. J., M. Bsibsi, S. B. Geutskens, R. Hassankhan, K. C. Verhulst, G. J. J. Stege, C. J. A. de Groot and J. M. van Noort (2000). "Differential expression of stress proteins in human adult astrocytes in response to cytokines." J Neuroimmunol **106**: 14-22.

Balchin, D., M. Hayer-Hartl and F. U. Hartl (2016). "In vivo aspects of protein folding and quality control." Science **353**: aac4354.

Ballinger, C. A., P. Connell, Y. Wu, Z. Hu, L. J. Thompson, L. Y. Yin and C. Patterson (1999). "Identification of CHIP, a novel tetratricopeptide repeat-containing protein that interacts with heat shock proteins and negatively regulates chaperone functions." Mol Cell Biol **19**: 4535-4545.

Batchelor, P. E., S. Tan, T. E. Wills, M. J. Porritt and D. W. Howells (2008). "Comparison of inflammation in the brain and spinal cord following mechanical injury." J Neurotrauma **25**: 1217-1225.

Batulan, Z., G. A. Shinder, S. Minotti, B. P. He, M. M. Doroudchi, J. Nalbantoglu, M. J. Strong and H. D. Durham (2003). "High threshold for induction of the stress response in motor neurons is associated with failure to activate HSF1." J Neurosci **23**: 5789-5798.

Batulan, Z., D. M. Taylor, R. J. Aarons, S. Minotti, M. M. Doroudchi, J. Nalbantoglu and H. D. Durham (2006). "Induction of multiple heat shock proteins and neuroprotection in a primary culture model of familial amyotrophic lateral sclerosis." Neurobiol Dis **24**: 213-225.

Bauer, P. O., A. Goswami, H. K. Wong, M. Okuno, M. Kurosawa, M. Yamada, H. Miyazaki, G. Matsumoto, et al. (2010). "Harnessing chaperone-mediated autophagy for the selective degradation of mutant huntingtin protein." Nat Biotech **28**: 256-263.

Bechtold, D. A. and I. R. Brown (2000). "Heat shock proteins Hsp27 and Hsp32 localize to synaptic sites in the rat cerebellum following hyperthermia." Mol Brain Res **75**: 309-320.

Beere, H. M. (2004). "`The stress of dying: The role of heat shock proteins in the regulation of apoptosis." J Cell Sci **117**: 2641-2651.

Benn, S. C., D. Perrelet, A. C. Kato, J. Scholz, I. Decosterd, R. J. Mannion, J. C. Bakowska and C. J. Woolf (2002). "Hsp27 upregulation and phosphorylation is required for injured sensory and motor neuron survival." Neuron **36**: 45-56.

Bersuker, K., M. S. Hipp, B. Calamini, R. I. Morimoto and R. R. Kopito (2013). "Heat shock response activation exacerbates inclusion body formation in a cellular model of Huntington disease." J Biol Chem **288**: 23633-23638.

Bharadwaj, S., A. Ali and N. Ovsenek (1999). "Multiple components of the HSP90 chaperone complex function in regulation of heat shock factor 1 in vivo." Mol Cell Biol **19**: 8033-8041.

Bilsland, L. G., N. Nirmalananthan, J. Yip, L. Greensmith and M. R. Duchen (2008). "Expression of mutant SOD1G93A in astrocytes induces functional deficits in motoneuron mitochondria." J Neurochem **107**: 1271-1283.

Blake, M. J., D. Gershon, J. Fargnoli and N. J. Holbrook (1990). "Discordant expression of heat shock protein mRNAs in tissues of heat-stressed rats." J Biol Chem **265**: 15275-15279.

Bogdan, C. (2001). "Nitric oxide and the immune response." Nat Immunol **2**: 907-916.

Boillée, S., C. Vande Velde and Don W. Cleveland (2006a). "ALS: A disease of motor neurons and their nonneuronal neighbors." Neuron **52**: 39-59.

Boillée, S., K. Yamanaka, C. S. Lobsiger, N. G. Copeland, N. A. Jenkins, G. Kassiotis, G. Kollias and D. W. Cleveland (2006b). "Onset and progression in inherited ALS determined by motor neurons and microglia." Science **312**: 1389-1392.

Bolanos, J. P. (1997). "Nitric oxide-mediated mitochondrial damage in the brain: Mechanisms and implications for neurodegenerative diseases." J Neurochem **68**: 2227-2240.

Bolanos, J. P., S. J. Heales, J. M. Land and J. B. Clark (1995). "Effect of peroxynitrite on the mitochondrial respiratory chain: differential susceptibility of neurones and astrocytes in primary culture." J Neurochem **64**: 1965-1972.

Bolanos, J. P., S. J. Heales, S. Peuchen, J. E. Barker, J. M. Land and J. B. Clark (1996). "Nitric oxide-mediated mitochondrial damage: a potential neuroprotective role for glutathione." Free Radic Biol Med **21**: 995-1001.

Bose, S. and J. Cho (2017). "Targeting chaperones, heat shock factor-1, and unfolded protein response: Promising therapeutic approaches for neurodegenerative disorders." Ageing Res Rev **35**: 155-175.

Boya, P., F. Reggiori and P. Codogno (2013). "Emerging regulation and functions of autophagy." Nat Cell Biol **15**: 713-720.

Bradford, J., J.-Y. Shin, M. Roberts, C.-E. Wang, X.-J. Li and S. Li (2009). "Expression of mutant huntingtin in mouse brain astrocytes causes age-dependent neurological symptoms." Proc Natl Acad Sci USA **106**: 22480-22485.

Bradford, J., J. Y. Shin, M. Roberts, C. E. Wang, G. Sheng, S. Li and X. J. Li (2010). "Mutant huntingtin in glial cells exacerbates neurological symptoms of Huntington disease mice." J Biol Chem **285**: 10653-10661.

Brehme, M., C. Voisine, T. Rolland, S. Wachi, J. H. Soper, Y. Zhu, K. Orton, A. Villella, et al. (2014). "A chaperome subnetwork safeguards proteostasis in aging and neurodegenerative disease." Cell Rep **9**: 1135-1150.

Brown, I. R. and S. J. Rush (1999). "Cellular localization of the heat shock transcription factors HSF1 and HSF2 in the rat brain during postnatal development and following hyperthermia." Brain Res **821**: 333-340.

Bruijn, L. I., T. M. Miller and D. W. Cleveland (2004). "Unraveling the mechanisms involved in motor neuron degeneration in ALS." Annu Rev Neurosci **27**: 723-749.

Bryantsev, A. L., S. Y. Kurchashova, S. A. Golyshev, V. Y. Polyakov, H. F. Wunderink, B. Kanon, K. R. Budagova, A. E. Kabakov, et al. (2007). "Regulation of stress-induced intracellular sorting and chaperone function of Hsp27 (HspB1) in mammalian cells." Biochem J **407**: 407-417.

Buell, A. K., C. Galvagnion, R. Gaspar, E. Sparr, M. Vendruscolo and T. P. Knowles (2014). "Solution conditions determine the relative importance of nucleation and growth processes in alpha-synuclein aggregation." Proc Natl Acad Sci U S A **111**: 7671–7676.

Bush, K. T., A. L. Goldberg and S. K. Nigam (1997). "Proteasome inhibition leads to a heat-shock response, induction of endoplasmic reticulum chaperones, and thermotolerance." J Biol Chem **272**: 9086-9092.

Calabrese, V., A. Copani, D. Testa, A. Ravagna, F. Spadaro, E. Tendi, V. G. Nicoletti and A. M. Giuffrida Stella (2000). "Nitric oxide synthase induction in astroglial cell cultures: Effect on heat shock protein 70 synthesis and oxidant/antioxidant balance." J Neurosci Res **60**: 613-622.

Carnemolla, A., H. Lazell, S. Moussaoui and G. P. Bates (2015). "In vivo profiling reveals a competent heat shock response in adult neurons: Implications for neurodegenerative disorders." PLoS One **10**: e0131985.

Cashikar, A. G., M. Duennwald and S. L. Lindquist (2005). "A chaperone pathway in protein disaggregation. Hsp26 alters the nature of protein aggregates to facilitate reactivation by Hsp104." J Biol Chem **280**: 23869-23875.

Cassina, P., A. Cassina, M. Pehar, R. Castellanos, M. Gandelman, A. de Leon, K. M. Robinson, R. P. Mason, et al. (2008). "Mitochondrial dysfunction in SOD1G93A-bearing astrocytes promotes motor neuron degeneration: Prevention by mitochondrial-targeted antioxidants." J Neurosci **28**: 4115-4122.

Cassina, P., H. Peluffo, M. Pehar, L. Martinez-Palma, A. Ressia, J. S. Beckman, A. G. Estévez and L. Barbeito (2002). "Peroxynitrite triggers a phenotypic transformation in spinal cord astrocytes that induces motor neuron apoptosis." J Neurosci Res **67**: 21-29.

Chafekar, S. M. and M. L. Duennwald (2012). "Impaired heat shock response in cells expressing full-length polyglutamine-expanded huntingtin." PLoS One **7**: e37929.

Charette, S. J., J. N. Lavoie, H. Lambert and J. Landry (2000). "Inhibition of Daxx-mediated apoptosis by heat shock protein 27." Mol Cell Biol **20**: 7602-7612.

Chaturvedi, R., M. Asim, N. D. Lewis, H. M. Algood, T. L. Cover, P. Y. Kim and K. T. Wilson (2007). "L-arginine availability regulates inducible nitric oxide synthase-dependent host defense against Helicobacter pylori." Infect Immun **75**: 4305-4315.

Chen, H.-J., J. C. Mitchell, S. Novoselov, J. Miller, A. L. Nishimura, E. L. Scotter, C. A. Vance, M. E. Cheetham, et al. (2016). "The heat shock response plays an important role in TDP-43 clearance: Evidence for dysfunction in amyotrophic lateral sclerosis." Brain **139**: 1417-1432.

Chen, H., Y. Wu, Y. Zhang, L. Jin, L. Luo, B. Xue, C. Lu, X. Zhang, et al. (2006). "Hsp70 inhibits lipopolysaccharide-induced NF-κB activation by interacting with TRAF6 and inhibiting its ubiquitination." FEBS Letters **580**: 3145-3152.

Chen, M. Z., N. S. Moily, J. L. Bridgford, R. J. Wood, M. Radwan, T. A. Smith, Z. Song, B. Z. Tang, et al. (2017). "A thiol probe for measuring unfolded protein load and proteostasis in cells." Nature Commun **8**: 474.

Chen, S., P. Sayana, X. Zhang and W. Le (2013). "Genetics of amyotrophic lateral sclerosis: an update." Mol Neurodegener **8**: 28.

Chen, Z., J. Hagler, V. J. Palombella, F. Melandri, D. Scherer, D. Ballard and T. Maniatis (1995). "Signal-induced site-specific phosphorylation targets I kappa B alpha to the ubiquitin-proteasome pathway." Genes Dev **9**: 1586-1597.

Cheroni, C., M. Marino, M. Tortarolo, P. Veglianese, S. De Biasi, E. Fontana, L. V. Zuccarello, C. J. Maynard, et al. (2009). "Functional alterations of the ubiquitin-proteasome system in motor neurons of a mouse model of familial amyotrophic lateral sclerosis." Hum Mol Genet **18**: 82-96.

Chiti, F. and C. M. Dobson (2006). "Protein misfolding, functional amyloid, and human disease." Annu Rev Biochem **75**: 333-366.

Choi, H. S., B. Li, Z. Lin, E. Huang and A. Y. Liu (1991). "cAMP and cAMP-dependent protein kinase regulate the human heat shock protein 70 gene promoter activity." J Biol Chem **266**: 11858-11865.

Ciryam, P., R. Kundra, R. I. Morimoto, C. M. Dobson and M. Vendruscolo (2015). "Supersaturation is a major driving force for protein aggregation in neurodegenerative diseases." Trends Pharmacol Sci **36**: 72-77.

Corish, P. and C. Tyler-Smith (1999). "Attenuation of green fluorescent protein half-life in mammalian cells." Protein Eng **12**: 1035-1040.

Cox, D. and H. Ecroyd (2017). "The small heat shock proteins αB-crystallin (HSPB5) and Hsp27 (HSPB1) inhibit the intracellular aggregation of α-synuclein." Cell Stress Chaperon **22**: 589-600.

Cox, D., E. Selig, M. D. W. Griffin, J. A. Carver and H. Ecroyd (2016). "Small heat shock proteins prevent alpha-synuclein aggregation via transient interactions and their efficacy is affected by the rate of aggregation." J Biol Chem **291**: 22618-22629.

Crippa, V., D. Sau, P. Rusmini, A. Boncoraglio, E. Onesto, E. Bolzoni, M. Galbiati, E. Fontana, et al. (2010). "The small heat shock protein B8 (HspB8) promotes autophagic removal of misfolded proteins involved in amyotrophic lateral sclerosis (ALS)." Hum Mol Gen **19**: 3440-3456.

Dabir, D. V., J. Q. Trojanowski, C. Richter-Landsberg, V. M. Lee and M. S. Forman (2004). "Expression of the small heat-shock protein alphaB-crystallin in tauopathies with glial pathology." Am J Pathol **164**: 155-166.

Danuser, G. (2011). "Computer Vision in Cell Biology." Cell **147**: 973-978.

Datskevich, P. N. and N. B. Gusev (2014). "Structure and properties of chimeric small heat shock proteins containing yellow fluorescent protein attached to their C-terminal ends." Cell Stress Chaperon **19**: 507-518.

Datskevich, P. N., L. K. Muranova and N. B. Gusev (2015). "Attempt to optimize some properties of fluorescent chimeras of human small heat shock protein HspB1 by modifying linker length and nature." Biochemistry (Moscow) **80**: 67-73.

Datskevich, P. N., E. V. Mymrikov, N. N. Sluchanko, A. A. Shemetov, M. V. Sudnitsyna and N. B. Gusev (2012). "Expression, purification and some properties of fluorescent chimeras of human heat shock proteins." Protein Expr Purif **82**: 45-54.

Daub, A., P. Sharma and S. Finkbeiner (2009). "High-content screening of primary neurons: Ready for prime time." Curr Opin Neurobiol **19**: 537-543.

Dawson, V. L., T. M. Dawson, E. D. London, D. S. Bredt and S. H. Snyder (1991). "Nitric oxide mediates glutamate neurotoxicity in primary cortical cultures." Proc Natl Acad Sci USA **88**: 6368-6371.

de Haas, A. H., H. W. G. M. Boddeke and K. Biber (2008). "Region-specific expression of immunoregulatory proteins on microglia in the healthy CNS." Glia **56**: 888-894.

De Vos, W. H., L. Van Neste, B. Dieriks, G. H. Joss and P. Van Oostveldt (2010). "High content image cytometry in the context of subnuclear organization." Cytometry A **77**: 64-75.

DeMeester, S. L., T. G. Buchman, Y. Qiu, K. Dunnigan, R. S. Hotchkiss, I. E. Karl and J. P. Cobb (1998). "Pyrrolidine dithiocarbamate activates the heat shock response and thereby induces apoptosis in primed endothelial cells." Shock **10**: 1-6.

Denis-Donini, S., J. Glowinski and A. Prochiantz (1984). "Glial heterogeneity may define the three-dimensional shape of mouse mesencephalic dopaminergic neurones." Nature **307**: 641-643.

Devi, L., V. Raghavendran, B. M. Prabhu, N. G. Avadhani and H. K. Anandatheerthavarada (2008). "Mitochondrial import and accumulation of α-synuclein impair complex I in human dopaminergic neuronal cultures and Parkinson disease brain." J Biol Chem **283**: 9089-9100.

Di Giorgio, F. P., M. A. Carrasco, M. C. Siao, T. Maniatis and K. Eggan (2007). "Non-cell autonomous effect of glia on motor neurons in an embryonic stem cell-based ALS model." Nat Neurosci **10**: 608-614.

Ditsworth, D., M. Maldonado, M. McAlonis-Downes, S. Sun, A. Seelman, K. Drenner, E. Arnold, S.-C. Ling, et al. (2017). "Mutant TDP-43 within motor neurons drives disease onset but not progression in amyotrophic lateral sclerosis." Acta Neuropathol **133**: 907-922.

Douglas, P. M. and A. Dillin (2010). "Protein homeostasis and aging in neurodegeneration." J Cell Biol **190**: 719-729.

Duncan, E. J., M. E. Cheetham, J. P. Chapple and J. van der Spuy (2015). "The role of Hsp70 and its co-chaperones in protein misfolding, aggregation and disease." Subcell Biochem **78**: 243-273.

Dwyer, D. S., Y. Liu, S. Miao and R. J. Bradley (1996). "Neuronal differentiation in PC12 cells is accompanied by diminished inducibility of Hsp70 and Hsp60 in response to heat and ethanol." Neurochem Res **21**: 659-666.

Ecroyd, H., S. Meehan, J. Horwitz, A. Aquilina, J. Benesch, C. Robinson, C. MacPhee and J. Carver (2007). "Mimicking phosphorylation of αB-crystallin affects its chaperone ability." Biochem J **401**: 129-141.

Faideau, M., J. Kim, K. Cormier, R. Gilmore, M. Welch, G. Auregan, N. Dufour, M. Guillermier, et al. (2010). "In vivo expression of polyglutamine-expanded huntingtin by mouse striatal astrocytes impairs glutamate transport: A correlation with Huntington's disease subjects." Hum Mol Genet **19**: 3053-3067.

Falsig, J., P. Pörzgen, S. Lund, A. Schrattenholz and M. Leist (2006). "The inflammatory transcriptome of reactive murine astrocytes and implications for their innate immune function." J Neurochem **96**: 893-907.

Farmer, W. T., T. Abrahamsson, S. Chierzi, C. Lui, C. Zaelzer, E. V. Jones, B. P. Bally, G. G. Chen, et al. (2016). "Neurons diversify astrocytes in the adult brain through sonic hedgehog signaling." Science **351**: 849-854.

Farrawell, N. E., I. A. Lambert-Smith, S. T. Warraich, I. P. Blair, D. N. Saunders, D. M. Hatters and J. J. Yerbury (2015). "Distinct partitioning of ALS associated TDP-43, FUS and SOD1 mutants into cellular inclusions." Sci Rep **5**: 13416.

Feinstein, D. L., E. Galea, D. A. Aquino, G. C. Li, H. Xu and D. J. Reis (1996). "Heat shock protein 70 suppresses astroglial-inducible nitric-oxide synthase expression by decreasing NFkappaB activation." J Biol Chem **271**: 17724-17732.

Ferrucci, M., F. Fulceri, L. Toti, P. Soldani, G. Siciliano, A. Paparelli and F. Fornai (2011). "Protein clearing pathways in ALS." Arch Ital Biol **149**: 121-149.

Firdaus, W. J. J., A. Wyttenbach, C. Diaz-Latoud, R. W. Currie and A.-P. Arrigo (2006). "Analysis of oxidative events induced by expanded polyglutamine huntingtin exon 1 that are differentially restored by expression of heat shock proteins or treatment with an antioxidant." FEBS J **273**: 3076-3093.

Frühbeis, C., D. Fröhlich, W. P. Kuo and E.-M. Krämer-Albers (2013). "Extracellular vesicles as mediators of neuron-glia communication." Front Cell Neurosci **7**: 182.

Fujimoto, M., E. Takaki, T. Hayashi, Y. Kitaura, Y. Tanaka, S. Inouye and A. Nakai (2005). "Active HSF1 significantly suppresses polyglutamine aggregate formation in cellular and mouse models." J Biol Chem **280**: 34908-34916.

Gai, W. P., J. H. Power, P. C. Blumbergs, J. G. Culvenor and P. H. Jensen (1999). "Alpha-synuclein immunoisolation of glial inclusions from multiple system atrophy brain tissue reveals multiprotein components." J Neurochem **73**: 2093-2100.

Gamerdinger, M., A. M. Kaya, U. Wolfrum, A. M. Clement and C. Behl (2011). "BAG3 mediates chaperone-based aggresome-targeting and selective autophagy of misfolded proteins." EMBO Rep **12**: 149-156.

Garcia-Abreu, J., V. M. Neto, S. L. Carvalho and L. A. Cavalcante (1995). "Regionally specific properties of midbrain glia: Interactions with midbrain neurons." J Neurosci Res **40**: 471-477.

Garrido, C., J.-M. Bruey, A. Fromentin, A. Hammann, A. P. Arrigo and E. Solary (1999). "HSP27 inhibits cytochrome c-dependent activation of procaspase-9." FASEB J **13**: 2061-2070.

Garvey, E. P., J. A. Oplinger, E. S. Furfine, R. J. Kiff, F. Laszlo, B. J. R. Whittle and R. G. Knowles (1997). "1400W is a slow, tight binding, and highly selective inhibitor of inducible nitric-oxide synthase in vitro and in vivo." J Biol Chem **272**: 4959-4963.

Gaudin, R. and N. S. Barteneva (2015). "Sorting of small infectious virus particles by flow virometry reveals distinct infectivity profiles." Nat Commun **6**: 6022.

Gidalevitz, T., V. Prahlad and R. I. Morimoto (2011). "The stress of protein misfolding: From single cells to multicellular organisms." Perspect Biol **3**: a009704.

Gifondorwa, D. J., M. B. Robinson, C. D. Hayes, A. R. Taylor, D. M. Prevette, R. W. Oppenheim, J. Caress and C. E. Milligan (2007). "Exogenous delivery of heat shock protein 70 increases lifespan in a mouse model of amyotrophic lateral sclerosis." J Neurosci **27**: 13173-13180.

Gillis, J., S. Schipper-Krom, K. Juenemann, A. Gruber, S. Coolen, R. van den Nieuwendijk, H. van Veen, H. Overkleeft, et al. (2013). "The DNAJB6 and DNAJB8 protein chaperones prevent intracellular aggregation of polyglutamine peptides." J Biol Chem **288**: 17225-17237.

Gomez-Pastor, R., E. T. Burchfiel, D. W. Neef, A. M. Jaeger, E. Cabiscol, S. U. McKinstry, A. Doss, A. Aballay, et al. (2017). "Abnormal degradation of the neuronal stress-protective transcription factor HSF1 in Huntington's disease." Nat Commun **8**: 14405.

Gómez, A. V., D. Galleguillos, J. C. Maass, E. Battaglioli, M. Kukuljan and M. E. Andrés (2008). "CoREST represses the heat shock response mediated by HSF1." Mol Cell **31**: 222-231.

Gordon, N. (2003). "Alexander disease." Eur J Paediatr Neurol **7**: 395-399.

Grabert, K., T. Michoel, M. H. Karavolos, S. Clohisey, J. K. Baillie, M. P. Stevens, T. C. Freeman, K. M. Summers, et al. (2016). "Microglial brain region-dependent diversity and selective regional sensitivities to aging." Nat Neurosci **19**: 504-516.

Gu, X., V. M. Andre, C. Cepeda, S. H. Li, X. J. Li, M. S. Levine and X. W. Yang (2007). "Pathological cell-cell interactions are necessary for striatal pathogenesis in a conditional mouse model of Huntington's disease." Mol Neurodegener **2**: 8.

Gu, X., C. Li, W. Wei, V. Lo, S. Gong, S. H. Li, T. Iwasato, S. Itohara, et al. (2005). "Pathological cell-cell interactions elicited by a neuropathogenic form of mutant Huntingtin contribute to cortical pathogenesis in HD mice." Neuron **46**: 433-444.

Guertin, M. J. and J. T. Lis (2010). "Chromatin landscape dictates HSF binding to target DNA elements." PLoS Genet **6**: e1001114.

Guettouche, T., F. Boellmann, W. Lane and R. Voellmy (2005). "Analysis of phosphorylation of human heat shock factor 1 in cells experiencing a stress." BMC Biochem **6**: 4.

Guo, Y., T. Guettouche, M. Fenna, F. Boellmann, W. B. Pratt, D. O. Toft, D. F. Smith and R. Voellmy (2001). "Evidence for a mechanism of repression of heat shock factor 1 transcriptional activity by a multichaperone complex." J Biol Chem **276**: 45791-45799.

Gupta, R., P. Kasturi, A. Bracher, C. Loew, M. Zheng, A. Villella, D. Garza, F. U. Hartl, et al. (2011a). "Firefly luciferase mutants as sensors of proteome stress." Nat. Methods **8**: 879-884.

Gupta, R., P. Kasturi, A. Bracher, C. Loew, M. Zheng, A. Villella, D. Garza, F. U. Hartl, et al. (2011b). "Firefly luciferase mutants as sensors of proteome stress." Nat Methods **8**: 879-884.

Gurney, M., H. Pu, A. Chiu, M. Dal Canto, C. Polchow, D. Alexander, J. Caliendo, A. Hentati, et al. (1994). "Motor neuron degeneration in mice that express a human Cu,Zn superoxide dismutase mutation." Science **264**: 1772-1775.

Gurney , M. E. (1994). "Transgenic-mouse model of amyotrophic lateral sclerosis." N Engl J Medicine **331**: 1721-1722.

Guzhova, I., K. Kislyakova, O. Moskaliova, I. Fridlanskaya, M. Tytell, M. Cheetham and B. Margulis (2001). "In vitro studies show that Hsp70 can be released by glia and that exogenous Hsp70 can enhance neuronal stress tolerance." Brain Res **914**: 66-73.

Hackett, E. A., R. K. Esch, S. Maleri and B. Errede (2006). "A family of destabilized cyan fluorescent proteins as transcriptional reporters in S. cerevisiae." Yeast **23**: 333-349.

Haim, L. B. and D. H. Rowitch (2017). "Functional diversity of astrocytes in neural circuit regulation." Nat Rev Neurosci **18**: 31-41.

Han, I., Y. You, J. H. Kordower, S. T. Brady and G. A. Morfini (2010). "Differential vulnerability of neurons in Huntington's disease: The role of cell type-specific features." J Neurochem **113**: 1073-1091.

Hanspal, M. A., C. M. Dobson, J. J. Yerbury and J. R. Kumita (2017). "The relevance of contact-independent cell-to-cell transfer of TDP-43 and SOD1 in amyotrophic lateral sclerosis." Biochim Biophys Acta **1863**: 2762-2771.

Hansson, E. (1984). "Cellular composition of a cerebral hemisphere primary culture." Neurochem Res **9**: 153-172.

Hansson, O., J. Nylandsted, R. F. Castilho, M. Leist, M. Jäättelä and P. Brundin (2003). "Overexpression of heat shock protein 70 in R6/2 Huntington's disease mice has only modest effects on disease progression." Brain Res **970**: 47-57.

Hartl, F. U., A. Bracher and M. Hayer-Hartl (2011). "Molecular chaperones in protein folding and proteostasis." Nature **475**: 324-332.

Haslbeck, M., T. Franzmann, D. Weinfurtner and J. Buchner (2005). "Some like it hot: The structure and function of small heat-shock proteins." Nat Struc Mol Biol **12**: 842-846.

Hatakeyama, S., M. Kitagawa, K. Nakayama, M. Shirane, M. Matsumoto, K. Hattori, H. Higashi, H. Nakano, et al. (1999). "Ubiquitin-dependent degradation of IkappaBalpha is mediated by a ubiquitin ligase Skp1/Cul 1/F-box protein FWD1." Proc Natl Acad Sci U S A **96**: 3859-3863.

Hatayama, T., H. Takahashi and N. Yamagishi (1997). "Reduced induction of Hsp70 in PC12 cells during neuronal differentiation." J Biochem **122**: 904-910.

Havasi, A., Z. Li, Z. Wang, J. L. Martin, V. Botla, K. Ruchalski, J. H. Schwartz and S. C. Borkan (2008). "Hsp27 inhibits Bax ativation and apoptosis via a phosphatidylinositol 3-kinase-dependent mechanism." J Biol Chem **283**: 12305-12313.

Hay, D. G., K. Sathasivam, S. Tobaben, B. Stahl, M. Marber, R. Mestril, A. Mahal, D. L. Smith, et al. (2004). "Progressive decrease in chaperone protein levels in a mouse model of Huntington's disease and induction of stress proteins as a therapeutic approach." Hum Mol Genet **13**: 1389-1405.

Hayashida, N., M. Fujimoto, K. Tan, R. Prakasam, T. Shinkawa, L. Li, H. Ichikawa, R. Takii, et al. (2010). "Heat shock factor 1 ameliorates proteotoxicity in cooperation with the transcription factor NFAT." EMBO J **29**: 3459-3469.

Haynes, C. M. and D. Ron (2010). "The mitochondrial UPR - Protecting organelle protein homeostasis." J Cell Sci **123**: 3849-3855.

Heemskerk, J., A. J. Tobin and L. J. Bain (2002). "Teaching old drugs new tricks." Trends Neurosci **25**: 494-496.

Hetz, C. (2012). "The unfolded protein response: Controlling cell fate decisions under ER stress and beyond." Nat Rev Mol Cell Biol **13**: 89-102.

Hipp, M. S., S. H. Park and F. U. Hartl (2014). "Proteostasis impairment in protein-misfolding and -aggregation diseases." Trends Cell Biol **24**: 506-514.

Hochstim, C., B. Deneen, A. Lukaszewicz, Q. Zhou and D. J. Anderson (2008). "The spinal cord contains positionally distinct astrocyte subtypes whose identities are specified by a homeodomain transcriptional code." Cell **133**: 510-522.

Holmberg, C. I., V. Hietakangas, A. Mikhailov, J. O. Rantanen, M. Kallio, A. Meinander, J. Hellman, N. Morrice, et al. (2001). "Phosphorylation of serine 230 promotes inducible transcriptional activity of heat shock factor 1." EMBO J **20**: 3800-3810.

Hooten, K. G., D. R. Beers, W. Zhao and S. H. Appel (2015). "Protective and toxic neuroinflammation in amyotrophic lateral sclerosis." Neurotherapeutics **12**: 364-375.

Houck, S. A. and J. I. Clark (2010). "Dynamic subunit exchange and the regulation of microtubule assembly by the stress response protein human alphaB crystallin." PLoS One **5**: e11795.

Houser, J. R., E. Ford, S. M. Chatterjea, S. Maleri, T. C. Elston and B. Errede (2012). "An improved short-lived fluorescent protein transcriptional reporter for Saccharomyces cerevisiae." Yeast **29**: 519-530.

Howarth, J. L., C. P. J. Glover and J. B. Uney (2009). "HSP70 interacting protein prevents the accumulation of inclusions in polyglutamine disease." J Neurochem **108**: 945-951.

Huang, C., B. Huang, F. Bi, L. H. Yan, J. Tong, J. Huang, X. G. Xia and H. Zhou (2014). "Profiling the genes affected by pathogenic TDP-43 in astrocytes." J Neurochem **129**: 932-939.

Ianaro, A., A. Ialenti, P. Maffia, B. Pisano and M. Di Rosa (2001). "HSF1/Hsp72 pathway as an endogenous anti-inflammatory system." FEBS Letters **499**: 239-244.

Iguchi, Y., M. Katsuno, K. Ikenaka, S. Ishigaki and G. Sobue (2013). "Amyotrophic lateral sclerosis: An update on recent genetic insights." J Neurol **260**: 2917-2927.

Ilieva, H., M. Polymenidou and D. W. Cleveland (2009). "Non–cell autonomous toxicity in neurodegenerative disorders: ALS and beyond." J Cell Biol **187**: 761-772.

Inobe, T. and A. Matouschek (2014). "Paradigms of protein degradation by the proteasome." Curr Opin Struc Biol **24**: 156-164.

Israël, A. (2010). "The IKK complex, a central regulator of NF-κB activation." CSH Perspect Biol **2**: a000158.

Ito, H., K. Kamei, I. Iwamoto, Y. Inaguma, D. Nohara and K. Kato (2001). "Phosphorylation-induced change of the oligomerization state of αB-crystallin." J Biol Chem **276**: 5346 - 5352.

Iwahashi, C. K., D. H. Yasui, H. J. An, C. M. Greco, F. Tassone, K. Nannen, B. Babineau, C. B. Lebrilla, et al. (2006). "Protein composition of the intranuclear inclusions of FXTAS." Brain **129**: 256-271.

Jackrel, M. E. and J. Shorter (2011). "Shock and awe: Unleashing the heat shock response to treat Huntington's disease." J Clin Invest **121**: 2972-2975.

Jespersen, T., M. Duch, M. L. Carrasco, S. Warming and F. S. Pedersen (1999). "Expression of heterologous genes from an IRES translational cassette in replication competent murine leukemia virus vectors." Gene **239**: 227-235.

Jia, Y. Y., J. Lu, Y. Huang, G. Liu, P. Gao, Y. Z. Wan, R. Zhang, Z. Q. Zhang, et al. (2014). "The involvement of NFAT transcriptional activity suppression in SIRT1-mediated inhibition of COX-2 expression induced by PMA/Ionomycin." PLoS One **9**: e97999.

Jing, Y., M. S. Fleete, N. D. Collie, H. Zhang and P. Liu (2013). "Regional variations and age-related changes in arginine metabolism in the rat brain stem and spinal cord." Neuroscience **252**: 98-108.

Jucker, M. and L. C. Walker (2013). "Self-propogation of pathogenic protein aggregates in neurodegenerative diseases." Nature **501**: 45-51.

Kabashi, E., J. N. Agar, Y. Hong, D. M. Taylor, S. Minotti, Denise A. Figlewicz and H. D. Durham (2008a). "Proteasomes remain intact, but show early focal alteration in their composition in a mouse model of amyotrophic lateral sclerosis." J Neurochem **105**: 2353-2366.

Kabashi, E., J. N. Agar, Y. Hong, D. M. Taylor, S. Minotti, D. A. Figlewicz and H. D. Durham (2008b). "Proteasomes remain intact, but show early focal alteration in their composition in a mouse model of amyotrophic lateral sclerosis." J Neurochem **105**: 2353-2366.

Kabashi, E., J. N. Agar, D. M. Taylor, S. Minotti and H. D. Durham (2004). "Focal dysfunction of the proteasome: A pathogenic factor in a mouse model of amyotrophic lateral sclerosis." J Neurochem **89**: 1325-1335.

Kaganovich, D., R. Kopito and J. Frydman (2008). "Misfolded proteins partition between two distinct quality control compartments." Nature **454**: 1088-1095.

Kakkar, V., C. Månsson, E. P. de Mattos, S. Bergink, M. van der Zwaag, M. A. W. H. van Waarde, N. J. Kloosterhuis, R. Melki, et al. (2016). "The S/T-rich motif in the DNAJB6

chaperone delays polyglutamine aggregation and the onset of disease in a mouse model." Mol Cell **62**: 272-283.

Kakkar, V., M. Meister-Broekema, M. Minoia, S. Carra and H. H. Kampinga (2014). "Barcoding heat shock proteins to human diseases: Looking beyond the heat shock response." Dis Models Mech **7**: 421-434.

Kalmar, B., G. Burnstock, G. Vrbova and L. Greensmith (2002). "The effect of neonatal nerve injury on the expression of heat shock proteins in developing rat motoneurones." J Neurotrauma **19**: 667-679.

Kalmar, B. and L. Greensmith (2009). "Induction of heat shock proteins for protection against oxidative stress." Adv Drug Deliv Rev **61**: 310-318.

Kalmar, B., C.-H. Lu and L. Greensmith (2014). "The role of heat shock proteins in Amyotrophic Lateral Sclerosis: The therapeutic potential of Arimoclomol." Pharmacol Ther **141**: 40-54.

Kalmar, B., S. Novoselov, A. Gray, M. E. Cheetham, B. Margulis and L. Greensmith (2008). "Late stage treatment with arimoclomol delays disease progression and prevents protein aggregation in the SOD1 mouse model of ALS." J Neurochem **107**: 339-350.

Kampinga, H. H. and S. Bergink (2016). "Heat shock proteins as potential targets for protective strategies in neurodegeneration." Lancet Neurol **15**: 748-759.

Kawamata, T., H. Akiyama, T. Yamada and P. L. McGeer (1992). "Immunologic reactions in amyotrophic lateral sclerosis brain and spinal cord tissue." Am J Pathol **140**: 691-707.

Kayatekin, C., K. E. Matlack, W. R. Hesse, Y. Guan, S. Chakrabortee, J. Russ, E. E. Wanker, J. V. Shah, et al. (2014). "Prion-like proteins sequester and suppress the toxicity of huntingtin exon 1." Proc Natl Acad Sci USA **111**: 12085-12090.

Khan, S., A. W. Rammeloo and J. J. Heikkila (2012). "Withaferin A induces proteasome hnhibition, endoplasmic reticulum stress, the heat shock response and acquisition of thermotolerance." PLoS One **7**: e50547.

Kiaei, M., K. Kipiani, S. Petri, J. Chen, N. Y. Calingasan and M. F. Beal (2005). "Celastrol blocks neuronal cell death and extends life in transgenic mouse model of amyotrophic lateral sclerosis." Neurodegener Dis **2**: 246-254.

Kieran, D., B. Kalmar, J. R. Dick, J. Riddoch-Contreras, G. Burnstock and L. Greensmith (2004). "Treatment with arimoclomol, a coinducer of heat shock proteins, delays disease progression in ALS mice." Nat Med **10**: 402-405.

Kilpatrick, K., J. A. Novoa, T. Hancock, C. J. Guerriero, P. Wipf, J. L. Brodsky and L. Segatori (2013). "Chemical induction of Hsp70 reduces alpha-synuclein aggregation in neuroglioma cells." ACS Chem Biol **8**: 1460-1468.

Kim, E., B. Wang, N. Sastry, E. Masliah, P. T. Nelson, H. Cai and F.-F. Liao (2016). "NEDD4-mediated HSF1 degradation underlies α-synucleinopathy." Hum Mol Genet **25**: 211-222.

Kim, Y. M., M. E. de Vera, S. C. Watkins and T. R. Billiar (1997). "Nitric oxide protects cultured rat hepatocytes from tumor necrosis factor-alpha-induced apoptosis by inducing heat shock protein 70 expression." J Biol Chem **272**: 1402-1411.

Kirkitadze, M. D., G. Bitan and D. B. Teplow (2002). "Paradigm shifts in Alzheimer's disease and other neurodegenerative disorders: The emerging role of oligomeric assemblies." J Neurosci Res **69**: 567-577.

Klucken, J., Y. Shin, E. Masliah, B. T. Hyman and P. J. McLean (2004). "Hsp70 Reduces alpha-Synuclein Aggregation and Toxicity." J Biol Chem **279**: 25497-25502.

Krishnan, J., K. Vannuvel, M. Andries, E. Waelkens, W. Robberecht and L. Van Den Bosch (2008). "Over-expression of Hsp27 does not influence disease in the mutant SOD1G93A mouse model of amyotrophic lateral sclerosis." J Neurochem **106**: 2170-2183.

Krueger, A. M., J. N. Armstrong, J. Plumier, H. A. Robertson and R. W. Currie (1999). "Cell specific expression of Hsp70 in neurons and glia of the rat hippocampus after hyperthermia and kainic acid-induced seizure activity." Brain Res Mol Brain Res **71**: 265-278.

Kulig, M. and H. Ecroyd (2012). "The small heat-shock protein alphaB-crystallin uses different mechanisms of chaperone action to prevent the amorphous versus fibrillar aggregation of alpha-lactalbumin." Biochem J **448**: 343-352.

Kwong, J. Q., M. F. Beal and G. Manfredi (2006). "The role of mitochondria in inherited neurodegenerative diseases." J Neurochem **97**: 1659-1675.

Labbadia, J., H. Cunliffe, A. Weiss, E. Katsyuba, K. Sathasivam, T. Seredenina, B. Woodman, S. Moussaoui, et al. (2011). "Altered chromatin architecture underlies progressive impairment of the heat shock response in mouse models of Huntington disease." J Clin Invest **121**: 3306-3319.

Labbadia, J., S. S. Novoselov, J. S. Bett, A. Weiss, P. Paganetti, G. P. Bates and M. E. Cheetham (2012). "Suppression of protein aggregation by chaperone modification of high molecular weight complexes." Brain **135**: 1180-1196.

Laemmli, U. K. (1970). "Cleavage of structural proteins during the assembly of the head of bacteriophage T4." Nature **227**: 680-685.

Leak, R. K. (2014). "Heat shock proteins in neurodegenerative disorders and aging." J Cell Commun Signal **8**: 293-310.

Lee, H.-J., J.-E. Suk, E.-J. Bae, J.-H. Lee, S. R. Paik and S.-J. Lee (2008). "Assembly-dependent endocytosis and clearance of extracellular a-synuclein." Int J Biochem Cell Biol **40**: 1835-1849.

Lee, J., S. J. Hyeon, H. Im, H. Ryu, Y. Kim and H. Ryu (2016). "Astrocytes and microglia as non-cell autonomous players in the pathogenesis of ALS." Exp Neurol **25**: 233-240.

Lee, S., K. Carson, A. Rice-Ficht and T. Good (2006). "Small heat shock proteins differentially affect amyloid-beta aggregation and toxicity." Biochem Biophys Res Commun **347**: 527-533.

Li, D., T. Xu, Y. Cao, H. Wang, L. Li, S. Chen, X. Wang and Z. Shen (2015). "A cytosolic heat shock protein 90 and cochaperone CDC37 complex is required for RIP3 activation during necroptosis." Proc Natl Acad Sci USA **112**: 5017-5022.

Li, J., T. McQuade, A. B. Siemer, J. Napetschnig, K. Moriwaki, Y. S. Hsiao, E. Damko, D. Moquin, et al. (2012). "The RIP1/RIP3 necrosome forms a functional amyloid signaling complex required for programmed necrosis." Cell **150**: 339-350.

Liddelow, S. A., K. A. Guttenplan, L. E. Clarke, F. C. Bennett, C. J. Bohlen, L. Schirmer, M. L. Bennett, A. E. Münch, et al. (2017). "Neurotoxic reactive astrocytes are induced by activated microglia." Nature **541**: 481-487.

Lin, P.-Y., S. M. Simon, W. K. Koh, O. Folorunso, C. S. Umbaugh and A. Pierce (2013). "Heat shock factor 1 over-expression protects against exposure of hydrophobic residues on mutant SOD1 and early mortality in a mouse model of amyotrophic lateral sclerosis." Mol Neurodegener **8**: 43-43.

Littlefield, O. and H. C. Nelson (1999). "A new use for the 'wing' of the 'winged' helix-turn-helix motif in the HSF-DNA co-crystal." Nat Struct Biol **6**: 464-470.

Liu, J., L. A. Shinobu, C. M. Ward, D. Young and D. W. Cleveland (2005). "Elevation of the Hsp70 chaperone does not effect toxicity in mouse models of familial amyotrophic lateral sclerosis." J Neurochem **93**: 875-882.

Liu, X., B. R. Miller, G. V. Rebec and D. E. Clemmer (2007). "Protein expression in the striatum and cortex regions of the brain for a mouse model of Huntington's disease." J Proteome Res **6**: 3134-3142.

Maatkamp, A., A. Vlug, E. Haasdijk, D. Troost, P. J. French and D. Jaarsma (2004). "Decrease of Hsp25 protein expression precedes degeneration of motoneurons in ALS-SOD1 mice." Eur J Neurosci **20**: 14-28.

MacDonald, M. E., C. M. Ambrose, M. P. Duyao, R. H. Myers, C. Lin, L. Srinidhi, G. Barnes, S. A. Taylor, et al. (1993). "A novel gene containing a trinucleotide repeat that is expanded and unstable on Huntington's disease chromosomes." Cell **72**: 971-983.

Malik, B., N. Nirmalananthan, A. L. Gray, A. R. La Spada, M. G. Hanna and L. Greensmith (2013). "Co-induction of the heat shock response ameliorates disease progression in a mouse model of human spinal and bulbar muscular atrophy: Implications for therapy." Brain **136**: 926-943.

Manzerra, P. and I. R. Brown (1992). "Expression of heat shock genes (Hsp70) in the rabbit spinal cord: Localization of constitutive and hyperthermia-inducible mRNA species." J Neurosci Res **31**: 606-615.

Manzerra, P., S. J. Rush and I. R. Brown (1997). "Tissue-specific differences in heat shock protein Hsc70 and Hsp70 in the control and hyperthermic rabbit." J Cell Physiol **170**: 130-137.

Mardones, P., G. Martínez and C. Hetz (2015). "Control of systemic proteostasis by the nervous system." Trends Cell Biol **25**: 1-10.

Marini, A. M., M. Kozuka, R. H. Lipsky and T. S. Nowak, Jr. (1990). "70-kilodalton heat shock protein induction in cerebellar astrocytes and cerebellar granule cells in vitro: comparison with immunocytochemical localization after hyperthermia in vivo." J Neurochem **54**: 1509-1516.

Marino, M., S. Papa, V. Crippa, G. Nardo, M. Peviani, C. Cheroni, M. C. Trolese, E. Lauranzano, et al. (2015). "Differences in protein quality control correlate with phenotype variability in 2 mouse models of familial amyotrophic lateral sclerosis." Neurobiol Aging **36**: 492-504.

Mathur, S. K., L. Sistonen, I. R. Brown, S. P. Murphy, K. D. Sarge and R. I. Morimoto (1994). "Deficient induction of human hsp70 heat shock gene transcription in Y79 retinoblastoma cells despite activation of heat shock factor 1." Proc Natl Acad Sci USA **91**: 8695-8699.

Matsumoto, G., S. Kim and R. I. Morimoto (2006). "Huntingtin and mutant SOD1 form aggregate structures with distinct molecular properties in human cells." J Biol Chem **281**: 4477-4485.

McAlary, L., J. A. Aquilina and J. J. Yerbury (2016). "Susceptibility of mutant SOD1 to form a destabilized monomer predicts cellular aggregation and toxicity but not in vitro aggregation propensity." Front Neurosci **10**: 499.

McCarthy, K. D. and J. de Vellis (1980). "Preparation of separate astroglial and oligodendroglial cell cultures from rat cerebral tissue." J Cell Biol **85**: 890-902.

Meissner, F., K. Molawi and A. Zychlinsky (2010). "Mutant superoxide dismutase 1-induced IL-1β accelerates ALS pathogenesis." Proc Natl Acad Sci USA **107**: 13046-13050.

Mimoto, T., N. Morimoto, K. Miyazaki, T. Kurata, K. Sato, Y. Ikeda and K. Abe (2012). "Expression of heat shock transcription factor 1 and its downstream target protein T-cell death associated gene 51 in the spinal cord of a mouse model of amyotrophic lateral sclerosis." Brain Res **1488**: 123-131.

Minami, Y., J. Hohfeld, K. Ohtsuka and F. U. Hartl (1996). "Regulation of the heat-shock protein 70 reaction cycle by the mammalian DnaJ homolog, Hsp40." J Biol Chem **271**: 19617-19624.

Molofsky, A. V., K. W. Kelley, H.-H. Tsai, S. A. Redmond, S. M. Chang, L. Madireddy, J. R. Chan, S. E. Baranzini, et al. (2014). "Astrocyte-encoded positional cues maintain sensorimotor circuit integrity." Nature **509**: 189-194.

Morano, K. A., C. M. Grant and W. S. Moye-Rowley (2012). "The response to heat shock and oxidative stress in saccharomyces cerevisiae." Genetics **190**: 1157-1195.

Morimoto, R. I. (2008). "Proteotoxic stress and inducible chaperone networks in neurodegenerative disease and aging." Gene Dev **22**: 1427-1438.

Morimoto, R. I. (2011). The heat shock response: Systems biology of proteotoxic stress in aging and disease. Cold Spring Harb Symp Quant Biol. **76:** 91-99.

Mosher, K. I. and T. Wyss-Coray (2014). "Microglial dysfunction in brain aging and Alzheimer's disease." Biochem Pharmacol **88**: 594-604.

Muchowski, P. J. and J. L. Wacker (2005). "Modulation of neurodegeneration by molecular chaperones." Nat Rev Neurosci **6**: 11-22.

Munch, C., J. O'Brien and A. Bertolotti (2011). "Prion-like propagation of mutant superoxide dismutase-1 misfolding in neuronal cells." Proc Natl Acad Sci USA **108**: 3548-3553.

Murphy, S. (2000). "Production of nitric oxide by glial cells: regulation and potential roles in the CNS." Glia **29**: 1-13.

Murshid, A., S. D. Chou, T. Prince, Y. Zhang, A. Bharti and S. K. Calderwood (2010). "Protein kinase A binds and activates heat shock factor 1." PLoS One **5**: e13830.

Nagai, M., D. B. Re, T. Nagata, A. Chalazonitis, T. M. Jessell, H. Wichterle and S. Przedborski (2007). "Astrocytes expressing ALS-linked mutated SOD1 release factors selectively toxic to motor neurons." Nat Neurosci **10**: 615-622.

Neef, D. W., A. Jaeger, R. Gomez-Pastor, F. Willmund, J. Frydman and D. J. Thiele (2014). "A direct regulatory interaction between chaperonin TRiC and stress responsive transcription factor HSF1." Cell Rep **9**: 955-966.

Neudegger, T., J. Verghese, M. Hayer-Hartl, F. U. Hartl and A. Bracher (2016). "Structure of human heat-shock transcription factor 1 in complex with DNA." Nat Struct Mol Biol **23**: 140-146.

Niforou, K., C. Cheimonidou and I. P. Trougakos (2014). "Molecular chaperones and proteostasis regulation during redox imbalance." Redox Biol **2**: 323-332.

Nishimura, R. N. and B. E. Dwyer (1996). "Evidence for different mechanisms of induction of HSP70i: A comparison of cultured rat cortical neurons with astrocytes." Brain Res Mol Brain Res **36**: 227-239.

Nishimura, R. N., B. E. Dwyer, K. Clegg, R. Cole and J. de Vellis (1991). "Comparison of the heat shock response in cultured cortical neurons and astrocytes." Mol Brain Res **9**: 39-45.

Nishitoh, H., H. Kadowaki, A. Nagai, T. Maruyama, T. Yokota, H. Fukutomi, T. Noguchi, A. Matsuzawa, et al. (2008). "ALS-linked mutant SOD1 induces ER stress- and ASK1-dependent motor neuron death by targeting Derlin-1." Gen Dev **22**: 1451-1464.

Novoselov, S. S., W. J. Mustill, A. L. Gray, J. R. Dick, N. Kanuga, B. Kalmar, L. Greensmith and M. E. Cheetham (2013). "Molecular chaperone mediated late-stage neuroprotection in the SOD1G93A mouse model of amyotrophic lateral sclerosis." PLos One **8**: e73944.

Oliveira, A. O., A. Osmand, T. F. Outeiro, P. J. Muchowski and S. Finkbeiner (2016). "AlphaB-crystallin overexpression in astrocytes modulates the phenotype of the BACHD mouse model of Huntington's disease." Hum Mol Genet **25**: 1677-1689.

Olshina, M. A., L. M. Angley, Y. M. Ramdzan, J. Tang, M. F. Bailey, A. F. Hill and D. M. Hatters (2010). "Tracking mutant huntingtin aggregation kinetics in cells reveals three major populations that include an invariant oligomer pool." J Biol Chem **285**: 21807-21816.

Olzscha, H., S. M. Schermann, A. C. Woerner, S. Pinkert, M. H. Hecht, G. G. Tartaglia, M. Vendruscolo, M. Hayer-Hartl, et al. (2011). "Amyloid-like aggregates sequester numerous metastable proteins with essential cellular functions." Cell **144**: 67-78.

Ormsby, A. R., Y. M. Ramdzan, Y.-F. Mok, K. D. Jovanoski and D. M. Hatters (2013). "A platform to view huntingtin exon 1 aggregation flux in the cell reveals divergent influences from chaperones Hsp40 and Hsp70." J Biol Chem **288**: 37192-37203.

Ortega, L., M. Calvillo, F. Luna, F. Pérez-Severiano, M. Rubio-Osornio, J. Guevara and I. D. Limón (2014). "17-AAG improves cognitive process and increases heat shock protein response in a model lesion with Aβ25–35." Neuropeptides **48**: 221-232.

Ortner, V., A. Ludwig, E. Riegel, S. Dunzinger and T. Czerny (2015). "An artificial HSE promoter for efficient and selective detection of heat shock pathway activity." Cell Stress Chaperon **20**: 277-288.

Outeiro, T. F., J. Klucken, K. E. Strathearn, F. Liu, P. Nguyen, J. C. Rochet, B. T. Hyman and P. J. McLean (2006). "Small heat shock proteins protect against alpha-synuclein-induced toxicity and aggregation." Biochem Biophys Res Commun **351**: 631-638.

Oza, J., J. Yang, K. Chen and A. C. Liu (2008). "Changes in the regulation of heat shock gene expression in neuronal cell differentiation." Cell Stress Chaperon **13**: 73-84.

Papageorgiou, I. E., A. Lewen, L. V. Galow, T. Cesetti, J. Scheffel, T. Regen, U. K. Hanisch and O. Kann (2016). "TLR4-activated microglia require IFN-gamma to induce severe neuronal dysfunction and death in situ." Proc Natl Acad Sci U S A **113**: 212-217.

Patel, P., J. P. Julien and J. Kriz (2014). "Early-stage treatment with withaferin A reduces levels of misfolded superoxide dismutase 1 and extends lifespan in a mouse model of amyotrophic lateral sclerosis." Neurotherapeutics **12**: 217-233.

Pavlik, A. and I. S. Aneja (2007). "Cerebral neurons and glial cell types inducing heat shock protein Hsp70 following heat stress in the rat." Prog Brain Res **162**: 417-431.

Pavlik, A., I. S. Aneja, J. Lexa and B. A. Al-Zoabi (2003). "Identification of cerebral neurons and glial cell types inducing heat shock protein Hsp70 following heat stress in the rat." Brain Res **973**: 179-189.

Pehar, M., P. Cassina, M. R. Vargas, R. Castellanos, L. Viera, J. S. Beckman, A. G. Estévez and L. Barbeito (2004). "Astrocytic production of nerve growth factor in motor neuron apoptosis: implications for amyotrophic lateral sclerosis." J Neurochem **89**: 464-473.

Pelham, H. R. (1982). "A regulatory upstream promoter element in the Drosophila Hsp 70 heat-shock gene." Cell **30**: 517-528.

Peteranderl, R. and H. C. M. Nelson (1992). "Trimerization of the heat shock transcription factor by a triple-stranded alpha-helical coiled-coil." Biochemistry **31**: 12272-12276.

Petrasch-Parwez, E., H. P. Nguyen, M. Lobbecke-Schumacher, H. W. Habbes, S. Wieczorek, O. Riess, K. H. Andres, R. Dermietzel, et al. (2007). "Cellular and subcellular localization of Huntingtin [corrected] aggregates in the brain of a rat transgenic for Huntington disease." J Comp Neurol **501**: 716-730.

Phatnani, H. P., P. Guarnieri, B. A. Friedman, M. A. Carrasco, M. Muratet, S. O'Keeffe, C. Nwakeze, F. Pauli-Behn, et al. (2013). "Intricate interplay between astrocytes and motor neurons in ALS." Proc Natl Acad Sci U S A **110**: E756-765.

Philips, T. and W. Robberecht (2011). "Neuroinflammation in amyotrophic lateral sclerosis: role of glial activation in motor neuron disease." Lancet Neurol **10**: 253-263.

Plumier, J. C., D. A. Hopkins, H. A. Robertson and R. W. Currie (1997). "Constitutive expression of the 27-kDa heat shock protein (Hsp27) in sensory and motor neurons of the rat nervous system." J Comp Neurol **384**: 409-428.

Polling, S., Y. F. Mok, Y. M. Ramdzan, B. J. Turner, J. J. Yerbury, A. F. Hill and D. M. Hatters (2014). "Misfolded polyglutamine, polyalanine, and superoxide dismutase 1 aggregate via distinct pathways in the cell." J Biol Chem **289**: 6669-6680.

Popiel, H. A., T. Takeuchi, H. Fujita, K. Yamamoto, C. Ito, H. Yamane, S.-i. Muramatsu, T. Toda, et al. (2012). "Hsp40 gene therapy exerts therapeutic effects on polyglutamine disease mice via a non-cell autonomous mechanism." PLoS One **7**: e51069.

Pountney, D. L., T. M. Treweek, T. Chataway, Y. Huang, F. Chegini, P. C. Blumbergs, M. J. Raftery and W. P. Gai (2005). "αB-Crystallin is a major component of glial cytoplasmic inclusions in multiple system atrophy." Neurotox Res **7**: 77-85.

Pramatarova, A., J. Laganiere, J. Roussel, K. Brisebois and G. A. Rouleau (2001). "Neuron-specific expression of mutant superoxide dismutase 1 in transgenic mice does not lead to motor impairment." J Neurosci **21**: 3369-3374.

Pratt, W. B., J. E. Gestwicki, Y. Osawa and A. P. Lieberman (2015). "Targeting Hsp90/Hsp70-based protein quality control for treatment of adult onset neurodegenerative diseases." Annu Rev Pharmacol **55**: 353-371.

Prell, T., J. Lautenschlager, O. W. Witte, M. T. Carri and J. Grosskreutz (2012). "The unfolded protein response in models of human mutant G93A amyotrophic lateral sclerosis." Eur J Neurosci **35**: 652-660.

Rabindran, S. K., R. I. Haroun, J. Clos, J. Wisniewski and C. Wu (1993). "Regulation of heat shock factor trimer formation: Role of a conserved leucine zipper." Science **259**: 230-234.

Ramdzan, Y. M., M. M. Trubetskov, A. R. Ormsby, E. A. Newcombe, X. Sui, M. J. Tobin, M. N. Bongiovanni, S. L. Gras, et al. (2017). "Huntingtin inclusions trigger cellular quiescence, deactivate apoptosis, and lead to delayed necrosis." Cell Rep **19**: 919-927.

Ramdzan, Y. M., R. Wood and D. M. Hatters (2013). "Pulse shape analysis (PulSA) to track protein translocalization in cells by flow cytometry: Applications for polyglutamine aggregation." Methods Mol Biol **1017**: 85-93.

Raoul, C., C. Barthelemy, A. Couzinet, D. Hancock, B. Pettmann and A. O. Hueber (2005). "Expression of a dominant negative form of Daxx in vivo rescues motoneurons from Fas (CD95)-induced cell death." J Neurobiol **62**: 178-188.

Raoul, C., E. Buhler, C. Sadeghi, A. Jacquier, P. Aebischer, B. Pettmann, C. E. Henderson and G. Haase (2006). "Chronic activation in presymptomatic amyotrophic lateral sclerosis (ALS) mice of a feedback loop involving Fas, Daxx, and FasL." Proc Natl Acad Sci USA **103**: 6007-6012.

Raoul, C., A. G. Estevez, H. Nishimune, D. W. Cleveland, O. deLapeyriere, C. E. Henderson, G. Haase and B. Pettmann (2002). "Motoneuron death triggered by a specific pathway downstream of Fas potentiation by ALS-linked SOD1 mutations." Neuron **35**: 1067-1083.

Raoul, C., C. E. Henderson and B. Pettmann (1999). "Programmed cell death of embryonic motoneurons triggered through the FAS death receptor." J Cell Biol **147**: 1049-1062.

Raychaudhuri, S., C. Loew, R. Körner, S. Pinkert, M. Theis, M. Hayer-Hartl, F. Buchholz and F. U. Hartl (2014). "Interplay of acetyltransferase EP300 and the proteasome system in regulating heat shock transcription factor 1." Cell **156**: 975-985.

Redinbaugh, M. G. and R. B. Turley (1986). "Adaptation of the bicinchoninic acid protein assay for use with microtiter plates and sucrose gradient fractions." Anal Biochem **153**: 267-271.

Resenberger, U. K., V. Müller, L. M. Munter, M. Baier, G. Multhaup, M. R. Wilson, K. F. Winklhofer and J. Tatzelt (2012). "The heat shock response is modulated by and interferes with toxic effects of scrapie prion protein and amyloid β." J Biol Chem **287**: 43765-43776.

Richter, K., M. Haslbeck and J. Buchner (2010). "The heat shock response: Life on the verge of death." Mol Cell **40**: 253-266.

Riva, L., M. Koeva, F. Yildirim, L. Pirhaji, D. Dinesh, T. Mazor, M. L. Duennwald and E. Fraenkel (2012). "Poly-glutamine expanded huntingtin dramatically alters the genome wide binding of HSF1." J Huntingtons Dis **1**: 33-45.

Roberts, K., R. Zeineddine, L. Corcoran, W. Li, I. L. Campbell and J. J. Yerbury (2013). "Extracellular aggregated Cu/Zn superoxide dismutase activates microglia to give a cytotoxic phenotype." Glia **61**: 409-419.

Rosser, M. F., E. Washburn, P. J. Muchowski, C. Patterson and D. M. Cyr (2007). "Chaperone functions of the E3 ubiquitin ligase CHIP." J Biol Chem **282**: 22267-22277.

Rothstein, J. D. (2009). "Current hypotheses for the underlying biology of amyotrophic lateral sclerosis." Ann Neurol **65**: S3-S9.

Ruiz, C., M. J. Casarejos, A. Gomez, R. Solano, J. G. de Yebenes and M. A. Mena (2012). "Protection by glia-conditioned medium in a cell model of Huntington disease." PLoS Curr **4**: e4fbca54a2028b.

Russo, C. D., P. E. Polak, P. R. Mercado, A. Spagnolo, A. Sharp, P. Murphy, A. Kamal, F. J. Burrows, et al. (2006). "The heat-shock protein 90 inhibitor 17-allylamino-17-demethoxygeldanamycin suppresses glial inflammatory responses and ameliorates experimental autoimmune encephalomyelitis." J Neurochem **99**: 1351-1362.

Sala, A. J., L. C. Bott and R. I. Morimoto (2017). "Shaping proteostasis at the cellular, tissue, and organismal level." J Cell Biol **216**: 1231-1241.

Sandqvist, A., J. K. Björk, M. Åkerfelt, Z. Chitikova, A. Grichine, C. Vourc'h, C. Jolly, T. A. Salminen, et al. (2009). "Heterotrimerization of heat-shock factors 1 and 2 provides a transcriptional switch in response to distinct stimuli." Mol Biol Cell **20**: 1340-1347.

Santoro, M. G., E. Garaci and C. Amici (1989). "Prostaglandins with antiproliferative activity induce the synthesis of a heat shock protein in human cells." Proc Natl Acad Sci USA **86**: 8407-8411.

Sasi, B. K., P. J. Sonawane, V. Gupta, B. S. Sahu and N. R. Mahapatra (2014). "Coordinated transcriptional regulation of Hspa1a gene by multiple transcription factors: Crucial roles for HSF-1, NF-Y, NF-κB, and CREB." J Mol Biol **426**: 116-135.

Satoh, J., T. Tabira, T. Yamamura and S. U. Kim (1994). "HSP72 induction by heat stress is not universal in mammalian neural cell lines." J Neurosci Res **37**: 44-53.

Saura, J. (2007). "Microglial cells in astroglial cultures: A cautionary note." J Neuroinflammation **4**: 26.

Saura, J., E. Angulo, A. Ejarque, V. Casado, J. M. Tusell, R. Moratalla, J. F. Chen, M. A. Schwarzschild, et al. (2005). "Adenosine A2A receptor stimulation potentiates nitric oxide release by activated microglia." J Neurochem **95**: 919-929.

Scarim, A. L., M. R. Heitmeier and J. A. Corbett (1998). "Heat shock inhibits cytokine-induced nitric oxide synthase expression by rat and human islets." Endocrinology **139**: 5050-5057.

Schett, G., K. Redlich, Q. Xu, P. Bizan, M. Groger, M. Tohidast-Akrad, H. Kiener, J. Smolen, et al. (1998). "Enhanced expression of heat shock protein 70 (hsp70) and heat shock factor 1 (HSF1) activation in rheumatoid arthritis synovial tissue. Differential regulation of hsp70 expression and hsf1 activation in synovial fibroblasts by proinflammatory cytokines, shear stress, and antiinflammatory drugs." J Clin Invest **102**: 302-311.

Schnell, L., S. Fearn, H. Klassen, M. E. Schwab and V. H. Perry (1999). "Acute inflammatory responses to mechanical lesions in the CNS: differences between brain and spinal cord." Eur J Neurosci **11**: 3648-3658.

Sharma, K., S. Schmitt, C. G. Bergner, S. Tyanova, N. Kannaiyan, N. Manrique-Hoyos, K. Kongi, L. Cantuti, et al. (2015a). "Cell type- and brain region-resolved mouse brain proteome." Nat Neurosci **18**: 1819-1831.

Sharma, S., R. Mishra, B. Walker, S. Deshmukh, M. Zampino, J. Patel, M. Anamalai, D. Simpson, et al. (2015b). "Celastrol, an oral heat shock activator, ameliorates multiple animal disease models of cell death." Cell Stress Chaperon **20**: 185-201.

Sharp, P. S., M. T. Akbar, S. Bouri, A. Senda, K. Joshi, H.-J. Chen, D. S. Latchman, D. J. Wells, et al. (2008). "Protective effects of heat shock protein 27 in a model of ALS occur in the early stages of disease progression." Neurobiol Dis **30**: 42-55.

Sharpe, J. and S. Wulff. (2005). "Small particle analysis." Retrieved 11/06/2016, from https://www.researchgate.net/publication/265185385_Small-Particle_Analysis.

Shi, Y., D. D. Mosser and R. I. Morimoto (1998). "Molecular chaperones as HSF1-specific transcriptional repressors." Gen Dev **12**: 654-666.

Shiber, A., W. Breuer and T. Ravid (2014). "Flow cytometric quantification and characterization of intracellular protein aggregates in yeast." Prion **8**: 276-284.

Shin, J. Y., Z. H. Fang, Z. X. Yu, C. E. Wang, S. H. Li and X. J. Li (2005). "Expression of mutant huntingtin in glial cells contributes to neuronal excitotoxicity." J Cell Biol **171**: 1001-1012.

Shinkawa, T., K. Tan, M. Fujimoto, N. Hayashida, K. Yamamoto, E. Takaki, R. Takii, R. Prakasam, et al. (2011). "Heat shock factor 2 is required for maintaining proteostasis against febrile-range thermal stress and polyglutamine aggregation." Mol Biol Cell **22**: 3571-3583.

Sittler, A., R. Lurz, G. Lueder, J. Priller, H. Lehrach, M. K. Hayer-Hartl, F. U. Hartl and E. E. Wanker (2001). "Geldanamycin activates a heat shock response and inhibits huntingtin aggregation in a cell culture model of Huntington's disease." Hum Mol Genet **10**: 1307-1315.

Sommer, C. and D. W. Gerlich (2013). "Machine learning in cell biology - teaching computers to recognize phenotypes." J Cell Sci **126**: 5529-5539.

Soncin, F., X. Zhang, B. Chu, X. Wang, A. Asea, M. A. Stevenson, D. B. Sacks and S. K. Calderwood (2003). "Transcriptional activity and DNA binding of heat shock factor-1 involve phosphorylation on threonine 142 by CK2." Biochem Biophys Res Commun **303**: 700 - 706.

Sorger, P. K. and H. R. Pelham (1988). "Yeast heat shock factor is an essential DNA-binding protein that exhibits temperature-dependent phosphorylation." Cell **54**: 855-864.

Strey, C. W., D. Spellman, A. Stieber, J. O. Gonatas, X. Wang, J. D. Lambris and N. K. Gonatas (2004). "Dysregulation of stathmin, a microtubule-destabilizing protein, and up-regulation of Hsp25, Hsp27, and the antioxidant peroxiredoxin 6 in a mouse model of familial amyotrophic lateral sclerosis." Am J Pathol **165**: 1701-1718.

Tafuri, F., D. Ronchi, F. Magri, G. P. Comi and S. Corti (2015). "SOD1 misplacing and mitochondrial dysfunction in amyotrophic lateral sclerosis pathogenesis." Front Cell Neurosci **9**: 336.

Tagawa, K., S. Marubuchi, M. L. Qi, Y. Enokido, T. Tamura, R. Inagaki, M. Murata, I. Kanazawa, et al. (2007). "The induction levels of heat shock protein 70 differentiate the vulnerabilities to mutant huntingtin among neuronal subtypes." J Neurosci **27**: 868-880.

Tak, P. P. and G. S. Firestein (2001). "NF-κB: a key role in inflammatory diseases." J Clin Invest **107**: 7-11.

Tashiro, Y., M. Urushitani, H. Inoue, M. Koike, Y. Uchiyama, M. Komatsu, K. Tanaka, M. Yamazaki, et al. (2012). "Motor neuron-specific disruption of proteasomes, but not autophagy, replicates amyotrophic lateral sclerosis." J Biol Chem **287**: 42984-42994.

Taylor, A. R., M. B. Robinson, D. J. Gifondorwa, M. Tytell and C. E. Milligan (2007). "Regulation of heat shock protein 70 release in astrocytes: Role of signaling kinases." Dev Neurobiol **67**: 1815-1829.

Taylor, J. P., R. H. Brown Jr and D. W. Cleveland (2016). "Decoding ALS: From genes to mechanism." Nature **539**: 197-206.

Thomas, S. C., M. A. Ryan, T. P. Shanley and H. R. Wong (1998). "Induction of the stress response with prostaglandin A1 increases I-κBα gene expression." FASEB J **12**: 1371-1378.

Tong, J., C. Huang, F. Bi, Q. Wu, B. Huang, X. Liu, F. Li, H. Zhou, et al. (2013). "Expression of ALS-linked TDP-43 mutant in astrocytes causes non-cell-autonomous motor neuron death in rats." EMBO J **32**: 1917-1926.

Towbin, H., T. Staehelin and J. Gordon (1979). "Electrophoretic transfer of proteins from polyacrylamide gels to nitrocellulose sheets: procedure and some applications." Proc Natl Acad Sci U S A **76**: 4350-4354.

Tremblay, R. G., M. Sikorska, J. K. Sandhu, P. Lanthier, M. Ribecco-Lutkiewicz and M. Bani-Yaghoub (2010). "Differentiation of mouse Neuro 2A cells into dopamine neurons." J Neurosci Methods **186**: 60-67.

Treweek, T. M., S. Meehan, H. Ecroyd and J. A. Carver (2015). "Small heat-shock proteins: Important players in regulating cellular proteostasis." Cell Mol Life Sci **72**: 429-451.

Trinklein, N. D., W. C. Chen, R. E. Kingston and R. M. Myers (2004a). "Transcriptional regulation and binding of heat shock factor 1 and heat shock factor 2 to 32 human heat shock genes during thermal stress and differentiation." Cell Stress Chaperon **9**: 21 - 28.

Trinklein, N. D., J. I. Murray, S. J. Hartman, D. Botstein and R. M. Myers (2004b). "The role of heat shock transcription factor 1 in the genome-wide regulation of the mammalian heat shock response." Mol Biol Cell **15**: 1254 - 1261.

Turner, B. J., J. D. Atkin, M. A. Farg, D. W. Zang, A. Rembach, E. C. Lopes, J. D. Patch, A. F. Hill, et al. (2005). "Impaired extracellular secretion of mutant superoxide dismutase 1

associates with neurotoxicity in familial amyotrophic lateral sclerosis." J Neurosci **25**: 108-117.

Tzeng, E., T. R. Billiar, P. D. Robbins, M. Loftus and D. J. Stuehr (1995). "Expression of human inducible nitric oxide synthase in a tetrahydrobiopterin (H4B)-deficient cell line: H4B promotes assembly of enzyme subunits into an active dimer." Proc Natl Acad Sci USA **92**: 11771-11775.

Vacher, C., L. Garcia-Oroz and D. C. Rubinsztein (2005). "Overexpression of yeast Hsp104 reduces polyglutamine aggregation and prolongs survival of a transgenic mouse model of Huntington's disease." Hum Mol Genet **14**: 3425-3433.

Varshavsky, A. (2012). "The ubiquitin system, an immense realm." Annu Rev Biochem **81**: 167-176.

Velichko, A., E. Markova, N. Petrova, S. Razin and O. Kantidze (2013). "Mechanisms of heat shock response in mammals." Cell Mol Life Sci **70**: 4229-4241.

Verbeke, P., J. Fonager, B. F. Clark and S. I. Rattan (2001). "Heat shock and aging: Mechanisms and implications." Cell Biol Int **25**: 845-857.

Vergnolle, N., J. L. Wallace, N. W. Bunnett and M. D. Hollenberg (2001). "Protease-activated receptors in inflammation, neuronal signaling and pain." Trends Pharmacol Sci **22**: 146-152.

Victoria, G. S. and C. Zurzolo (2017). "The spread of prion-like proteins by lysosomes and tunneling nanotubes: Implications for neurodegenerative diseases." J Cell Biol **216**: 2633-2644.

Vihervaara, A. and L. Sistonen (2014). "HSF1 at a glance." J Cell Sci **127**: 261-266.

Vihma, H., M. Luhakooder, P. Pruunsild and T. Timmusk (2016). "Regulation of different human NFAT isoforms by neuronal activity." J Neurochem **137**: 394-408.

Vleminckx, V., P. Van Damme, K. Goffin, H. Delye, L. Van Den Bosch and W. Robberecht (2002). "Upregulation of Hsp27 in a transgenic model of ALS." J Neuropathol Exp Neurol **61**: 968-974.

Vlug, A. S., E. Teuling, E. D. Haasdijk, P. French, C. C. Hoogenraad and D. Jaarsma (2005). "ATF3 expression precedes death of spinal motoneurons in amyotrophic lateral sclerosis-SOD1 transgenic mice and correlates with c-Jun phosphorylation, CHOP expression, somato-dendritic ubiquitination and Golgi fragmentation." Eur J Neurosci **22**: 1881-1894.

Vonsattel, J. P. and M. DiFiglia (1998). "Huntington disease." J Neuropathol Exp Neurol **57**: 369-384.

Vos, M. J., M. P. Zijlstra, B. Kanon, M. A. van Waarde-Verhagen, E. R. Brunt, H. M. Oosterveld-Hut, S. Carra, O. C. Sibon, et al. (2010). "HSPB7 is the most potent polyQ aggregation suppressor within the HSPB family of molecular chaperones." Hum Mol Genet **19**: 4677-4693.

Walker, A. K., K. Y. Soo, V. Sundaramoorthy, S. Parakh, Y. Ma, M. A. Farg, R. H. Wallace, P. J. Crouch, et al. (2013). "ALS-associated TDP-43 induces endoplasmic reticulum stress, which drives cytoplasmic TDP-43 accumulation and stress granule formation." PLoS One **8**: e81170.

Walter, P. and D. Ron (2011). "The unfolded protein response: From stress pathway to homeostatic regulation." Science **334**: 1081-1086.

Wang, J., E. Martin, V. Gonzales, D. R. Borchelt and M. K. Lee (2008). "Differential regulation of small heat shock proteins in transgenic mouse models of neurodegenerative diseases." Neurobiol Aging **29**: 586-597.

Wang, J., H. Slunt, V. Gonzales, D. Fromholt, M. Coonfield, N. G. Copeland, N. A. Jenkins and D. R. Borchelt (2003). "Copper-binding-site-null SOD1 causes ALS in transgenic mice: Aggregates of non-native SOD1 delineate a common feature." Hum Mol Genet **12**: 2753-2764.

Wang, J., G. Xu, H. Li, V. Gonzales, D. Fromholt, C. Karch, N. G. Copeland, N. A. Jenkins, et al. (2005). "Somatodendritic accumulation of misfolded SOD1-L126Z in motor neurons mediates degeneration: αB-crystallin modulates aggregation." Hum Mol Gen **14**: 2335-2347.

Wang, W., L. Wang, J. Lu, S. L. Siedlak, H. Fujioka, J. Liang, S. Jiang, X. Ma, et al. (2016). "The inhibition of TDP-43 mitochondrial localization blocks its neuronal toxicity." Nat Med **22**: 869-878.

Watanabe, S., N. Ageta-Ishihara, S. Nagatsu, K. Takao, O. Komine, F. Endo, T. Miyakawa, H. Misawa, et al. (2014). "SIRT1 overexpression ameliorates a mouse model of SOD1-linked amyotrophic lateral sclerosis via HSF1/HSP70i chaperone system." Mol Brain **7**: 62.

Wengenack, T. M., S. S. Holasek, C. M. Montano, D. Gregor, G. L. Curran and J. F. Poduslo (2004). "Activation of programmed cell death markers in ventral horn motor neurons during early presymptomatic stages of amyotrophic lateral sclerosis in a transgenic mouse model." Brain Res **1027**: 73-86.

Westerheide, S. D., J. D. Bosman, B. N. A. Mbadugha, T. L. A. Kawahara, G. Matsumoto, S. Kim, W. Gu, J. P. Devlin, et al. (2004). "Celastrols as inducers of the heat shock response and cytoprotection." J Biol Chem **279**: 56053-56060.

Westwood, J. T. and C. Wu (1993). "Activation of Drosophila heat shock factor: Conformational change associated with a monomer-to-trimer transition." Mol Cell Biol **13**: 3481-3486.

Weydt, P., E. C. Yuen, B. R. Ransom and T. Moller (2004). "Increased cytotoxic potential of microglia from ALS-transgenic mice." Glia **48**: 179-182.

Williams, K. L., S. Topp, S. Yang, B. Smith, J. A. Fifita, S. T. Warraich, K. Y. Zhang, N. Farrawell, et al. (2016). "CCNF mutations in amyotrophic lateral sclerosis and frontotemporal dementia." Nat Commun **7**: 11253.

Winner, B., R. Jappelli, S. K. Maji, P. A. Desplats, L. Boyer, S. Aigner, C. Hetzer, T. Loher, et al. (2011). "In vivo demonstration that α-synuclein oligomers are toxic." Proc Natl Acad Sci USA **108**: 4194-4199.

Wong, H. R., M. Ryan and J. R. Wispe (1997). "Stress response decreases NF-kappaB nuclear translocation and increases I-kappaBalpha expression in A549 cells." J Clin Invest **99**: 2423-2428.

Wong, P. C., C. A. Pardo, D. R. Borchelt, M. K. Lee, N. G. Copeland, N. A. Jenkins, S. S. Sisodia, D. W. Cleveland, et al. (1995). "An adverse property of a familial ALS-linked SOD1 mutation causes motor neuron disease characterized by vacuolar degeneration of mitochondria." Neuron **14**: 1105-1116.

Wu, C. (1995). "Heat shock transcription factors: Structure and regulation." Annu Rev Cell Dev Biol **11**: 441-469.

Wyatt, A. R., J. J. Yerbury, H. Ecroyd and M. R. Wilson (2013). "Extracellular chaperones and proteostasis." Annu Rev Biochem **82**: 295-322.

Xiao, H. and J. Lis (1988). "Germline transformation used to define key features of heat-shock response elements." Science **239**: 1139-1142.

Xiao, Q., W. Zhao, D. R. Beers, A. A. Yen, W. Xie, J. S. Henkel and S. H. Appel (2007). "Mutant SOD1(G93A) microglia are more neurotoxic relative to wild-type microglia." J Neurochem **102**: 2008-2019.

Xu, Q., Y. Hu, R. Kleindienst and G. Wick (1997). "Nitric oxide induces heat-shock protein 70 expression in vascular smooth muscle cells via activation of heat shock factor 1." J Clin Invest **100**: 1089-1097.

Xu, Y.-M., D.-Y. Huang, J.-F. Chiu and A. T. Y. Lau (2012). "Post-translational modification of human heat shock factors and their functions: A recent update by proteomic approach." J Proteome Res **11**: 2625-2634.

Xue, C., T. Y. Lin, D. Chang and Z. Guo (2017). "Thioflavin T as an amyloid dye: Fibril quantification, optimal concentration and effect on aggregation." R Soc Open Sci **4**: 160696.

Yamanaka, K., S. J. Chun, S. Boillee, N. Fujimori-Tonou, H. Yamashita, D. H. Gutmann, R. Takahashi, H. Misawa, et al. (2008). "Astrocytes as determinants of disease progression in inherited ALS." Nat Neurosci **11**: 251-253.

Yamashita, H., J. Kawamata, K. Okawa, R. Kanki, T. Nakamizo, T. Hatayama, K. Yamanaka, R. Takahashi, et al. (2007). "Heat-shock protein 105 interacts with and suppresses aggregation of mutant Cu/Zn superoxide dismutase: Clues to a possible strategy for treating ALS." J Neurochem **102**: 1497-1505.

Yang, J., J. Oza, K. Bridges, K. Y. Chen and A. Y. Liu (2008). "Neural differentiation and the attenuated heat shock response." Brain Res **1203**: 39-50.

Yerbury, J. J., D. Gower, L. Vanags, K. Roberts, J. A. Lee and H. Ecroyd (2013). "The small heat shock proteins alphaB-crystallin and Hsp27 suppress SOD1 aggregation in vitro." Cell Stress Chaperon **18**: 251-257.

Yerbury, J. J., L. Ooi, A. Dillin, D. N. Saunders, D. M. Hatters, P. M. Beart, N. R. Cashman, M. R. Wilson, et al. (2016). "Walking the tightrope: Proteostasis and neurodegenerative disease." J Neurochem **137**: 489-505.

Zeineddine, R., N. E. Farrawell, I. A. Lambert-Smith and J. J. Yerbury (2017a). "Addition of exogenous SOD1 aggregates causes TDP-43 mislocalisation and aggregation." Cell Stress Chaperon **22**: 893-902.

Zeineddine, R., J. F. Pundavela, L. Corcoran, E. M. Stewart, D. Do-Ha, M. Bax, G. Guillemin, K. L. Vine, et al. (2015). "SOD1 protein aggregates stimulate macropinocytosis in neurons to facilitate their propagation." Mol Neurodegener **10**: 57.

Zeineddine, R., D. R. Whiten, N. E. Farrawell, L. McAlary, M. A. Hanspal, J. R. Kumita, M. R. Wilson and J. J. Yerbury (2017b). "Flow cytometric measurement of the cellular propagation of TDP-43 aggregation." Prion **11**: 195-204.

Zeineddine, R. and J. J. Yerbury (2015). "The role of macropinocytosis in the propagation of protein aggregation associated with neurodegenerative diseases." Front Physiol **6**: 277.

Zhang, S., M. B. Tang, H. Y. Luo, C. H. Shi and Y. M. Xu (2017). "Necroptosis in neurodegenerative diseases: a potential therapeutic target." Cell Death Dis **8**: e2905.

Zhao, W., D. R. Beers, S. Bell, J. Wang, S. Wen, R. H. Baloh and S. H. Appel (2015). "TDP-43 activates microglia through NF-kappaB and NLRP3 inflammasome." Exp Neurol **273**: 24-35.

Zheng, X., J. Krakowiak, N. Patel, A. Beyzavi, J. Ezike, A. S. Khalil and D. Pincus (2016). "Dynamic control of Hsf1 during heat shock by a chaperone switch and phosphorylation." eLife **5**: e18638.

Zheng, Z., J. Y. Kim, H. Ma, J. E. Lee and M. A. Yenari (2008). "Anti-inflammatory effects of the 70 kDa heat shock protein in experimental stroke." J Cereb Blood Flow Metab **28**: 53-63.

Zinkie, S., B. J. Gentil, S. Minotti and H. D. Durham (2013). "Expression of the protein chaperone, clusterin, in spinal cord cells constitutively and following cellular stress, and upregulation by treatment with Hsp90 inhibitor." Cell Stress Chaperon **18**: 745-758.

Zoghbi, H. Y. and H. T. Orr (2000). "Glutamine repeats and neurodegeneration." Annu Rev Neurosci **23**: 217-247.

Zourlidou, A., T. Gidalevitz, M. Kristiansen, C. Landles, B. Woodman, D. J. Wells, D. S. Latchman, J. de Belleroche, et al. (2007). "Hsp27 overexpression in the R6/2 mouse model of Huntington's disease: chronic neurodegeneration does not induce Hsp27 activation." Hum Mol Genet **16**: 1078-1090.

Zuccato, C., N. Belyaev, P. Conforti, L. Ooi, M. Tartari, E. Papadimou, M. MacDonald, E. Fossale, et al. (2007). "Widespread disruption of repressor element-1 silencing transcription factor/neuron-restrictive silencer factor occupancy at its target genes in Huntington's disease." J Neurosci **27**: 6972-6983.

Zuo, J., R. Baler, G. Dahl and R. Voellmy (1994). "Activation of the DNA-binding ability of human heat shock transcription factor 1 may involve the transition from an intramolecular to an intermolecular triple-stranded coiled-coil structure." Mol Cell Biol **14**: 7557-7568.

Zuo, J., D. Rungger and R. Voellmy (1995). "Multiple layers of regulation of human heat shock transcription factor 1." Mol Cell Biol **15**: 4319 - 4330.

Zurcher, N. R., M. L. Loggia, R. Lawson, D. B. Chonde, D. Izquierdo-Garcia, J. E. Yasek, O. Akeju, C. Catana, et al. (2015). "Increased in vivo glial activation in patients with amyotrophic lateral sclerosis: assessed with [(11)C]-PBR28." Neuroimage Clin **7**: 409-414.

Appendix

pminHsp70p-EGFP plasmid map:

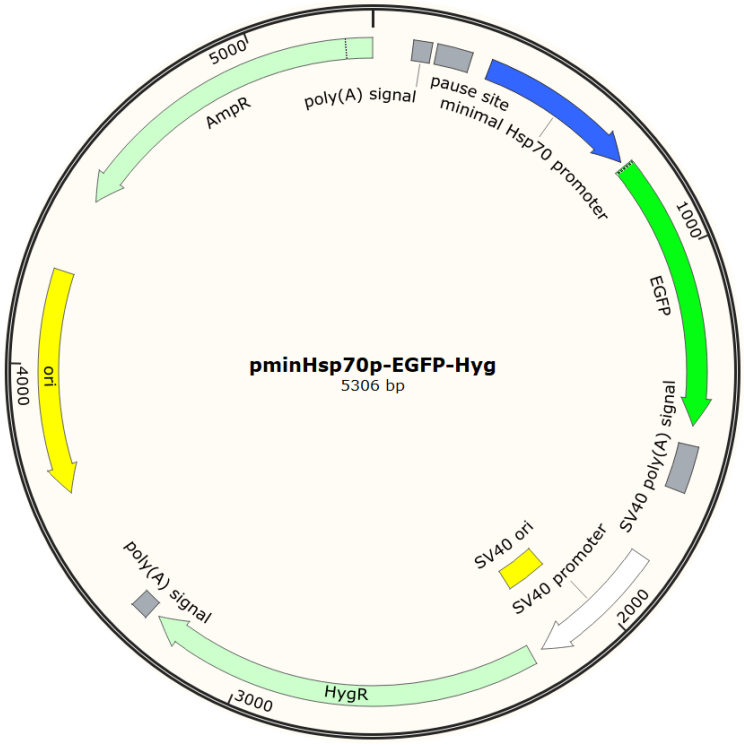

pminHsp70p-EGFP sequence:

TCGAGGCGCGTCCTCAGAGCCAGCCGGGAGGAGCTAGAACCTTCCCCGCGTTTCT
TTCAGCAGCCCTGAGTCAGAGGCGGGCTGGCCTGGCATAGCCGCCCAGCCTCTC
GGCTCACGGCCCGATCCGCCCGAACCTTCTCCCGGGGTCAGCGCCGCGCTGCGCC
GCCCGGCTGACTCAGCCCGGGCGGGCGGGCGGGAGGCTCTCGACTGGGCGGAA
GGTGCGGGAAGGTTCGCGGCGGCGGGGTCGGGGAGGTGCAAAAGGATGAAAAG
CCCGTGGAAGCGGAGCTGAGCAGATCCGAGCCGGGCTGGCGGCAGAGAAACCG
CAGGGAGAGCCTCACTGCTGAGCGCCCCTCGACGGCGGAGCGGCAGCAGCCTCC
GTGGCCTCCAGCATCCGACAAGAAGCTCTCTAGTCGACGGTATCGATAAGCTTCT
TAACATATGGTGAGCAAGGGCGAGGAGCTGTTCACCGGGGTGGTGCCCATCCTG
GTCGAGCTGGACGGCGACGTAAACGGCCACAAGTTCAGCGTGTCCGGCGAGGGC
GAGGGCGATGCCACCTACGGCAAGCTGACCCTGAAGTTCATCTGCACCACCGGC
AAGCTGCCCGTGCCCTGGCCCACCCTCGTGACCACCCTGACCTACGGCGTGCAGT
GCTTCAGCCGCTACCCCGACCACATGAAGCAGCACGACTTCTTCAAGTCCGCCAT
GCCCGAAGGCTACGTCCAGGAGCGCACCATCTTCTTCAAGGACGACGGCAACTA
CAAGACCCGCGCCGAGGTGAAGTTCGAGGGCGACACCCTGGTGAACCGCATCGA
GCTGAAGGGCATCGACTTCAAGGAGGACGGCAACATCCTGGGGCACAAGCTGGA
GTACAACTACAACAGCCACAACGTCTATATCATGGCCGACAAGCAGAAGAACGG
CATCAAGGTGAACTTCAAGATCCGCCACAACATCGAGGACGGCAGCGTGCAGCT
CGCCGACCACTACCAGCAGAACACCCCCATCGGCGACGGCCCCGTGCTGCTGCC
CGACAACCACTACCTGAGCACCCAGTCCGCCCTGAGCAAAGACCCCAACGAGAA
GCGCGATCACATGGTCCTGCTGGAGTTCGTGACCGCCGCCGGGATCACTCTCGGC
ATGGACGAGCTGTACAAGTAA

Appendix A: Plasmid map and sequence of the pminHsp70-EGFP-Hyg^{r} construct used to generate the Neuro-2a (HSE:EGFP) and HEK293 (HSE:EGFP) stable cell line reporters of the HSR. Sequence corresponding to the human minimal Hsp70 promoter (minHsp70p) is shown in blue and the EGFP gene in green. The 8 putative heat shock elements (NGAAN) in the minHsp70p sequence are underlined.

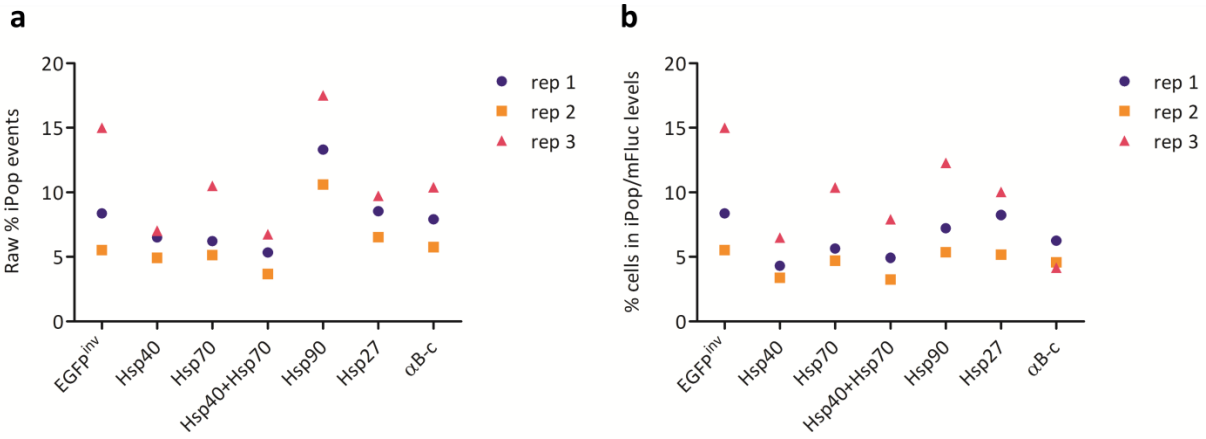

Appendix B. Graphs of raw percent of cells in the iPop gate. Cells were co-transfected with mFluc-EGFP and each of the Hsp-encoding bicistronic constructs and 48 h post-transfection the effect of each expressing each Hsp on mFluc inclusion formation was analysed by flow cytometry. (**a**) Raw percent of cells in the iPop gate within each sample across each of the three biological replicates, ● rep 1, ■ rep 2 and ▲ rep 3. (**b**) The percent of cells in the iPop gate normalised to relative mFluc expression levels in each respective sample across the three biological replicates. We found that the raw percent of cells with inclusions varied between biological replicates, for example, the third biological replicate demonstrated a consistently higher proportion of cells with inclusions across all samples. However, despite the differences in the raw percent of cells in the iPop gate, the trends across the Hsp expressing samples remained constant between experiments. Therefore, the data shown in Fig. 3 is expressed as a fold change rather than a raw percent to better reflect the chaperone activities of each Hsp in the mFluc protein aggregation assay.